Doctoral Dissertation

Doctoral Program in Chemical Engineering (34th Cycle)

Aqueous phase reforming for biorefinery stream valorization

By

Giulia Zoppi

******

Supervisor(s):

Prof. Samir Bensaid

Doctoral Examination Committee:

Prof. Massimo Migliori, Referee, Università degli Studi della Calabria

Prof. Gianluca Landi, Referee, Istituto di ricerca sulla combustione-CNR

Prof. Claudio Ampelli, Referee, Università degli studi di Messina

Prof. Silvia Tabasso, Referee, Università di Torino

Prof. Fabio Deorsola, Referee, Politecnico di Torino

Politecnico di Torino

2022

Declaration

I hereby declare that, the contents and organization of this dissertation constitute my own original work and does not compromise in any way the rights of third parties, including those relating to the security of personal data.

Giulia Zoppi

2022

* This dissertation is presented in partial fulfillment of the requirements for **Ph.D. degree** in the Graduate School of Politecnico di Torino (ScuDo)

Abstract

The growing energy demands led the attention on the necessity to find alternatives to fossil sources. Biomass may be one of the keys to solve this challenge, and its conversion into chemicals, fuels and energy is called biorefinery. To be sustainable from economic and environmental point of view biorefineries need to recover as much as possible of the carbon in the feedstock; however, in most of the process there is a production of a liquid side streams which contains organic compounds. For example, among the exiting processes, hydrothermal liquefaction aims to produce a biocrude, which after an upgrade step can be used as fuel. However, next to the desired product, a gas phase, a solid char and a wastewater (HTL-AP) are produced.

Aim of the thesis is testing the feasibility of the aqueous phase reforming reaction application to liquid side streams, containing diluted organics; especially the attention of this work focuses on the hydrothermal process of lignin rich feed, starting from model molecules up to pilot-plant testing looking also at environmental and economic feasibility. The water formed during the Fischer-Tropsch water was also tested to deeper understand the feasibility of APR in the various industrial frames.

Most of the works in literature focuses on simple compounds, especially alcohols and polyalcohols; however, they are not representative of a complex mixture as the HTL-AP. Starting from literature or from direct characterization of side streams, model compounds of different classes were selected and tested.

Fischer-Tropsch fraction contains small alcohols and carboxylic acids, their reactivity was assessed thanks to single compound tests and then their synthetic mixture was compared to the water produce by low temperature Fischer-Tropsch. Increase of temperature and time had beneficial effect on the conversion of the feedstock and good hydrogen productivity was obtained thanks to the presence of linear alcohols in the water. From the tests on single molecules insights into the reaction mechanism and product distribution were obtained and the importance of the hydroxyl group position was highlighted.

Then, carboxylic and bicarboxylic acids, hydroxyacids, alcohols, cycloketones and aromatics were identified as representative for HTL of lignin rich stream and tested. The tests were performed with a Pt/C catalyst and the influence of the carbon concentration (0.3–1.8 wt. C%) was investigated. Glycolic acid, acetic acid, lactic acid were mixed together and tested to understand the behaviors of single compound, with acetic acid which seems to suffer of adsorption competition on the active site. Finally residual waters from HTL of lignin were tested for the first time after a deep characterization. Deactivation of the catalyst was observed, and it was ascribed to the presence of aromatics in the water. The extent of deactivation was correlated to the reduction of surface area, which may be due to the adsorption on the catalyst of phenolic oligomers. Simple aromatics like guaiacol and phenol, were proved not to be the cause of the deactivation thanks to the use of a multi-component synthetic mixture. Solutions to mitigate the phenomena were studied, such as active carbon adsorption and liquid-liquid extraction for the selective removal of aromatics.

Finally, the knowledge gained with batch tests were used to understand the feasibility of APR at industrial level. To do that lab scale continuous reactor was used. Indeed, the continuous mode is a necessary step to get closer to industrial application and to deeper study the stability of the catalyst.

Thanks to the characterization of the HTL water fraction synthetic mixture were prepared as close as possible and tested in continuous to study the influence of temperature and flow rate on the conversion and hydrogen production. Preliminary tests were conducted in a pilot-plant scale with the same synthetic mixture and the results were comparable with lab scale reactor.

Aqueous phase reforming can be combined with hydrothermal liquefaction to clean its water and produce a gas rich in hydrogen which can be used in the upgrading step of biocrude. A conceptual design of the HTL APR combined plant was carried out to understand the feasibility of the combination of the processes. Two cases were studied: one with lignin and one with corn stover as feedstock of HTL. Based on the plant techno-economic and environmental assessment were carried out and proved the potential of aqueous phase reforming to produce hydrogen starting from water waste. The analysis shows that the minimum selling prices for the biofuel are 1.20 for lignin rich stream and 1.17 €/kg for corn stover.

Content

1. Chapter 1 9
2. Introduction 9
    1.1. Global warming 9
    1.2. Aqueous phase reforming 14
    1.1.1. Theory 14
    1.1.2. Parameter influence on APR reaction 16
    1.1.3. Industrial application 22
    Lignocellulosic biomass: biorefineries approach 22
    Hydrolysis 22
    Thermochemical conversion technology 29
    Food industry 32
    Crude glycerol 37
    Perspectives: towards industrial APR application 38
    1.3. Aim of the work 42
3. Chapter 2 43
4. Material and methods 43
    2.1. Materials 43
    2.2. Methods 45
    2.2.1. Aqueous phase reforming tests 45
    2.2.2. Reproducibility tests 47
    2.2.3. Adsorption tests 48
    2.2.4. Analytical methods 48
    2.2.5. Catalyst characterization 49
5. Chapter 3 50
6. Fischer-Tropsch 50

3.1. Characterization of the FT product water 52
3.2. Aqueous phase reforming of FT product water 52
3.2.1. Influence of reaction temperature 52
3.2.2. Influence of reaction time 55
3.2.3. Aqueous phase reforming of single compounds 57
3.2.4. Catalyst stability 62
3.2.5. Conclusion 63
7. Chapter 4 64
8. Hydrothermal liquefaction water fraction 64
4.1. Model compound 66
4.1.1. Influence of carbon concentration 66
4.1.2. Influence of reaction time 69
4.1.3. HTL aqueous phase synthetic mixture 71
4.1.4. Case study: APR of the water fraction from HTL of lignin 74
Characterization of the aqueous phase 74
4.1.5. HTL-AP catalytic test 77
4.1.6. Deactivation of the catalyst 79
4.2. Catalyst deactivation 90
4.2.1. Synthetic aqueous phase – effect of aromatic monomers and inorganics 91
4.2.2. Actual aqueous phase – effect of physical pretreatment 94
4.2.3. Evaluation of catalyst deactivation 99
4.2.4. Solid characterization 101
4.3. Influence of solvent extraction 102
Conclusion 106
9. Chapter 5 108
10. Continuous tests 108
5.1. Lab scale continuous tests 108

5.1.1. Model compounds and synthetic mixtures 108
5.1.2. Influence of weight-hourly space velocity 113
5.1.3. Influence of sulfate concentration 115
5.2. Pilot plant continuous tests 119
11. Chapter 6 122
12. Techno-economic and life cycle assessment 122
6.1. Methodology techno-economic assessment 123
6.1.1. Process description 124
6.1.2. Economic assessment 125
Fixed cost 125
Operative costs 126
Minimum selling price 127
Sensitivity analysis 129
6.2. Methodology life cycle assessment 129
6.3. Mass and Energy balances 131
6.3.1. Mass balance 131
6.3.2. Hydrothermal liquefaction and separation 131
6.3.3. Aqueous phase reforming 132
6.3.4. Aqueous phase recycling 133
6.3.5. Purification and upgrading 134
6.3.6. Overall 135
6.3.7. Energy balance 137
6.4. Process and equipment design 139
6.4.1. Pre-treatment 141
6.4.2. HTL reaction 141
6.4.3. Products separation 142
6.4.4. APR reaction 143
6.4.5. Purification 143

6.5. Economic analysis 144
6.5.1. Fixed costs 144
6.5.2. Material and utilities costs 145
6.5.3. Minimum selling prices and economic indicators 146
6.5.4. Sensitivity analysis 148
6.5.5. Comparison with literature data 152
6.6. LCA results 155
6.6.1. Goal and scope 155
6.6.2. Inventory list 158
6.6.3. Life cycle assessment 159
6.6.4. Interpretation step 162
6.6.5. Non-biogenic carbon 165
6.6.6. Literature comparison 165
6.7. Catalyst deactivation 167
6.7.1. Liquid-liquid extraction 168
6.7.2. Adsorption with activated carbon 168
6.7.3. Char activation 169
6.7.4. Inert catalyst support 170
6.8. Conclusion 170
13. Chapter 7 172
14. Conclusion 172
15. Acknowledgment 173
16. Bibliography 174

List of Figures

Figure 1: energetic world consumption by sources, 1971-2019 (EJ) [1]. 9

Figure 2: oil total final consumption by sector, 1971–2019 (EJ). 10

Figure 3: biorefinery concept modified from [15]. 11

Figure 4: Advantages and challenges of state of technology for HTL-AP (Aqueous phase from Hydrothermal liquefaction) valorization [26]. 12

Figure 5: aqueous phase reforming applied to HTL water. 13

Figure 6. Thermodynamic equilibrium for hydrogen production, modified from [39]. 14

Figure 7: reactions pathway of ethylene glycol, proposed in[39]. 16

Figure 8. Influence of chain length on APR performance [41]. 17

Figure 9: effect on feedstock concentration[37]. 17

Figure 10. Design of heterogeneous catalyst from [49]. 18

Figure 11. Relative rates of reactions under APR reaction conditions, C-C cleaving (white bar), water gas shift (grey bar), methanation (black bar). as reported in [50]. 19

Figure 12: effect of hydrogen pressure on sorbitol conversion (open circle) and hydrogen selectivity (black circle) from [54] 20

Figure 13: some model compounds use for APR studies[58]. 21

Figure 14. APR of wheat straw hydrolysate with different catalysts. Reaction conditions: 250 °C, 2 h, 50 mL hydrolysate (data from [64]). 23

Figure 15. Influence of carbon concentration on the hydrogenation of a glucose-xylose mixture (A) and on the APR of the hydrogenated feed (B). Hydrogenation reaction conditions: 0.188 g Ru/C catalyst, 1 h reaction time, 180 °C, 15 bar H2 pressure. APR reaction conditions: 0.375 g Pt/C catalyst, 2 h reaction time, 270 °C (from [44]). 24

Figure 16. Thermochemical conversion routes and main outputs of biomass. 29

Figure 17. A: Influence of glycerol grade on the hydrogen content in the gaseous stream, reaction conditions: 250 °C/20 bar, 10 wt.% glycerol, flow rate 0.5 mL/min, 0.3 g catalyst (from [105]). B:

Influence of catalyst on APR of pure and crude glycerol, reaction conditions: 225 °C/29 bar, 3 h, 0.3 g catalyst (data from [109]).....38

Figure 18. Parr top reactor component scheme. 45

Figure 19. Influence of stirring speed on glycolic acid APR. Reaction conditions: 270 °C, 0.05 g 5% Pt/C, 1 h, 1.3 wt.% glycolic concentration. 46

Figure 20: continuous reactor set up 47

Figure 21. On the left, HPLC chromatograms of the Fischer-Tropsch product water (1: acetic acid 2: propionic acid 3: methanol 4: ethanol 5: butanoic acid 6: 2-propanol 7:1-propanol 8: butanol); on the right, quantification of the main organic and inorganic compounds. 52

Figure 22: Influence of the reaction temperature on the APR of FT product water. Gas performance indicators. Reaction conditions: 0.375 g Pt/C catalyst, 75 mL FT product water, 2 hours reaction time.....53

Figure 23: HPLC chromatograms of the feed and products (1: acetic acid 2: propionic acid 3: methanol 4: ethanol 5: butanoic acid 6: 2-propanol 7:1-propanol 8: butanol), together with COD data. Reaction conditions: 0.375 g Pt/C catalyst, 75 mL FT product water, 2 hours reaction time. 54

Figure 24: conversion of the main molecules present in the feed. Reaction conditions: 0.375 g Pt/C catalyst, 75 mL FT product water, 2 hours reaction time. 55

Figure 25: Influence of reaction time on the APR of the FT product water. Gas performance indicators. 0.375 g Pt/C catalyst, 75 mL FT product water, 270 °C reaction temperature. 56

Figure 26: Influence of reaction time on the APR of the FT product water. Conversion of the main alcohols in the feed. 0.375 g Pt/C catalyst, 75 mL FT product water, 270 °C reaction temperature 56

Figure 27: Influence of reaction time on the APR of the FT product water. left: evolution of the liquid species; right: evolution of the gaseous species and H_2/CO_2 ratio. Reaction conditions: 0.375 g Pt/C catalyst, 75 mL FT product water, 270 °C reaction temperature. 57

Figure 28. Influence of the feed on the gas (A) and liquid (B) composition. Reaction conditions: 0.375 g Pt/C catalyst, 75 mL solution 0.9 wt.% C, 270 °C reaction temperature, 2 hours reaction time. 59

Figure 29. Suggested reaction mechanism for APR of primary (a) and secondary (b) alcohols.60

Figure 30. Influence of catalyst re-use on the APR performance of FT product water. Reaction conditions: 0.1 g Pt/C, 75 mL FT product water, 270 °C reaction temperature, 2 hours reaction time. 63

Figure 31: Block flow diagram of a HTL-APR integrated plant. HTL: hydrothermal liquefaction; HT: hydrotreatment (upgrade block). 65

Figure 32. Amount-time profile for APR of acetic acid (A), glycolic acid (B), Lactic acid (C-D). Reaction conditions: Liquid phase amount: 75 g, 0.375 g Pt/C, 0.9 wt. % C feed, 270 °C reaction temperature.....70

Figure 33. Proposed reaction scheme for lactic acid APR. 71

Figure 34: Amount-time profile for APR of a synthetic ternary mixture. Reaction conditions: Liquid phase amount: 75 g, 0.375 g Pt/C, total 0.9 wt.% C glycolic, acetic and lactic acid (0.3 wt.% C per component), 270 °C reaction temperature..... 72

Figure 35: Influence of carbon concentration on the reaction parameters (A) and conversion (B) of APR of the synthetic mixture. Reaction conditions: Liquid phase amount: 75 g, 270°C reaction temperature, 2 h reaction time..... 73

Figure 36: Influence of reaction temperature on the reaction parameters of APR of the synthetic mixture. Reaction conditions: Liquid phase amount: 75 g, 1.8 wt. % C, 2 h reaction time. 73

Figure 37: Effect of the filtration of the feed on the APR of the HTL-AP sample. Reaction conditions: 0.8 wt.% C, 270 °C reaction temperature, 2 h reaction time..... 75

Figure 38: HPLC chromatograms of the HTL-AP (1: glycolic acid, 2: lactic acid, 3: glycerol, 4: acetic acid, 5: acetaldehyde, 6: methanol, 7: catechol, 8: phenol, 9: guaiacol). 76

Figure 39: Influence of carbon concentration on reaction parameters of APR of the HTL-AP. Reaction conditions: Liquid phase amount: 75 g , 270°C reaction temperature, 2 h reaction time. . 77

Figure 40: HPLC chromatograms of the feed and product for the first test (left) and second test (right) of the HTL-AP sample. Reaction conditions: 1% wt.% C, 270°C reaction temperature, 2 reaction time (1: glycolic acid 2: lactic acid 3: glycerol 4: acetic acid 5: acetaldehyde 6: methanol 7: catechol 8: phenol 9: propionic acid)..... 78

Figure 41: H_2 productivity (A) and H_2 production (B) for the APR of HTL-AP. Reaction conditions: Liquid phase amount: 75 g, 270°C reaction temperature, 2 h reaction time..... 79

Figure 42: APR of glycolic acid with different catalysts. Reaction conditions: Liquid phase amount: 75 g, 0.9 wt.% C glycolic acid, reaction temperature 270°C, reaction time 2 h..... 80

Figure 43: HPLC chromatograms of HTL-AP and treated HTL-AP feeds (1: glycolic acid 2: lactic acid 3: glycerol 4: acetic acid 5: acetaldehyde 6: methanol 7: catechol 8: phenol 9: guaiacol 10: DEE). 81

Figure 44: Influence of carbon concentration and DEE pre-treatment on the H_2 production for APR of different batches. Reaction conditions: Liquid phase amount: 75 g, 270 °C reaction temperature, 2 h reaction time..... 82

Figure 45: TGA-IR of fresh catalyst. Analysis conditions: heat from 30 °C to 1000 °C @ 20 °C/min in nitrogen atmosphere with a purge rate of 20 mL/min under nitrogen. A: TG results; B: IR-Absorption peak during TGA. 84

Figure 46: TGA-IR of spent catalyst after APR 1st test of HTL-AP. Reaction conditions: 0.8 wt.% C, reaction temperature 270 °C, reaction time 2 h. Analysis conditions: heat from 30 °C to 1000 °C @ 20 °C/min in nitrogen atmosphere with a purge rate of 20 mL/min under nitrogen. A: TG results; B: IR-Absorption peak during TGA of water, CO_2, CH_4, aliphatic fragments and primary alcohols; C: Infrared spectra at 408°C. 85

Figure 47: TGA-IR of spent catalyst after APR of treated HTL-AP 1. Reaction conditions: 0.8 wt.% C, reaction temperature 270 °C, reaction time 2 h. Analysis conditions: heat from 30 °C to 1000 °C @ 20 °C/min in nitrogen atmosphere with a purge rate of 20 mL/min under nitrogen. A: TG results; B: IR-Absorption peak during TGA. 85

Figure 48:TGA-IR of spent catalyst after APR of treated HTL-AP 2. Reaction conditions: 0.8 wt.% C, reaction temperature 270 °C, reaction time 2 h. Analysis conditions: heat from 30 °C to 1000 °C @ 20 °C/min in nitrogen atmosphere with a purge rate of 20 mL/min under nitrogen. A: TG results; B: IR-Absorption peak during TGA; C: Infrared spectra at 380°C. 86

Figure 49: TGA-IR of spent catalyst after APR 2nd test of HTL-AP. Reaction conditions: 0.8 wt.% C, reaction temperature 270 °C, reaction time 2 h. Analysis conditions: heat from 30 °C to 1000 °C @ 20 °C/min in nitrogen atmosphere with a purge rate of 20 mL/min under nitrogen. A: TG results; B: IR-Absorption peak during TGA; C: Infrared spectra at 198°C; D: Infrared spectra at 298 °C... 88

Figure 50: TGA-IR of spent catalyst after APR second test of HTL-AP 1. Reaction conditions: 0.8 wt.% C, reaction temperature 270 °C, reaction time 2 h. Analysis conditions: heat from 30 °C to 1000 °C @ 20 °C/min in nitrogen atmosphere with a purge rate of 20 mL/min under nitrogen. A: TG results; B: IR-Absorption peak during TGA; C: Infrared spectra at 270 °C..... 88

Figure 51: TGA-IR of spent catalyst after APR of HTL-AP 3. Reaction conditions: 0.8 wt.% C, reaction temperature 270 °C, reaction time 2 h. Analysis conditions: heat from 30 °C to 1000 °C @ 20 °C/min in nitrogen atmosphere with a purge rate of 20 mL/min under nitrogen. A: TG results; B: IR-Absorption peak during TGA; C: Infrared spectra at 270 °C. 89

Figure 52: XPS spectra of fresh and spent catalysts after aqueous phase reforming. Reaction conditions: 0.8 wt.% C feed (HTL-AP or treated HTL-AP 3), 270 °C reaction temperature, 2 h reaction time. 90

Figure 53. APR results of model mixtures. Reaction conditions: 0.375 g Pt/C, 270 °C, 2 hours. 92

Figure 54. Adsorption of the components of the model mixture. Adsorption conditions: 0.375 g Pt/C, 75 mL Acids + Aromatics solution, room temperature. 93

Figure 55. Influence of temperature of physical pretreatment. Reaction conditions: 0.375 g Pt/C, 270 °C, 0.375 g Pt/C, 2 hours. 95

Figure 56. Adsorption of the actual phase with 0.375 g activated carbon (A) and 0.375 g Pt/C catalyst (B). Adsorption conditions: 75 mL solution, room temperature. 97

Figure 57. HPLC chromatograms (PDA wavelength: 212 nm) of synthetic (A) and actual (B) mixtures on Pt/C catalyst. 1: glycolic acid, 2: lactic acid, 3: acetic acid, 4: propionic acid, 5: phenol, 6: guaiacol, 7: catechol, 8: 3-methoxycathecol. Adsorption conditions: 75 mL solution, 0.375 g Pt/C catalyst, room temperature, 4 hours. Reaction conditions: 75 mL solution, 0.375 g Pt/C catalyst, 270 °C, 2 hours. 98

Figure 58. GC-MS analysis of the acetone solution derived from the washing step of the Pt/C catalyst. From left to right: creosol, 4-ethylguaiacol, syringol, 4-propylguaiacol, 2,4-di-tert-buthylphenol..... 98

Figure 59. APR of glycolic acid using second-use Pt/C catalysts and corresponding textural properties. Reaction conditions: 0.375 g Pt/C, 270 °C, 0.9 wt.% C glycolic acid, 2 hours. 99

Figure 60. XRD patterns of as-received and regenerated catalyst. 101

Figure 61. ATR spectra of solid deposits formed during the storage of the aqueous phase. 102

Figure 62. A: Organic acids recovery after liquid-liquid extraction and HPLC-RID chromatograms (1: glycolic acid, 2: lactic acid, 3: acetic acid); B: aromatics recovery after liquid-liquid extraction and HPLC-PDA (212 nm) chromatograms (4: catechol, 5: 3-methoxycatechol, 6: phenol, 7: guaiacol). 104

Figure 63. Influence of the nature and amount of the solvent on the APR performance. Reaction conditions: 75 mL aqueous phase, 270 °C, 2 h, 0.375 g 5% Pt/C. 105

Figure 64. APR of glycolic acid with a spent catalyst. Reaction conditions: 75 mL aqueous phase 2.85 wt.% glycolic acid, 270 °C, 2 h, 0.200 g 5% Pt/C (spent). 106

Figure 65. APR of model compounds (A: glycolic acid; B: ethanol; C: lactic acid; D: acetic acid). Reaction conditions: 270 °C, 60 bar, flow 0.6 mL/min, feed concentration 0.3 – 1 wt.% C. 109

Figure 66. Performance of APR synthetic mixture. 270 °C, 60 bar, A: 0.2 ml/min B: 0.4 ml/min C: 0.6 ml/min 109

Figure 67: HPLC chromatogram of HTL-AP and synthetic mixture. 110

Figure 68. Performance of APR of synthetic mixture 270 °C, 60 bar, 0.8 ml/min without DEE (left) and with DEE (Right) 110

Figure 69. Gas composition of APR of synthetic mixture. 270 °C, 60 bar, 0.8 ml/min. 111

Figure 70: Influence of reaction temperature on acetic acid conversion 111

Figure 71. Influence of reaction temperature on substrate conversion. Reaction conditions: 1 g_{feed}/g_{cat} min 112

Figure 72. Influence of WHSV on substrate conversion. Reaction conditions: 0.6-0.8 ml/min, 270 °C, 60 bar. 114

Figure 73. performance of APR of HTL-AP. 270°C, 60 bar, 0.8 ml/min(left); Performance of II use HTL-AP APR. 270°C, 60 bar, 0.8 ml/min (right) 115

Figure 74. Influence of sulfate 270°C 0.6 mL/min 116

Figure 75: effect of loading in the AC adsorption. 117

Figure 76: adsorption of four types of Amberlite (left) and mechanism of adsorption (right). 117

Figure 77: influence of IRA 67 loading 118

Figure 78: effect of resin pretreatment, 270°C 118

Figure 79: pilot plant pictures, BEST 119

Figure 80: reaction conditions 263°C, 58 bar and 0.56 WHSV 120

Figure 81: conversion of compounds 121

Figure 82: Block flow diagram of the HTL-APR integrated plant. Block numbers are identifiers of plant sections. 123

Figure 83: The four steps followed to carry out the life cycle assessment. 130

Figure 84: Example of impact categories and factors [245]. 131

Figure 85: Mass flow for L case (a) and CS (b) 136

Figure 86: Block diagram and energy stream for LRS and CS 138

Figure 87: Plant layout. 140

Figure 88: Grassroot costs distribution between sections, with LRS case (left) and CS case (right) 144

Figure 89: Grassroot costs distribution between equipment, with LRS case (left) and CS case (right). 144

Figure 90: Operative costs, with LRS case (left) and CS case (right) 146

Figure 91: MSP10% variations after feedstock, electricity, natural gas price variation and with an HTL-APR plant operating at 20% solid loading. 148

Figure 92: plant configurations for hydrogen supply. A) APR+electrolysis, B) APR alone, C) APR+SR, D) SR alone, E) Electrolysis alone, F) No upgrading. The percentage values refer to the variation of the $MSP^{10\%}$ of the considered configuration compared to the respective base case (A for LRS and B for CS). 152

Figure 93: Example of system boundaries in a LCA [245]. 156

Figure 94: system boundary of studied LCA 156

Figure 95: GABI model of HTL+APR plant. LRS above and CS below. 161

Figure 96: distribution of GWP among the main processes (1 MJ biofuel). 163

Figure 97:distribution of AP (1) and EP (2) and of abiotic depletion (3) among the main processes (1 MJ biofuel) 164

Figure 98: comparison of synfuels and fossil fuels from [268] 167

List of Tables

Table 1. APR reaction stoichiometry and theoretical hydrogen yield for common oxygenated present in wastewater fraction. 1 g of carbon was assumed as basis for the calculation. [59] 21

Table 2. APR of different lignocellulosic biomass. n.a.: not available 27

Table 3: APR of model compounds and differences with theoretical values. Reaction conditions: 5% Pt/Al2O3 catalyst, temperature 270 °C, reaction time 2 h, feed concentration 133 mM, 75 mL batch reactor (data from [88]) 31

Table 4. Main characterization and results of APR of wastewaters derived from different food-processing. Inorganics: sum of phosphate, sulfate, sodium chloride; LSC: low salt content – HSC: high salt content. 34

Table 5: Summary of wastewater sources with corresponding characteristics, advantages and disadvantages in the field of APR. 39

Table 6: tested compounds. 43

Table 7: acetic acid APR reproducibility tests. Reaction conditions: 270°C, 0-3 h 13 mmol acetic acid 47

Table 8: Reaction conditions: reproducibility test in continous reactor. 270°C, 1 g of Pt/C, 0.8 ml/min 47

Table 9. Main products of APR of alcohols. 61

Table 10. Linear combination of single model compound in comparison with FT water fraction results. 62

Table 11*:* Influence of carbon concentration on APR of model compounds. Reaction conditions: Liquid phase amount: 75 g, Temperature 270°C, Reaction time 120 min.....68

Table 12: co-adsorptiont tests.....74

Table 13: HTL-AP quantification of main compounds and ICP analysis. 76

Table 14: Aqueous phase reforming of synthetic mixtures with and without DEE. Reaction conditions: Liquid phase amount: 75 g, 0.9 wt.% C acids + 0.9 wt.% C DEE, 270 °C reaction temperature, 2 h reaction time.....82

Table 15. Composition of the model aqueous phase tested in the APR set-up. 91

Table 16. Description of pretreatments performed on the samples subjected to APR. 94

Table 17. Influence of reaction temperature on gas production; average values were reported. Reaction conditions: 1 g_{feed}/g_{cat} min.....113

Table 18: gas production. Reaction conditions: 0.6-0.8 ml/min, 270 °C, 60 bar 114

Table 19. Surface analysis of fresh and spent Pt/C catalyst. 115

Table 20: gas production of glycolic acid APR 120

Table 21: gas composition.....121
Table 22: Plant sections and unit operations. 124
Table 23: Data for the operative costs. 127
Table 24: Economic set parameters. 128
Table 25: Phase compositions and LHV of feedstocks and products. 132
Table 26: APR performances obtained from the HTL-AP valorization of LRS and CS. 133
Table 27: Main inorganic elements present in LRS and in its HTL products. 133
Table 28: Hydrotreatment product distribution. 135
Table 29: Main input and output streams. 135
Table 30: Electric and thermal yearly inputs of the plant. 138
Table 31: Economic parameters and main indicators for LRS and CS case 146
Table 32: $MSPs^{10\%}$ for different plant configurations for hydrogen supply. 150
Table 33: MSPs comparison with literature data 154
Table 34: Life cycle inventory of 1 kg biofuel for LRS and CS cases. 158
Table 35: Environmental impacts of the HTL-APR biorefinery for LRS and CS scenarios (1 MJ biofuel). 163
Table 36: comparison of impacts of different biofuels 166

Chapter 1

Introduction

1.1. Global warming

The energy demand in the world is constantly increasing. From Figure 1 it is clear that the energy consumption is rising steadily, and fossil fuels (coal, natural gas, oil) still represent the 80% of energy sources [1].

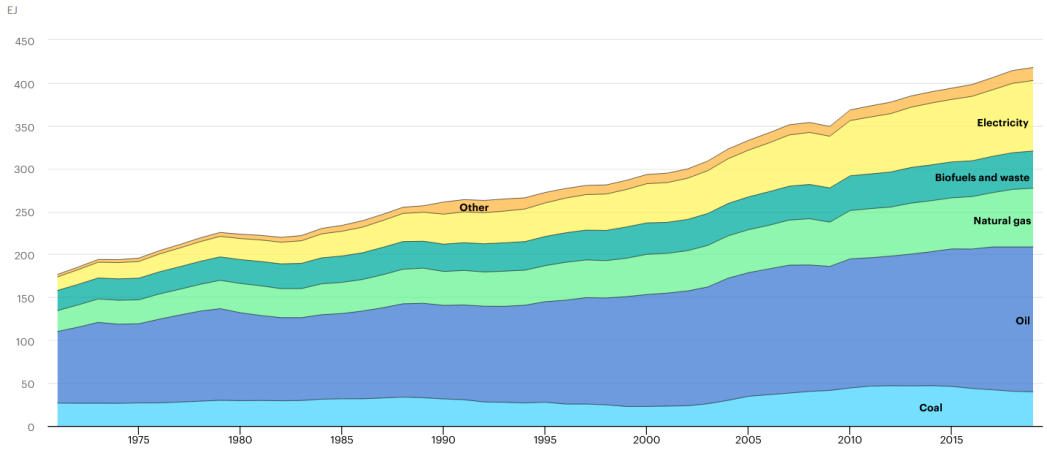


Figure 1: energetic world consumption by sources, 1971-2019 (EJ) [1].

There are several issues related with fossil fuel consume: countries are energetically dependent from others; they have the highest impact in the greenhouse gas emissions. They still are the most convenient option, from an economical point of view, but the interest of the world into renewable sources has driven the attention to other possibilities of energy production.

Renewable energy is, according to the definition of the International Energy Agency: "*Energy derived from natural processes (e.g. sunlight and wind) that are replenished at a faster rate than they are consumed. Solar, wind, geothermal, hydro, and some forms of biomass are common sources of renewable energy*"

Figure 2 highlights that an important fraction of consumption is given by the transportation sector.

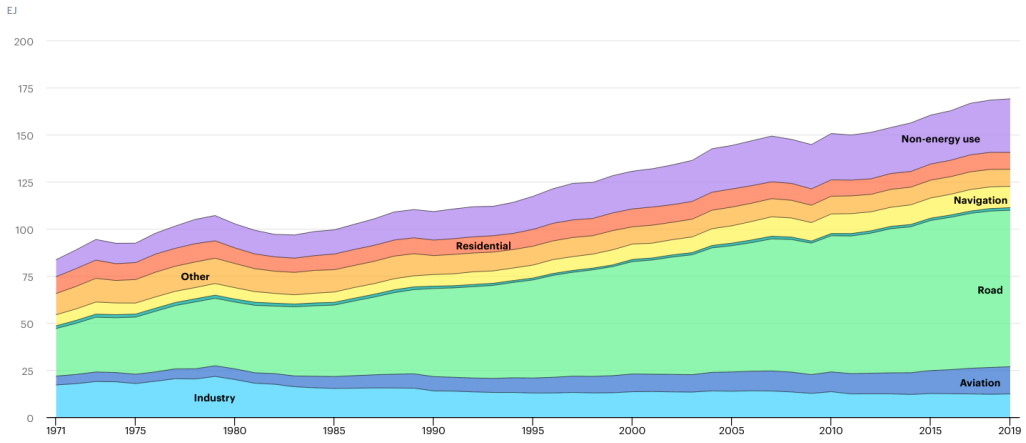


Figure 2: oil total final consumption by sector, 1971–2019 (EJ).

The increase of industrialization brought, other than an increase of pollution, an escalation in the production of waste water streams from human activity [2]. Human activities (industrial, agricultural, domestic and commercial) consume fresh water to produce polluted water; this is a problem addressed in the 2030 Agenda, the sustainable development goal (SDG) number 6 is indeed dedicated to water. The goal is to improve the water quality and halving the percentage of untreated wastewater [3]. Furthermore, the exploitation of the remaining organic content to produce chemicals or fuels, meets another SDG, the number 12, which is related to the sustainable production and consumption.

Food and agricultural sector have an important water footprint since they consume fresh water and produce contaminated aqueous streams; the characteristic of these streams vary according with the type of industry. For example: brewery industries lead to 3-10 liters of wastewater per liter of beer [4]; beer has a production of 191 billion liters in the world [5]. Soybean processing produces 7-10 tons of wastewater (Chemical Oxygen Demand (COD) in the range of 10-20 g/L) which contains a wide range of compounds; cheese making to 9 kg of cheese whey for each kg of cheese [6] and dairy industries produces 0.2-10 liter of water per liter of milk [7]. Also, biorefineries can suffer from strong impact regarding water effluent. Indeed the water produced from thermochemical processes contain organics, whose concentration may vary in a large range (2.38-104.2 g/L) [8], several classes of compounds are dissolved in water such as alcohols, carboxylic acid, aromatics and so on [9]. The usual treatment is a combination of different technologies such as physical, chemical and biological process to reduce its organic content to the environmental regulation [10]. Other possible treatments are ozonation, chlorination, filtration through the use of activated carbon or membrane [11]. One of the main limitations in the development of an effective treatment regards the lack of characterization of water fractions [12].

One of the renewables alternatives of fossil sources in the transportation sector is represented by biofuels. Biofuels are liquid or gaseous transportation fuels (e.g. biodiesel and bioethanol) made from biomass. The biorefinery concept is defined by IEA: a biorefinery is the sustainable processing of biomass into a spectrum of marketable products [13].

The biomass can be broadly divided into different categories according to its origin [14]:

- First generation biomass refers to biomass which is also edible feedstock such as oils seeds, sugar beet, corn. It brings social and environmental issue related to the fuel vs food competition.
- Second generation biomass refers to non-food biomass like agricultural, forest residues or waste.
- Third generation biomass refers to algae-based matter. Their main advantage consists of the possibility to use marginal lands or water for their production

In the following Figure 3 the biorefinery concept is represented. The aim of the biorefinery should be to exploit as much as feedstock possible producing fuels materials, and chemicals.

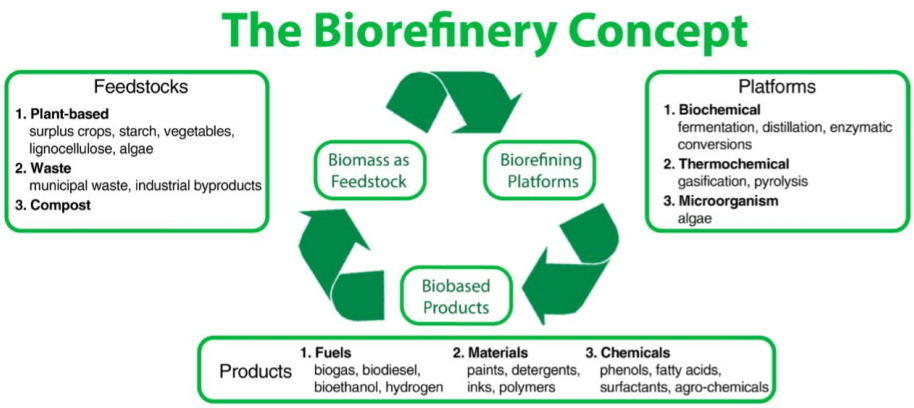


Figure 3: biorefinery concept modified from [15].

The processes carried out in a biorefinery can be divided in two main categories: biochemical and thermochemical [16]. Some of the most common biochemical processes are fermentation and anaerobic digestion. The fermentation aims to produce bioethanol starting from sugar monomers with the use of yeast. The anaerobic digestion instead produced the biogas (mixture of methane and carbon dioxide) thanks to the ability of bacteria to decompose the organic matter [17].

Thermochemical processes instead occur in presence of heat. Thermochemical process can be wet or dry. Dry route consists of three main reactions: combustion, gasification or pyrolysis. These are distinguished by the oxygen content. Combustion is the production of energy heat and power by the biomass reaction with (at least) stoichiometric O_2. Gasification process deals with the biomass reacting with oxygen (lower than stoichiometry) to produce a hydrogen/carbon monoxide mixture (syngas) to be used for petrochemical industry, or for energy production [18]. Finally pyrolysis works without oxygen and convert the biomass into three different phases: a solid char (inorganics and unconverted carbon), a gas phase and a liquid organic phase, that can be used as a fuel after proper upgrading steps [19].

Wet route instead deals with biomass with high moisture content; thanks to the possibility to avoid an expensive drying step the hydrothermal technologies are gaining attention [20].

The hydrothermal technologies can be divided with the operative temperature:

- Hydrothermal carbonization working at 160-250 °C aims to produce a solid fuel [21];
- Hydrothermal liquefaction working at 300-350 °C produces a biocrude similar to the oil derived from pyrolysis [22];
- Hydrothermal gasification working at 350-400 °C or 600-700 °C (near-critical or super-critical conditions) converts the biomass into a gas mixture with different gas composition with hydrogen being the main component at higher temperatures, while methane at lower temperatures [23].

These processes along with their desired products generate an aqueous fraction which contain for 20 up to 50% of the initial carbon [24]. However, the entire biomass should be valorized to reach economic and environmental sustainability of the process. Moreover, it was estimated that the waste disposal is pivotal point for the industrialization of thermochemical process; in terms of cost is the second most important voice in the variable costs [25]. Most of literature focus on the optimization of the reactions conditions to obtain the biocrude with the highest quality, but there is a lack of study regarding the characterization and valorization of the aqueous fractions.

Some options have been tested but they all presented advantages and disadvantages. In the following Figure 4 the main technologies are summarized.

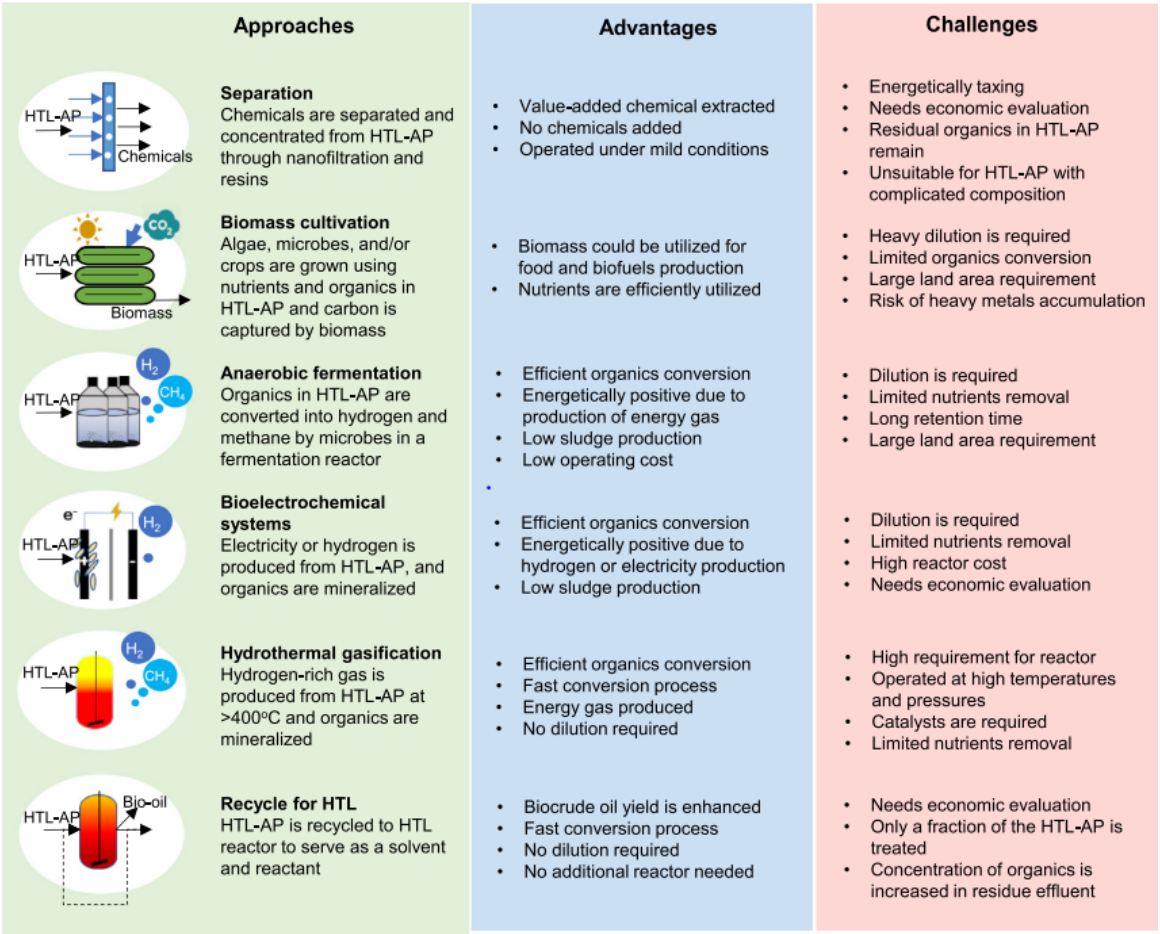


Figure 4: Advantages and challenges of state of technology for HTL-AP (Aqueous phase from Hydrothermal liquefaction) valorization [26].

Anaerobic digestion converts the organics into hydrogen and methane, but it requires dilution, long reaction time and some of the dissolved organics may be toxic for the microorganisms [27]. Algae cultivation has the objective to use the compounds to growth aquatic biomass, which is able to exploit its loading of organic and inorganic nutrients [28]. However high dilution and large area are necessary and there are risks of accumulation of metals. Hydrothermal gasification is another option to produce a hydrogen rich gas, the conversion is fast and efficient, but a catalyst and high temperature and pressure are required [29].

Another issue related to hydrothermal liquefaction is the production of a crude with high oxygen content which requires hydrogen to be upgraded.

Hydrogen is mainly produced from non-renewable and unsustainable sources, such as steam reforming of natural gas and partial oxidation of heavy oil fractions. There are some renewable options under investigation such as the steam reforming of the aqueous fraction of bio-oil [30], [31]; supercritical water reforming [32], [33]; Bio-processes like photo-fermentation or dark fermentation [34], [35].

The solution studied in this thesis is the aqueous phase reforming. A reforming reaction of oxygenated hydrocarbon in liquid phase which can convert the organic content of the water in a gas phase rich in hydrogen. This solution can help the biorefineries to increase their carbon recovery and reduce the amount of wastewater using the waste to produce renewable hydrogen.

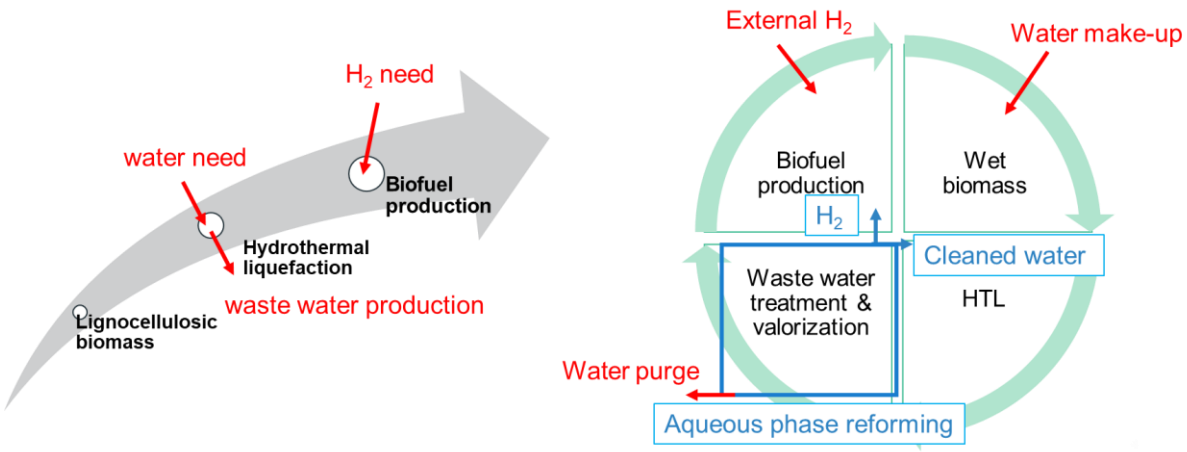


Figure 5: aqueous phase reforming applied to HTL water.

1.2. Aqueous phase reforming

Aqueous phase reforming reaction was proposed in 2002 by Dumesic et al. [36] in a work in which oxygenated hydrocarbons, glucose sorbitol and glycerol in aqueous phase were catalytically converted into a gas phase rich in hydrogen at mild temperature and pressure.

Starting from this paper APR has been proposed as a route to valorize wastewater stream to produce renewable hydrogen. In this chapter the theory of APR is reported together with its application to actual water fractions.

1.1.1. Theory

Aqueous phase reforming is a reforming reaction carried out in liquid phase at mild temperature (200-270°C) and pressure (15-60 bar) in the presence of a catalyst [37].

As reported in Figure 6 the reforming of oxygenated hydrocarbons (blue lines), such as methanol, ethylene glycol and so on, is more favorable at lower temperature compared to the reforming of alkanes (red lines). In the same range of temperature water as shift reactions (green line) is also favorable. Thus, the APR presents two main advantages: first there is a reduction of energy requirement compared to traditionally steam reforming, which works at high temperature (800°C) and the reaction is carried out in liquid phase avoiding the need of vaporization. Second it is possible to produce a gas phase rich in hydrogen with low concentration of carbon monoxide thanks to the possibility of having in the same reactor both reforming and WGS [38]. Concluding, APR allows to produce a hydrogen-rich gas in a single reactor at moderate temperature.

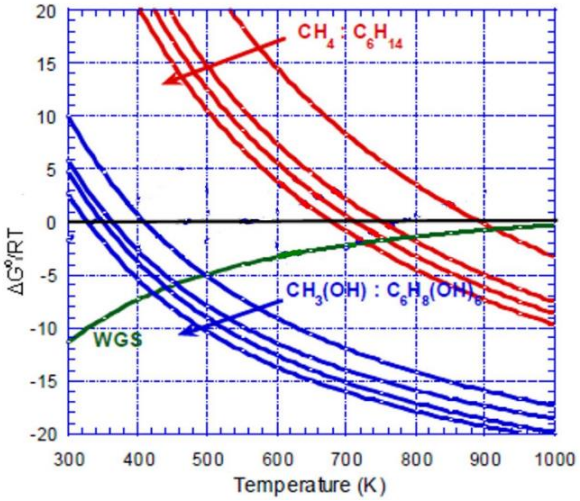


Figure 6. Thermodynamic equilibrium for hydrogen production, modified from [39].

Equation 1 is the reaction of steam reforming from alkanes to produce CO and H_2; Equations 2 and 3 are the reactions involved in the APR of oxygenated hydrocarbons. The first one represents the decomposition of the molecule into carbon monoxide and hydrogen, while the second is the water gas shift (WGS) reaction, which convert the carbon monoxide into hydrogen and carbon dioxide.

$$C_nH_{2n+2} + nH_2O \leftrightarrow nCO + (2n+1)H_2 \quad \text{(Eq. 1)}$$

$$C_nH_{2y}O_n \leftrightarrow nCO + yH_2 \quad \text{(Eq. 2)}$$

$$CO + H_2O \leftrightarrow CO_2 + H_2 \quad \text{(Eq. 3)}$$

$$C_nH_{2y}O_n + nH_20 \leftrightarrow nCO_2 + (y+n)H_2 \quad \text{(Eq. 4)}$$

The combination of WGS and the reaction involving the oxygenated hydrocarbons lead to Equation 4 that is the reforming of carbohydrates.

Apart from the thermodynamic point of view, selectivity issues must be highlighted due to the presence of side reactions. Coronado et al. [37] reported some side reactions that can be present during aqueous phase reforming, in both liquid and gas phases. These undesired reactions can be methanation and Fisher-Tropsch in the gas phase, where they both consume hydrogen to produce short chain alkanes. Hydrogen can be consumed in liquid phase in hydrogenation reaction producing liquid by-products. The choice of the right catalyst is pivotal in the production of hydrogen from the aqueous phase reforming of oxygenated hydrocarbons. An efficient catalyst must promote the C-C bond cleavage and the WGS reaction minimizing at the same time the undesired side reactions to produce alkanes.

In Figure 7 is reported the reaction pathways proposed by Dumesic for the reforming of ethylene glycol. The first step I is the dehydrogenation, this stage creates an intermediate adsorbed on the surface catalyst; the type of adsorption metal-carbon bond (path A) and/or metal and oxygen (Path B) depends on the nature of active site. In the case of platinum based catalyst the formation of Pt-C bonds is favored than Pt-O ones [40]; nevertheless, it might be formed. The first pathway involved the C-C cleavage leading to the formation of hydrogen and carbon monoxide; at this point the latter can react with water through the water gas shift reaction (step III) to produce H_2 and CO_2. Consecutive reaction of CO_2 and or CO (IVa; IVb) consumes hydrogen to produce water and methane. This step is pivotal for the reaction mechanism, it is necessary a catalyst able to activate the WGS and to reduce side reactions which consume hydrogen.

The path B) refers to the possibility of formation of metal-oxygen bond; the following reaction involves hydrogen as reactant and C-O cleavage step (pathway II) to form an alcohol. The alcohol can undergo further reaction on the metal surface, to produce hydrogen but also alkanes. Another parallel pathway involves the rearrangement of the adsorbed species to form an acid that can start to react again to form, as the alcohol, methane, carbon monoxide, carbon dioxide, ethane, hydrogen and water. Finally, it is worthy to cite the possibility (not reported in the figure) of a first step of dehydration of the molecule, mainly influenced by the acidity/basicity properties of the support [39].

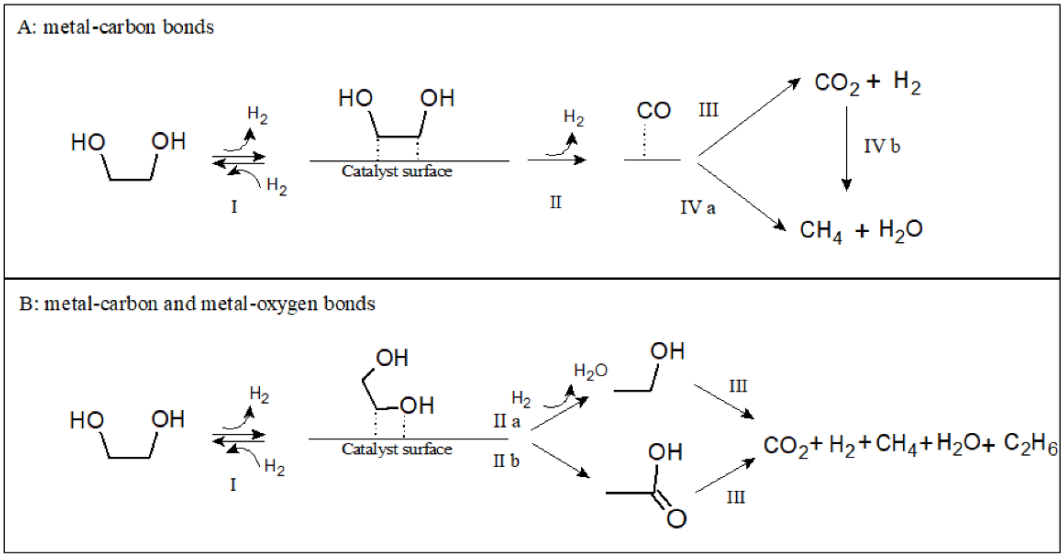


Figure 7: reactions pathway of ethylene glycol, proposed in[39].

In the next paragraphs the parameters that influence the hydrogen productivity will be reported and in the final paragraph the main applications of APR are summarized.

1.1.2. Parameter influence on APR reaction

The choice of the catalyst (metal and support) is not the only parameter that has an influence in the selectivity and gas product distributions. The nature of the feed, its concentration, the pH of the solution, and the reactions condition (temperature and pressure) can strongly affect the activity and the product yield of the APR.

It has been reported that the chain length affects the hydrogen yield, shorter molecules have an higher hydrogen production, from methanol to glucose hydrogen selectivity decreases from 99% to 33% as showed in Figure 8. Davda et al. [36] reported that the selectivity for hydrogen production improves with the following order:

$$\text{glucose} < \text{sorbitol} < \text{glycerol} < \text{ethylene glycol} < \text{methanol}$$

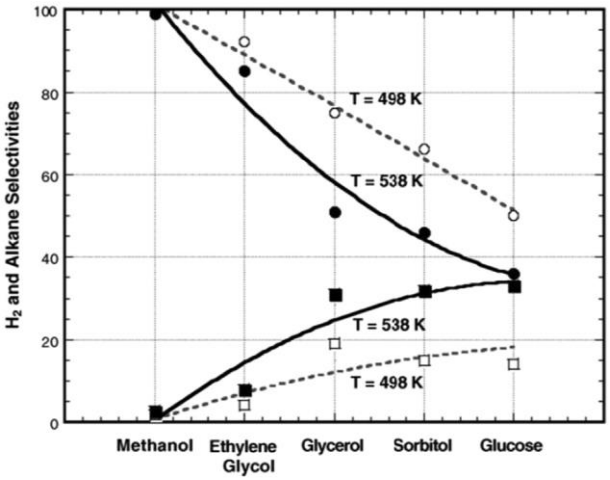


Figure 8. Influence of chain length on APR performance [41].

Regarding the concentration it was proved that some molecules, as polyols, are insensitive to the feedstock concentration [39], however other compounds are affected by the increase in concentration: more diluted feedstock showed higher carbon to gas and hydrogen yield conversion, as summarized in Figure 9. For sugars it must be considered that the rate of homogeneous decomposition of glucose, for example, increases with an increase of glucose concentration, leading to lower hydrogen production. Indeed reforming reactions are fractional order for hydrogen production (0.8 for methanol, 0.3-0.5 for ethylene glycol [42]); instead homogeneous reactions are first order reactions [43]. To overcome this issue with sugars the operating condition such as temperature, change of pH of solution and increase of active sites has been proposed another possibility consists in prehydrogenate the sugars to the corresponding sugar-alcohols to avoid the homogenous decomposition reactions [44], [45]

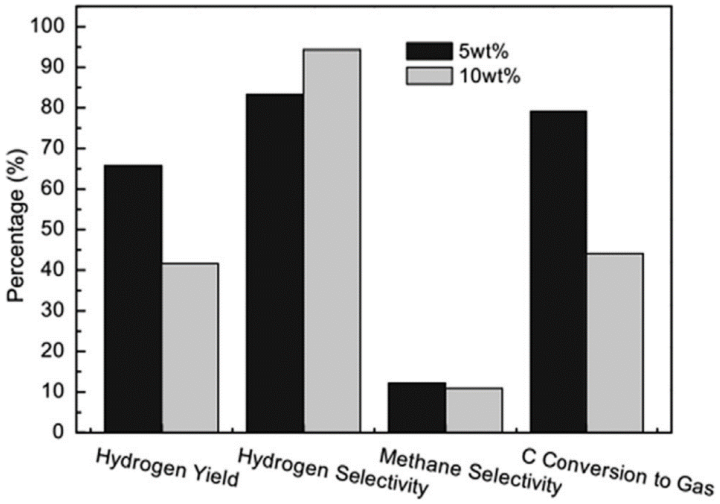


Figure 9: effect on feedstock concentration[37].

The acidity of solution can also influence the performance of APR, the nature of the by-product, the intermediate compounds formed during the reaction and the CO_2 dissolved in water, can influence

the pH of the aqueous solution. More acid solution led to higher alkanes formation compared to basic or neutral solutions which promote hydrogen production.

Reaction temperature are between 200 and 270°C, in this condition the reforming and WGS are favoured but also methanation and Fischer-Tropsch which are undesired reaction. Increase in reaction temperature led to an increase in the conversion of the feed to gas product[46], thanks to the increase on bond breaking reactions. However hydrogen selectivity decrease in favour of carbon dioxide, carbon monoxide and methane [47]. The pressure of the system should be enough to keep the water in the liquid phase. Increase of pressure has important effects: higher pressure can reduce the hydrogen production due to the reduction of product desorption from the catalyst [48].

Finally, the catalyst choice has a fundamental role to convert successfully the feedstock into hydrogen without being deactivate quickly. As reported in Figure 10 the catalyst decision involves the metal, the promoters, the support, and the preparation technique.



Figure 10. Design of heterogeneous catalyst from [49].

Looking to the reaction network reported in Figure 7 it is suggested that the optimal catalyst should maximize the C-C bond breaking and water gas shift activity, while the C-O bond breaking, methanation and Fischer-Tropsch activity should be hindered; moreover, the support should not allow dehydration reactions.

From the reaction network presented in Figure 7 , the optimal catalyst should have high activity for C-C- bond cleavage and water gas shift, on the other hand it should hinder the C-O breaking, the methanation and Fischer-Tropsch reaction. The support should avoid the dehydration reactions.

Davda et al. reported a comparative study of the activity and selectivity of different metal of the VIII group. These metal show high activity for C-C cleavage; the metal activity decreases in the following order[39]:

$$\mathrm{Pt{\sim}Ni} > \mathrm{Ru} > \mathrm{Rh} - \mathrm{Pd} > \mathrm{Ir}$$

Among these catalysts only platinum and palladium exhibited also a moderately high selectivity for the hydrogen production; this is due because not only the activity to break the C-C bond is necessary, but it should also be able to activate WGS (as reported in Figure 11). Moreover, they

showed a low activity for the side reactions (C-O cleavage, methanation and Fischer-Tropsch). Indeed, platinum-based catalysts are the most used in literature.

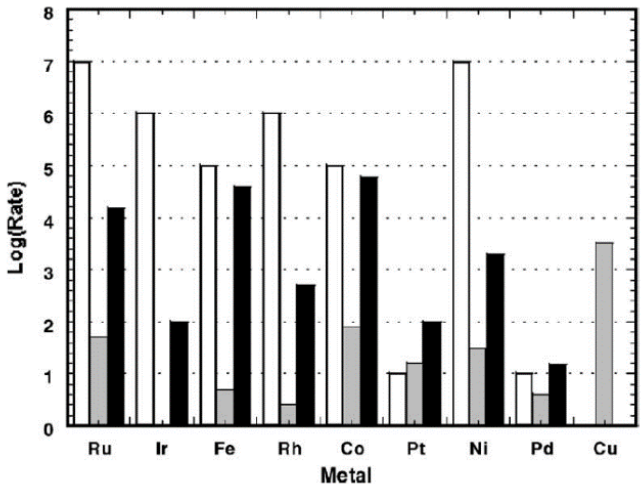


Figure 11. Relative rates of reactions under APR reaction conditions, C-C cleaving (white bar), water gas shift (grey bar), methanation (black bar). as reported in [50].

The support plays an important role in the performance of the catalyst, being Pt the most active it is often chosen for the study of the effect of the support [51]. The support of the catalyst plays an important role too in regards of the hydrogen selectivity. Hydrogen formation was favored by basic support, that showed higher H2 yield; in contrast neutral and acid supports lead to higher production in alkanes. The effect of Pt catalyst support with different acidity was studied by Wen et al [52]. The authors showed that the scale of hydrogen yield was SAPO-11 < AC < HUSY< SiO_2 < MgO < Al_2O_3, which is coherent with the range of acidity. Most of works focus on platinum supported on γ-Al_2O_3; however, γ-alumina, during the aqueous phase reforming reaction, goes under catalyst deactivation. Alumina transform into boehmite (AlO(OH)), sintering of the supported metal particles, and deposit on the surface of carbonaceous material. Boehmite is the stable form under APR condition, it increases the acidity of support, however according to some research once formed the boehmite performed phase stability and also stable activity with high hydrogen yield. This may be due to the presence of OH group, which are fundamentals for water activation[53]. Carbon supports are considered stable under APR conditions, but they showed lower hydrogen yield.

Finally, the last parameter which can influence the APR reaction is the reactor system. APR requires a three-phase system with solid catalyst, liquid feedstock, and gas products. Most of work in literature refers to fixed bed reactors, however due to its complex configuration it is possible that transport of products from the catalyst play an important role. In general, aqueous phase reforming is still in laboratory scale, where the experiments are carried out in laboratory scale tubular packed-bed and batch reactor. For research purpose a stirred reactor is a suitable option to overcome mass transfer limitation, but it is not easy to study deactivation and stability of catalyst. For this reason, the reactor design is important as well as the catalyst selection, however few works evaluated the effect of reactor configuration or gas addition to overcome transport of products issue.

Neira D'Angelo et al. evaluated the use of a microchannel reactor for the APR of sorbitol and compare its performance with a fixed bed reactor [54]. The conversion was not affected by the reactor, but the hydrogen selectivity was higher in the microchannel type; this may be due to the more effective mass transport compared to fixed bed. The formed hydrogen is transferred quickly to gas phase avoid to further react inside reactions. Moreover, in the same work the effect hydrogen/nitrogen mixture co-feeding in different ratio was studied. In Figure 12 is reported a decrease of sorbitol conversion (open circle) and hydrogen selectivity (black circle) when the hydrogen partial pressure increases probably due to an adsorption of hydrogen in the active sites. Finally, the addition of nitrogen flow increased the hydrogen production, since adding an inert reduced the hydrogen concentration in the gas phase and its partial pressure.

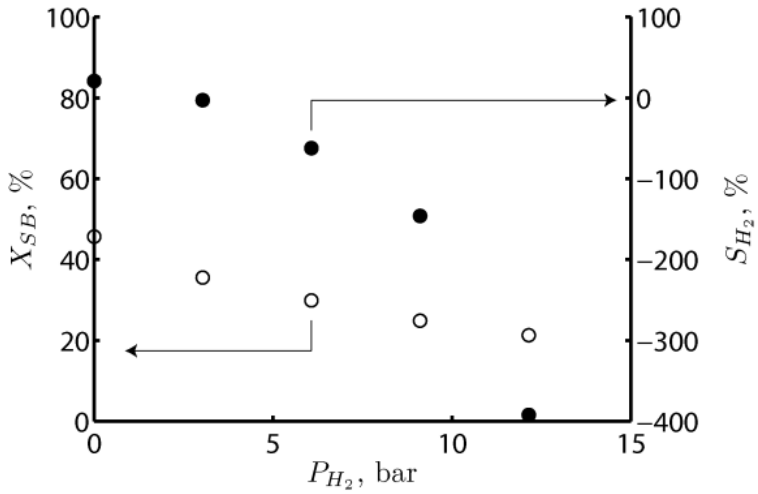


Figure 12: effect of hydrogen pressure on sorbitol conversion (open circle) and hydrogen selectivity (black circle) from [54]

Entezary et al. studied structured catalyst in microreactors for APR of ethylene glycol and glycerol over Pt/Al_2O_3 and Pt/CeO_2-Al_2O_3 catalysts [55]. The structured catalyst reduces the risk of by-pass and a stricter control on residence time. Moreover, the microreactors led to higher hydrogen yield compared to fixed bed reactor. These works confirm the importance of coupling the right catalyst to an effective reactor configuration to increase the hydrogen yield.

Despite the potential of the reaction APR has been mostly studied with simple model compounds; especially: glycerol, ethylene glycol, methanol, sorbitol ([42], [56], [57]) Few works tested also ethanol, acetic acid, acetaldehyde, acetol, butanol, fructose, sucrose, furfural, galacticol, cyclic compounds and xylitol. In Figure 13 some model compounds are reported. However more complex solutions, such as multi-component synthetic mixtures or even actual wastewaters, have been less deepened.

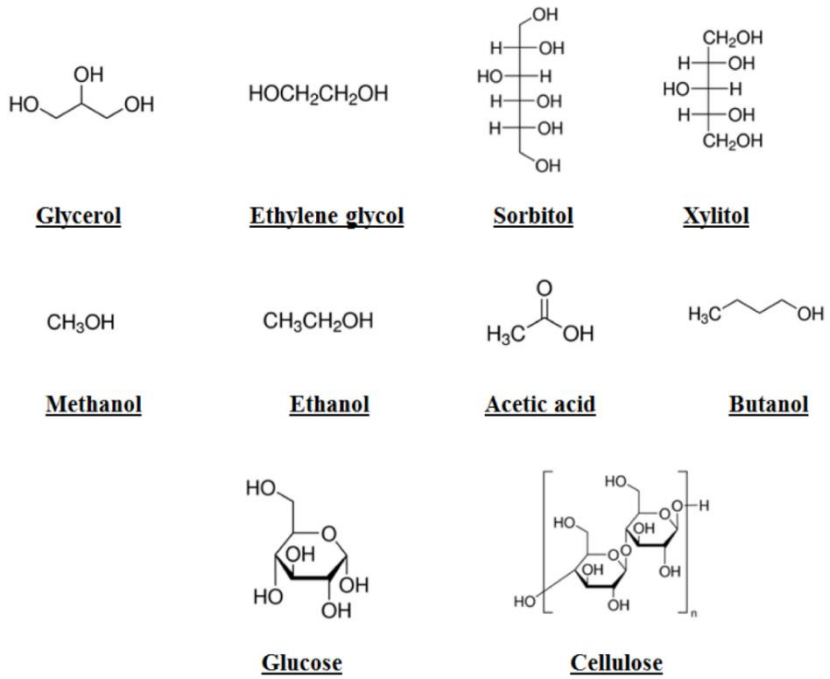


Figure 13: some model compounds use for APR studies[58].

The following Table 1 reports the APR stoichiometry and the theoretical hydrogen yield for the single compounds. Organic acids and sugars were added to the most studied molecules to include other molecules commonly present in wastewater.

Table 1. APR reaction stoichiometry and theoretical hydrogen yield for common oxygenated present in wastewater fraction. 1 g of carbon was assumed as basis for the calculation. [59]

Compound	APR Reaction	H_2 yield (mg H_2/g C)
Glycerol	$C_3H_8O_3 + 3H_2O \rightarrow 3CO_2 + 7H_2$	390
Methanol	$CH_4O + H_2O \rightarrow CO_2 + 3H_2$	500
Glycolic acid	$C_2H_4O_3 + H_2O \rightarrow 2CO_2 + 3H_2$	250
Acetic acid	$C_2H_4O_2 + 2H_2O \rightarrow 2CO_2 + 4H_2$	330
Ethanol	$C_2H_6O + 3H_2O \rightarrow 2CO_2 + 6H_2$	500
Lactose	$C_{12}H_{22}O_{11} + 13H_2O \rightarrow 12CO_2 + 24H_2$	330
Glucose	$C_6H_{12}O_6 + 6H_2O \rightarrow 6CO_2 + 12H_2$	330

For this reason, the next paragraphs summarize the available literature which, over the past 15 years, focused on the valorization of diluted wastewater streams through APR to produce a gas phase rich in hydrogen. Only works with synthetic mixtures or actual streams, also containing the molecules above presented, will be considered. The theoretical hydrogen yield is not often reached for several reasons, which will be presented and discussed.

1.1.3. Industrial application

This paragraph presents the overview of the application of APR; the data were collected by literature survey and were summarized in a published work [59]. These paragraphs will be firstly dedicated to lignocellulosic biomass after that is presented the wastewater valorization from food processing and then biodiesel plant is reviewed. In conclusion different industrial scenario and the perspective of the APR with future challenge for its applications are reported.

Lignocellulosic biomass: biorefineries approach

Lignocellulosic biomass is constituted by cellulose, hemicellulose and lignin. Each of these fractions is potentially able to produce hydrogen via APR. In the following, experimental results on several real (kenaf, pine sawdust, wheat straw, sorghum, switchgrass, miscanthus, corn kernel) and synthetic lignocellulosic-derived compounds will be reported. Moreover, some studies focused to the valorization of the whole biomass (i.e. in a solid form) will be reported as well. In fact, if the proposed technologies can convert each portion of the biomass, lignocellulosic feedstock may have a chance to substitute fossil fuel.

Hydrolysis

Lignocellulosic biomass can be subjected to hydrolysis to remove the lignin fraction, increase the porosity of the material and reduce cellulose crystallinity [60]. In this way, sugar monomers are released from the structure of the biomass and can be valorized following different pathways [61].

Kenaf is reported as an interesting substrate because of its fast growth rate and large production. Irmak and Ozturk performed the APR of the liquid phase obtained from kenaf hydrolysis (150 and 250 °C – 27.58 MPa carbon dioxide) and of the solid biomass itself on a 5% Pt/C catalyst [62]. They showed that the hydrolysate constituted by low-molecular weight compounds (i.e. the one obtained at 250 °C) produced more gas than the one with higher molecular weight (104.2 vs 16 mL), also due to the higher carbon concentration in the feed (4431 mg C/L vs 1504 mg C/L). The conversion of the single components of the mixture was not reported, likely because of its complexity: in fact, only xylose was recognized as simple monosaccharide in the starting solution. A comparison with glucose at the same concentration was performed as well. In this case, the TOC removal (i.e. the fraction of carbon that was converted into a gas/solid species after the reaction) increased by 60%, while the hydrogen yield was almost three times higher. In order to better understand the efficiency of the process, we compared this value with the theoretical one reported in Table 1 which is equal to 330 mg H_2/g C). The authors reported that the TOC removal was 80%, so the yield should have been approximately 260 mg H_2/g C; the presence of other gaseous species, such as methane and ethane, and the lower H_2/CO_2 ratio compared to the stoichiometric one, infers reaction pathways other than the simple reforming.

APR of solid kenaf biomass increased the gas production, but the hydrogen content globally decreased. Kenaf was also used for the production of activated carbon as support for Pt-based catalysts for APR [63].

The APR of wheat straw hydrolysate was investigated in [64]. 5% Pt/carbon, 5% Pt/alumina and Raney Ni 2400 were used as catalysts, with the latter producing far more gaseous species than the formers (Figure 14). It is worthy to highlight that the use of an inexpensive Ni-based catalyst can be advantageous under the economical point of view. The gas phase also presented a higher hydrogen concentration than the Pt-based cases (68.9 mol.%) and no carbon monoxide. It is interesting to observe that the gas production was also higher than the case of kenaf hydrolysate previously reported, also considering the similar organic carbon (4965 mg C/L vs 4431 mg C/L) [62]. This difference may be ascribed to the different hydrolysate composition.

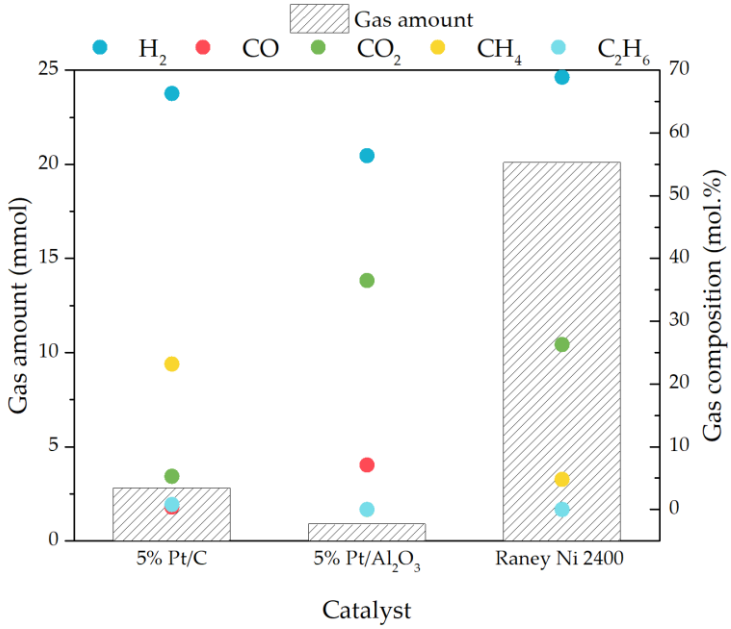


Figure 14. APR of wheat straw hydrolysate with different catalysts. Reaction conditions: 250 °C, 2 h, 50 mL hydrolysate (data from [64]).

The authors did not mention the formation of a solid residue. Pipitone et al. tested wheat straw hydrolysate with different concentration (0.3-1.8 C wt.%) using a 5% Pt/C [44]. The authors reported the presence of a solid residue due to humins formation from glucose and xylose. Humins are water insoluble compounds that derive from the polymerization and condensation of furfurals in the hydrothermal environment [65]. In fact, glucose and xylose may be dehydrated via an acid-catalyzed mechanism into hydroxymethylfurfural (HMF) and furfural, respectively; afterwards, it can be rehydrated to 2,5-dioxo-6-hydroxyhexanal, which polymerize via aldol condensation to form humins. Two important consequences are correlated to humins formation. On one side, hydrogen yield was reduced because of alternative pathways taken by the intermediate products; on the other side, the catalyst surface was covered by this material, blocking the active sites. The authors observed that humin formation increased with the increase of feedstock concentration and with the decrease of reaction temperature. The first outcome was because this is a homogeneous first order reaction, so it is more favored by the concentration increase than the reforming reaction, which is fractional order. The second result was related to the more favorable C-C breaking reaction by increasing the temperature, so decreasing the humin formation.

Since HMF and furfural are intermediates from sugars, a pre-hydrogenation step to sugar alcohols was evaluated to avoid homogeneous reactions. In Figure 15-A the hydrogenation of a glucose-xylose solution at different carbon concentration is reported (5% Ru/C catalyst was used in this case). The solution was almost completely hydrogenated, and in a selective way (without side-products). The APR of this solution was further subjected to APR and the results are reported in Figure 15-B. The net hydrogen production, i.e. mole $H_{2\ produced}$ – mole $H_{2\ consumed}$, in the two-steps case was much higher than the one-pot case (without pre-hydrogenation). This difference is due to the more selective reforming of sugar alcohols compared to sugars.

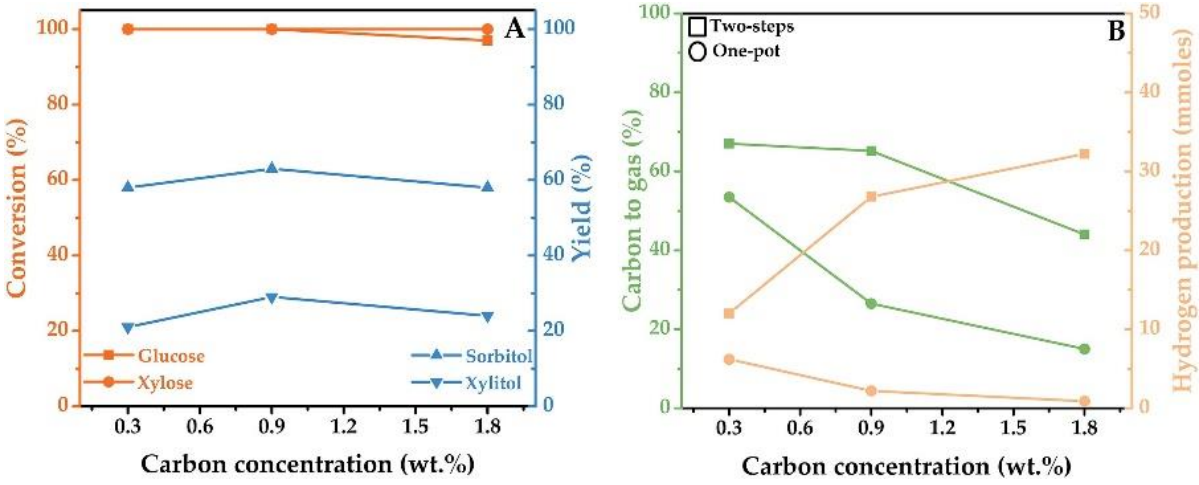


Figure 15. Influence of carbon concentration on the hydrogenation of a glucose-xylose mixture (A) and on the APR of the hydrogenated feed (B). Hydrogenation reaction conditions: 0.188 g Ru/C catalyst, 1 h reaction time, 180 °C, 15 bar H2 pressure. APR reaction conditions: 0.375 g Pt/C catalyst, 2 h reaction time, 270 °C (from [44]).

A similar approach was reported for kenaf hydrolysate [66], sucrose [67] and maltose [68], which were pre-reduced to increase the hydrogen selectivity. The attempt for an in situ hydrogenation of xylose to xylitol thanks to the conversion of formic acid into hydrogen in the reactant mixture did not succeed, overall decreasing the hydrogen selectivity for xylose APR [69].

Different carbon supports for Pt catalysts have been studied thanks to their tunable properties for the APR of wheat straw hydrolysate [70]. The results reported that activated carbon was the support with the highest hydrogen production (2.17 mmoles), followed by single wall carbon nanotube (1.72 mmoles), graphene oxide (1.10 mmoles), super-darco carbon (0.66 mmoles) and multi wall carbon nanotube (0.59 mmoles). Graphene oxide produced the gas phase with the highest hydrogen concentration (56 mol%). Due to the large dimension of the molecules present in the hydrolysate, the support should have proper textural characteristics to permit the accessibility of the active site. Interestingly, in this work the liquid phase after APR was characterized as well. Activated carbon also allowed a higher formation of sugar alcohols in the liquid phase (e.g. glycerol, xylitol, sorbitol etc.) and breaking down of soluble organic compounds derived from lignin fraction (4-methoxyphenol, vanillin, syringaldehyde etc.).

Sorghum hydrolysate may be an alternative feedstock due to its drought tolerance, fast growth rate, high starch content together with low ash, fat and protein [71]. Response surface methodology was used to investigate the effects of temperature (200-270 °C), feed flow rate (0.3-1 mL/min) and biomass feed concentration (1000-4000 mg C/L) on the APR process using a Raney nickel catalyst. The former variable was the main factor on the H_2 yield, which was higher at higher temperature. In fact, working at this condition suppressed methanation, and hydrogen production increased by three times moving from 200 to 270 °C.

The use of microwaves for the pretreatment of switchgrass and miscanthus has been investigated for the deconstruction of the recalcitrant crystalline cellulose fraction [72]. Similarly with previous works, the composition of the hydrolysate was not reported. Once treated with microwaves, they were hydrolyzed in subcritical water and subjected to APR with a Pt/C catalyst to evaluate its hydrogen productivity. Miscanthus produced 20% more hydrogen than switchgrass, likely due to the higher organic content (for the untreated, it was 1350 mg C/L vs 1132 mg C/L). The lower TOC in the case of the microwave-treated feedstock decreased the hydrogen production; moreover, it increased the formation of solid carbon residue after APR. As reported earlier, this is a problem for the implementation because it severely affects the catalyst lifetime.

Corn kernel may be a suitable feed for APR application, since it is present in excess in the US for its valorization into bioethanol [73]. Irmak and Tiryaki, with a preliminary economic analysis based only on the price of the feeds, showed that the cost of the corn kernel is about 1.7 times higher than methane to produce the same amount of hydrogen. The hydrolysis of corn kernel at 200 °C produced an aqueous solution with approximately 2500 mg/L TOC concentration and yielded 2.3 times more hydrogen then corn stover biomass (5.8 mmol H_2/g C vs 2.6 mmol H_2/g C, respectively) [74]. Various corn kernels were evaluated for gas production (field corn, non-genetically modified field corn, yellow field corn, white field corn and popcorn) [75]. The hydrolysate TOC ranged between 5230 and 5850 mg C/L, with the field corn showing the highest concentration of glucose. No significant differences were found among the varieties in terms of gas production and hydrogen yield, with the latter being 130 mL/g corn on average.

Finally, using a systematic approach, Irmak et al. investigated the APR of the cellulose, hemicellulose and lignin fraction of kenaf and wheat straw [45]. The hydrolysis of each biomass fraction was conducted a 250 °C in a CO_2 atmosphere of 17.24 MPa. The results showed that the hydrolysis of the cellulose fraction led to the highest TOC content, whereas lignin to the lowest one. The obtained hydrolysates (only the polysaccharide weight distribution was reported) were subjected to APR at 250 °C for 2 h using a Pt/C catalyst. The highest hydrogen yield was obtained in both cases from the cellulose fraction, while hemicellulose was the most selective. Furthermore, lignin did not report any hydrogen production, despite it presented the highest TOC removal. Apart from the higher gas production, kenaf left less solid residue. Further investigation on APR of lignin can be found in [76].

In Table 2 a summary of the main results obtained with different biomass discussed in the paragraph is reported. The hydrolysis and APR conditions were reported, specifying also the used

catalyst. It can be observed that Pt is the most used metal among the reviewed investigation. This choice leads primarily to an economic drawback, but the challenges of actual streams require high activity, selectivity and stability to justify its use. So, its use can be meaningful since it is commonly the one with the best performances (among the monometallic catalysts).

Apart from the cited exceptions, the characterization of the starting and product solutions is not evaluated, likely because of the complexity of the liquid phase. The ash content is commonly reported, but the possible influence is not investigated. Most commonly, the molecular weight distribution of the polysaccharides and the TOC were showed. From the latter, it can be observed that these solutions have most of the TOC close or below 5000 mg C/L, hindering their catalytic treatment and increasing the costs since larger equipment are necessary. The TOC removal is often showed, without info on conversion or selectivity. The gas composition was reported in terms of volume percentage of hydrogen, alkane (sum of methane, ethane and propane) and carbon dioxide. Carbon monoxide concentration was not reported since it is commonly negligible. Among the results, it is interesting to observe that Raney Ni 2400 reached the highest hydrogen yield; furthermore, low selectivity towards methanation was observed, in contrast with common results reported in literature [77]. On the other hand, high concentration of the hydrolysate and the lignin-fraction of the biomass led to negligible hydrogen yields.

This comparison may be further studied in deep with the aim to find suitable substrates for hydrogen production via APR. However, the differences in the hydrolysis and APR conditions can affect a rigorous analysis at this stage.

Table 2. APR of different lignocellulosic biomass. n.a.: not available

Biomass	Hydrolysis conditions	APR conditions	Catalyst	Feed TOC (mg C/L)	TOC removal (%)	Gas composition			H_2 yield (mg H_2/g C)	Ref
						% H_2	% Alkane	% CO_2		
Kenaf	7.5 g solid in 350 mL water, pretreated 20 kHz, 27.58 MPa CO_2, 150 °C	50 mL, 250 °C, 2 h, batch reactor	0.12 g 5% Pt/C	1504	n.a.	49.6	4.3	38.8	9.4	[62]
	7.5 g solid in 350 mL water, pretreated 20 kHz, 27.58 MPa CO_2, 250 °C			4431	50	60.0	7.6	32.4	25.2	
Glucose	-	50 mL, 250 °C, 2 h, batch reactor	0.12 g 5% Pt/C	4400	80	57.4	8.6	34.0	72.7	[62]
Wheat straw	10 g solid in 350 mL water, pretreated 20 kHz, 27.58 MPa CO_2, 250 °C	50 mL, 250 °C, 2 h, batch reactor	0.12 g 5% Pt/C	4964	27	66.3	24	7.3	15.0	[64]
			0.12 g 5% Pt/Al_2O_3	4964	37	56.4	n.d.	36.5	4.2	
			0.6 g Raney Ni 2400	4964	52	68.9	4.8	26.3	111.8	
Wheat straw	Enzymatic hydrolysis (from a commercial plant – PROESA™ technology)	75 mL, 270 °C, 2 h, batch reactor	0.375 g 5% Pt/C	3000	47	40.5	13.6	45.9	25.6	[44]
				9000	20	24.0	11.4	64.5	5.3	
				18000	10	6.0	4.5	86.2	0.5	
Wheat straw	10 g solid in 350 mL water, pretreated 20 kHz, 27.58 MPa CO_2, 250 °C	50 mL, 250 °C, 2 h, batch reactor	0.12 g 5% Pt/C	n.a.	n.a.	49.0	11.0	39.0	n.a.	[70]

Switchgrass	5 g solid in 350 mL water, 25.52 MPa CO_2, 220 °C, no pretreat microwave	50 mL, 250 °C, 2 h, batch reactor	0.12 g 5% Pt/C	1132	20	72.1	6.2	21.1	85.9	[72]
	5 g solid in 350 mL water, 25.52 MPa CO_2, 220 °C, 120 °C microwave			1541	15	65.4	6.1	27.2	51.2	
	5 g solid in 350 mL water, 25.52 MPa CO_2, 220 °C, 150 °C microwave			1679	11	67.5	5.9	25.4	39.8	
Miscanthus	5 g solid in 350 mL water, 25.52 MPa CO_2, 220 °C, no pretreat microwave	50 mL, 250 °C, 2 h, batch reactor	0.12 g 5% Pt/C	1350	22	71.4	5.6	24.7	88.8	[72]
	5 g solid in 350 mL water, 25.52 MPa CO_2, 220 °C, 60 °C microwave			1550	13	67.9	5.8	24.9	47.7	
	5 g solid in 350 mL water, 25.52 MPa CO_2, 220 °C, 80 °C microwave			1742	13	71.0	6.2	22.2	56.0	
Corn kernel	6 g solid in 350 mL water, 13.79 MPa CO_2, 200 °C	350 mL, 250 °C, 1.5 h, batch reactor	0.2 g 5% Pt/C	5670	n.a.	71.7	n.a.	24.4	17.6	[74]
Wheat straw - cellulose	4 g solid in 200 mL water, 17. 24 MPa CO_2, 250 °C	50 mL, 250 °C, 2 h, batch reactor	0.12 g 5% Pt/C	5256	19	20.7	9.9	67.6	8.5	[45]
Wheat straw - hemicellulose				4180	11	27.0	13.5	58.8	7.3	
Wheat straw - lignin				595	32	0.0	7.2	92.8	0.0	
Kenaf - cellulose	4 g solid in 200 mL water, 17.24 MPa CO_2, 250 °C	50 mL, 250 °C, 2 h, batch reactor	0.12 g 5% Pt/C	5216	22	21.1	10.3	66.9	10.1	[45]
Kenaf - hemicellulose				4985	17	24.0	8.0	68.0	9.5	
Kenaf - lignin				606	31	0.0	8.3	91.7	0.0	

Valenzuela et al. reported APR of solid actual biomass, pine sawdust, for the first time [78]. The presence of platinum catalyst doubled the hydrogen production compared to the one acid-catalyzed (5% H_2SO_4). Sulfur poisoning was considered the main cause for deactivation (S/Pt elemental ratio equals to 24.3).

Cellulose is a more readily available feedstock than glucose. Degreased cotton, filter paper and microcrystalline cellulose were investigated looking at the effect of different degree of polymerization [79]. Filter paper gave 20.3 mmol H_2/g of cellulose, much higher than Valenzuela et al. [78] (0.96 mmol/g). The authors observed that the hydrogen selectivity increased with the increase of the degree of crystallinity. In fact, it is related to the hydrolysis rate of cellulose. Since hydrogen selectivity is negatively affected by glucose concentration, slower hydrolysis caused lower local concentration, favoring hydrogen production. No measurable leaching and sintering were observed for Pt, while carbon deposition was mainly considered (just 80.3% carbon balance). Despite not comparable with gasification performance (43.2 mmol), it was more energy effective.

Thermochemical conversion technology

In the recent years, due to the growth of energy demand, thermochemical conversion technologies (TCC) have been revisited. As a matter of fact, they are not a recent route to convert biomass, but they were abandoned due to low petroleum price. The main TCC process are gasification, hydrothermal liquefaction (HTL), pyrolysis, direct combustion, and supercritical fluid extraction [80].

Figure 16 summarizes the thermochemical conversion routes of biomass [81]. Heat is the main output from combustion; a CO/H_2 mixture (syngas) is the main product of gasification, which can be used as building block for the petrochemical sector or trough Fischer-Tropsch (FT) synthesis can be converted into transport fuels; pyrolysis and hydrothermal liquefaction are processes able to convert biomass into a crude biofuel, which, upon upgrade to reduce its oxygen content, can be used in conventional engines. They also produce an aqueous phase (AP) with organic compounds dissolved in, which should be valorized to minimize carbon waste.

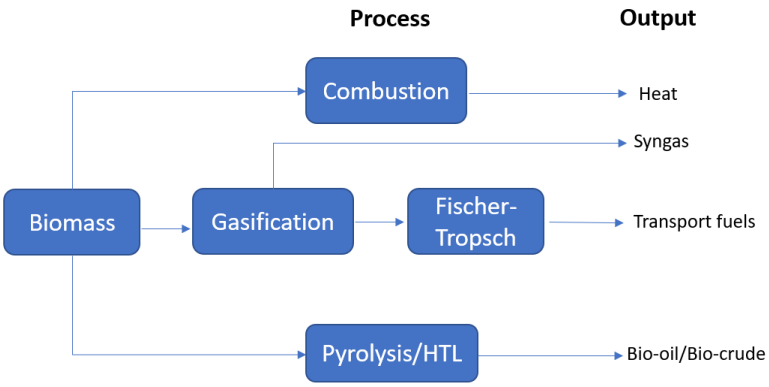


Figure 16. Thermochemical conversion routes and main outputs of biomass.

The aqueous phase produced by HTL process contains an organic content varying between 15-50% of initial carbon [82] and must be valorized to make the hydrothermal processes economically feasible. The complexity of the mixture and the high dilution of the organic compound makes difficult

their recovery. Davidson et al. studied other possible routes of valorization such as catalytic upgrading of carboxylic acids and the improvement of steam reforming thanks to a dual bed in combination with a cleanup process of the aqueous phase [82].

Leng at al. [8] reviewed the main options for HTL water phase treatment proposed by the state of the art so far. The water treatment after hydrothermal processing is a key point for its industrial development. However, these streams are very complex and they contain inhibitory substances. The reported technologies are anaerobic digestion, super critical water gasification (SCWG), microbial fuel cell, microbial electrolysis cell, microalgae cultivation and recirculation of the aqueous phase to HTL. All these routes present advantages and disavantages and are strongly related to the starting feedstock. SCWG is the one which can be applied to most phases but it is higly energy expensive and the catalyst deactives quickly. The anaerobic digestion, the bioelectrochemical treatment and the microalgae options suffer from the presence of inhibitory compounds; finally the AP recirculation can limit the application to the dry biomass and can cause the building up of undesired compounds.

A deep characterization of the water fraction is generally adviced to determine which is the best treatment applicable to these streams. Panisko et al. [83] found in the AP from corn stover HTL several classes of compounds, from alcohols to carboxylic acids, from hydroxyacids to ketones and aromatics. Starting from this knowledge and following simulations [84], the work carried out by Pipitone et al. [85] had the goal to understand the reactivity of the molecules dissolved in the aqueous phase, with particular attention to the tendency to hydrogen production; furthermore, synthetic binary and ternary mixtures were tested. The tests were devoted to the study of compounds not usually subjected to APR, such as hydroxyacids, carboxylic and bicarboxylic acids, ketones and aromatics. The increase of the temperature between 230 and 270 °C showed mainly a benefic effect on the activity, without affecting the selectivity.

In Table 3 the experimental hydrogen yield produced by some of the molecules is compared with the theoretical one, i.e. considering complete conversion of the substrate and selectivity. Furthermore, alkane yield was reported.

Interestingly, the glycolic acid, which was never tested before, showed great hydrogen production, thanks to its OH group. Its lower hydrogen production than the theoretical one was ascribed to the parasite formation of acetic acid in the liquid phase, which derived from glycolic acid hydrogenation. Acetic acid APR led to a gas phase constituted by roughly 50% carbon dioxide and 50% methane, so that only 4% of the theoretical hydrogen was produced. It derived a general consideration for carboxylic acids, which followed the path reported in Eq. 4.Ethanol produced a gas mixture rich in hydrogen (50%), but with the 25% of it being methane, which increased the gap between theoretical and experimental hydrogen produced. For ethanol, and in general for molecules with C:OH ratio different than one, a modified APR stoichiometry can be written, which takes into consideration also the real mechanism of reaction [86], [87]. In fact, when only one hydroxylic group is present in the molecule, only one CO group can be extracted and converted to H_2 and CO_2 (Eq. 5). Consequently, the corrected theoretical hydrogen is three times lower (167 mg H_2/g C) and closer to the experimental one.Ethylene glycol thanks to its C:OH ratio equal to 1 had a good accordance between theoretical and real hydrogen production, even if the alkane yield was three times higher than the one obtained by APR of glycolic acid.

Finally, glycerol reached a complete conversion. However, the discrepancy between the two values could be explained in this case not by the different C:OH ratio (which is equal to 1 and has a molecular structure similar to ethylene glycol). The higher molecular weight and complexity of the molecule caused the presence of alternative reaction pathways which lead to gaseous (methane) and liquid by-products (hydroxyacetone, propylene glycol, acetic acid) decreasing the hydrogen production.

$$CH_3COOH_n \leftrightarrow CH_4 + CO_2 \quad \text{(Eq. 5)}$$

$$CH_3CH_2OH + H_2O \leftrightarrow 2H_2 + CO_2 + CH_4 \quad \text{(Eq. 6)}$$

Table 3: APR of model compounds and differences with theoretical values. Reaction conditions: 5% Pt/Al2O3 catalyst, temperature 270 °C, reaction time 2 h, feed concentration 133 mM, 75 mL batch reactor (data from [88])

Molecule	Theoretical	Experimental		
	H_2 yield (mg H_2/g C)	H_2 yield (mg H_2/g C)	Alkane yield (mg alkane/g C)	Substrate conversion (%)
Glycolic acid	250	184.6	19.9	100
Acetic acid	330	12.0	327.9	56
Ethanol	500	121.4	515.8	99
Ethylene glycol	420	351.0	59.5	100
Glycerol	390	233.2	168.7	100

The study of binary and ternary mixtures allowed to understand that acetic acid (one of most present compound) in mixture suffered from competitive adsorption on the active site of the catalyst. Consequently, the theoretical gas production ideally obtained from the linear combination of the present compound was different from the real one.

The low-boiling fraction of the bio-oil derived from fast pyrolysis of rice husk was subjected to APR using a Pt/Al_2O_3 catalyst [88]. The increase of reaction temperature allowed the increase of the gas production, moving from 20.3 mmol at 503 K to 52.9 mmol at 563 K; at the same time, the hydrogen selectivity remained constant, and its concentration of the gas phase was about 65 vol.%. In the liquid phase, acetic acid was the main compound, with its area in the GC-MS chromatogram being 86% of the total area.

As reported in Figure 16, gasification of biomass is a process which converts the solid feedstock into hydrogen, carbon monoxide and carbon dioxide (syngas). It can be further coupled to a Fischer-Tropsch (FT) reactor to produce liquid fuels. In this process a contaminated water is also obtained, containing light oxygenates at low carbon concentration. A possible route for the valorization of this side stream was reported in [89]. Coronado et al. performed the kinetic modelling of FT water APR on a Ni-Cu catalyst supported on ceria-zirconia [90]. The results showed that C2-C4 alcohols adsorbed similarly to the catalyst surface and addition increased the

stability of the catalyst, at the expense of the hydrogen yield [91]. reacted with analogous rate and mechanism. Moreover, using a synthetic mixture, it was reported that copper

Food industry

Containing a high concentration of water, hydrothermal valorization of food processing side-streams has been proposed thanks to the energetic advantage of avoiding the drying step [92].

Tuna cooking waste water was subjected to APR since the high salinity and different organic loads can make difficult the use of a biological treatment [93]. Pt supported on different carbon materials were used as catalysts. The characterization of the wastewater is reported in Table 4. In the absence of catalyst, hydrothermal carbonization occurred and was responsible for 20% TOC removal. The catalyst caused a lower TOC removal than the bare support since the high surface area was assumed responsible for the adsorption (e.g., 70% vs 50% for CAPSUPER – commercial - and Pt/CAPSUPER, respectively). However, a higher production of hydrogen and alkanes was obtained adding Pt (5.4 vs 1.4 μmol). A comparison between batch and semi-continuous set-up showed similar amount of valuable gases. However, alkane percentage was reduced, suggesting that hydrogen-consuming reactions (e.g., methanation, hydrogenation etc.) were prevented thanks to the decrease in the hydrogen partial pressure inside the reactor [94]. The observed catalyst deactivation was ascribed to the presence of acetic and phosphoric acids or chloride; for example, P species can prevent CO adsorption on Pt, hindering the WGS. The authors admitted that it was not possible to ascribe the catalyst deactivation to single compounds due to the complexity of the wastewater. The increase of platinum particle size was responsible for the decrease of methanation and increase of hydrogen concentration in the gas phase.

Breweries produce 3-10 liter of wastewater per liter of beer. The conventional treatment of this effluent consists of chemical, biological and physical step, but APR may be considered as an option [95]. A synthetic representative mixture was prepared using malt and yeast extract, peptone, maltose, ammonium sulfate, ethanol, monosodium and disodium phosphate. Without the catalyst, the hydrothermal carbonization (HTC) led to a reduction of COD and TOC of about 50%. In this case, the APR with Pt/C increased the carbon removal significantly (about 80%). It was reported that the presence of hydrogen in the produced gas phase increased with the increase of the concentration (range 474-414 mg C/L initial TOC), despite the TOC and COD removal decreased from 99% to 51%. The presence of carbonaceous compounds has been considered as the cause for the observed catalyst deactivation (in terms of hydrogen yield, not TOC removal). In Table 4 the hydrogen production is reported for different Pt-based catalysts at 200 °C and 225 °C. The better performance obtained by Pt/ENS250 were ascribed to its mesoporous texture and basic property. The mesoporosity can be beneficial to avoid mass-transfer limitations, since it facilitated the motion of reactants and products; the basicity could promote the water gas shift reaction, because it aided the water dissociation [96].

Since cleaning-in-place operations are performed in such plants with the use of alkaline solutions, the effect of NaOH and KOH was evaluated as well [97]. The characterization of the synthetic (using malt and yeast extract, peptone, maltose, ammonium sulfate and ethanol) and real brewery wastewater is reported in Table 4, together with the test results with specific attention to the carbon black samples,

which did not present microporosity. Base addition was found useful to favor the hydrogen production thanks to the removal of CO_2 and hence supporting WGS, mainly when KOH was added, through the following Eq. 7

$$CO_2 + 2\,KOH \rightarrow K_2CO_3 + H_2O \qquad \text{(Eq. 7)}$$

This concept is similar to the one previously reported, which takes advantage of the surface basic properties of the support. Moreover, C-O bond cleavage can be favored on C-C bond cleavage. The results between the two samples showed higher hydrogen production for the real one. One important reason can be ascribed to the different composition between real and synthetic sample. Acetate, formate, glycolate, phosphate, sulfate and maleate were identified and quantified in the initial samples. However, these species accounted only for 6% of the initial TOC, making difficult further discussion on the different performance. Finally, the influence of inorganics on the stability of the catalyst was not discussed.

Due to the sugar content of fruit juice wastewater, APR was explored as a possible alternative to conventional biological methods, since the variation of the organic load, pH, and salinity may hinder optimal performance [98]. The synthetic fruit juice wastewater was constituted by glucose, fructose, citric acid, ascorbic acid and galacturonic acid. Coherently with [97], the increase of pH increased the hydrogen yield together with a decrease of the carbon dioxide via carbonatation. The increase of the salinity did not affect the TOC and COD removal, while the hydrogen yield decreased: the authors attributed this outcome to catalyst deactivation, which in turn increased the contribution of the homogenous hydrothermal carbonization to the product distribution.

In Table 4 the results from APR of food processing are summarized. It can be observed that in the case of food processing wastewater the TOC of the feed is even lower than the one reported by hydrolysate, being always lower than 2500 mg C/L. The feed dilution hinders the application for very diluted streams since it means larger equipment in each section of the plant, feed pretreatment (heating/cooling and pumping), reaction and separation zone. The gas composition differs significantly moving from one type of substrate to the other. For example, tuna cooking led mainly to carbon dioxide; this percentage decreased for other side streams, but a high concentration of alkane was anyway obtained. Nevertheless, typically higher hydrogen yields are observed compared to the one obtained from hydrolysate

Table 4. Main characterization and results of APR of wastewaters derived from different food-processing. Inorganics: sum of phosphate, sulfate, sodium chloride; LSC: low salt content – HSC: high salt content.

Wastewater origin	COD (mg/L)	Acetate (mg/L)	Formate (mg/L)	Inorganics (mg/L)	Initial pH	APR conditions	Catalyst	Feed TOC (mg/L)	TOC removal (%)	% H_2	% Alkane	% CO_2	H_2 yield (mg H_2/ g C)	Ref
Tuna cooking	4996	1895	10	4354	6.1	20 mL wastewater, 200 °C, 4 h, batch reactor	0.4 g Pt/CAPSUPER	1895	54	1.8	1.3	96.9	2.8	[93]
							0.4 g Pt/SXPLUS		54	0.5	3.5	96.0	3.3	
							0.4 g Pt/ENSACO		41	8.7	9.3	82.0	25.5	
Breweries - synthetic	6229	<1	<1	987	6.9	15 mL wastewater, 200 °C, 4 h, batch reactor	0.3 g Pt/CAP	1968	82	5.7	36.1	58.3	30.5	[95]
						15 mL wastewater, 225 °C, 4 h, batch reactor			86	19.1	32.4	48.6	133.4	
						15 mL wastewater, 200 °C, 4 h, batch reactor	0.3 g Pt/ENS250		79	35.4	26.8	37.8	318.9	
						15 mL wastewater, 225 °C, 4 h, batch reactor			88	48.9	22.7	28.4	829.2	
						15 mL wastewater, 200 °C, 4 h, batch reactor	0.3 g Pt/ENS350		80	19.2	26.8	54.0	88.8	
						15 mL wastewater, 225 °C, 4 h, batch reactor			88	34.3	23.9	41.7	296.5	
						15 mL wastewater, 200 °C, 4 h, batch reactor	0.3 g Pt/C_MESO		60	33.2	21.3	45.5	19.5	
						15 mL wastewater, 225 °C, 4 h, batch reactor			74	41.1	19.6	39.2	31.1	
Breweries - synthetic	5846	2	1	696	7	15 mL wastewater, 220 °C, 4 h, batch reactor	0.3 g Pt/ENS	1871	60	46.7	21.3	32.0	595.4	[97]
					11	15 mL wastewater + NaOH, 220 °C, 4 h, batch reactor			66	51.4	23.0	25.6	387.3	
					11	15 mL wastewater + KOH, 220 °C, 4 h, batch reactor			70	52.7	22.2	25.1	594.8	
					7	15 mL wastewater, 220 °C, 4 h, batch reactor	0.3 g Pt/KJB		83	23.5	19.6	56.9	91.2	
					11	15 mL wastewater + NaOH, 220 °C, 4 h, batch reactor			75	32.7	22.8	44.5	130.0	
					11	15 mL wastewater + KOH, 220 °C, 4 h, batch reactor			78	38.6	21.7	39.7	236.9	
Breweries - real	4764	172	37	56	11	15 mL wastewater, 220 °C, 4 h, batch reactor	0.3 g Pt/ENS	1646	52	51.1	20.1	28.8	485.7	[97]
							0.3 g Pt/KJB		69	53.6	19.9	26.5	798.1	
Fruit juice	5925	-	-	-	2	15 mL wastewater, 220 °C, 4 h, batch reactor	0.3 g Pt/ENSACO	2317	92	27.8	11.9	60.1	288.3	[98]
					7				74	34.9	15.7	49.3	371.8	
					10				61	40.8	14.1	45.1	425.3	
					12				63	40.0	11.8	48.2	362.5	

Fruit juice - LSC	5925	-	-	483	10	15 mL wastewater, 220 °C, 4 h, batch reactor	0.3 g Pt/ENSACO	2317	63	38.1	15.5	46.4	419.6	[98]
Fruit juice - HSC				967	10				65	35.1	16.3	48.6	269.4	

Cheese whey valorization via APR has been explored due to the environmental concern prompted by its co-production during cheese making processes, since about 9 kg/kg cheese are obtained [6]. Lactose is the primary compound in cheese whey, approximately 5 wt.%. Only one third is recovered, and the remaining is sent to waste treatment or even field spread. It is estimated that the full reforming of lactose produced by the U.S. cheese industry could generate up to 0.33 million tons of hydrogen (about 9% hydrogen production capacity of U.S. refineries in 2014) [99].

Traditionally, the treatment is addressed through filtration technologies or biological treatments (aerobic/anaerobic digestion, lactose fermentation). The effect of temperature (200-240 °C), pressure (38-50 bar), lactose concentration (1-10 wt.%) and catalyst (Ni-La/Al_2O_3) mass/lactose mass flow rate ratio (10-40 g cat min/g lactose) were investigated using a design of experiment approach for the APR of a model lactose solution. The lactose conversion was complete in each of the investigated conditions. It turned out that the gas production is favored by high temperature and pressure, together with high $W/m_{lactose}$ and lactose concentration [6]. Beside gas production, the carbon conversion to liquid ranged from 33 to 97%, and the liquid products were constituted by aldehydes, carboxylic acids, alcohols, ketones and furans. Similarly with the results reported for sugar solutions, a portion of the carbon was converted in a solid phase, within a range 0-59% according with the reaction conditions. This is an important topic because the presence of insoluble compounds in a catalytic reaction can easily cause the deactivation of the catalyst by fouling. Despite this risk has been highlighted for concentrated sugar solutions, the authors reported that similar solid production can be obtained even at dilute conditions (1 wt.% lactose).

Overlayer bimetallic Pt on Ni or Co catalysts supported on alumina were tested for lactose APR [99]. Ni-Pt showed the highest hydrogen yield and selectivity. Interestingly, the work reported that the use of pseudomorphic overlayer bimetallic catalysts helped to decrease the H_2 and CO binding strength, favoring the H_2 production.

Finally, a comparison between cheese whey, filtered cheese whey (i.e. cheese whey with lower fat and protein fraction) and lactose solution was performed using a Ni-La/Alumina [100]. The cheese whey was mainly constituted by lactose (4.71 wt.%), sorbic acid (1.81 wt.%) and acetic acid (1.37 wt.%); moreover, ashes were present as well (0.52 wt.%). Cheese whey experiments showed less gas production than lactose experiments, attributed to the high formation of char in the former case; the filtration allowed to increase the gas production and reduced the char formation, suggesting that fats and protein could play a role in its formation due to their high molecular weight. Moreover, it has been suggested that salts, promoting dehydration reactions, may be responsible of the great amount of char using the real feedstock compared to the model lactose solution. Test performed in the continuous set-up clearly showed a decrease of the conversion to gas with the time on stream caused by char formation, which eventually clogged the reactor.

Despite the potential interest of cheese whey as feedstock for APR, the low selectivity is a main obstacle. Alternative strategies, similar to the ones cited for sugar streams, or the optimization of the reaction conditions should be evaluated to assess its implementation beyond the laboratory scale.

Crude glycerol

During the production of biodiesel, a crude glycerol stream is obtained (0.1 kg crude glycerol/kg of biodiesel). Apart from being an environmental issue, this inconvenience may hinder the development of the biodiesel itself as alternative fuel. This is the reason why various valorization routes for glycerol have been explored [101]–[104].

Glycerol is the most studied molecule for APR. However, it is mainly used in reagent grade, therefore the corresponding results will not be reported in the present work since out of the scope. Far more interesting in this context is understanding the effect of the impurities (methanol, soap, salts) which are present in crude glycerol.

Lehnert and Claus compared for the first time the performance of pharma grade glycerol and crude glycerol on Pt catalyst and ascribed the decrease of the hydrogen production to the blocking of the active sites caused by inorganic salts [105]. The rate of hydrogen production at the steady state was 7.6 mmol/min·g_{cat} for pure glycerol whereas it was 1 mmol/min·g_{cat} for crude glycerol. In Figure 17-A the difference in the hydrogen content between pharma grade and crude glycerol is reported.

Remon et al. studied the effect of acetic acid (up to 3 wt.%), potassium hydroxide (up to 2.8 wt.%) and methanol (up to 5 wt.%) at 220 °C using a Ni-La/Al_2O_3 catalyst [106]. The influence of one, two and three impurities on the glycerol conversion, carbon distribution, gas and liquid composition was systematically evaluated. Acetic acid decreased the carbon conversion to gas without affecting the glycerol conversion; potassium hydroxide increased the carbon conversion to gas, as well as the hydrogen concentration in the gas phase; methanol decreased the glycerol conversion. When the impurities were present in binary or ternary mixtures, neutralization and esterification could occur. Finally, acidic conditions promoted Ni and La leaching, whereas basic conditions favored Al leaching.

The influence of acidic and basic impurities have been further investigated in [107]. The acid impurities were acetic acid, sulfuric acid and phosphoric acid: these may be found due to the neutralization step; the basic impurities were potassium hydroxide and sodium hydroxide, since they may be used as catalyst during the transesterification for the biodiesel production. The authors reported that the impurities did not affect the catalytic performance (i.e. carbon conversion to gas or liquid or solid) during the first hour of experiment. However, they did deactivate the catalyst, mainly via fouling/poisoning and leaching mechanisms. The latter was independent by the type of present impurities, confirming that leaching depended just on the pH of the solution (which was maintained constant in the experimental campaign at 7). Carbon deposition was negligible (less than 0.28 mg C/g catalyst). K deposition could help S and P deposition thanks to the higher electron deficiency of the catalyst, contributing to its deactivation. Furthermore, the type of acid and base influenced the alumina transition into boehmite. In the presence of KOH, the lowest transition was observed with H_3PO_4, while in the presence of NaOH it was the lowest with H_2SO_4. Unfortunately, no comparison with pure glycerol was reported in the work.

The effect of NaCl was studied in [108]. The authors reported that 1.25 wt.% NaCl did not affect the gas and liquid product distribution, but decreased the conversion to liquid products, using a silica-alumina supported nickel catalyst.

Finally, it is important to highlight that the support of the catalytic system plays a key role on the resistance to the impurities. Boga et al. observed a drastic decrease of the hydrogen selectivity moving from a pure 6.85 wt.% glycerol solution (64% selectivity) to a crude glycerol solution constituted by glycerol, soaps, methanol and ester (1% selectivity) [109]. However, active carbon support maintained the performance similarly to the case of pure glycerol (Figure 17-B). The separate investigation of the contaminants allowed to identify sodium oleate as the most dangerous one, due to its irreversible adsorption. In this sense, the use of activated carbon able to adsorb selectively the fatty acid improved the hydrogen selectivity from 1 to 18%.

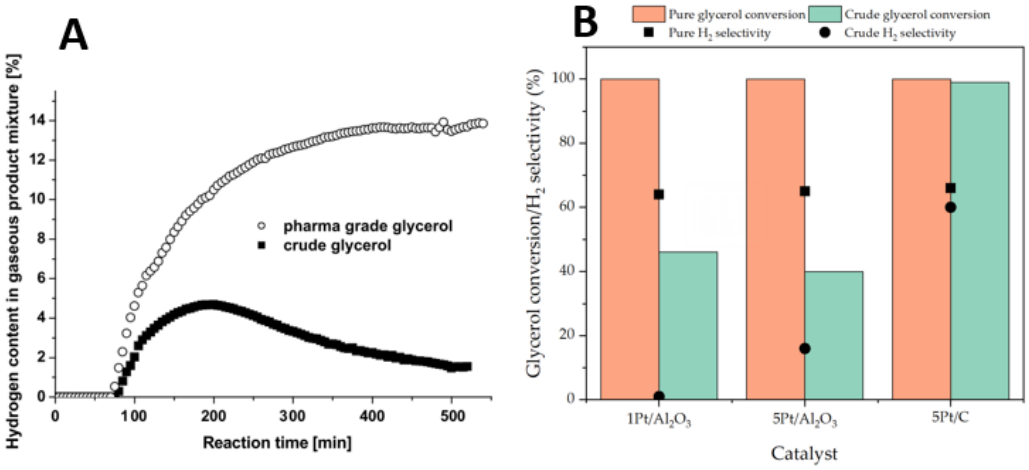


Figure 17. A: Influence of glycerol grade on the hydrogen content in the gaseous stream, reaction conditions: 250 °C/20 bar, 10 wt.% glycerol, flow rate 0.5 mL/min, 0.3 g catalyst (from [105]). B: Influence of catalyst on APR of pure and crude glycerol, reaction conditions: 225 °C/29 bar, 3 h, 0.3 g catalyst (data from [109]).

Perspectives: towards industrial APR application

To the best of our knowledge, only one commercial demonstration of the APR process is currently active, the BioForming Technology by Virent Energy Systems Co. in cooperation with several partners [110]. This plant has not the objective of producing hydrogen as main product; instead, it aims at the production of drop-in hydrocarbons from sugar-based aqueous solution.

The aim of this paragraph is to evaluate the possibility that an APR unit for hydrogen production can be integrated in an existing plant, comparing the results obtained with other technologies reported in literature, when available.

In Table 5 a summary of the wastewater mentioned in the review with their main difficulties and advantages regarding the APR application is presented. This table could be considered an initial screening for suitable APR substrates. That is, once an aqueous fraction is present in a plant, some characteristics could make it more appropriate than others for APR reaction.

First, higher organic content is favorable. This can be trivial in most of the cases; however, attention should be put in the case of sugar-laden water fractions, where homogeneous reactions can drastically reduce the hydrogen yield. Most of the investigated aqueous streams are really diluted, and only crude

glycerol from biodiesel production and cheese whey from dairy industries present concentration higher than 5 wt.%. Looking at the composition, mono and polyalcohols, together with hydroxyacids should be favored, thanks to the presence of a C:OH moiety in the molecule, which can be activated producing hydrogen via dehydrogenation and water gas shift of the intermediate CO. Carboxylic acids are usually recalcitrant and with higher tendency to alkane formation. Ketones and aromatics are very stable compounds at the typical APR conditions, showing negligible conversion.

Table 5: Summary of wastewater sources with corresponding characteristics, advantages and disadvantages in the field of APR.

Sources	Main characteristics	Main difficulties	Main advantages	Ref
Biodiesel production	kg crude glycerol/kg biodiesel 68.5-80 wt.% glycerol, 1-20 wt.% methanol, 0-5 wt.% sodium chloride, 1.5-14 wt.% water, 2-16.2 wt.% soaps	Inorganic salt Soaps Dilution is typically performed before APR	High concentration of the substrate High hydrogen yield thanks to the optimal C:OH ratio	[47], [109]
Dairy	9 kg cheese whey/kg cheese COD: 50-102 kg/m^3 4.5-6 wt.% lactose, 0.6-1.1 wt.% protein, 0.8-1 wt.% minerals, 93-94 wt.% water, fats and lactic acid below 1 wt.%	Char formation/Humin deposition due to salts presence	High concentration of lactose in the wastewater	[6], [100]
Brewery	3-10 L/L beer TOC 2000 mg C/L COD 6200 mg C/L 1000 mg/L malt extract, 500 mg/L yeast extract, 150 mg/L peptone, 860 mg/L maltose, 1000 mg/L ammonium sulfate, 2.8 mL/L ethanol	Carbonaceous deposits on the catalyst Diluted water fraction	High removal of TOC and COD, with production of hydrogen and alkanes	[95]
Hydrothermal liquefaction	10-50% of initial feedstock carbon ends up in the aqueous phase TOC 5000-20000 mg C/L	Competitive adsorption of carboxylic acids Diluted water fraction	Methanol, glycerol and glycolic acid presence improved the H_2 production	[83], [85]
Fischer-Tropsch	TOC 5000-10400 mg C/L C1-C5 alcohols and corresponding carboxylic acids	Diluted water fraction	Alcohol are the main compounds so high hydrogen yield is obtained	[90], [91]
Carbohydrate processing	TOC: 5000-18000 mg C/L C5-C6 sugars	Humins deposition	With pre-hydrogenation step high H_2 production and TOC reduction is obtained	[44], [45]

Preliminary process design studies were performed for APR [111], [112]. They highlighted that no external heat can be provided if the gaseous alkanes by-products are used as fuel. Moreover, the

facility may be located close to pulp mills for a stand-alone green diesel production plant where small-scale methane steam reformers would be not economically attractive [111]. This points out the possible synergy between two technologies. An important issue derived from the cost of the feedstock is also arose. Sladkovskiy et al. simulated a 500 kg/h hydrogen plant from sorbitol to satisfy the need of a 100000 T/y green diesel plant [112]. With the current cost of sorbitol syrup, the hydrogen production costs would be seven times higher than the actual one with conventional technologies (roughly 13 $/kg vs 2 $/kg), and the feedstock would account from about 92% of the total production cost [112]. For this reason, the use of waste or readily available feedstocks seems pivotal for its application at the industrial scale. In this sense, APR was applied to waste water fractions associated to the valorization of municipal waste [113]–[115], or in the treatment of sludge for reuse purpose thanks to the removal of micro-pollutants such as ibuprofen and caffeine [116].

The possibility to use the hydrogen directly in situ is the best condition for the applicability of APR combined with biorefineries or industries producing water.

Besides stand-alone options, the integration with other facilities should be foreseen, especially in the case where the aqueous stream is particularly diluted. These refer not only to the one cited regarding the upgrade of intermediate biofuels [117], [118]. For example, the integration with dimethyl ether production, where its exothermicity may be coupled with the endothermicity of the reforming reaction, which in turn produces the syngas necessary for DME [119]. Another possibility is the use of the hydrogen *in situ* to produce other chemicals like methane [120] or deoxygenate fatty acids [121].

A comparison of APR performance with other technologies can be mentioned. Looking at the brewery wastewater, about 294 mL H_2/g COD was obtained with APR, while it was 150 mL H_2/g COD for the anaerobic digestion [122]. A techno-economic assessment compared hydrogen produced by glycerol reforming in aqueous and gaseous phase (80 kg/h size) [123]. The investigation estimated 3.65 $/kg cost production from glycerol steam reforming and 3.55 $/kg for glycerol APR. These values are comparable or even lower than other renewable hydrogen routes, such as biomass gasification (1.77-2.05 $/kg), dark fermentation (2.57 $/kg), solar thermal electrolysis (5.10-10.49 $/kg) [124].

The carbohydrate to hydrogen technologies have been recently reviewed in [61]. This research showed that the APR hydrogen yield (mol H_2/mol glucose) is comparable or higher than other technologies like anaerobic fermentation, photo-fermentation, electrohydrogenesis and ethanol partial oxidation reforming.

In view of the possible use of APR to industrial contexts, some important issues should be investigated and solved.

The characterization of the complex aqueous stream is often lacking. Nevertheless, it is necessary to identify the most suitable treatment and/or catalytic system. For example, microporous supports should be avoided in the case of large molecules in the feed, while they can be used when small organics (alcohols, carboxylic acids) are present, so that the dispersion of the active phase is maximized.

The development of active, selective and stable catalyst is crucial for the industrial application. Lange depicted some catalytic performance criteria that should be targeted by biorefineries to reach the industrial scale, such as selectivity, activity, catalyst consumption and product concentration [125]. It is worthy trying to understand where APR is. Industrial catalyst activity ranges from 0.1 to 1000 tons of product per ton of catalyst per hour. Despite it is not rigorous for batch reactors, we can roughly evaluate if APR is within this range. Looking at the results reported in [62], it can be estimated that the catalytic activity would be equal to 0.09 tons of hydrogen per ton of catalyst per hour, and 0.27 in the case of glucose. Regarding the catalyst consumption, it is reported that it should be disposed at least after having produced 1000-100 000 times higher product than its mass. No long runs are available for APR and even small tests showed important deactivation phenomena such as poisoning and fouling. Most of the experiments were carried out in batch reactors, which prevented the study of the catalyst deactivation. This is the real enemy for the use of noble metals. These issues are often overcome for model compounds, but inevitably appear moving to actual streams.

As it commonly happens in the conventional industrial chemistry, pretreatments to clean the feed should be adopted when noble metals are used. Proper pre-treatment of the aqueous phase may be envisioned, involving the removal of large macromolecules which may poison the catalyst. Some examples were already reported, such as pre-hydrogenation of sugars to corresponding sugar alcohols, or liquid-liquid extraction/adsorption of the aromatics in HTL-derived water. In addition, apart from the cited works with crude glycerol, limited information on the effect of inorganic impurities such as sulfur and phosphorous were reported by the literature ([78], [93]).

Most of the cited works used noble metal catalysts. In our survey, only Ni-based catalysts were reported as alternatives ([6], [64], [71], [90]). Cheaper catalyst formulations would be necessary to increase the cost-effectiveness of the process. Furthermore, the addition of promoters able to facilitate the adsorption of carboxylic acids should be investigated, since the observed competitivity with other classes of compounds limited the organic abatement of the wastewater.

One final comment should be reserved to the effluent of the APR reactor. It has been reported that the conversion level does not affect the hydrogen selectivity in the case of methanol and ethylene glycol [39]. For the real streams, Remon et al. showed that changing the space velocity can have different effects depending also on the reaction temperature and substrate concentration [6]. According to Murzin and coworkers, the pressure swing adsorption (PSA) may be the most efficient method to purify the gas products derived from APR, which is characterized by high hydrogen recovery (85-95%) and low pressure-drop for the purified gas [112]. Apart from the gas phase, the liquid effluent should be carefully checked. In the ideal case, the TOC and COD removal should have been sufficient to meet the environmental legislation. If this is not the case, further treatments or recycle loops should be proposed. In view of a possible industrial implementation of APR, also these rarely cited practical implications (downstream processing such as hydrogen separation from gas mixtures, regulatory COD and BOD levels) should be verified.

1.3. Aim of the work

To conclude the introduction is important to notice that industrial processes, including biorefineries, produce side water streams which contain complex mixture of diluted organics. This is a limitation for biorefineries, since up to 50% of initial carbon can be lost in the water. To really improve biomass processing it is necessary to exploit all the side products and increase the carbon recovery of the entire process. In this frame aqueous phase reforming may be a valuable option thanks to its ability to convert the organic content as a whole and produce a gas rich in hydrogen. The APR reaction condition have higher energy efficiency compared to steam reforming and allows to conduct both reforming and water gas shift in the same reactor.

As reported in the introduction the APR of representative industrial aqueous streams is still poorly investigated, most of works focus on model compounds. There is also a lack of characterization of these waters, which are pivotal for the applicability of APR in industrial scale.

Aim of this work is understand the possibility of aqueous phase reforming application. Single model compounds and synthetic mixture were tested; then, two water fractions from Fischer-Tropsch (FT) process and from hydrothermal liquefaction of lignin were deeply studied. Attention was paid to catalyst stability trying to find solutions to the deactivation. Batch and continuous set up were studied and preliminary tests were conducted in a pilot scale plant. Finally, the experimental results were used to design the combined HTL+APR plant and the techno-economic (TEA) and environmental assessments (LCA) were carried out.

In the next chapters the results will be presented. Chapter 2 deals with the materials and method used; chapter 3 presents the campaign on FT water; chapter 4 summarized the results of the HTL of lignin rich feed with a focus on catalyst deactivation; chapter 5 is dedicated to the continuous tests results and finally chapter 6 include both LCA and TEA methods and results.

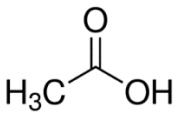
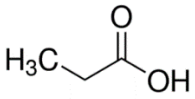
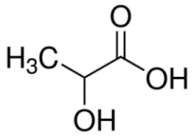
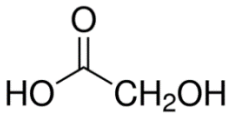
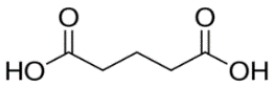
Chapter 2

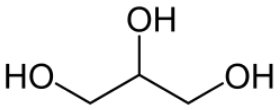
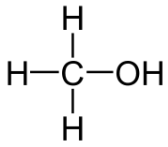
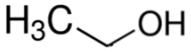
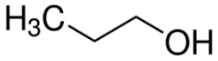
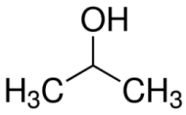
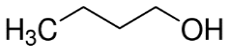
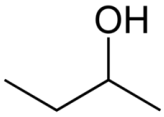
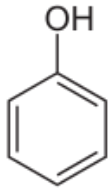
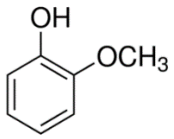
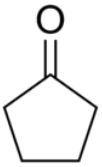
Material and methods

2.1. Materials

Several compounds were tested as representative of industrially relevant water fractions such as Fischer-Tropsch and Hydrothermal liquefaction. They were purchased by Sigma Aldrich and Flucka. The choice of compounds was before based on a deep study of the literature and then adjusted thanks to the characterization of actual water phases provide by RE-CORD (Renewable Energy Consortium for Research and Demonstration) for the HTL-side stream; by Tu-Wien and BEST for the FT water. The compounds are reported in Table 6 below where are they are summarized together with the condition of their tests and in which waters can be found.

Table 6: tested compounds.

Class	**Compound**		**Studied conditions**	**Water**
Carboxylic acid	Acetic acid		Concentration, time, mixture, adsorption	FT, HTL
	Propionic acid		Concentration	FT, HTL
Hydroxyacid	Lactic acid		Concentration, time, mixture	HTL
	Glycolic acid		Concentration, time, mixture, Adsorption	HTL
Dicarboxylic acid	Glutaric acid		Concentration	HTL

Alcohols and polyalcohols00	Glycerol		Concentration, time, mixture	HTL
	Methanol		Concentration, time, mixture	FT, HTL
	Ethanol		Concentration, time, mixture	FT, HTL
	1-propanol		Time, mixture	FT
	2-propanol		Time, mixture	FT
	Butanol		Time, mixture	FT
	2-Butanol		Time, mixture	FT
Aromatics	Phenol		Adsorption	HTL
	Guaiacol		Adsorption, concentration	HTL
	Cyclopentanone		Concentration	HTL

Deionized water was obtained in laboratory with a RO Cubic S2 system.

The used catalyst is a platinum-based catalyst (5 wt% Pt/ C), provided as developmental catalyst by commercial supplier in both powder and pellet form. The Pt dispersion of 58% was measured by H_2 pulse chemisorption (details in paragraph 2.2.4). The 80% of the catalyst, in powder form, had a size of < 106 µm; the pellet are provided in grit shape with 1 mm average particle size. The catalyst was used without any further pretreatment. The carbon support is activated carbon with high surface area (950 m2/g) Activated carbon (Darco – 100 mesh particle size), Amberlite IRA-67, IRA-400,

IRA-410 and IRA-900, used for the adsorption tests, were purchased from Sigma Aldrich. The effect of inorganics was studied with the addition of SO^{4-} from H_2SO_4 and Na from NaCl.

2.2. Methods

2.2.1. Aqueous phase reforming tests

The batch tests have been conducted in a 300 mL 4560 series mini bench top reactor (Parr), represented in Figure 18 equipped with a 4848-model reactor controller (Parr). Glass liners were used in order to resist to all the desired set temperatures. The reactor was filled with 75 ml of the desired solution and with the desired Pt-based catalyst. Once closed the reactor was purged with nitrogen to eliminate the oxygen and then pressurized to 0.3 MPa of N_2. Time and temperature were varied between 0-8 hours and 230-270 °C respectively to study their influence; at the end of the reaction the reactor was cooled down thanks to an internal cooling loop and/or external water bath. Before opening the reactor, the gas phase is collected in a syringe and analyzed by μGC. The liquid phase was filtered by gravity to separate the catalyst and then analyzed through TOC and HPLC analysis. The recovered catalyst was dried in an oven overnight (105°C) and weighted afterward; for the reuse tests the catalyst was use without pretreatment.

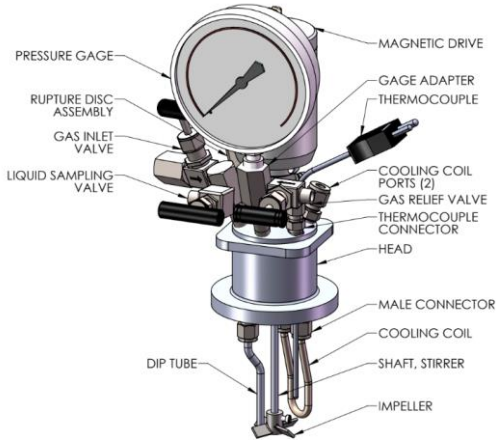


Figure 18. Parr top reactor component scheme.

Since APR environment is a three-phase system, prior to perform any kinetic evaluation, the presence of any mass transfer resistance should be excluded.

The external mass transfer was checked at the most conservative conditions, being 270 °C with glycolic acid, which is the most active compound, and 5% Pt/C, which is the most active catalyst. The agitation speed was varied between 0 and 400 rpm, and its effect on conversion of the substrate and hydrogen yield is reported in Figure 19. It could be observed that in the absence of stirring, the glycolic conversion and hydrogen yield were 18.7% and 13.9%, respectively; however, they increased up to about 34.3% and 26.7% already at 200 rpm, and remained constant even after increasing the stirring rate. The lower values in the unstirred conditions could be correlated to the

inevitable stratification of the solid catalyst, which hindered the contact with the reagent, affecting its conversion. This outcome evidenced that external mass transfer limitations should be discarded at the conditions used in this work (400 rpm).

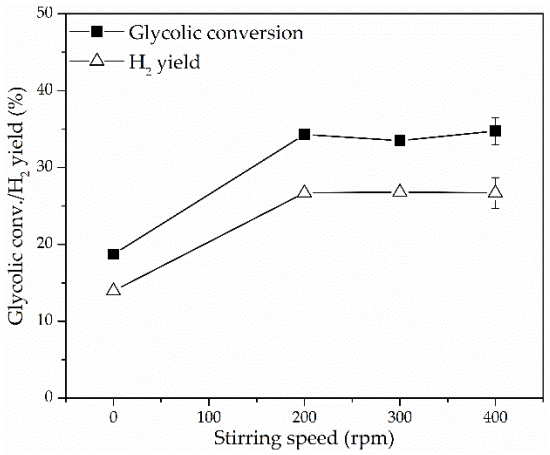


Figure 19. Influence of stirring speed on glycolic acid APR. Reaction conditions: 270 °C, 0.05 g 5% Pt/C, 1 h, 1.3 wt.% glycolic concentration.

Internal mass transfer limitations were evaluated using the Weisz-Prater criterion [126].
The value of the criterion was equal to 0.27, therefore internal mass transfer limitations were absent.

Continuous test have been carried out in unit design and built by PID (Process Integral Development Eng & Tech, Spain): it is constituted by stainless steel tubular reactor (9 mm internal diameter), equipped with temperature control and electric furnace. The solution is fed by a HPLC pump (Gilson, 307 model). The system has a six-valve system to decide if feeding upward or downward; The system pressure was maintained constant thanks to a micrometric valve and the set value was fixed equal to the autogenous pressure at the chosen reaction temperature (plus five bars). The separation system consists of a Peltier system (2 ml dead volume) to cool down up to 10°C; the liquid is then collected at bottom part and analysed with HPLC, finally the gas depressurized and analysed with micro-GC passing through a mass flow meter

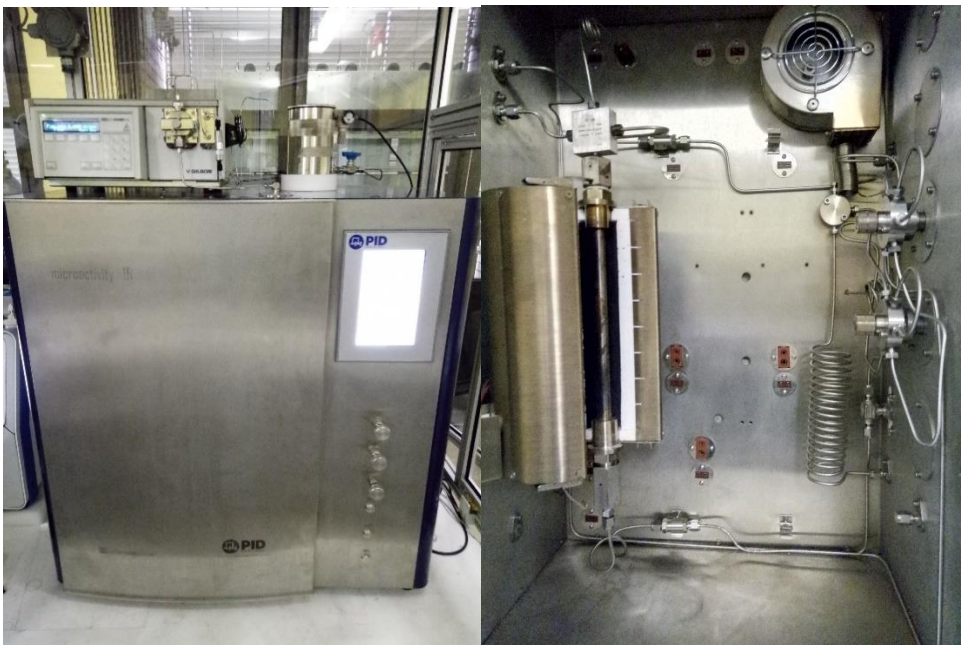


Figure 20: continuous reactor set up

2.2.2. Reproducibility tests

The reproducibility of the reactors was tested with repetition of some reference tests and based on these results the following results are commented.

The batch stability was tested with acetic acid APR. In Table 7 the conversion of first and second test at three different reaction time are reported and the tests have standard deviation of 3-4%

Table 7: acetic acid APR reproducibility tests. Reaction conditions: 270°C, 0-3 h 13 mmol acetic acid

Time (h)	Test 1	Test 2
0.5	32.8	27.8
1	23.7	29.3
3	33.7	37.6

Instead, the continuous reaction was studied with a synthetic mixture test. The conversion of the two tests were similar, in the table below the conversion of glycolic acid at different time on stream is reported.

Table 8: Reaction conditions: reproducibility test in continous reactor. 270°C, 1 g of Pt/C, 0.8 ml/min

Time (min)	Test 1	Test 2
100	92.1	90
300	89	90.8
500	90.3	92.5

2.2.3. Adsorption tests

Aqueous solution with the same composition used for the catalytic test was used for the adsorption tests. Preliminary analysis, not reported, showed that equilibrium was reached within 90 minutes. The tests have been conducted at room temperature. Pre-weighted amount of activated carbon or Amberlite were added to the solution and the stirring was started. At the end of the experiment, 1 mL was taken to perform HPLC and ion chromatography analysis.

2.2.4. Analytical methods

The gas phase was analysed with a SRA Micro-GC equipped with a Pora PLOT U (column temperature: 85 °C) with Helium, as carrier, for for the separation of carbon dioxide, ethane and propane and a Molsieve 5A column for the analysis of hydrogen, nitrogen, methane and carbon monoxide with Argon (column temperature: 100 °C). The detection of the species is performed with a TCD detector. The injection temperature was fixed at 100 °C and the pressure at 30 psi. The micro-GC has been calibrated constantly, in the necessary range to find and calculate the composition of the produced gas phase. HPLC analysis (Shimadzu) was performed with a Rezex ROA-Organic acid H^+ (8%) column (300 mm * 7.8 mm) to determine the composition of the liquid phase. The mobile phase is 5mm H2SO4 in water and the flow rate was fixed at 0.7 ml/min with a temperature oven of 50°C. The compounds were determined using a refractive index detector (RID) and quantified by external calibration. Photo diode array (PDA) detector was used to identify aromatic compounds thanks to its higher sensitivity compared to RID. The total carbon analysis was made using a Shimadzu TOC-V_{CSH} analyzer equipped with a nondispersive infrared detector. The analysis of the inorganics was performed using a Thermo Scientific iCAP Q ICP-MS (Thermo Fischer).

To evaluate the performance of the process five parameters were defined:

- the carbon to gas conversion: the ratio between the moles of carbon in the gas product $mol_{fin}C_{gas}$ and the moles of carbon in the feed $mol_{in}C_{feedstock}$ (eq.9);
- H_2 yield: the ratio between the moles of hydrogen produced and the initial mol in feedstock times (y+n) parameter reported in the stoichiometry (eq. 10);
- the H_2 gas distribution: the ratio between the moles of hydrogen present in the gas phase as molecular hydrogen (mol_{fin} H_2) after the reaction and the moles of total hydrogen present in the final gas phase (that is, also as alkanes) (eq.11);
- the H_2 productivity: moles of hydrogen produced $mmol_{fin}H_2$ divided by the moles of carbon in the feed $mol_{in}C_{feedstock}$ (eq. 11). This parameter is useful especially for real water fractions where the complex composition does not allow to use parameters involving the classical reaction stoichiometry;
- the conversion: the ratio between the number of moles reacted (mol_{in} i – mol_{fin} i) and the number of moles in the feed (mol_{in} i) (eq. 12).

$$\text{Carbon to gas (\%)} = 100 * \frac{\text{mol}_{\text{fin}}\ \text{C}_{\text{gas}}}{\text{mol}_{\text{in}}\ \text{C}_{\text{feedstock}}} \qquad \text{(Eq. 8)}$$

$$\text{APR} - \text{H}_2 \text{ yield } (\%) = 100 * \frac{\text{mol}_{\text{fin}}\, \text{H}_2}{(\text{y+n}) * \text{mol}_{\text{in}}\, \text{feedstock}} \quad \text{(Eq. 9)}$$

$$\text{H}_2 \text{ gas distribution } (\%) = \frac{\text{mol}_{\text{fin}}\, \text{H}_2}{\text{mol}_{\text{fin}}(\text{H}_2 + 2 * \text{CH}_4 + 3 * \text{C}_2\text{H}_6 + 4 * \text{C}_3\text{H}_8)} \quad \text{(Eq. 10)}$$

$$\text{APR H}_2 \text{ selectivity}(\%) = 100 * \frac{\text{mol}_{\text{fin}}(\text{H}_2/\text{CO}_2)}{(\text{H}_2/\text{CO}_2)_{\text{teo}}} \quad \text{(Eq. 11)}$$

$$\text{H}_2 \text{ productivity} = \frac{\text{mol}_{\text{fin}}\, \text{H}_2}{\text{mol}_{\text{in}}\, \text{C}_{\text{feedstock}}} \quad \text{(Eq. 12)}$$

The quantification of the gaseous products has been performed using the initial moles of nitrogen as an internal standard. Being nitrogen inert the moles of gaseous products can be derived knowing the molar fraction of nitrogen in the final mixture.

2.2.5. Catalyst characterization

N_2 adsorption/desorption isotherms of the fresh and spent catalysts at 77 K were measured with a Micromeritics Tristar 3020 instrument. The samples were pre-treated at 200 °C under nitrogen flow for 2 h through a Micromeritics Flow Prep 060 degassing system. The specific surface area was calculated according to the Brunauer-Emmet-Teller (BET) equation. X-ray diffraction (XRD) of fresh and spent catalysts was performed through a Panalytical X'Pert Pro diffractometer (Cu Kα radiation). Inorganics analysis in the water (leaching of platinum) was measured via a Thermo Scientific iCAP Q ICP-MS (Thermo Fisher). XPS measurements were carried out with a PHI Model 5000 electron spectrometer equipped with an aluminum anode (1486 eV) monochromatic source, 25.0 W power, and high-resolution scan with 11.75 eV pass energy. The binding energies obtained by XPS analysis were corrected for specimen charging by referencing the C1s = 284.6 eV.
Temperature-programmed reduction (TPR) was carried out using a TPDRO-1100 equipment (Thermo Scientific). The sample (approximately 100 mg) was heated at 5 K/min in a 20 mL/min flow of 5% H_2/Ar from 323 K to 1073 K. The TPR profile did not show any peak associated with Pt reduction, confirming the metallic state of the sample and the possibility to use it without any pretreatment.

Chapter 3

Fischer-Tropsch

This chapter including results, figure and table is based on published work [87]

The hydrogenation of CO is a very old process and first insights were already published at the beginning of the 20th century [127]–[131]. The FT product contains mainly water, alkanes, alkenes and to a minor extent oxygenates such as alcohols ((Eq. 1), carbonyl groups aldehydes and ketones, and carboxylic acids[132]–[135]. The mechanisms describing the formation of these substance classes were discussed in further literature [132], [135]–[139].

1. $(2n+1)\,H_2 + n\,CO \rightarrow C_nH_{2n+2} + n\,H_2O$ (Eq. 13)

$2n\,H_2 + n\,CO \rightarrow C_nH_{2n} + n\,H_2O$ (Eq. 14)

$2n\,H_2 + n\,CO \rightarrow C_nH_{2n+2}O + (n-1)\,H_2O$ (Eq. 15)

$(2n-1)\,H_2 + n\,CO \rightarrow C_nH_{2n}O + (n-1)\,H_2O$ (Eq. 16)

$(2n-2)\,H_2 + n\,CO \rightarrow C_nH_{2n}O_2 + (n-2)\,H_2O\,, (n>1)$ (Eq. 17)

The desired product is the organic phase, which could be used to produce transportation fuels or basic chemicals [140]–[143].

Experiments performed at Güssing's research center showed that on a mass basis more than half of the condensable FT product was water. It is polluted with short-chained organic oxygenates, with alcohols being the most prominent substance class.

The design of the product separation and applied temperatures levels affect the phase-preference of short organic oxygenates. From a process point of view, the amount of oxygen-containing products increases if i) the hydrogenation potential of the FT catalyst decreases, ii) the hydrogen partial pressure decreases or iii) temperature increases [143].

Literature suggests that organic oxygenates account for about 1 wt.% of the FT water produced by cobalt-based low-temperature Fischer-Tropsch (LTFT) [135], [144].

The composition of the FT product water depends on operating conditions and catalyst type. The recovery of oxygenates from the product water is complex, especially when the oxygenate concentration is low. Therefore, if these compounds are not removed, the water has to be treated to minimize the environmental impact [145]. Purification of the acidic reaction water needs to be performed to permit its recycling within the FT facility or disposal.

Different approaches and technologies regarding wastewater treatment of FT product water were summarized by Miglio et al. [144]. One possibility is the physical separation through distillation steps, also involving extractive systems. However, this option is not cost-efficient due to the high dilution of the organics. Another option is exploiting the biological routes, producing methane thanks to the anaerobic digestion process.

Majone et al. investigated the anaerobic treatment of synthetic wastewater from an FT process at mesophilic conditions, obtaining up to 96% of COD removal and almost complete conversion to methane [146]. Wang et al. recently proposed the addition of magnetite to increase COD removal efficiency and methane production [147]. However, the performance of the process is sensitive to key parameters such as the pH of the solution or the flowrate of the feed, making the anaerobic digestion difficult to operate.

Aqueous phase reforming (APR) can be a suitable process to reduce the carbon content of FT product water, at the same time producing a gas phase rich in hydrogen. Coronado et al. [91] studied the conversion of FT representative alcohols (methanol, ethanol, 1-propanol, and 2-propanol) with active-nickel based catalysts, proposing several reaction pathways looking at the product distribution. However, only single model compounds were tested in the cited work. Recently, the same research group reported the study of a kinetic modelling of a Fischer-Tropsch real water using a nickel-copper catalyst supported on ceria-zirconia [90]. Chen and co-workers suggested for the first time to use catalytic aqueous phase hydrodeoxygenation (APHDO) for converting FT aqueous effluent into fuel gas, using a Ru catalyst [148]. The same research group looked to the stability issues regarding the catalyst, proposing titania and zirconia as the most promising support due to their hydrothermal stability [89]. Despite, the interesting results, a high consumption of hydrogen is necessary for the APHDO that is produced using fossil-based sources.

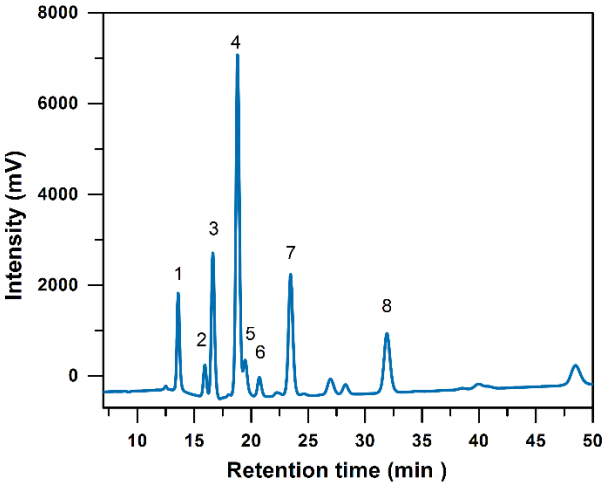
In the present chapter, the results of the aqueous phase reforming application to the real aqueous stream derived from the FT process are shown. The purpose is double: reducing the organic content of the water and producing renewable hydrogen. The aqueous effluent derived from a pilot-scale FT plant was characterized and subjected to APR using a Pt/C reference catalyst. This catalyst formulation was chosen because it provides high performance in terms of activity, selectivity and stability for aqueous phase reforming of alcohols. Dedicated tests with representative model compounds were performed to understand the results obtained with the real phase.

The novel approach proposed in this thesis shows an alternative pathway to utilize the FT product water contaminated with light oxygenates, at the same time increasing the carbon efficiency and producing a valuable gas phase.

3.1. Characterization of the FT product water

In Figure 21 the HPLC chromatogram of the FT product water is reported, together with the main information on its composition summarized in the table on the right (please note that only the compounds with weight concentration higher than 0.01% were reported). As reported in the introduction, the wastewater of the Fischer Tropsch process is typically constituted by alcohols and carboxylic acids. Alcohol formation may be due to parallel reactions that involve the insertion of carbon monoxide into a methylene- or methyl-metal bond [149]. As a matter of fact, the main compounds observed in the examined water fraction are low molecular weight primary alcohols C1-C4 such as methanol, ethanol, propanol, and butanol, together with their corresponding carboxylic acids. Secondary alcohols such as 2-propanol are present to a minor extent.

The quantification of these compounds is reported in the displayed table. The total organic content is around 4700 mg C/L. The HPLC quantification accounted for 95% of the total carbon content. The use of GC-MS (not shown results) allowed to increase the range of identified compounds up to C6 alcohols and corresponding carboxylic acids. The main inorganic species identified and quantified by ICP-MS are calcium, sodium, and potassium.



TOC (mg C/L)	Alcohols		Inorganics	
4700	Compounds	wt.%		ppm
	Methanol	0.41	Na	412 ± 21
	Ethanol	0.29	K	10 ±4
	1-Propanol	0.07	Ca	2392 ± 47
	2-Propanol	0.01		
	1-Butanol	0.05		
	1-Pentanol	0.02		
	Carboxylic acids			
	Acetic acid	0.06		
	Propionic acid	0.02		
	Butanoic acid	0.03		

Figure 21. On the left, HPLC chromatograms of the Fischer-Tropsch product water (1: acetic acid 2: propionic acid 3: methanol 4: ethanol 5: butanoic acid 6: 2-propanol 7:1-propanol 8: butanol); on the right, quantification of the main organic and inorganic compounds.

3.2. Aqueous phase reforming of FT product water

3.2.1. Influence of reaction temperature

In this section, the influence of reaction temperature applied in APR of Fischer-Tropsch product water is discussed.

In Figure 22 the gas performance indicators of APR are reported at different temperatures in the range between 230-270 °C. It can be observed that each of the three indicators has been positively influenced by the increase of the reaction temperature. The carbon to gas increased from 40% to more than 60%, due to the more favorable C-C bond breaking with enhanced reaction temperature. Moreover, the hydrogen gas distribution was affected by the higher temperature. This is an important point, as it implies that the desired reactions (i.e. breaking of the C-C bonds and water gas shift) are more favored compared to undesired reactions (such as methanation) with the increase of the temperature. The combination of the higher carbon conversion and H_2 gas distribution led to higher hydrogen productivity, that is a major finding when complex mixtures are tested.

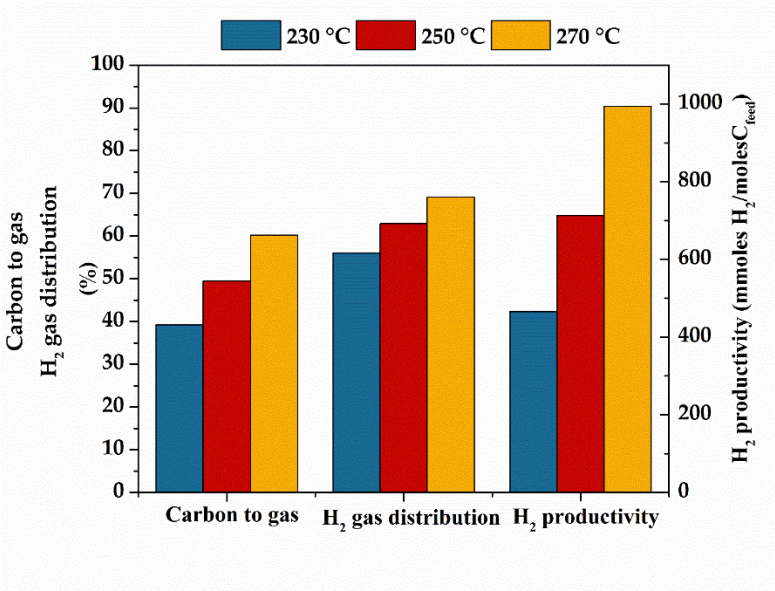


Figure 22: Influence of the reaction temperature on the APR of FT product water. Gas performance indicators. Reaction conditions: 0.375 g Pt/C catalyst, 75 mL FT product water, 2 hours reaction time.

The HPLC chromatograms reported in Figure 23 compare the feed with the liquid products obtained after APR at different temperatures. Firstly, it is important to observe that minor differences are present in the liquid phase composition among the investigated range of temperatures. At 230 °C, most of the alcoholic compounds converted, with only methanol showing a lower conversion and a higher dependency on the reaction temperature (Figure 24). Its conversion stopped at 40% at 230 °C, while the conversion of ethanol and 1-propanol reached 85% and 92%, respectively. The reason for the observed behavior may be ascribed to slight competitive issues in the mixture with the other molecules, reducing its reactivity. Shabaker et al. reported that the order of reaction of methanol reforming is higher than ethylene glycol on Pt because of the weaker adsorption of the former on the metal sites compared to the latter adsorbed in a bidentate mode [42]. Being ethanol adsorption mode similar to the one of ethylene glycol, it can be assumed that its higher reactivity can be explained by analogous reasonings [150].

Looking at the comparison between primary alcohols at equal temperature, it is observed that there is an increase in the activity with the increase of the chain length, and the difference is more visible at low temperatures (230-250 °C).

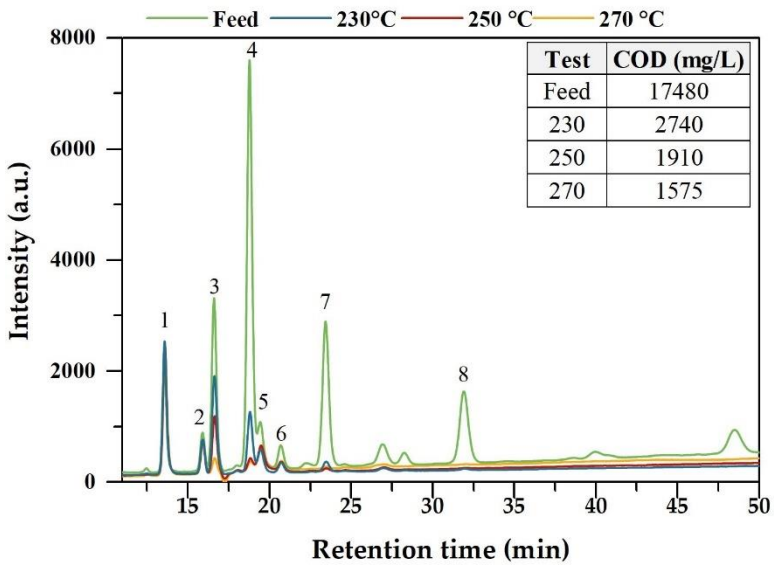


Figure 23: HPLC chromatograms of the feed and products (1: acetic acid 2: propionic acid 3: methanol 4: ethanol 5: butanoic acid 6: 2-propanol 7:1-propanol 8: butanol), together with COD data. Reaction conditions: 0.375 g Pt/C catalyst, 75 mL FT product water, 2 hours reaction time.

Alcohols are known to be highly reactive to produce hydrogen via APR [39]. On the contrary, carboxylic acids remained almost entirely in the liquid phase. The concentration of acetic acid increased, moving from 630 to 730 ppm; this is the reason why an apparent negative conversion is reported in Figure 24. Acetic acid can follow two different routes. It can be converted by reforming, leading to methane and carbon dioxide[85]; at the same time, it can be produced by primary alcohol (mainly ethanol) reforming, as reported in paragraph 3.2.3. During APR of ethanol, acetic acid was the only observed liquid by-product, to produce 100 ppm of acetic acid 2.5% of the starting ethanol should react trough hydro-dehydrogenation reaction to produce it. As detailed later, ethanol may be firstly dehydrogenated to acetaldehyde, which in turn can lead to acetic acid via Cannizzaro/ Tishchenko-like reactions. Moreover, acetic acid can suffer from competitive adsorption when it is in mixture with alcohols. In our previous work with a platinum-based catalyst supported in alumina, we reported that in the case of a binary mixture of ethanol/acetic acid, the conversion of the latter was negligible [85]. Therefore, due to the recalcitrance of the carboxylic acid when present in a mixture, in the current conditions its concentration globally increased. This is a major finding that was not reported yet in literature for the valorization of FT effluent because it was conventionally modeled only by alcohols. Interestingly, propionic acid's conversion showed a decreasing trend with temperature. Analogously with acetic acid, it can convert mainly producing ethane and carbon dioxide; at the same time, it can be produced by 1-propanol reforming, as reported later. It is likely that in this case, due to the lower concentration of 1-propanol compared to ethanol, less propionic acid is obtained, globally leading to a positive conversion.

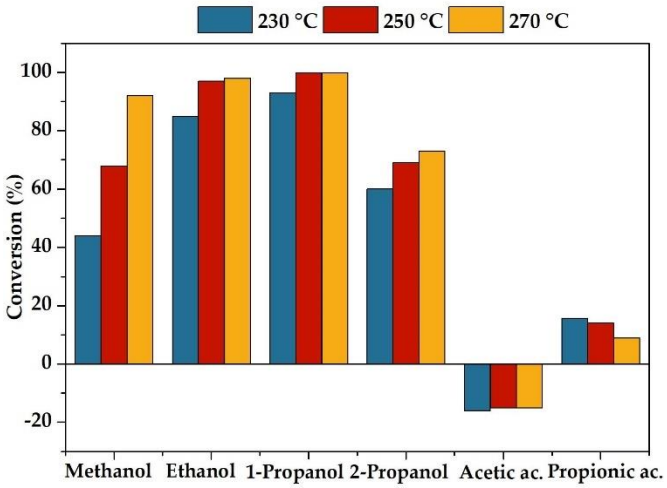


Figure 24: conversion of the main molecules present in the feed. Reaction conditions: 0.375 g Pt/C catalyst, 75 mL FT product water, 2 hours reaction time.

Finally, it is interesting to observe that the reforming of the product water considerably decreased the COD (chemical oxygen demand) of the stream as showed in the table enclosed in Figure 23. Indeed, it was reduced by more than 80% at 230°C and up to 90% at 270 °C. These results are comparable to the ones obtained by Majone et al. using a packed bed biofilm reactor to decrease the organic content of a synthetic FT product water [146].

3.2.2. Influence of reaction time

The obtained results showed that two hours are not enough time to convert a sufficient amount of organic oxygenates and reduce the COD down to legislative wastewater regulations, being methanol and carboxylic acids still present in the liquid APR product. In order to assess if more time could lead to a higher conversion of the organic alcohols and increase the hydrogen production, the influence of reaction time on the performance indicators was studied.

Figure 25 shows the progression of the main gas performance indicators at the different reaction time investigated. Please note that the point at 0 hours indicates the achievement of the operating temperature (270 °C), that is the starting point for the reaction time. For this reason, the evolution of the molecules in the liquid and gaseous phase (Figure 27) originates at "-1", taking into account the time necessary to heat the solution to 270 °C.

The three indicators constantly raised until two hours, whereas increasing the reaction time up to 4 hours did not improve appreciably the performance. Similarly, with the temperature increase, both the carbon to gas conversion and the H_2 gas distribution increased, indicating that the FT product water did not suffer from series-selectivity issues in the current reaction conditions.

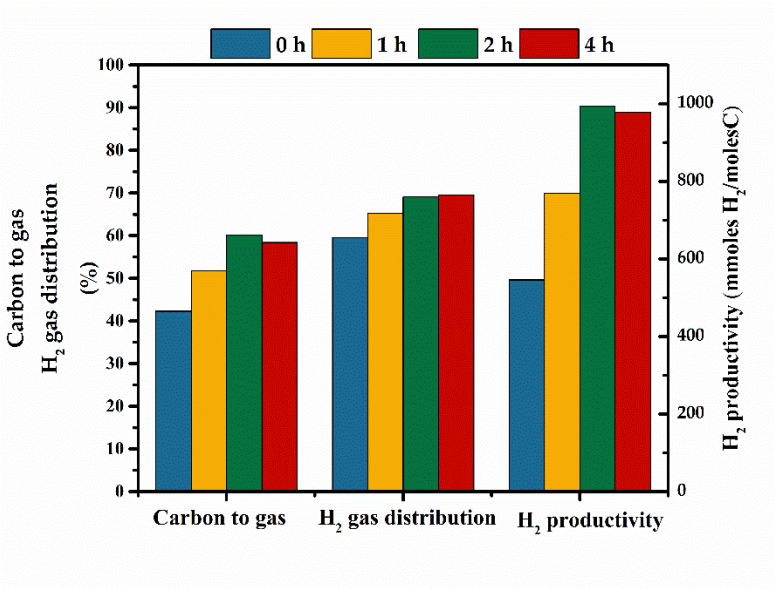


Figure 25: Influence of reaction time on the APR of the FT product water. Gas performance indicators. 0.375 g Pt/C catalyst, 75 mL FT product water, 270 °C reaction temperature.

In the liquid phase, each of the alcohols started to react to a high extent already during the heating time of the reactor (0 h), as reported in Figure 26.

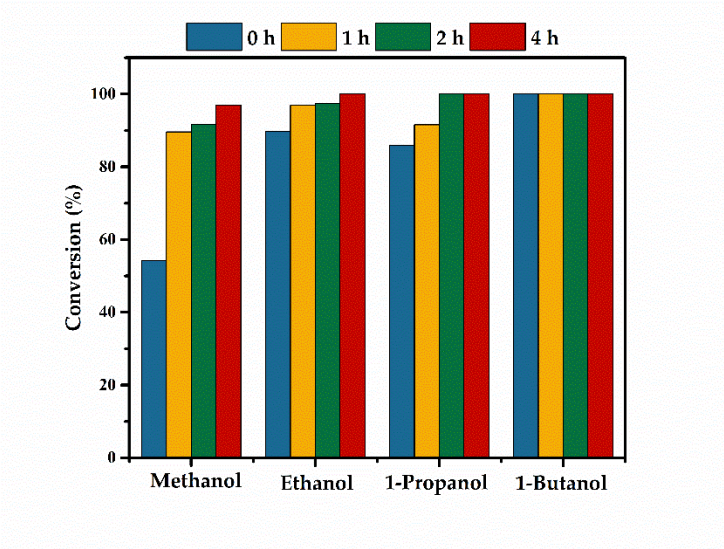


Figure 26: Influence of reaction time on the APR of the FT product water. Conversion of the main alcohols in the feed. 0.375 g Pt/C catalyst, 75 mL FT product water, 270 °C reaction temperature

From this point on, methanol was almost the only compound present in the liquid phase (Figure 27 left). Methanol conversion rate was approximately 5.2 mmol/h, while ethanol conversion rate was about 4.3 mmol/h; however, methanol's concentration in the FT water is almost double than the ethanol's concentration. Therefore, it was reasonable to expect a higher difference between the two conversion rates. This outcome, consistent with the results reported in the previous paragraph, may suggest that methanol suffer from competitive adsorption with the other alcohols (mainly ethanol in the current case), reducing its consumption rate.

The hydrogen production constantly increased over time (Figure 27 right); at 0 hour, 17 millimoles of hydrogen were produced, which increased up to 31 at 4 hours; it can be motivated by an almost complete conversion of 1-propanol and ethanol at this time. Indeed, as we reported in the previous paragraph, ethanol and 1-propanol reached a high conversion already at 230°C. On the other hand, methanol, having a slower conversion over time, can cause an increase of hydrogen and CO_2 observed during longer reaction time. In fact, the H_2/CO_2 ratio tends to be close 3, which is the theoretical H_2/CO_2 ratio for methanol APR (equation 18). Looking at methane and ethane, their production reached its plateau already at 0 hour; as reported in the following paragraph, methane is produced by the conversion of ethanol and ethane by the conversion of 1-propanol; indeed, they both converted already at 0 hour and, for this reason, their presence does not increase after that point.

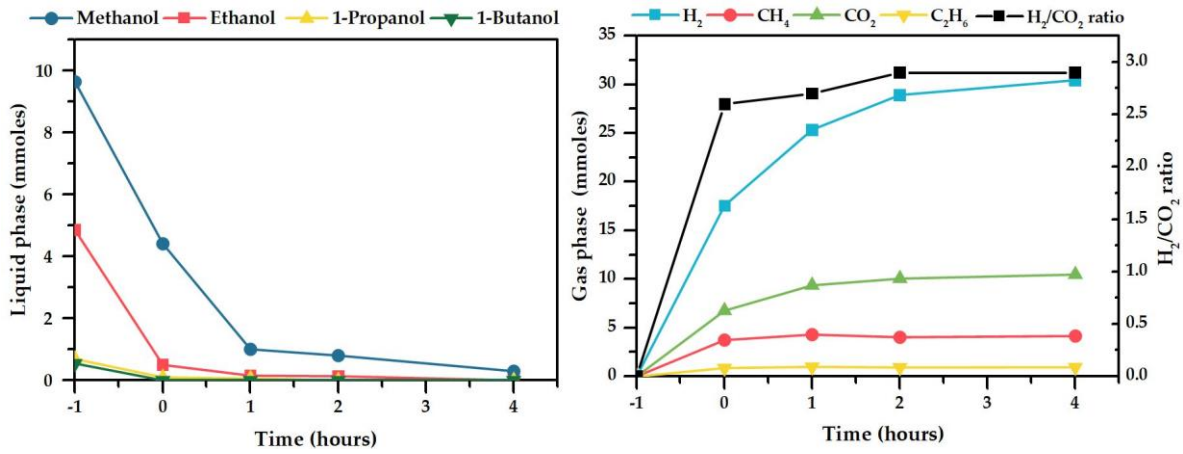


Figure 27: Influence of reaction time on the APR of the FT product water. left: evolution of the liquid species; right: evolution of the gaseous species and H_2/CO_2 ratio. Reaction conditions: 0.375 g Pt/C catalyst, 75 mL FT product water, 270 °C reaction temperature.

3.2.3. Aqueous phase reforming of single compounds

The complexity of the FT product water does not allow us to get qualitative information on the reactions that lead to the observed product distribution. To get deeper into these outcomes, in this section the results obtained from the APR of the main compounds present in the FT product water are discussed.

APR tests of ethanol, methanol, 1-propanol, 2-propanol, 1-butanol, and 2-butanol at 0.9 wt. % of carbon were carried out at the optimal reaction conditions identified for the real mixture (5% Pt/C catalyst, 270°C, 2 hours).

In Figure 28-A the gas composition obtained from the APR of single-compound solutions is reported.

Methanol follows the conventional aqueous phase reforming stoichiometry. In fact, the reforming ratio (i.e. the ratio between moles of hydrogen and carbon dioxide), calculated from the gas composition reported in Figure 28, is 3.5 and it is close to the theoretical value (i.e. 3) derived from eq. 13. The higher ratio can be explained by the contribution of hydrogen-producing reactions

(dehydrogenation), commonly considered the first step of the APR reaction mechanism, not leading to the contemporary production of a mole of carbon dioxide (such in the case of water gas shift reaction).

C:OH = 1:1 $CH_3OH + H_2O \rightarrow CO_2 + 3H_2$ (Eq. 18)

Looking at the gas composition obtained from the APR of C2-C4 primary alcohols, it is highlighted that, despite the difference, the gas composition can be considered analogous. Indeed, the APR of primary alcohols is accompanied by a gas composition with 2:1:1 ratio in hydrogen: carbon dioxide: methane (or ethane, or propane) from ethanol (or 1-propanol, or 1-butanol).

Looking at the conversion of the primary alcohols, no main differences were found between the tests, and they converted almost completely (Figure 26). The corresponding aldehydes, largely reported in the literature as the first reaction intermediates of APR, were not observed in the liquid phase. This difference should not be ascribed to a change in the reaction mechanism. It can be due to the high reactivity of both reactants and intermediates, together with the high conversion reached in this work compared to some of the commonly reported low conversions in other researches [151]; moreover, due to the high volatility of the aldehydes, they can be lost during the filtration step.

The liquid phase derived from methanol APR was constituted only by the unconverted molecule (Figure 28-B). On the other hand, the C2-C4 primary alcohols produced the homologous carboxylic acid as the main by-product. This is likely due to a Cannizzaro or Tishchenko reactions, as suggested by Lobo et al. [152]. Therefore, it is supposed that the aldehyde formed during the dehydrogenation of the primary alcohol may lead to the corresponding carboxylic acid via condensation of two aldehydes, followed by hydrolysis.

In our previous work with Pt/Al_2O_3, it was reported a similar behavior of primary alcohols in the range 230-270 °C [85]. Lobo et al. carried out the APR of 1-propanol on platinum supported on several materials (alumina, titania, ceria), finding different activities among the catalytic systems, but similar selectivity in the product distribution [152]. These results suggest that the support does not play a role in determining the gas product distribution of primary alcohols APR.

Coronado and co-workers reported results with a Ni-based catalysts on APR of methanol, ethanol, and 1-propanol [91]. Regardless of the composition of the catalyst (undoped or doped with Cu/Ce), the molar fraction of hydrogen in the APR of ethanol and 1-propanol was higher than 50% as it was in the present work, ranging from 63% to 85%. Several reasons may justify this difference. It should be excluded that the higher concentration of hydrogen is due to more favorable WGS, as it was reported the presence of CO with the use of Ni catalysts, while it was not detected in the current work; it can be suggested that Pt is more prone to activate the decarbonylation of the aldehyde (Figure 29-A, with the APR scheme of 1-butanol for the sake of representativeness), leading to a higher production of gaseous products. This hypothesis would explain also the difference regarding the composition of the liquid phase. In fact, we observed no other liquid products apart from the unconverted alcohol and the corresponding carboxylic acid; on the other hand, the use of a Ni catalyst led only to the corresponding aldehyde as liquid product [91].

Comparing in a rigorous way the two results is complex due to the different reaction conditions (starting from the use of a batch and a continuous reactor). However, having reported that the APR selectivity of primary alcohols is quite insensitive to different reaction temperature and concentration of the feedstock, we may ascribe the reported differences to the nature of the active site.

Most of the literature highlights the importance of the C:O ratio for aqueous phase reforming [39]. However, as already mentioned by Godina et al., only one carbon can be removed as CO in molecules where only one OH group is present [86]. Afterward, it can react with water through WGS reaction producing H_2 and CO_2. As reported in [85] for the linear alcohols with only one OH, the real reaction path in the APR reaction using a platinum catalyst are the following (eq. 19-21)

C:OH = 2:1 $C_2H_5OH + H_2O \rightarrow 2H_2 + CH_4 + CO_2$ (Eq. 19)

C:OH = 3:1 $C_3H_7OH + H_2O \rightarrow 2H_2 + C_2H_6 + CO_2$ (Eq. 20)

C:OH = 4:1 $C_4H_9OH + H_2O \rightarrow 2H_2 + C_3H_8 + CO_2$ (Eq. 21)

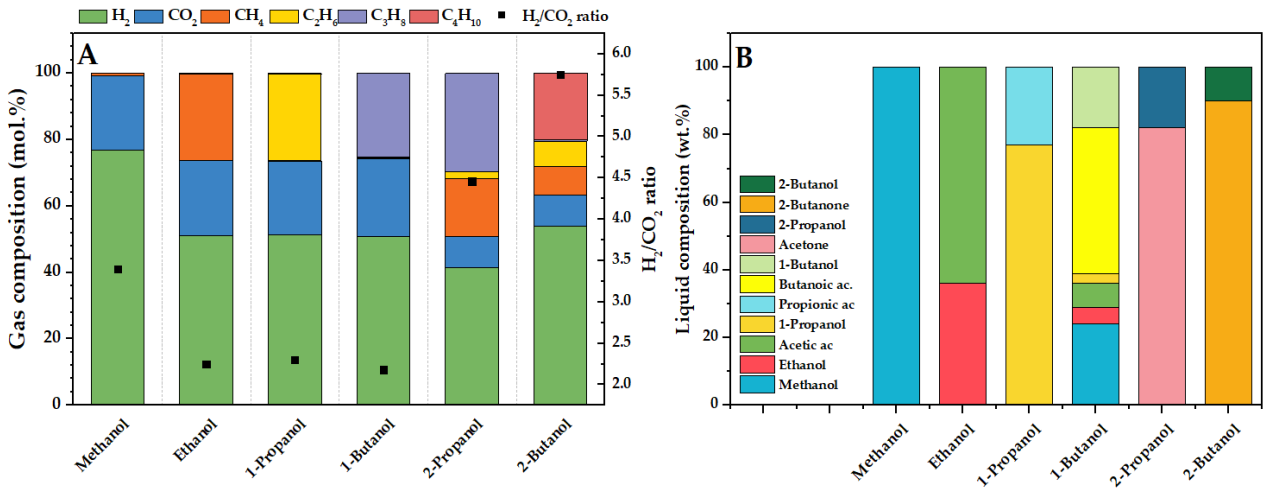


Figure 28. Influence of the feed on the gas (A) and liquid (B) composition. Reaction conditions: 0.375 g Pt/C catalyst, 75 mL solution 0.9 wt.% C, 270 °C reaction temperature, 2 hours reaction time.

On the other hand, secondary alcohols such as 2-propanol and 2-butanol showed a completely different reaction path. As reported in Figure 28-A, two main differences can be highlighted in the gas phase. The first one regards the hydrogen/carbon dioxide ratio, equal to 4.5 from 2-propanol and 5.7 from 2-butanol. The second one regards the presence of the corresponding alkane, i.e. 28% of propane from 2-propanol and 20% of butane from 2-butanol. The much higher ratio between hydrogen and carbon dioxide than the one proposed by the APR, together with the presence of alkanes with the same number of carbon atoms, let us suppose that other mechanisms are involved in the hydrogen production, without water gas shift and C-C bond breaking. The difference in the gas composition between primary and secondary alcohols is reflected also in the liquid composition (Figure 28-B), where acetone from 2-propanol APR and 2-butanone from 2-butanol APR were found as only liquid products.

From this information on the gas and liquid phase, it can be proposed that the main reaction in which the secondary alcohols are involved is the dehydrogenation (Figure 29-B). The presence of butane suggests that also hydrogenation reactions are involved in the mechanism. Furthermore, smaller alkanes are present in the gas phase, such as ethane and methane. We propose that one hydrogen molecule is involved in the cleavage of the C-C bond, leading to the formation of one molecule of methane and one mole of the linear alcohol (1-propanol in the case of 2-butanol APR). At this point, the latter can react giving the already known products, that are hydrogen, carbon dioxide and ethane. The suggested mechanism is confirmed by the relative composition of the gas phase, where a 1:1:1 ratio is reported between methane, carbon dioxide, and ethane. Even if not reported in the figure, an analogous pathway can be suggested for 2-propanol, where is coherently observed a 2:1 ratio between methane and carbon dioxide (in this case, ethanol is the intermediate primary alcohol that is consumed).

The reported results underline not only the importance of the C:OH ratio but also the effect of the position of the hydroxyl group. To the best of our knowledge, it has been reported here for the first time for 2-butanol, allowing to confirm the peculiar behavior of secondary alcohols reported by us and other authors in previous works [85], [91].

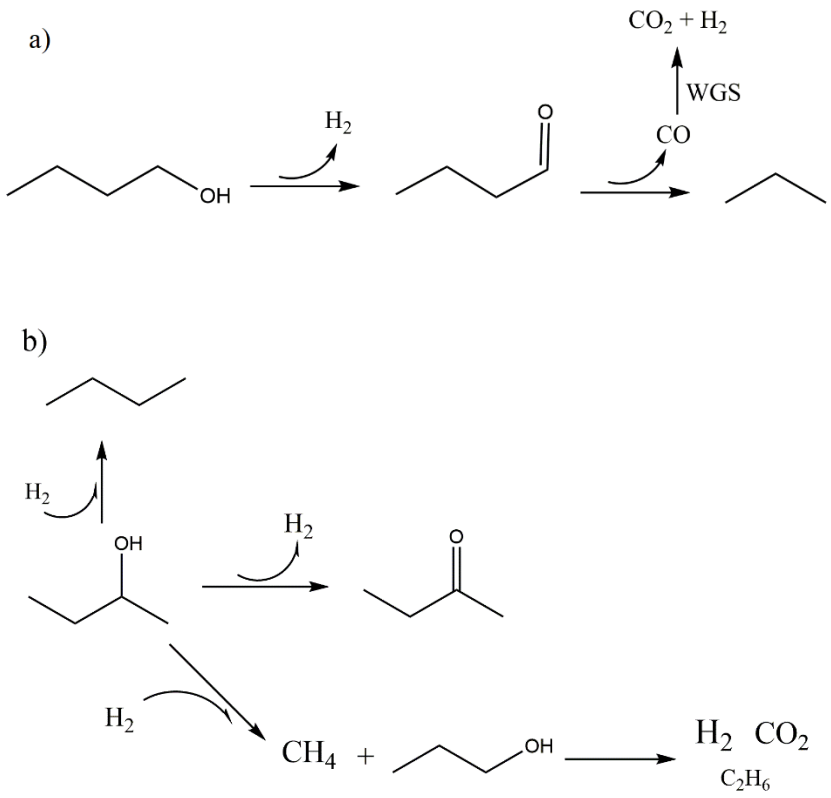


Figure 29. Suggested reaction mechanism for APR of primary (a) and secondary (b) alcohols.

To summarize the differences between primary and secondary alcohols, the following Table 9 depicts the main products (liquid and gas) observed from their APR.

Table 9. Main products of APR of alcohols.

	H_2	***CO_2***	***Alkanes***	***Ketones***	***Carboxylic acids***
MeOH	X	X	no	no	no
EtOH	X	X	CH_4	no	Acetic acid
1-PropOH	X	X	C_2H_6	no	Propionic acid
1-ButOH	X	X	C_3H_8	no	Butanoic acid
2-PropOH	X	X	C_3H_8, CH_4	Acetone	no
2-ButOH	X	X	C_4H_{10}, C_2H_6	2-Butanone	no

Based on the APR of the single compounds and the conversion of FT product water, it is possible to address the contribution of each component of the liquid phase to determine possible interferences among the reactions that involve each alcohol (Table 10). For the sake of comparison, the gas products obtained during the APR of FT water fraction at 270 °C and 2 h reaction time was reported.

The linear combination of the single reactions was calculated with the following equation 22 for each gas:

$$n_{H_2} = n_{H_{2methanol}} + n_{H_{2ethanol}} + n_{H_{2\,1-propanol}} + n_{H_{2\,1-butanol}} \quad \text{(Eq. 22)}$$

where $n_{H_{2methanol}} = \frac{n_{H_2 methanol_{SCT}}}{n_{conv\ methanol_{SCT}}} \cdot n_{conv\ methanol_{FT}}$

n_{H_2} is the number of moles of hydrogen reported in Table 3 in the row named "Total". Obviously, the same can be written for CO_2, CH_4, etc. They are calculated summing the moles of H_2 produced by each alcohol during the corresponding test (e.g. $n_{H_{2methanol}}$ refers to the moles of hydrogen produced during the APR of methanol). However, the amount of alcohol used during the single-compound test (SCT) is different from the amount of alcohol present in the FT water. Therefore, if we assume that the moles of product ($n_{H_2 methanol_{SCT}}$) per mole of alcohol reacted ($n_{conv\ methanol_{SCT}}$) remain constant between the single-compound test and the FT test (i.e. the selectivity remains constant), we can obtain the "ideal" contribution of each compound multiplying this ratio by the moles of alcohols reacted during the FT test ($n_{conv\ methanol_{FT}}$) to obtain the final value.

As it can be observed, the product distribution in the case of the FT water APR is consistent with the summation of the results obtained in the case of single-compound APR.

Thank to this outcome, we may assume that no interference is present between the alcohols. This result is consistent with previous outcomes reported with a mixture of polyols [44].

Table 10. Linear combination of single model compound in comparison with FT water fraction results.

Test	*H_2 (mmoles)*	*CO_2 (mmoles)*	*CH_4 (mmoles)*	*C_2H_6 (mmoles)*	*C_3H_8 (mmoles)*
FT- 270 °C 2h	**29.0**	**10.4**	**4.1**	**0.9**	**0.5**
Methanol	23.6	7.2	0	0	0
Ethanol	7.1	3.1	3.3	0	0
1-Propanol	0.9	0.4	0	0.4	0
1-Butanol	0.8	0.4	0	0	0.4
Total	32.4	11.1	3.3	0.4	0.4

3.2.4. Catalyst stability

To assess the feasibility of the exploitation of the FT product water a test in which the catalyst was reused at 270°C was performed.

The tests were performed using 100 mg of catalyst to reduce the conversion of the reactants and detect possible catalyst deactivation. After the first use, the catalyst was recovered and dried in the oven overnight at 105 °C. In Figure 30 the conversion of the main compounds is reported at each test, together with the hydrogen productivity. The plot highlights that no deactivation occurred during the three tests. Moreover, a slight increase of the hydrogen productivity was reported due to the increase of the selectivity. This result may be coherent with the outcome reported by Lehnert et al., who showed that higher particle size led to similar glycerol conversion but higher hydrogen selectivity [105]. We may assume that during the current reaction conditions, our catalyst suffers from slight sintering phenomena, as reported with platinum-based catalysts used in previous works [153]. In a previous work, we saw a quick deactivation of the catalyst with real feedstock [44]. It is noteworthy that the Fischer-Tropsch water fraction may be an ideal feedstock for APR valorization. Indeed, it was reported that the hydrolysate derived from a commercial bioethanol plant can deactivate the catalyst because of the formation of solid deposits (humins) derived from homogeneous reactions of the sugars [44]. Therefore, due to the absence of unstable compounds in the solution (like sugars), the FT water fraction may not constitute a challenging feed to be valorized via APR, from the point of view of the catalyst stability. Further research with a continuous reactor is suggested to better evaluate this phenomenon.

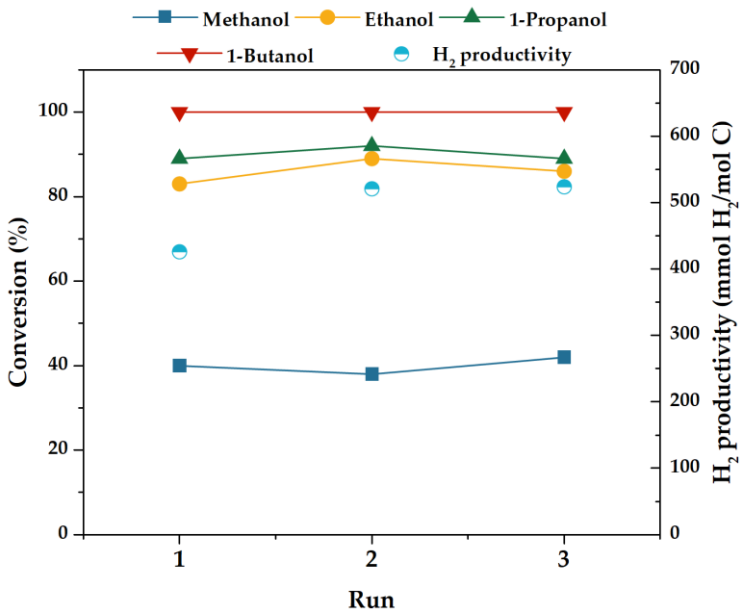


Figure 30. Influence of catalyst re-use on the APR performance of FT product water. Reaction conditions: 0.1 g Pt/C, 75 mL FT product water, 270 °C reaction temperature, 2 hours reaction time.

3.2.5. Conclusion

The water fraction produced by Fischer-Tropsch synthesis has been investigated for its valorization via aqueous phase reforming. The influence of reaction temperature and time on the performance of the process was investigated, using a reference platinum-based catalyst. The increase of temperature affected both the activity and the selectivity of the catalyst, increasing the hydrogen production. The COD of the mixture was reduced up to 90% of the original one, working at 270 °C and with 2 hours. Representative model compounds have been tested in similar conditions to understand the phenomena involved in the APR of the real mixture. Methanol reached the complete conversion after 4 hours, while higher alcohols converted at shorter reaction time. Despite the complexity of the mixture, neither interference between the molecules nor deactivation phenomena were observed in the aqueous phase reforming. The difference in the product distribution for primary and secondary alcohols reforming pointed out the importance of the position of the hydroxyl group in the molecule and helped to propose a general reaction mechanism for the studied substrates.

Chapter 4

Hydrothermal liquefaction water fraction

This chapter including results, figure and table is based on published works [154] and [155]

Among the possible biomass conversion pathways, hydrothermal liquefaction (HTL) has been studied to produce an intermediate energy carrier, namely biocrude, with an oxygen content depending on the feedstock used and the reaction conditions [156]. The main advantage of HTL with respect to similar processes (e.g. pyrolysis) is the possibility to treat feeds with a high moisture content (up to 90 wt.%, such as in the case of aquatic biomass), eliminating or drastically reducing the need for a drying pre-treatment [157].

As well as the desired biofuel, HTL also produces a gas phase (rich in carbon dioxide), a solid phase (containing most of the inorganics present in the feed) and an aqueous phase, which contains short chain oxygenated hydrocarbons that are not soluble in the organic phase The aqueous phase derived from hydrothermal liquefaction is a primary concern for the development of the technology, as confirmed by the U.S. Department of Energy [158]. It cannot be disposed of without a proper post-treatment; moreover, the recycle of the aqueous phase may be a key element to improve the economic feasibility of the entire process, significantly reducing the demand for freshwater at the inlet of the HTL reactor [159]. For this reason, some options have been proposed in literature, such as hydrothermal gasification and anaerobic digestion [160], [161].

Panisko et al. characterized the aqueous phase obtained from the HTL of pine forestry residuals showing that it is mainly constituted by organic acids, such as glycolic acid and acetic acid, as well as alcohols (methanol and ethanol) and ketones (acetone and cyclopenta-ones) [83]. Overall, the wastewater contains about 2 wt.% of organic carbon; however, it is even more important to highlight that the carbon yields in the aqueous phase (i.e. the fraction of carbon that ended up in the aqueous phase with respect to the original carbon content in the biomass feed) are in a range of 28 – 45 wt.%. This result not only points out the need to valorize also the organic compounds in the HTL-derived water, if the entire carbon heritage of the feedstock is to be exploited, but it also underlines the necessity to treat this water phase in order to allow its recycling within the process, thereby reducing the make-up of fresh water in the HTL feed. Similar considerations derive from the characterization of the aqueous fraction originating from the HTL of algae and municipal/food industry wastes [162], [163].

Confirming the strategic importance of the valorization of secondary streams, two reviews have recently been published addressing the urgent need for of new processes to tackle this challenge [24], [164].

In the present chapter, the conversion of the water-soluble organic compounds derived from HTL through the aqueous phase reforming (APR) was approached, with the purpose of producing renewable hydrogen to be integrated into biorefinery processes.

The aim is to investigate if APR can be a viable option to valorize the water stream derived from a hydrothermal liquefaction process. Indeed, the APR can also contribute to the production of the hydrogen necessary for upgrading the HTL biocrude through hydrotreatments. In this context, the aqueous phase reforming would be perfectly integrated in a biorefinery concept, reducing the dependency from external sources of hydrogen, helping to generate a biofuel with an oxygen level compatible with the final specification downstream processing (Figure 31). We initially investigated the APR of model compounds, looking at the influence of the nature of the substrate, its concentration and the reaction time. The majority of the literature research has been devoted to the study of alcohols and poly-alcohols such as methanol and glycerol (for example [36], [41], [42], [91], [105], [165], [166]), but most of the remaining compounds have not been studied yet in detail for aqueous phase reforming (i.e. glycolic acid, propionic acid, cyclopentanone, guaiacol), despite their importance for the sustainability of the process. A ternary mixture was also tested to simulate a possible multi-component aqueous phase composition. Finally, in order to be as close as possible to the actual application, we performed the APR of a water produced by the hydrothermal liquefaction of a biorefinery-derived lignin-rich stream. A thorough study was performed in order to evaluate how the solvent, used during the extraction of the aqueous phase, affects the following APR step, referring in particular to the influence on the activity and stability of the catalyst.

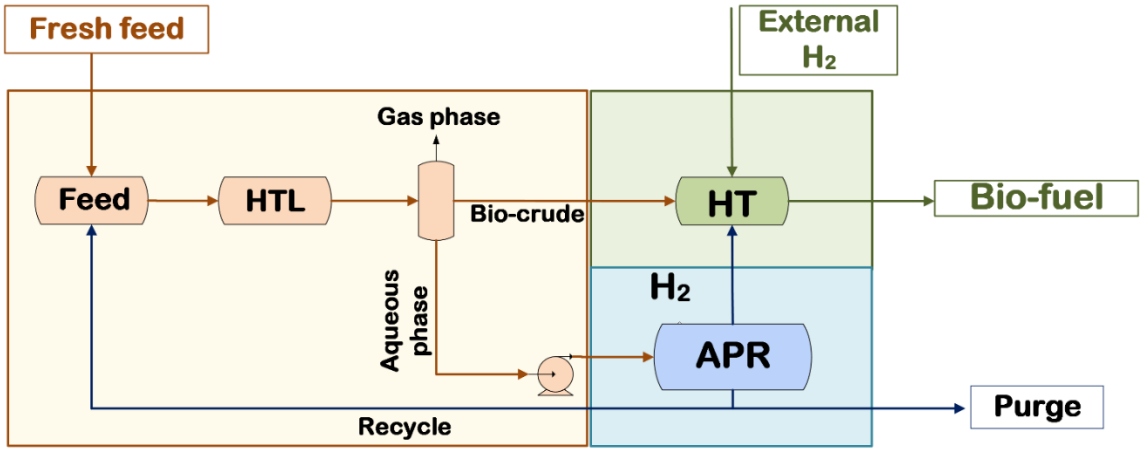


Figure 31: Block flow diagram of a HTL-APR integrated plant. HTL: hydrothermal liquefaction; HT: hydrotreatment (upgrade block).

4.1. Model compound

4.1.1. Influence of carbon concentration

Based on the analysis of the literature ten compounds were selected for the evaluation of the influence of the concentration on the APR process [83], [85].

The main results are reported in Table 11 for each compound in the range 0.3 – 1.8 wt.% of carbon. This range was chosen in order to investigate the diluted conditions commonly observed in literature.

Acetic acid and propionic acid were chosen to represent the carboxylic acids class. Both compounds showed a drastic decrease of the carbon conversion to gas with the increase of the concentration in the solution, moving from 80% to 15% for acetic acid and from 75% to 5% for propionic acid. Even if the reaction conditions did not allow to extrapolate kinetics, we may assume that there was a strong inhibiting effect of the feed, as the levels of conversion are inversely proportional to the concentration [42]. On the other hand, the selectivity towards alkane formation (i.e. the hydrogen gas distribution) and the H_2/CO_2 ratio remained constant on the whole range. It should indicate that new reaction pathways are not favored.

As we reported in [85], in which a Pt/Al_2O_3 catalyst was used, acetic acid and propionic acid mainly lead to the formation of a gas mixture composed by 50% carbon dioxide and 50% methane (or ethane in the case of propionic acid). This result was confirmed with the active carbon support used in this work, highlighting that the gas product distribution is neither influenced by the concentration nor by the support used for the catalyst, the nature of the active sites being the main responsible of the catalytic decomposition to CO_2 and alkanes. Given the low H_2 selectivity, the APR-H_2 yield was low at each tested concentration.

Glycolic acid and lactic acid were chosen as the most representative hydroxyacids in the aqueous effluent of hydrothermal liquefaction. Indeed, glycolic acid was reported as the main compound in the aqueous phase coming from the HTL of corn stover [83]. Despite a decrease of the carbon conversion to gas, the influence of the concentration is less evident as compared to the case of the carboxylic acids. On the other hand, a strong difference between the two compounds can be observed looking at their hydrogen yield. Glycolic acid showed a decrease in the hydrogen production due to the lower conversion, but maintained at least 30% yield at 1.8 wt.% C. Instead, the lactic acid yield was always below 5%, despite similar levels of conversion. As reported in the following section 3.1.2, lactic acid produces carbon dioxide and ethane due to the formation of propionic acid as reaction intermediate, recalcitrant to hydrogen production. On the other hand, the glycolic acid led only to a slight production of acetic acid, while selectively produced carbon dioxide and hydrogen in a ratio close to the stoichiometric one. Please note that the APR H2 selectivity higher than 100% are ascribed to further hydrogen-producing reactions, such as dehydrogenation (the same comment is valid for methanol).

Methanol and ethanol were investigated as they are likely present in the post-HTL aqueous phase [83]. The carbon conversion to gas of methanol decreased with the increase of the carbon

concentration from 58% to 20%, while the APR-H_2 selectivity and H_2 gas distribution remained almost constant and close to 100%. Methanol was largely investigated as model compound for APR since it is the simplest alcohol to perform this kind of investigation [36], [42], [91], [167]–[169]. These results can be explained by the structure of the alcohol that is readily dehydrogenated producing only hydrogen and carbon monoxide, reducing parallel and consecutive reactions (e.g. methanation or Fischer-Tropsch) involving different fragments of the molecule (such as alkyl groups); afterwards, the carbon monoxide is converted to carbon dioxide and hydrogen by reaction with activated water. Ethanol showed higher carbon to gas conversion than methanol thanks to the production of methane, together with carbon dioxide. Due to the production of the alkane, the hydrogen gas distribution was nearly 50%, constant in the whole range of concentration. It is interesting to observe that no difference in performance were reported between 0.3% and 0.9%. This fact should be due to the lower strength of adsorption of ethanol compared to methanol, that caused an apparently linear rate of consumption up to 0.9% of carbon.

Cyclopentanone was reported as one of the most present ketones in the post-HTL aqueous phase [83]. It is a valuable compound used, for example, in the preparation of specialty chemicals for the pharmaceutical or cosmetic sector [170]. Nevertheless, as it is present in very diluted concentrations, it is uneconomically envisaging a selective recovery. It was almost unreactive in the investigated reaction conditions (with about 20% of conversion of the feed in the whole range of concentration), showing the lowest carbon conversion to gas among the ten screened compounds. It is interesting to observe that the hydrogen gas distribution and the APR-H_2 selectivity were strongly influenced by the carbon concentration. The latter increased strongly with the increase of the concentration, thanks to the fact that the hydrogen production linearly increased in the studied range, while the carbon dioxide production had a maximum at 0.9% wt.% carbon. Moreover, it was observed that the weight of the catalyst recovered was higher than the initial 375 mg (the accuracy of the recovery procedure should be in ±5% range, assessed in organics-free blank tests). For this reason, it can be assumed that high-molecular weight compounds may be produced by aldol-condensation [171].

Glutaric acid was chosen as a typical example of bi-carboxylic acid. A strong decrease in the carbon conversion to gas was observed with the increase of the concentration, from 75% down to 25%. Interestingly, the analysis of the liquid phase showed an increase of the selectivity toward the formation of liquid products, mainly butanoic acid. In fact, while the conversion to gas phase decreased, the conversion of the feed remained approximately constant, favoring the formation of liquid by-products (propionic and acetic acid together with the butanoic acid). In analogy with the mono-carboxylic acid, the first reaction seems to be therefore the decarboxylation. Afterwards, as they are recalcitrant towards hydrogen production, the APR-H_2 yield remained low in all the investigated concentration range.

Guaiacol was studied as representative aromatic compound. As reported in the next paragraph 3.3, aromatics can be present in the aqueous phase in the case of the hydrothermal liquefaction of lignin. As shown in the Table 1, the carbon conversion to gas decreased from 20% to 3%, while the hydrogen gas distribution and APR-H_2 selectivity increased. This is due to an increase of the hydrogen production, together with a decrease of the formation of methane and carbon dioxide. The analysis of the liquid phase can give a hint on the reason behind these results. The methane can be

obtained by breaking the ether bond of the guaiacol, leading to catechol [172]. The HPLC chromatograms showed a decrease of the catechol production with the increase of the concentration, resulting in a greater hydrogen gas distribution. Phenol, the second most present by-product, can be obtained by consecutive deoxygenation from catechol itself.

Glycerol was also investigated in order to include in our study molecules not strictly related to the aqueous phase post lignin HTL, but still generally interesting for the valorization of organics dissolved in water. Glycerol can be found as soluble organic in the water phase, in particular from the hydrothermal liquefaction of aquatic biomass [173], [174]. This is due to the hydrolysis of triglycerides, that lead to fatty acids (ending up in the biocrude) and glycerol (ending up in the aqueous phase). The carbon to gas conversion constantly decreased from 73% to 30%; contrarily to the other compounds screened in the present work, a clear influence of the carbon concentration was observed also in the case of the hydrogen gas distribution and APR-H_2 selectivity, due to the change of selectivity in the intermediate liquid products (i.e. hydroxyacetone).

Table 11*:* Influence of carbon concentration on APR of model compounds. Reaction conditions: Liquid phase amount: 75 g, Temperature 270°C, Reaction time 120 min.

Concentration (wt. %C)	***APR H_2 yield (%)***	***Carbon to gas (%)***	***APR selectivity (%)***	***H_2 gas distribution (%)***
		Glycolic acid		
0.3	65.1	65.9	99.8	98.8
0.9	55.3	53.2	104.4*	99.4
1.8	31.1	33.9	92.4	99.1
		Acetic acid		
0.3	1.2	79.2	3.3	2.9
0.9	0.6	33.5	4.1	3.4
1.8	0.5	16.0	7.0	6.0
		Lactic acid		
0.3	2.3	66.8	8.1	7.0
0.9	1.0	32.7	5.6	7.4
1.8	0.8	19.9	5.8	11.5
		Propionic acid		
0.3	2.2	75.1	8.8	6.3
0.9	0.8	28.2	7.7	5.9
1.8	0.2	4.4	8.5	8.0
		Glutaric acid		
0.3	2.5	76.6	3.4	7.1
0.9	0.8	37.1	1.7	6.3
1.8	0.4	22.6	1.3	6.7
		Glycerol		
0.3	58.9	74.4	102*	80.6
0.9	37.8	53.4	96.4	76.0
1.8	19.9	31.9	85.7	73.6
		Methanol		
0.3	58.8	54.7	109.9*	98.4

0.9	32.1	29.2	113.5*	98.2
1.8	19.9	19.4	105.4*	98.0
		Guaiacol		
0.3	0.3	18.6	2.8	4.2
0.9	0.2	12.5	3	2.9
1.8	0.2	2.2	20	14.5
		Ethanol		
0.3	23.8	70.0	75.4	48.4
0.9	24.4	70.5	75.0	49.3
1.8	17.0	51.0	70.9	48.8
		Cyclopentanone		
0.3	0.9	4.4	25.7	65.0
0.9	0.8	3.9	35.2	42.4
1.8	0.5	0.4	131*	96.9

*APR selectivity higher than 100% is associated to the fact that the stoichiometry (used in the definition of APR selectivity) is not followed completely. Other reactions (e.g dehydrogenation) are present.

4.1.2. Influence of reaction time

Based on results available in literature [83], three compounds were selected as the most representative ones of a post-HTL aqueous stream: glycolic acid, acetic acid and lactic acid. The APR of these compounds was performed at different reaction times to evaluate the presence of reaction intermediates and suggest a plausible reaction pathway. Since the sampling of the gas phase during the reaction is experimentally difficult, a series of tests was carried out at different time durations with the same initial conditions. For the sake of clarity, 0 h is intended as the point in which the set temperature is reached (heating time approximately 60 minutes).

Acetic acid converted up to 35% before reaching the set temperature, producing a gas mixture with a 1:1 carbon dioxide/methane ratio (Figure 32A). It is clear that the consumption of acetic acid moles is almost entirely ascribed to the formation of methane and carbon dioxide. The relative production of the gas remained almost constant during the investigated reaction times. Hydrogen was present in small amount. This is due to the favorable cracking of the C-C bond, as confirmed in literature at different reaction conditions, and in our previous work with an alumina-supported Pt catalyst [85].

Glycolic acid reached a 28% conversion during the heating time and almost complete conversion after 2 hours. Hydrogen was the main product in the gas phase at each reaction time, reaching a plateau at about 2 hours, while carbon dioxide slightly increased up to 8 hours. According to the reaction mechanism suggested in our previous work, glycolic acid should produce 1.5 moles of hydrogen per mole of carbon dioxide [85]. This ratio is higher during the heating time, likely because the dehydrogenation (first step of APR) is predominant on the reaction mechanism compared to the reforming. In the following, it decreases also because of the formation of acetic acid, the only quantifiable liquid product. It may be obtained by the hydrogenation of the hydroxyl group of the glycolic acid, arising an issue of series-selectivity. As reported by Neira D'Angelo, the reactor configuration might be designed to allow the hydrogen to escape from the solution once formed,

without being consumed in parasite reactions using a microchannel reactor, together with an inert gas stripping [54]. Acetic acid did not appreciably react because methane was barely detected in the gas phase.

Finally, lactic acid converted completely during the heating time. For this reason, it was decided to stop the heating period after 20 min (where reached temperature was about 165 °C) and 40 min (about 245 °C). While there was no conversion during the first step, at 245 °C a small conversion of the lactic acid was already observed. Two parallel but interacting pathways have been proposed for lactic acid (Figure 33). In analogy with acetic acid behavior, lactic acid can be decarboxylated producing ethanol and carbon dioxide (light blue frame); subsequently, ethanol can readily react producing methane, carbon dioxide and hydrogen (red frame); for this reason, ethanol may not be observed by HPLC analysis. The second pathway involves the hydrogenation of lactic acid (using the hydrogen produced from ethanol APR) leading to propionic acid (green frame), that will subsequently lead to ethane and carbon dioxide, as reported in [85].

We tried to prove this hypothesis looking at the time evolution. At 0 h, 3.5 mmoles of methane have been produced; it follows that, according to the proposed reaction scheme, 7 mmoles of hydrogen and carbon dioxide should be obtained as well (experimentally 8.6 mmoles of CO_2 were quantified). This amount of hydrogen disappeared almost completely as it readily produces propionic acid (9.6 mmoles). From this point on, only propionic acid slowly reacted: from 0 to 8 h, 4.5 mmoles converted into carbon dioxide (+ 3.7 mmoles) and ethane (+ 3.4 mmoles).

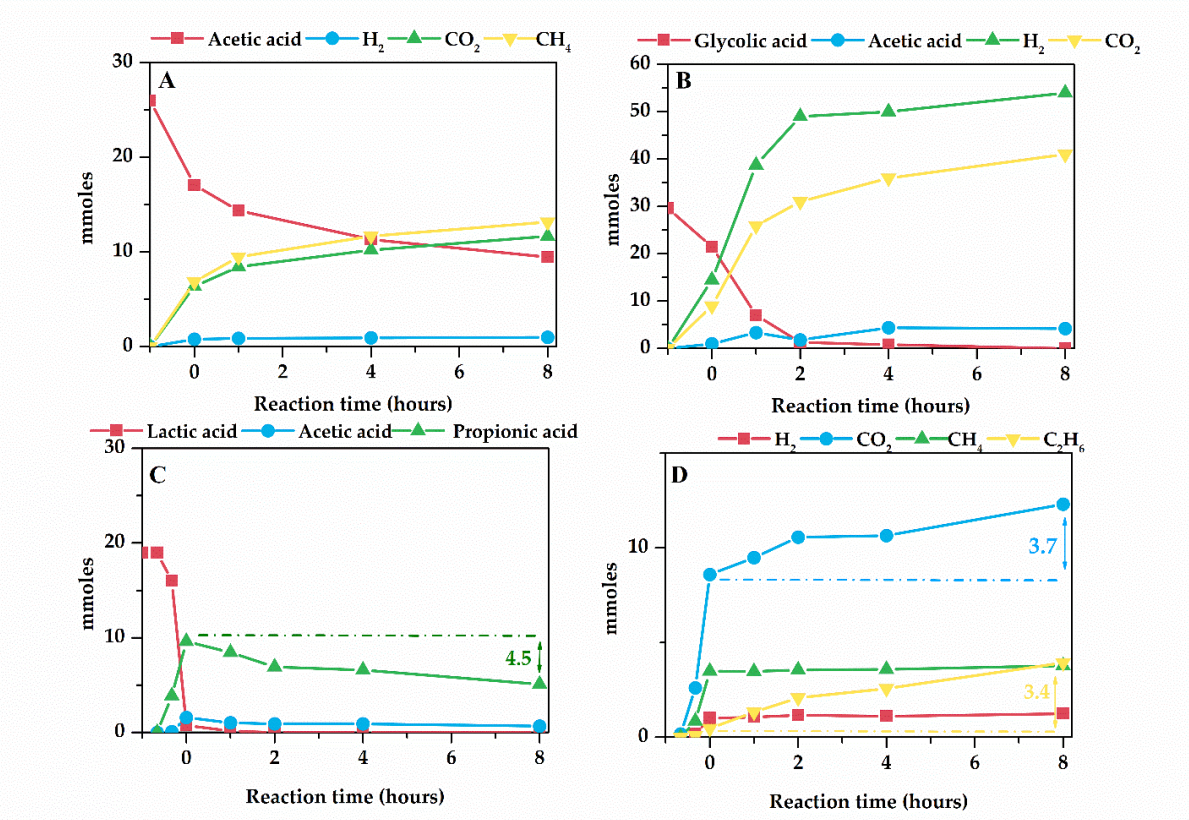


Figure 32. Amount-time profile for APR of acetic acid (A), glycolic acid (B), Lactic acid (C-D). Reaction conditions: Liquid phase amount: 75 g, 0.375 g Pt/C, 0.9 wt. % C feed, 270 °C reaction temperature.

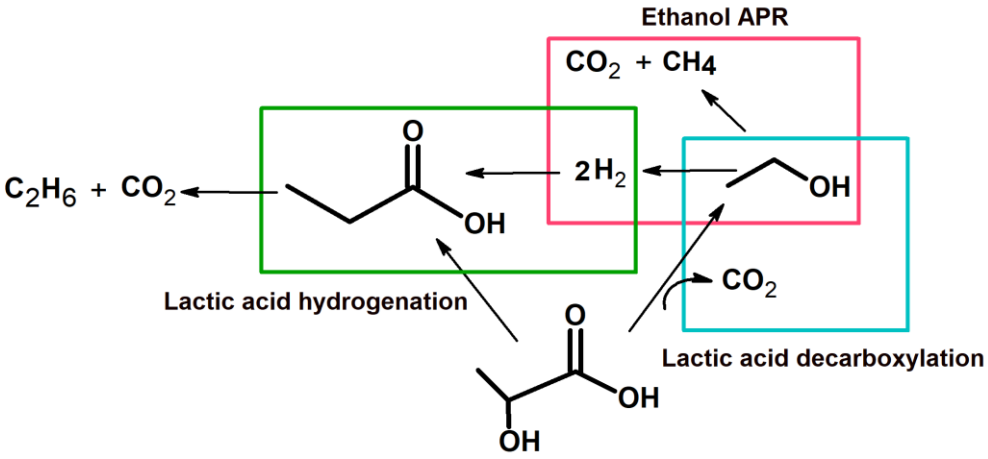


Figure 33. Proposed reaction scheme for lactic acid APR.

4.1.3. HTL aqueous phase synthetic mixture

Glycolic, acetic and lactic acid were tested in a ternary mixture with global 0.9 wt.% C concentration, equally divided in each component (Figure 34). It was previously observed that the molecules own different reactivity if they are tested alone or in mixture, likely because of competitive adsorption issues [85]. In the present study, we further investigated this aspect, looking at the influence of the reaction time.

Some characteristic outcomes can be highlighted. First of all, it was observed that glycolic acid was the compound with the highest initial rate of consumption, reaching 92% of conversion during the heating period. Hydrogen and carbon dioxide were produced from glycolic acid with the same selectivity reported in the single test, i.e. about 1:1.5 ratio hydrogen: carbon dioxide, and 1 mole of CO_2 per mole of glycolic acid converted. On the other hand, lactic acid, that almost disappeared in the test reported in the previous section, showed an initial low conversion. This result suggests a competition in the adsorption of the molecules on the active sites. In the case of the mixture, the adsorption of a reactant implicates also the displacement of the other adsorbed specie, leading to a more complex scenario compared to the test with a single compound [175]. It can be hypothesized that glycolic acid and lactic acid, co-adsorbing on the surface sites, limited the adsorption of acetic acid and, as a consequence, decreased strongly its reactivity [176]. This hypothesis is further studied and presented at the end of the paragraph.

The conversion of acetic acid from 2 h to 8 h led to the selective increase of carbon dioxide and methane in 1:1 ratio, with the same selectivity noted in the single test.

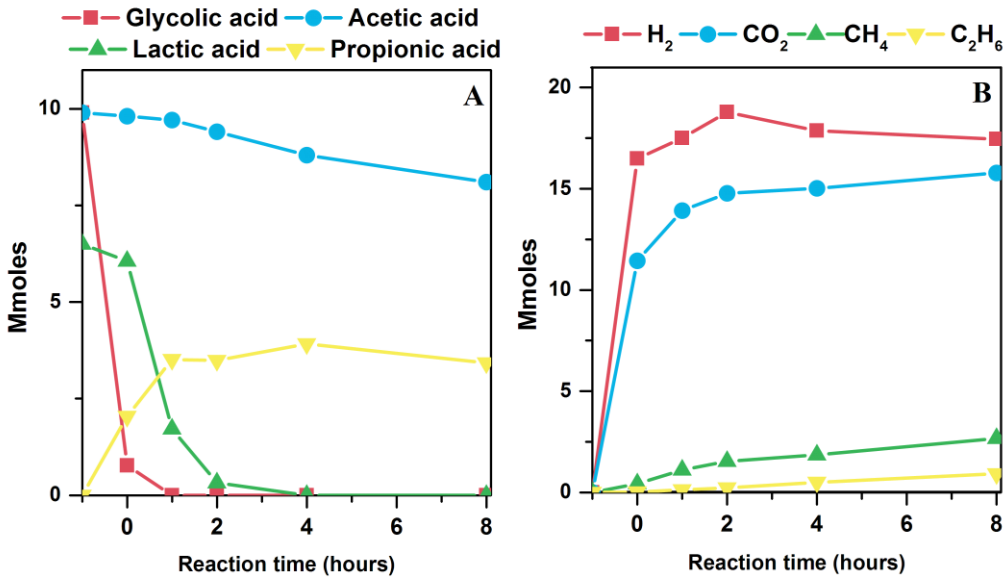


Figure 34: Amount-time profile for APR of a synthetic ternary mixture. Reaction conditions: Liquid phase amount: 75 g, 0.375 g Pt/C, total 0.9 wt.% C glycolic, acetic and lactic acid (0.3 wt.% C per component), 270 °C reaction temperature.

In the following Figure 35A the influence of the total carbon concentration on the APR parameters is reported. A decrease in the carbon conversion to gas from 35 to 20% was observed, while the hydrogen gas distribution and the APR H_2 selectivity increased from 59% to 82% and from 47% to 68% respectively. The different trends between the conversion and the selectivity led to an almost constant hydrogen yield in the investigated range of carbon concentration. To understand this behavior of the mixture, it is interesting to observe the conversion of each molecule (Figure 35B). Moving from 0.3 to 0.9 wt.% of carbon, glycolic acid still fully converted and lactic acid up to 90%, while acetic acid remained almost unconverted. Due to this different reactivity, likely linked to the previously described influence of reaction time, the carbon conversion to gas decreased, but the selectivity increased (mainly thanks to the intrinsic high selectivity of glycolic acid). In an analogous way the increase of the selectivity from 0.9 to 1.8 wt.% can be explained. Indeed, as the conversion of the lactic acid decreased to 20%, the produced gas phase was mainly ascribed to the conversion of glycolic acid.

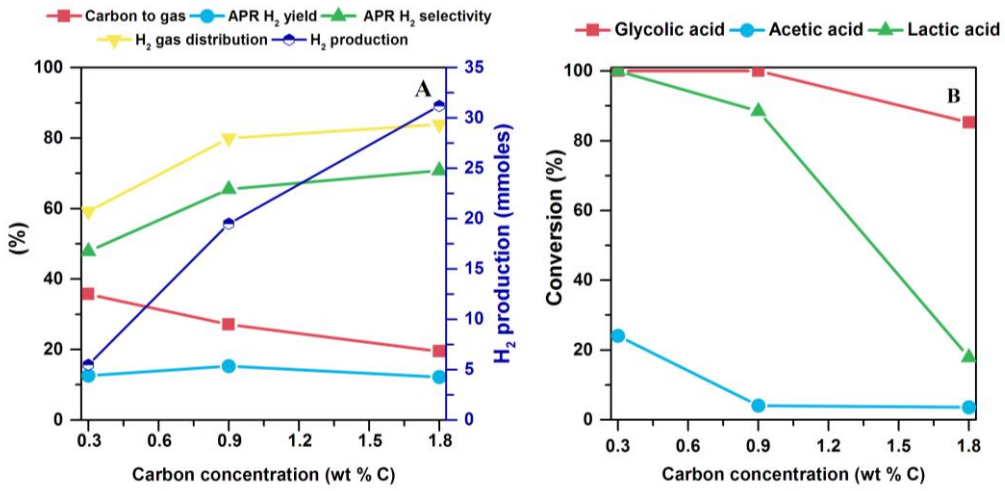


Figure 35: Influence of carbon concentration on the reaction parameters (A) and conversion (B) of APR of the synthetic mixture. Reaction conditions: Liquid phase amount: 75 g, 270°C reaction temperature, 2 h reaction time.

Finally, the influence of the reaction temperature is reported in Figure 36. A constant increase of the carbon to gas conversion was observed, in accordance to literature, due to the more readily breakable C-C bond [39]. The APR-H_2 selectivity decreased slightly from 250 and 270 °C because of the higher carbon dioxide production due to the higher conversion of acetic acid. At the same time, the higher reactivity of acetic acid at higher temperature led to higher production of methane and, therefore, to a smaller hydrogen gas distribution.

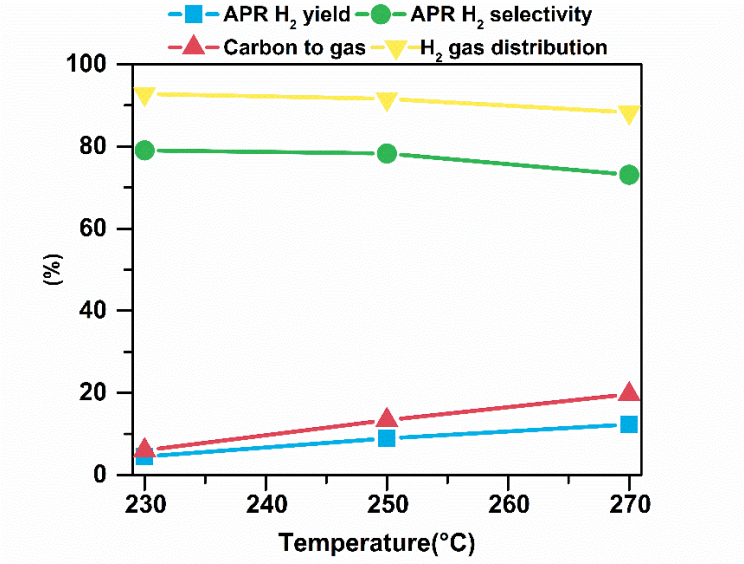


Figure 36: Influence of reaction temperature on the reaction parameters of APR of the synthetic mixture. Reaction conditions: Liquid phase amount: 75 g, 1.8 wt. % C, 2 h reaction time.

To verify the co-adsorption hypothesis some tests of binary mixture in different concentrations were performed and the results of conversion are reported in the table below.

Table 12: co-adsorptiont tests

Test	Compound	Conversion (%)
Glyolic acid alone (13.2 mmoles)	Glycolic acid	75
Lactic acid alone (13.2 mmoles)	Lactic acid	98
Acetic acid alone (13.2 mmoles)		25
Glycolic and acetic acid mixture (13.2 mmoles each)	Glycolic acid	70
	Acetic acid	0
Glycolic lactic acid mixture (13.2 mmoles each)	Glycolic acid	58
	Lactic acid	26

Looking at glycolic and acetic acid mixture, the glycolic acid conversion was almost constant (75% and 70%) comparing the single test with the one in equimolar mixture with of acetic acid. On the other hand, the acetic acid conversion passed from 25% (alone) to 0% (mixture), indicating that it was not able to adsorb on the active site due to the strong competition with glycolic acid. This phenomenon is far less evident if we look at the glycolic-lactic acid mixture. In fact, both molecules showed a reduction in their conversion when in mixture, despite to a different extent: glycolic acid conversion decreased by 22%, while lactic acid conversion decreased by 73%. This result may confirm the hypothesis that competitive adsorption phenomena are present during APR, and they influence the observed conversion and hydrogen production with respect to the results obtained in single tests.

4.1.4. Case study: APR of the water fraction from HTL of lignin

Characterization of the aqueous phase

In order to assess the possible valorization of the aqueous phase from biomass hydrothermal liquefaction via APR, an organics-laden aqueous stream originated from the HTL of lignin was investigated. Indeed, the available literature lacks on knowledge about the APR real water streams, underestimating the complexity deriving from mixtures of compounds, inorganics etc.

Few works reported an extensive characterization of the products of lignin HTL [177]. In the following Table 2, the classification and quantification of the main compounds present in the water are reported. While the sample named simply “HTL-AP” was obtained with a separation by gravity filtration, the samples named “Treated HTL-AP x” were obtained washing with an excess diethyl ether in a 5:1 ratio to reduce the phenolic compounds concentration, whose motivation will be clearer n the following. From the HPLC and GC analysis, it was possible to identify most of the compounds

in the water fraction (approximately 70% of the total organic content). Figure 38 shows the HPLC chromatograms of the HTL-AP sample. Several classes of compounds were identified, such as carboxylic acids (e.g. acetic acid, glycolic acid, lactic acid), alcohols (methanol, ethanol, 2-propanol), ketones (acetone), polyalcohols (glycerol), aromatics (phenol, catechol, guaiacol) and aldehydes. As it can be noticed, the screening of model compounds performed in the paragraph 3.1 reflects the species found in the actual aqueous phase.

Methanol is the most present compound, followed by lactic acid, phenolic compounds, glycolic acid, acetic acid and glycerol. Moreover, the quantification of inorganic species (sodium, calcium, potassium, sulfur and phosphorous) is given in the same table. Since the presence of inorganics can affect the catalyst lifetime, an investigation was performed in paragraph 3.3.3. As far as the total organic content is concerned, the tested samples have a carbon content of around 1 wt.% C. This value is lower than the typical ones reported in literature from the hydrothermal liquefaction of lignocellulosic biomass [83].

The storage of the sample was carried out at -5°C: despite the low temperature, the formation of solid particles was observed during storage, likely due to oligomerization reactions involving the phenolic compounds [178]. To evaluate the influence of this solid phase, two tests were performed with and without a filtration of the aqueous phase (results reported in Figure 37). Both carbon conversion and hydrogen production were negatively affected by the presence of the particles. For this reason, as they can contribute to affect the activity and the stability of the catalyst, a pre-filtration of the as-received liquid phase was performed in the following experimental campaign with a 0.2 µm nylon filter.

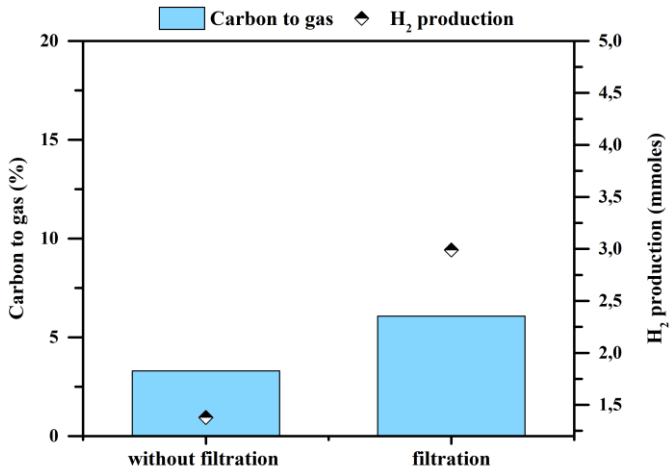


Figure 37: Effect of the filtration of the feed on the APR of the HTL-AP sample. Reaction conditions: 0.8 wt.% C, 270 °C reaction temperature, 2 h reaction time.

Table 13: HTL-AP quantification of main compounds and ICP analysis.

	Carbon weight concentration (wt. % C)					
Sample	**Glycolic**	**Lactic**	**Acetic**	**Methanol**	**Glycerol**	**Phenolic compounds**
HTL-AP	0.047	0.112	0.083	0.138	0.029	0.116
Treated HTL-AP 1	0.049	0.102	0.078	0.124	0.022	0.056
Treated HTL-AP 2	0.051	0.109	0.051	0.099	0.020	0.017
Treated HTL-AP 3	0.050	0.099	0.044	0.096	0.020	≈ 0

Sample	**Inorganic species (ppm)**					
HTL-AP	**Na**	**K**	**Ca**	**S**	**P**	**Total organic carbon (mgC/L)**
Treated HTL-AP 1	518	281	13	116	11	11558
Treated HTL-AP 2	190	140	15	19	1	10810*
Treated HTL-AP 3	n.a.	n.a.	n.a.	n.a.	n.a.	10540*
Sample	350	233	0	53	43	10358*

**excluding DEE*

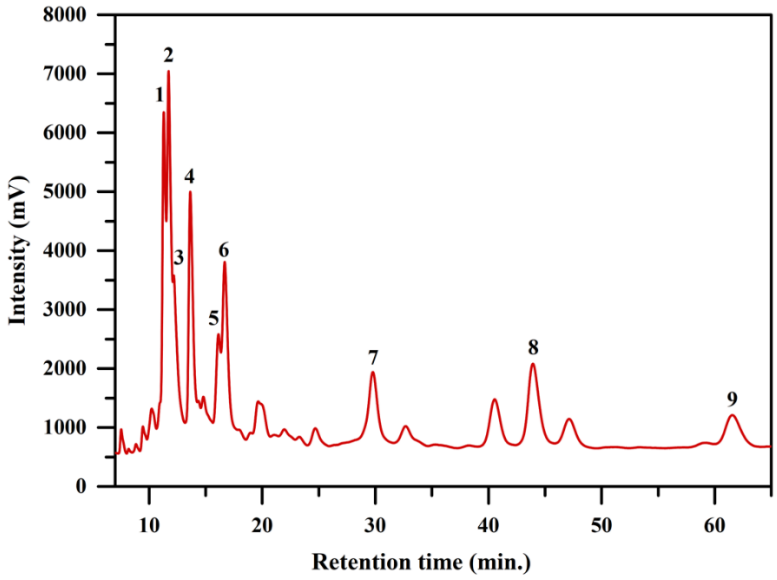


Figure 38: HPLC chromatograms of the HTL-AP (1: glycolic acid, 2: lactic acid, 3: glycerol, 4: acetic acid, 5: acetaldehyde, 6: methanol, 7: catechol, 8: phenol, 9: guaiacol).

4.1.5. HTL-AP catalytic test

The influence of the carbon concentration on the carbon to gas conversion and hydrogen production of the APR of the HTL-AP is shown in the Figure 39. It is important to highlight that the amount of hydrogen (reported in mmoles) obtained in the gas phase decreased strongly at increasing carbon concentration. This was a surprising result, as the increase of the concentration may surely negatively affect the hydrogen yield, but the amount of product should at least remain constant (unless of the rare case of kinetics with negative reaction orders).

In Figure 40 (left) the chromatogram of the feed and liquid product of the APR performed on 1 wt.% C HTL-AP is reported (named in the figure Product 1st test). It is possible to notice a similar peak intensity of most of the present molecules in the APR product (glycolic acid, lactic acid, glycerol, methanol) with respect to their original content in the feed, leading to a low carbon conversion to gas and a negligible hydrogen production. This outcome was not coherent with the previous results reported for the synthetic mixture (paragraph 3.2), where glycolic and lactic acid were highly reactive and converted completely before the end of the reaction.

In order to exclude an experimental error, the obtained solution after the filtration was subjected again to an APR test, using a fresh catalyst. The HPLC chromatogram of the liquid APR product obtained at the end of the 2nd test is reported in Figure 40 (right) and is compared to the one at the beginning of the test, which in fact is the liquid phase obtained after the 1st test.

As it can be noticed, thanks to the 2nd test, most of the initially present compounds were converted, being the peaks of glycolic acid, lactic acid, glycerol and methanol almost disappeared. Please note that the higher conversion cannot be due to the global longer reaction time (as the HTL-AP was subjected in this way to two runs, each one at 2 hours) because a test performed on a HTL-AP for 4 h reaction time led to the same result obtained with the 2 h test.

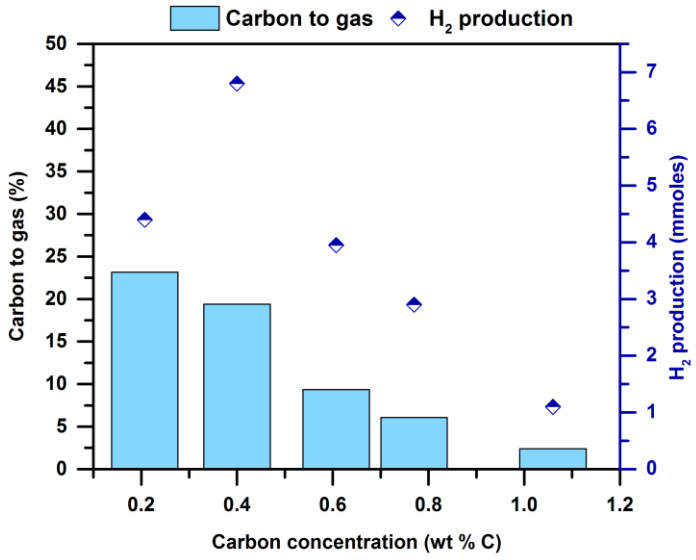


Figure 39: Influence of carbon concentration on reaction parameters of APR of the HTL-AP. Reaction conditions: Liquid phase amount: 75 g , 270°C reaction temperature, 2 h reaction time.

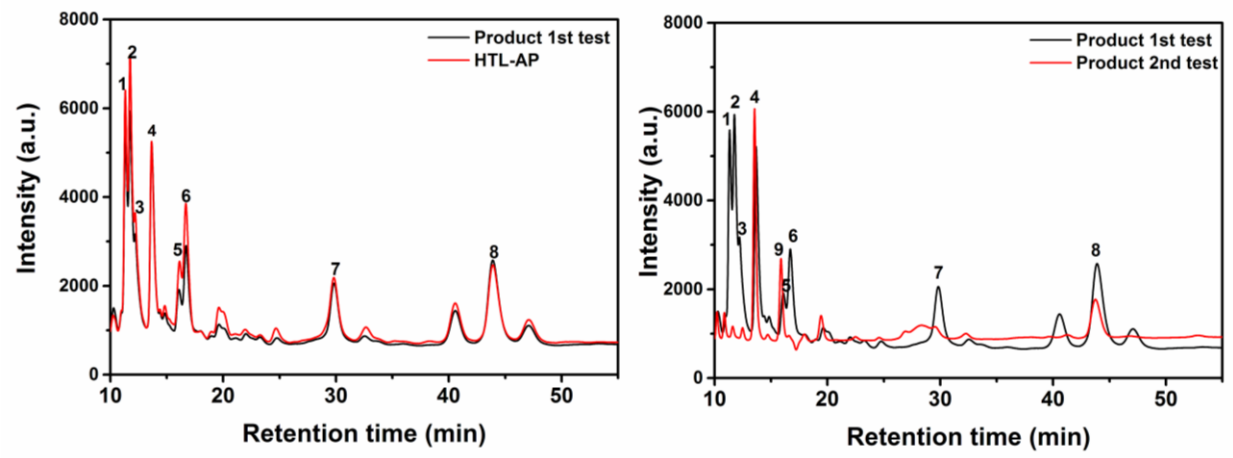


Figure 40: HPLC chromatograms of the feed and product for the first test (left) and second test (right) of the HTL-AP sample. Reaction conditions: 1% wt.% C, 270°C reaction temperature, 2 reaction time (1: glycolic acid 2: lactic acid 3: glycerol 4: acetic acid 5: acetaldehyde 6: methanol 7: catechol 8: phenol 9: propionic acid).

The higher conversion in the 2nd test led to a higher hydrogen production, as showed in Figure 41A, where the hydrogen productivity (i.e. the hydrogen production normalized by the moles of carbon in the feed) is reported for the 1st and 2nd tests. It can be observed that the 2nd test reported a higher and almost constant hydrogen productivity, contrarily to the trend obtained by the 1st runs, that was decreasing in the entire range of carbon concentrations investigated. It is highlighted here how the 2nd test had a lower starting carbon concentration compared to the corresponding 1st test. This is due to the impossibility to recover the entire liquid phase after the first reaction and, secondarily, to the low but not negligible conversion obtained during the 1st test.

The sum of the hydrogen mmoles produced during 1st test (black) and 2nd test (red) are showed in Figure 41-B. It can be observed that the decreasing trend observed in the 1st runs, was substituted by an almost constant hydrogen production (about 10 mmoles) if the 2nd tests are added to the 1st ones.

The dramatic difference in the performance between 1st and 2nd test denoted the probable deactivation of the catalyst because of species (organic or inorganic) present during the first test. For this reason, the next paragraph is devoted to the investigation of this important issue, hardly reported in literature because of the lack of study on HTL-derived actual streams.

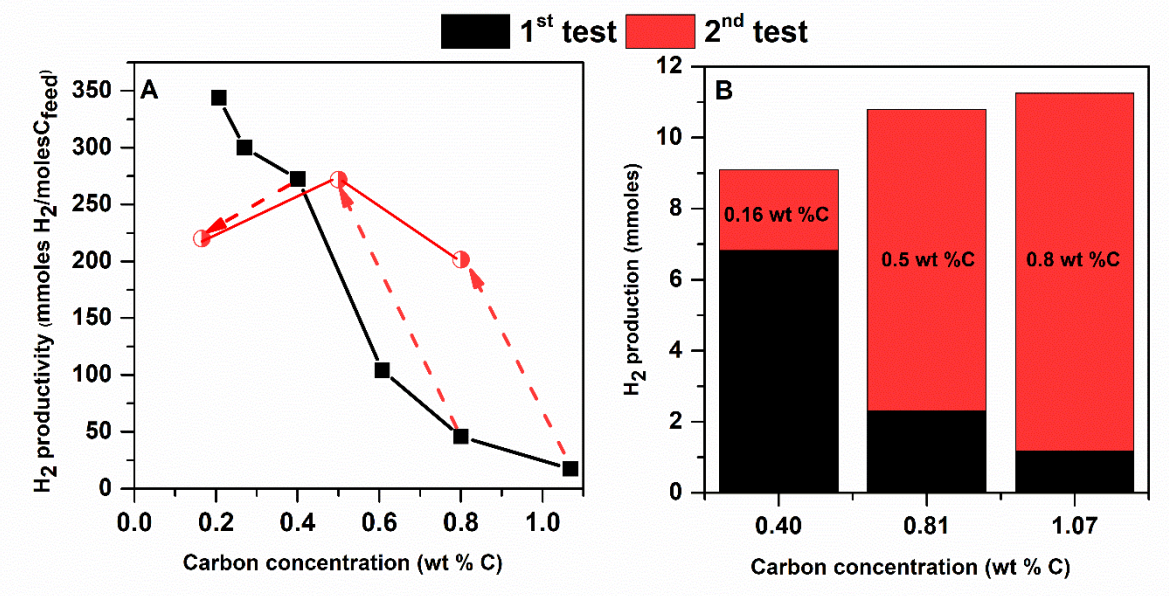


Figure 41: H_2 productivity (A) and H_2 production (B) for the APR of HTL-AP. Reaction conditions: Liquid phase amount: 75 g, 270°C reaction temperature, 2 h reaction time

4.1.6. Deactivation of the catalyst

In order to assess the hypothesis of catalyst deactivation, further experiments were performed, and the spent catalysts characterized.

As it was assumed an endogenous deactivation, the stability of the catalyst could not be evaluated with the common procedure of re-using the catalyst with a fresh solution. In fact, we would have observed still a negligible conversion, and no other conclusion could have been drawn. For this reason, it was decided to test the stability of the catalyst versus a reactive reference compound. The catalyst used during the 1st APR run on HTL-AP was recovered, dried overnight (105°C) and used for the APR of glycolic acid (formerly proven to provide high H_2 yields).

The carbon to gas conversion and hydrogen production of the reference test (obtained with a fresh catalyst) and of the runs with two used catalysts are compared in the following Figure 42. We previously assessed that the stability of the catalyst was maintained after an APR run with glycolic acid, therefore the differences cannot be ascribed to the hydroxyacid itself.

The catalyst used with the HTL-AP showed a serious deactivation: the conversion of the glycolic acid in the liquid phase decreased from 91% to 20%. On the other hand, the test named "Treated HTL-AP 3" is the APR of glycolic performed with the catalyst that had previously undergone an APR test with the treated HTL-AP 3 aqueous phase reforming. It is important to observe that the deactivation was still present, but at a lower extent than the previous one referred to the APR of an untreated feed (HTL-AP). Indeed, the conversion of glycolic acid raised to 42%, with the carbon to gas and the hydrogen production more than doubled.

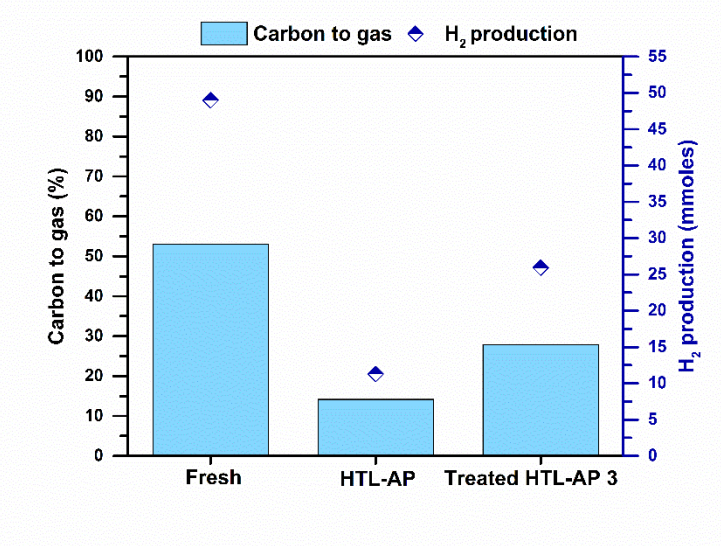


Figure 42: APR of glycolic acid with different catalysts. Reaction conditions: Liquid phase amount: 75 g, 0.9 wt.% C glycolic acid, reaction temperature 270°C, reaction time 2 h.

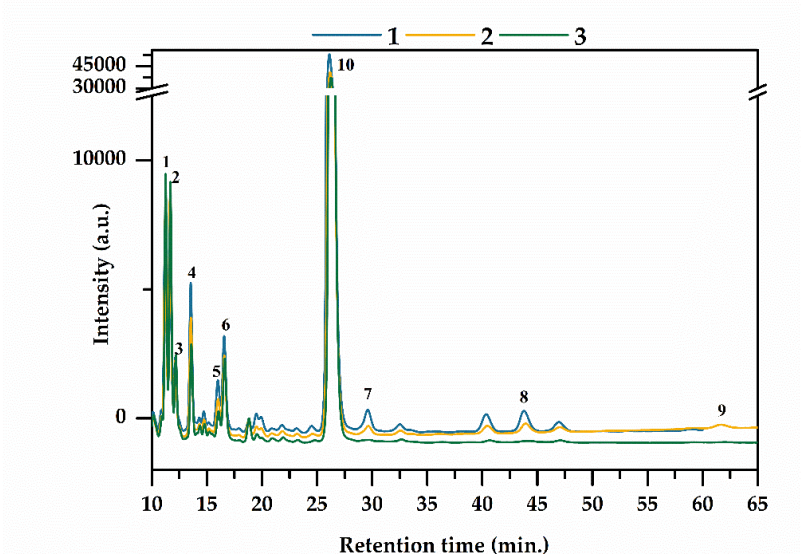
Two main reasons were investigated to explain the deactivation of the catalyst, i.e. the presence of phenolic oligomers and sulfur-containing molecules.

HTL-AP solution washed with diethyl-ether had the effect of selectively removing the phenolic compounds from the water, while keeping the other organic compounds nearly unchanged in terms of concentration in the water. Afterwards, they were tested to assess if the phenolics can be associated to the catalyst deactivation. Few works studied the deactivation of noble metal catalyst in the presence of phenolics, and no works were found in the currently investigated APR conditions with Pt/C as a catalyst. APR of glycerol with the purpose of hydrogenating phenol in-situ was studied with Raney Ni® [179]: the investigation showed an improvement of glycerol conversion due to the shift of the equilibrium. On the other hand, other researchers reported catalyst deactivation due to deposits formation on the catalyst surface, in different reaction conditions. Hydrodeoxygenation (HDO) of guaiacol with noble metal catalysts (Pt, Pd, Rh, Ru) supported on activated carbon led to catalyst deactivation due to polyaromatic deposits in different extents for each catalyst [180]. The catalytic wet air oxidation of phenol was studied on Pt/Al_2O_3 and Pt/CeO_2 during the reaction deposit of carbonaceous material were deposited on the catalyst leading to a catalyst deactivation [181]. De Souza et al. studied the HDO of phenol over Pd catalyst with different supports; they assessed a deactivation of the catalyst supported on Al_2O_3, SiO_2, TiO_2 and ZrO_2 [182].

From a preliminary glance, it is not possible to infer in our case that the deactivation is due to the presence of phenolic monomers (phenol, guaiacol, catechol). As reported in Figure 40 (left), there is no apparent difference between the feed and the 1st test product in terms of the phenolics amount. However, there was an improvement of the performance in 2nd test: it is more likely that phenolic oligomers, not visible in the HPLC analysis, underwent polymerization during the 1st reaction, blocking the pores of the catalyst (as suggested by the textural analysis in the following), which therefore acted as a sacrificial adsorbent that removed them from the product of the 1st test.

Consequently, these compounds were likely absent in the 1st test product and consequently did not affect the catalyst in the 2nd test.

For this reason, the phenolic compounds were removed via an HTL-AP treatment with DEE, whose effect was is showed in Figure 43. As observed in the chromatogram, the main consequence of washing the aqueous phase with the organic solvent is the elimination of phenolics (monomers and presumably also oligomers), without affecting the concentration of the remaining compounds. This is an important result, because it allows an easier interpretation of the results as only the different concentration of aromatics can be considered. Each treatment was able to extract different amount of phenolics, depending on *a-posteriori* evaluated effectiveness of the procedure. In the side-table, the phenolic content (guaiacol peak number 10, phenol peak number 9 and catechol peak number 8) of these batches are reported.



Sample	C wt.%
Treated HTL-AP 3	~ 0
Treated HTL-AP 2	0.017
Treated HTL-AP 1	0.05
HTL-AP	0.16

Figure 43: HPLC chromatograms of HTL-AP and treated HTL-AP feeds (1: glycolic acid 2: lactic acid 3: glycerol 4: acetic acid 5: acetaldehyde 6: methanol 7: catechol 8: phenol 9: guaiacol 10: DEE).

The hydrogen production as a function of carbon concentration (excluding diethyl-ether) is reported in the following Figure 44; when the phenolics content increased, the hydrogen production decreased to reach almost zero at the highest phenolics content. Moreover, it is clearly highlighted the difference in the hydrogen production between 1st and 2nd test on the HTL-AP, but in comparison to the treated HTL-AP 1. Finally, it can be observed that the treated HTL-AP 3 (with no detected phenolics) led to a trend analogous to the synthetic mixture, with a hydrogen productivity almost constant on the investigated carbon concentration range, equal to 300 mmol H_2/mol C.

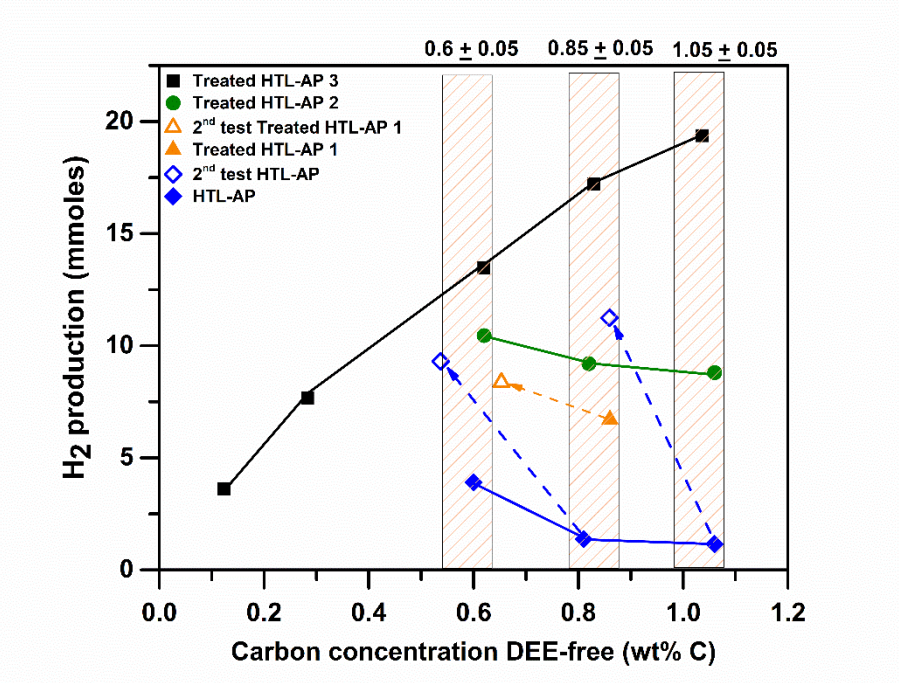


Figure 44: Influence of carbon concentration and DEE pre-treatment on the H_2 production for APR of different batches. Reaction conditions: Liquid phase amount: 75 g, 270 °C reaction temperature, 2 h reaction time.

In order to assess the contribution of DEE to the hydrogen production, we performed the APR of DEE alone and together with the synthetic mixture glycolic/acetic/lactic acid. As reported in the Table 14:, the amount of the main produced gas during the aqueous phase reforming of the synthetic mixture with and without DEE is almost identical. This means that the addition of the solvent for the removal of the phenolics did not change the product distribution and the hydrogen yield. It is highlighted that, despite the APR of DEE (0.9 wt.% C) produced considerable amount of hydrogen, the different selectivity in terms of methane/hydrogen ratio in the synthetic mixture + DEE test and in the DEE-alone test suggests that its conversion is negligible in the mix test, therefore negligible in terms of hydrogen production. The reason may be ascribed to the competitive adsorption of DEE against, for example, glycolic and lactic acid, which are readily converted.

Table 14: Aqueous phase reforming of synthetic mixtures with and without DEE. Reaction conditions: Liquid phase amount: 75 g, 0.9 wt.% C acids + 0.9 wt.% C DEE, 270 °C reaction temperature, 2 h reaction time.

Test	Hydrogen (mmoles)	Carbon dioxide (mmoles)	Methane (mmoles)
Synthetic mixture	19.5	16.1	2.0
Synthetic mixture + DEE	20.6	16.5	2.2
DEE	4.9	3.6	4.0

The textural analysis of some selected catalysts, together with the characterization of the fresh one, is reported in the Table 4. The catalyst used for the APR of the HTL-AP (i.e. with the highest content of phenolics) showed the highest decrease of the surface area and pore volume, indicating that high

molecular weight compounds blocked the pore of the catalysts, reducing the availability of active sites for the reaction. Coherently with the reported results, both the pore volume and surface area of the catalyst used for the 2nd test of the HTL-AP sample were higher than the former. Analogously, the catalyst used for the APR of the treated HTL-AP 3 (i.e. with negligible content of phenolics) showed a minor loss of textural properties compared to the untreated feed. It can be noticed anyway a strong difference compared to the fresh catalyst, that is in line with the results reported with the glycolic acid (Figure 44), where a worsening of the performance was noticed anyway.

Table 4: Textural characteristic of the fresh and spent catalysts. Reaction conditions: 270 °C, 2 h reaction time.

Sample	BET surface area (m^2/g)	Pore Volume (cm^3/g)	Average pore size (nm)
Fresh	923	0.632	5.1
HTL-AP 0.8% C	195	0.344	5.7
HTL-AP 1.1% C	216	0.361	5.6
HTL-AP 1.1% 2nd test	430	0.480	5.2
Treated HTL-AP 3 0.8% C	410	0.471	5.3

The spent catalysts were also characterized thanks to thermogravimetric analysis coupled with infrared spectroscopy.

The fresh catalyst showed a total weight loss equal to 15 wt.% when exposed to a heating treatment up to 1000 °C under inert flow, divided into three different steps: the first one, with a maximum at 80°C, due to the loss of adsorbed water; the second step, between 200°C and 600°C, was due to the decomposition of the carbon support, which is composed from a certain percentage of oxygen, with formation of carbon dioxide; the third step is a further decomposition of the carbon substrate with formation of carbon monoxide [183]. In fact, the infrared analysis of the curves of developed gasses showed a maximum for water at around 100°C, a maximum at 600°C for CO_2 and an increase in CO concentration over the 600°C (Figure 45).

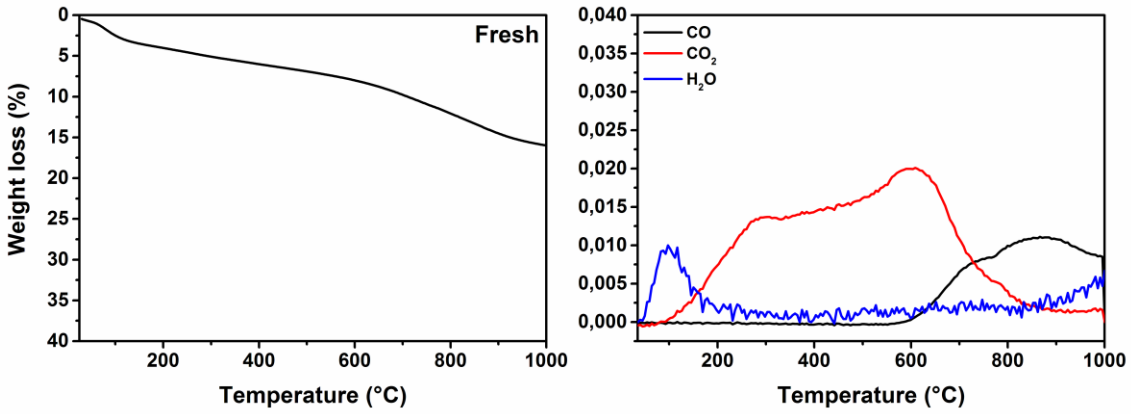


Figure 45: TGA-IR of fresh catalyst. Analysis conditions: heat from 30 °C to 1000 °C @ 20 °C/min in nitrogen atmosphere with a purge rate of 20 mL/min under nitrogen. A: TG results; B: IR-Absorption peak during TGA.

The TGA analyses of the spent catalysts showed that the weight loss is quite similar for all the catalysts, ranging from 15 to 20 wt.%. Please note that this information cannot be directly linked to the amount of deposits on the catalyst as the tests were not performed in an oxidative environment to allow the IR analysis of the evolved species. However, the degradation products were quite different whether the catalyst was used for a 1st or 2nd test (Figure 46 and Figure 49, respectively).

On one hand, the spent catalysts used for the 1st tests showed the presence of degradation products such as CO_2, CO, H_2O, aliphatic fragments and the presence of primary alcohols; for the sake of representativeness, the TGA-IR of the sample HTL-AP is reported in Figure 46 (analogous results were obtained for the samples treated HTL-AP 1 and treated HTL-AP 2 and are reported in Figure 47 and Figure 48).

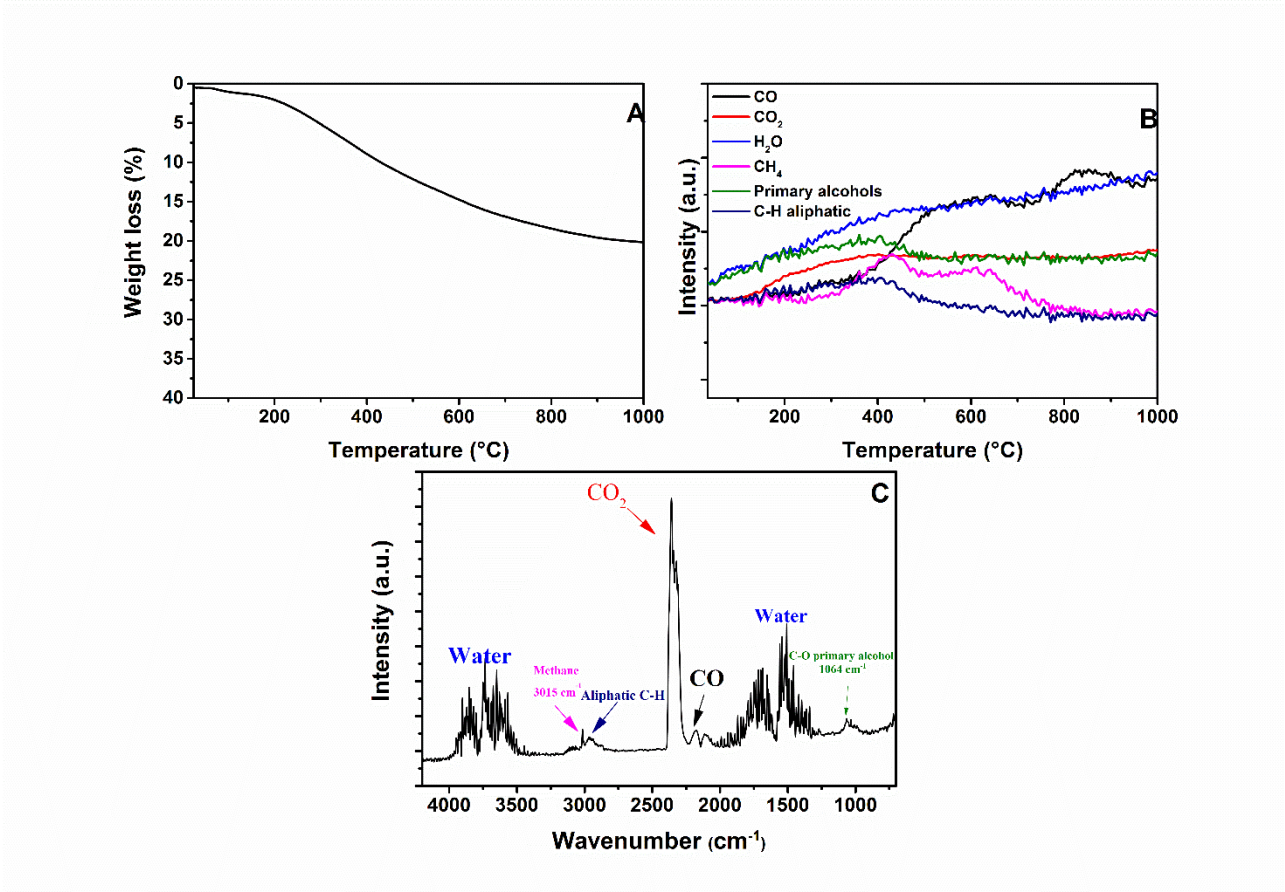


Figure 46: TGA-IR of spent catalyst after APR 1st test of HTL-AP. Reaction conditions: 0.8 wt.% C, reaction temperature 270 °C, reaction time 2 h. Analysis conditions: heat from 30 °C to 1000 °C @ 20 °C/min in nitrogen atmosphere with a purge rate of 20 mL/min under nitrogen. A: TG results; B: IR-Absorption peak during TGA of water, CO_2, CH_4, aliphatic fragments and primary alcohols; C: Infrared spectra at 408°C.

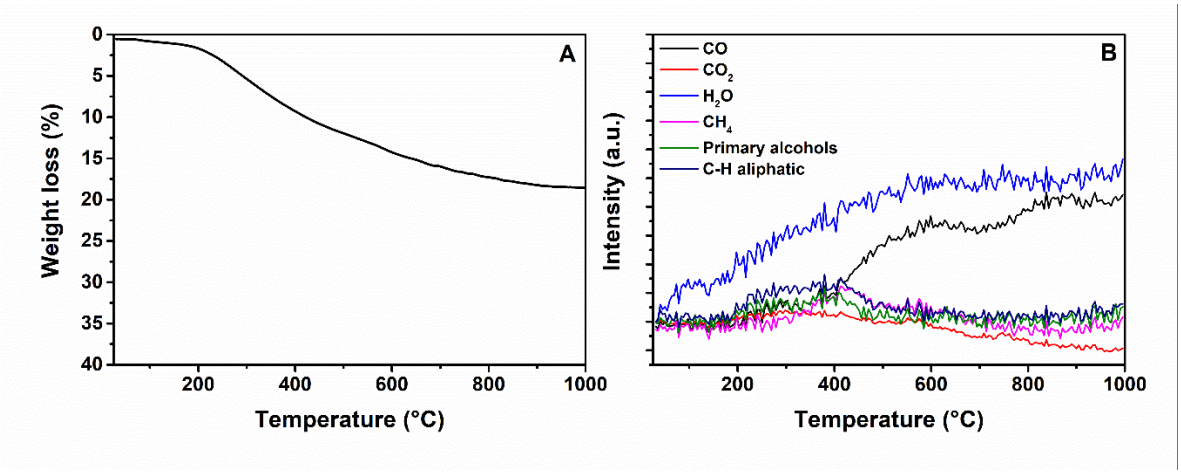


Figure 47: TGA-IR of spent catalyst after APR of treated HTL-AP 1. Reaction conditions: 0.8 wt.% C, reaction temperature 270 °C, reaction time 2 h. Analysis conditions: heat from 30 °C to 1000 °C @ 20 °C/min in nitrogen atmosphere with a purge rate of 20 mL/min under nitrogen. A: TG results; B: IR-Absorption peak during TGA.

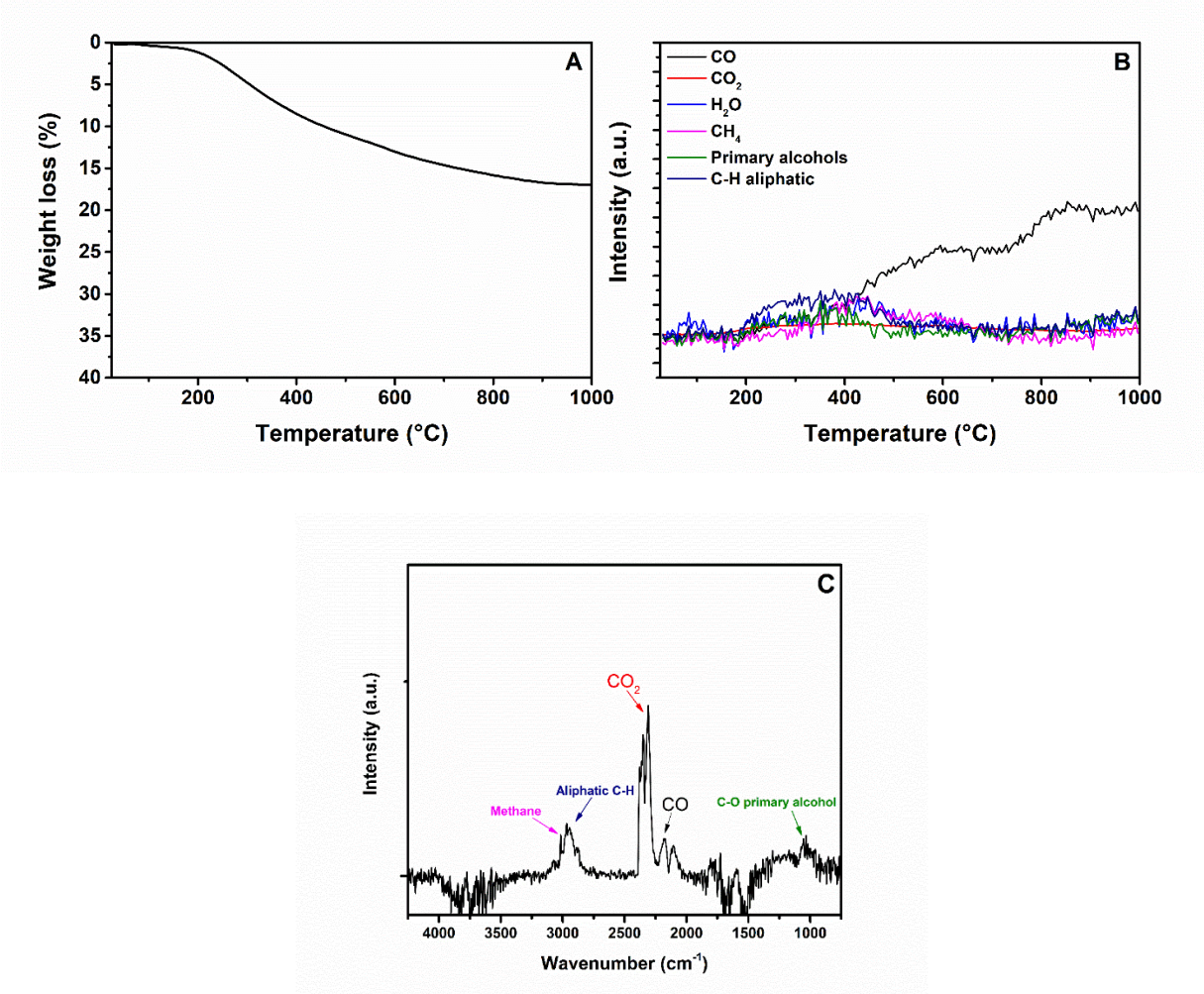


Figure 48:TGA-IR of spent catalyst after APR of treated HTL-AP 2. Reaction conditions: 0.8 wt.% C, reaction temperature 270 °C, reaction time 2 h. Analysis conditions: heat from 30 °C to 1000 °C @ 20 °C/min in nitrogen atmosphere with a purge rate of 20 mL/min under nitrogen. A: TG results; B: IR-Absorption peak during TGA; C: Infrared spectra at 380°C.

The degradation of the catalyst occurred in a single step with a maximum of degradation speed at about 383 °C (from the slope of the weight loss curve in Figure 49 A. The main volatile products of this degradation were visible in the infrared spectra at 408 °C (Figure 49 C). The infrared spectra showed the presence of water, carbon dioxide, carbon monoxide, and methane derived from the degradation of the organic substrate adsorbed on the catalyst. The spectra showed also more complex degradation products: between 2800 and 3000 cm^{-1} the stretching of CH_2 and CH_3 from aliphatic fragments were easily recognized, while the band at 1064 cm^{-1} is typical of primary alcohols. From the figure it was possible to consider that the first part degradation is mainly due to the evaporation of aliphatic compounds containing alcohols, while at higher temperatures the organic compounds (presumably of higher molecular weight and non-volatile at these temperatures) decomposed to form carbon monoxide, carbon dioxide, methane and water. The presence of alcoholic species can be considered as an indication of the low reactivity of these catalysts. Indeed, it was showed throughout the present work as the alcohols are characterized by high reactivity: for this reason, their presence on the surface of the catalyst states the sites are not available for activating the breaking of the molecules. The characteristic band of phenolics in the gaseous phase are located at about 3650 cm^{-1},

3100-3000 cm^{-1} and 1600-1500 cm^{-1}. However, these bands are covered from water and methane, therefore it was not possible to recognize the presence of phenol, guaiacol, catechol or other molecules containing phenolic groups.

On the other hand, different phenomena were observed for the catalysts used for the 2nd tests investigation and similarly for the treated HTL-AP 3 (that is the batch without phenolic content and with the best performance). In these cases, the main degradation step of the catalyst used for the second test of the feed HTL-AP, had a maximum at 322 °C (Figure 49 A). The degradation products in the first part of this step, namely below 200 °C, were mainly CO_2 and volatile organic molecules with anhydride functionalities as underlined from the CO asymmetric and symmetric stretching at 1792 and 1773 cm^{-1} and from the COC stretching at 1174 cm^{-1} in Figure 49 B and from the IR adsorption peak during TGA (Figure 49 D). Above 300 °C, more complex organic fragments are produced with an increase of the stretching of CH_2 and CH_3 from aliphatic fragments between 2800 and 3000 cm^{-1} and the appearance of a small quantity of water (Figure 49 C-D). At temperatures higher than 500 °C the degradation products are mainly water, CO_2 and CO (Figure 49 B). This behavior was similar for all the spent catalysts with high conversion in APR experiments (i.e. used in the 2nd tests or in the absence of detectable phenolic content) and is reported in Figure 50 and Figure 51. In these cases, the alcohols were not identified, giving an indication of the higher reactivity of these catalysts; at the same time, anhydride peaks were present. It can be supposed that the anhydrides derived from the reaction of the carboxylic acids formed during dehydrogenation reaction that underwent dehydration during the TGA. The presence of carboxylic acids can be a further proof of the better performance of the catalysts as they are by-products of alcohols reforming [85].

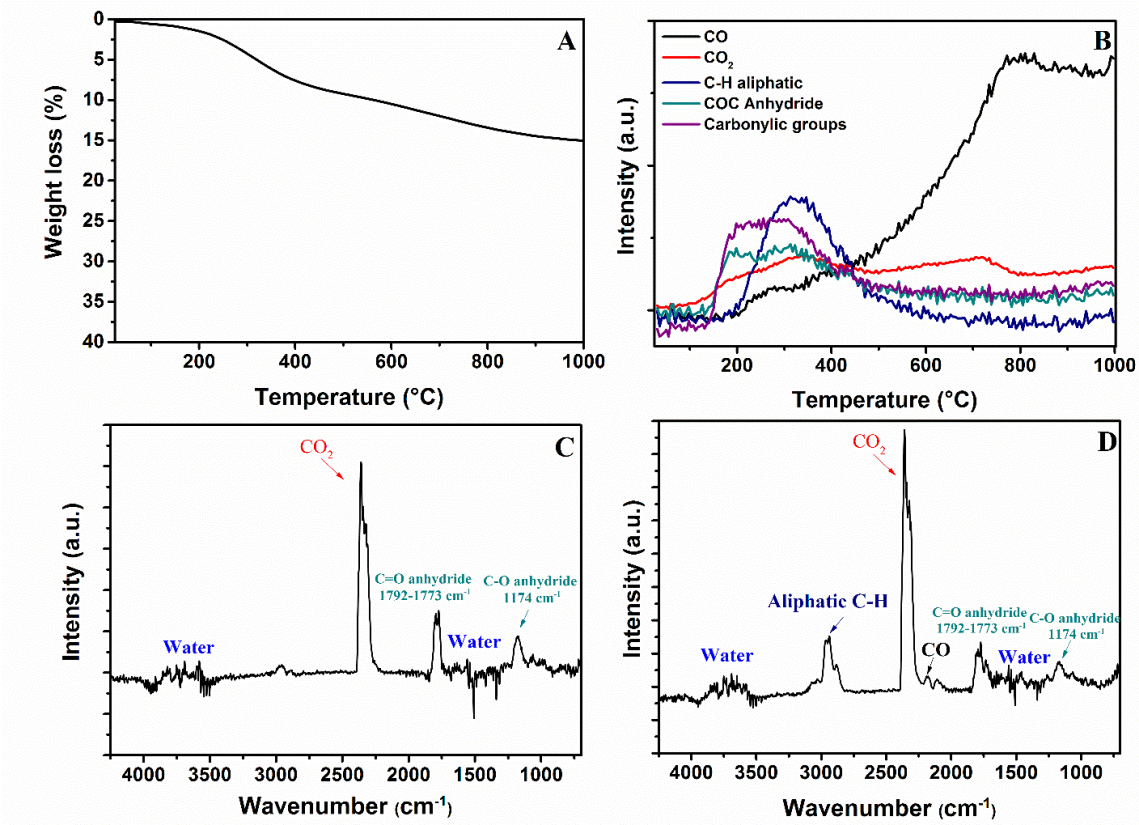
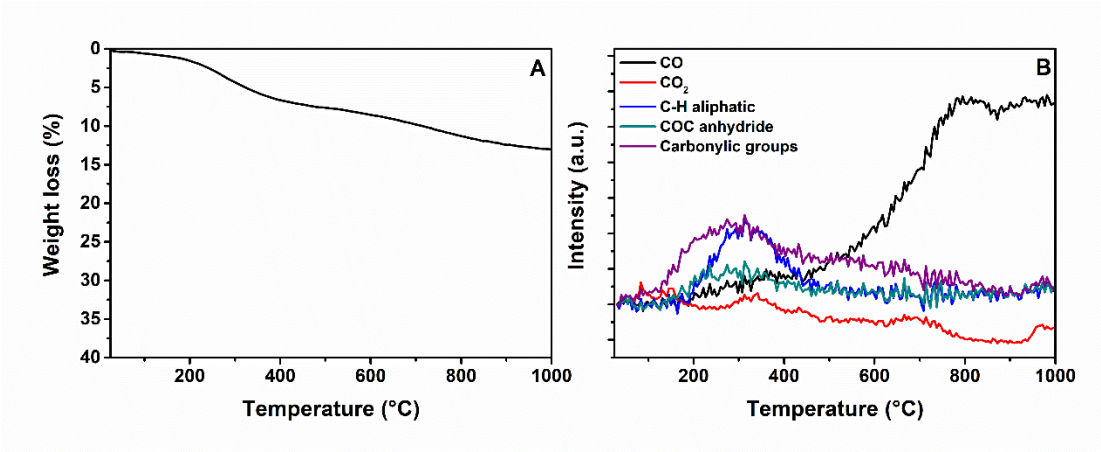


Figure 49: TGA-IR of spent catalyst after APR 2nd test of HTL-AP. Reaction conditions: 0.8 wt.% C, reaction temperature 270 °C, reaction time 2 h. Analysis conditions: heat from 30 °C to 1000 °C @ 20 °C/min in nitrogen atmosphere with a purge rate of 20 mL/min under nitrogen. A: TG results; B: IR-Absorption peak during TGA; C: Infrared spectra at 198°C; D: Infrared spectra at 298 °C.



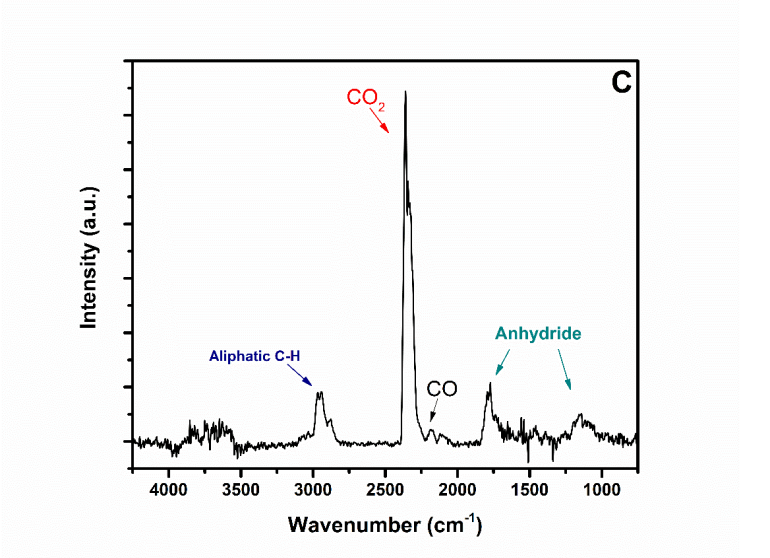


Figure 50: TGA-IR of spent catalyst after APR second test of HTL-AP 1. Reaction conditions: 0.8 wt.% C, reaction temperature 270 °C, reaction time 2 h. Analysis conditions: heat from 30 °C to 1000 °C @ 20 °C/min in nitrogen atmosphere with a purge rate of 20 mL/min under nitrogen. A: TG results; B: IR-Absorption peak during TGA; C: Infrared spectra at 270 °C

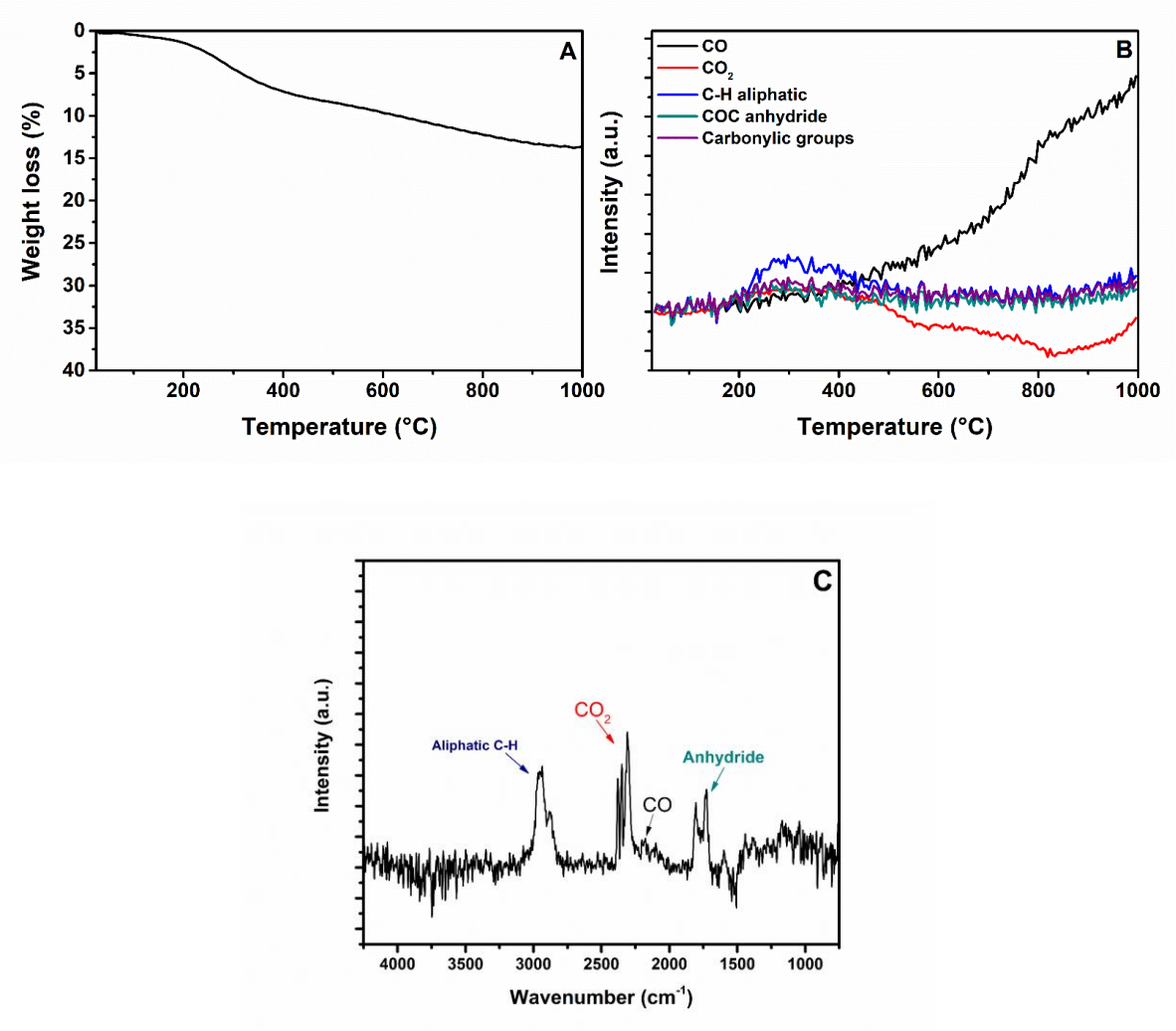


Figure 51: TGA-IR of spent catalyst after APR of HTL-AP 3. Reaction conditions: 0.8 wt.% C, reaction temperature 270 °C, reaction time 2 h. Analysis conditions: heat from 30 °C to 1000 °C @ 20 °C/min in nitrogen atmosphere with a purge rate of 20 mL/min under nitrogen. A: TG results; B: IR-Absorption peak during TGA; C: Infrared spectra at 270 °C.

The second possible cause of deactivation is related to the presence of organosulfur compounds, derived from lignin. As it is known, sulfur can chemisorb irreversibly on the Pt sites, leading to their deactivation.

ICP-MS analysis was performed on the spent catalyst to assess the presence of sulfur. The catalysts used for APR of HTL-AP and treated HTL-AP 3 showed the existence of sulfur on the catalyst, in the 0.08-0.2 wt.% range. This amount may be enough to explain the worsening of the performance; on the other hand, only the ICP-MS does not allow to understand the degree of interaction of the sulfur with the catalyst.

For this reason, potential chemical bonds between platinum and sulfur have been investigated by XPS. In Figure 52, the XPS spectra of Pt_{4f} of fresh and spent catalysts after APR of HTL-AP and treated HTL-AP 3 are reported. First, it is observed that the binding energies of the doublet in the fresh catalyst agree with the literature data regarding Pt metal, with the typical 3.33 eV splitting.

Moreover, none of the spent catalysts showed an increase in the binding energies, being an indication of the lack of strong (chemical) interactions between the platinum and sulfur [184]. Therefore, based on this result, the sulfur poisoning can be reasonably excluded as cause for the catalyst deactivation and its presence may be ascribed to the physical adsorption of S-containing species compounds on the high surface-area carbon support and to a negligible extent to the chemisorption on the active sites. Further investigation on the inorganic sulfur effect will be reported in chapter 5.

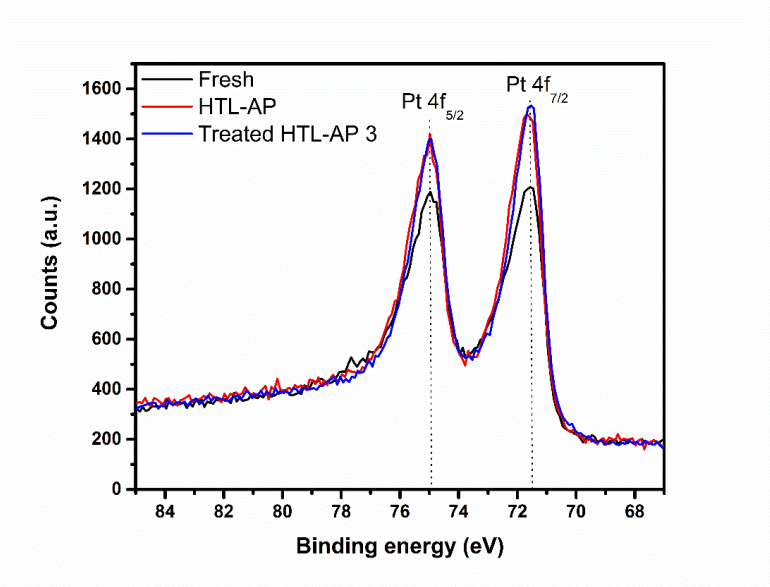


Figure 52: XPS spectra of fresh and spent catalysts after aqueous phase reforming. Reaction conditions: 0.8 wt.% C feed (HTL-AP or treated HTL-AP 3), 270 °C reaction temperature, 2 h reaction time.

4.2. Catalyst deactivation

In the previous paragraphs, we enlarged the portfolio of possible compounds, looking also at molecules more representative of waste streams deriving from HTL. Moreover, a real aqueous phase derived from lignin-rich hydrothermal liquefaction has been tested, increasing the level of complexity of the investigation. In this context, it has been reported that the process performance strongly depended on the aqueous phase composition. It has been suggested that phenolic oligomers may deactivate the catalyst, leading to the necessity of a liquid-liquid extraction with an organic solvent as pretreatment.

It is widely described in the literature that most of the processes involving lignin as feedstock (such as pyrolysis, hydrothermal liquefaction, supercritical water conversion) suffer the problem of solid deposit formation. The variability of the reaction conditions and feedstocks led also to different names, for instance, phenolic char, pyrolytic lignin, phenolic oligomers [185]. Several studies have been carried out to improve the stability of the bio-oils during storage [186], [187] or hinder char formation [188], [189]. The same kind of deposit has been found in the juice and wine storage where phenolic molecules are present [190]. The study of pyrolytic lignin highlighted that it contains linkages that were not present in the original lignin, proving the

presence of condensation reaction [178]. The catalytic process of valorization of bio-oil has to face the formation of carbonaceous materials from phenols polymerization [191].

The present paragraph of the thesis aims to investigate the deactivation of the catalyst after the aqueous phase reforming of lignin-rich hydrothermal liquefaction. Multi-component synthetic mixtures have been used to evaluate the contribution of simple aromatics (phenol and guaiacol) and inorganics to the deactivation. Furthermore, physical pretreatment such as the adsorption on activated carbon has been assessed, looking at the influence on the performance of APR. Finally, the degree of deactivation has been evaluated using a model reaction (APR of glycolic acid) as a means of comparison.

4.2.1. Synthetic aqueous phase – effect of aromatic monomers and inorganics

Previously we hypothesized that the aromatic compounds might interact with the platinum catalyst, drastically reducing the hydrogen productivity. This suggestion derived from the observation that the hydrogen yield monotonically decreased with the increase of the aromatic content in the aqueous phase derived from lignin-rich hydrothermal liquefaction.

In an attempt to evaluate the effect of the aromatic molecules, the composition of the actual aqueous phase was modeled considering five representative compounds. In the following Table 1, the concentration of each compound is reported.

Table 15. Composition of the model aqueous phase tested in the APR set-up.

Acetic acid	2.85E-02
Glycolic acid	2.21E-02
Guaiacol	3.29E-03
Lactic acid	1.74E-02
Phenol	8.66E-03

The influence of the aromatics was investigated looking at three different tests: the first one in which the five-compounds mixture was subjected to APR; the second one, in which guaiacol and phenol were excluded; the third one in which only the aromatics were present. In Figure 53, the comparison between the 3-components mixture (namely Acids) and the 5-components mix (namely Acids + Aromatics) is reported. Given the different initial carbon content, the comparison of indicators such as the carbon conversion to gas may be misleading; for this reason, looking at quantitative indicators such as the amount of produced gas may be more appropriate.

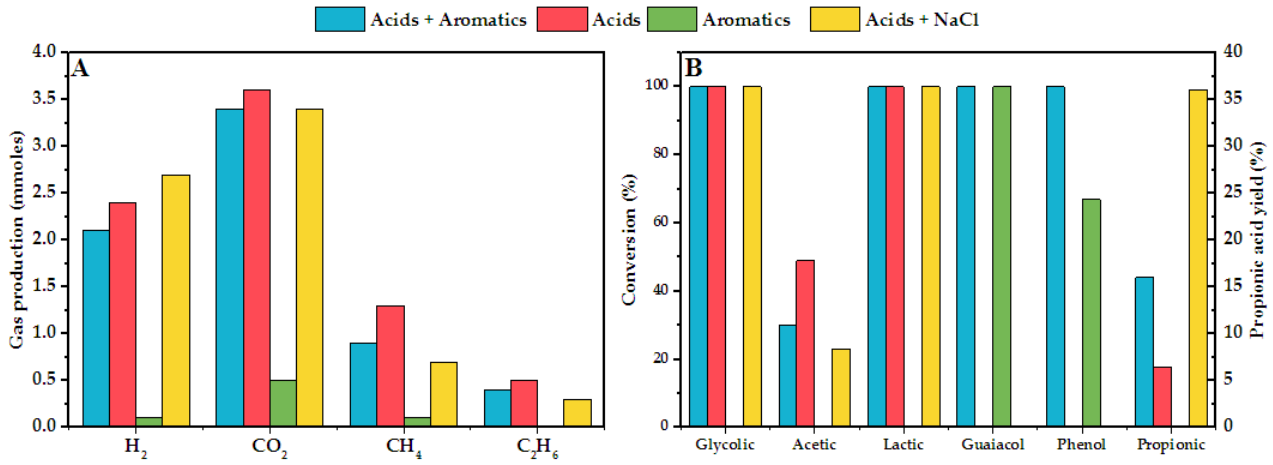


Figure 53. APR results of model mixtures. Reaction conditions: 0.375 g Pt/C, 270 °C, 2 hours.

The 5-components mixture led to the production of a gas phase constituted by carbon dioxide at 50%, followed by hydrogen at about 30%. In the liquid phase (Figure 53-B), glycolic acid and lactic acid converted at 100%, while acetic acid stopped at 30%. Moreover, propionic acid was produced (16% yield), likely deriving from lactic acid conversion as previously suggested. Please note that the propionic acid yield was defined as the ratio between the moles of propionic acid and the initial moles of lactic acid. At the same time, guaiacol and phenol apparently converted completely, as they were not recognized in the HPLC analysis.

The 3-components mixture, i.e. only constituted by glycolic, lactic and acetic acid, did not show dramatically different results compared to the case in which also the aromatics were present. The total gas production only slightly increased by 15%, while in the liquid phase acetic acid conversion increased up to 50%. It is known from previous studies that in the current working conditions one mole of acetic acid catalytically converted into one mole of carbon dioxide and one mole of methane. Starting from this knowledge, we can perform some calculations. In the 5-components test, about 0.6 mmoles of acetic acid converted, therefore being responsible for 0.6 mmoles out of 0.9 totally produced of CH_4 and 0.6 out of 3.4 mmoles in the case of CO_2. On the other hand, in the 3-components test, 0.9 mmoles of acetic acid converted, so likely being the reason why methane and carbon dioxide production increased.

The reported results highlight that phenol and guaiacol do not affect the conversion of glycolic and lactic acid, as it was observed in the case of the real aqueous phase reported in the previous paragraph, where both the acids decreased appreciably their conversion in the case of high concentration of aromatics. For this reason, it can be excluded that aromatic monomers are the cause of the observed deactivation in the actual stream.

For the sake of completeness, a test was performed in which only phenol and guaiacol were present. In this case, the gas production was negligible, highlighting that the aromatic molecules are recalcitrant in the current reaction condition towards the production of a valuable gas (70 mol.% was constituted by carbon dioxide). In the liquid phase, while guaiacol converted completely, phenol converted up to 67%, and catechol was produced.

It is worthy to highlight here that some carbon balance issues raised when guaiacol and phenol were tested. This was due to the adsorption affinity of aromatics with the carbonaceous support, as reported by [192]. We investigated at room conditions the physisorption affinity of the components of the model mixture to evaluate this phenomenon, sampling 1 mL of the solution each 30 minutes up to 2 hours, and the results are reported in the following Figure 54. When we refer to Relative Intensity in the figure, it is meant as the ratio between the area obtained in the chromatogram by the single component after the adsorption and the area at the initial conditions.

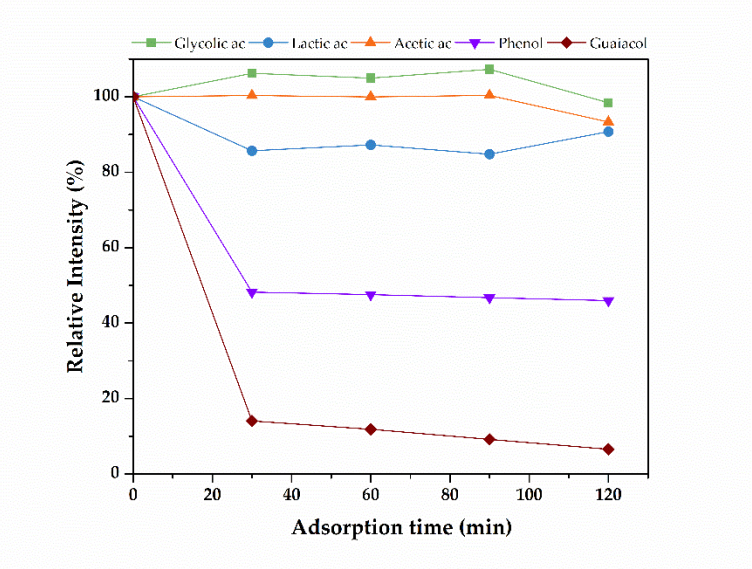


Figure 54. Adsorption of the components of the model mixture. Adsorption conditions: 0.375 g Pt/C, 75 mL Acids + Aromatics solution, room temperature.

Guaiacol and phenol sharply decreased their concentration after 30 minutes, with the former being present at about 10%, while the latter was steadily at 50%. On the other hand, the concentration of glycolic, acetic and lactic acid was higher. It is known that activated carbons are used for the removal of aromatic pollutants in wastewaters [193]. Villacanas et al. studied the adsorption of model aromatic compounds on activated carbons [192]. The lower concentration of guaiacol and phenol could be explained by the hydrophobic bonding between hydrophobic molecules, like aromatic molecules, and the hydrophobic carbon surface [193]. There was evidence to indicate that guaiacol was adsorbed with a higher extent to the active carbon, being more hydrophobic than phenol because of its methoxy group.

Finally, the effect of inorganics was evaluated using NaCl as a representative compound. 500 ppm of Na were added to the Acids mixture, mimicking its concentration in the actual aqueous phase. The APR of this mixture did not report any worsening of the performance compared to the mixture without inorganics. Even more, the production of methane reduced, leading to an increase in the hydrogen gas distribution. The influence of inorganics salts has been poorly investigated for APR. Lehnert et al. suggested that the deactivation observed during APR of crude glycerol was due to the presence of NaCl [105]; however, no experimental evidence was present in their work. On the other hand, Boga et al. ascribed the deactivation mainly to the presence of organic salts (like sodium oleate), studying separately the influence of several possible poisons [109]. In our reaction conditions, NaCl

did not affect the production of hydrogen, therefore it cannot be considered as a poison for the process in the current range.

4.2.2. Actual aqueous phase – effect of physical pretreatment

It was showed in the previous paragraph that a liquid-liquid extraction with DEE allowed to increase the stability of the catalyst, improving at the same time the hydrogen production. In this work, it was evaluated the possibility to carry out physical pretreatment to improve the performance of the process. In fact, if it is supposed that high molecular weight compounds are responsible for the deactivation, and if they have a hydrophobic nature, it is possible that they may interact with a solid sorbent, being removed from the aqueous phase that, afterward, can be subjected to reforming. In the present research, activated carbon was used due to its high surface area and ability to adsorb organic molecules.

For the sake of clarity, in the following Table 16, the names of the tests were reported together with a brief description of the pretreatments they have been subjected to.

Table 16. Description of pretreatments performed on the samples subjected to APR.

Test	Pretreatment
HTL-AP	APR was performed without any pretreatment of the sample
AC + HTL-AP	The sample was put in contact with activated carbon at room temperature for 2 hours; afterward, it was subjected to APR
270 AC + HTL-AP	The sample was put in contact with activated carbon at 270 °C for 2 hours; afterward, it was subjected to APR
DEE + HTL-AP	The sample was washed with excess DEE; afterward, it was subjected to APR
270 AC + DEE + HTL-AP	The sample was washed with excess DEE; afterward, it was put in contact with activated carbon at 270 °C for 2 hours; finally, it was subjected to APR

Two different adsorption conditions were evaluated. The first one was performed at room temperature; in the second one, the same temperature of the APR (270 °C) was used. In Figure 55 the results of the influence of the temperature of the physical pretreatment (AC + HTL-AP and 270 AC + HTL-AP) was compared with the results reported in the previous paragraph with same reaction conditions, where the aqueous phase was reformed without any pretreatment (HTL-AP) and after a liquid-liquid extraction with diethyl ether (DEE + HTL-AP). Finally, a test was performed where both pretreatments were used (270 AC + DEE + HTL-AP).

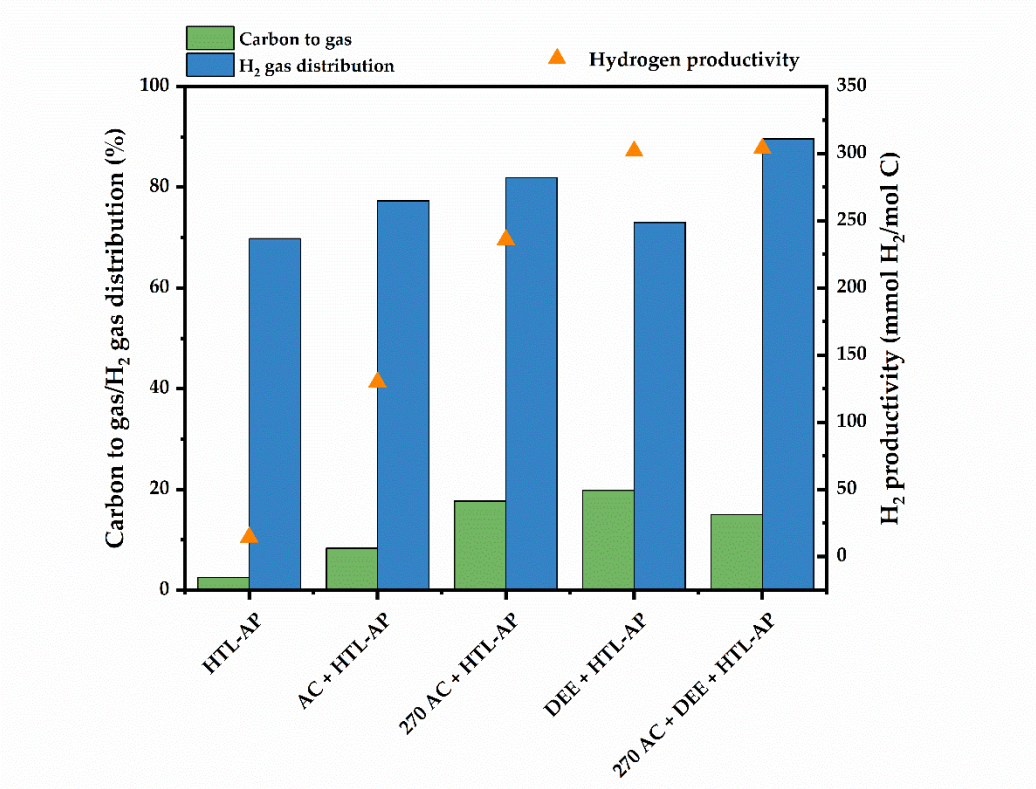


Figure 55. Influence of temperature of physical pretreatment. Reaction conditions: 0.375 g Pt/C, 270 °C, 0.375 g Pt/C, 2 hours.

The APR of HTL-AP led to less than 5% of carbon conversion to gas and negligible hydrogen productivity. This result derived from the small conversion of the mixture components that were prone to hydrogen production, like glycolic acid, glycerol, and methanol. Interestingly, if the APR test was performed after a room temperature pretreatment in which the aqueous phase was in contact with activated carbon (AC + HTL-AP), both the indicators improved. The carbon to gas conversion reached 10%, while the hydrogen productivity raised to 125 mmoles H_2/mol C. It is suggested that the phenolic oligomers present in the solution, because of the affinity with the hydrophobic solid, may be adsorbed into the activated carbon. The depolymerization of lignin during the hydrothermal liquefaction can lead to phenolic monomers and oligomers that are soluble in the water fraction [194]. Decomposition of lignin forms formaldehyde and phenolic monomer (guaiacol, catechol, syringol) and it has been reported that cross-linking reactions can occur between these molecules and residual lignin to form solid deposit [189]. In general, HTL and pyrolysis of lignocellulosic biomass form products with a wide range of very reactive molecules (acids, phenols aldehydes, ketones), including also free radicals; these molecules probably repolymerized to form high molecular weight condensation products [186]. The aqueous phase post HTL contained, despite in more diluted conditions, the same kind of molecules. Therefore, they may be involved in similar reactions.

When the aqueous phase was subjected to a high-temperature adsorption (270 AC + HTL-AP), the results of APR further improved in terms of carbon conversion to gas and hydrogen productivity. This was an interesting result, which suggested that the temperature influenced the formation of high molecular weight compounds, responsible for the deactivation of the catalyst. Performing the

pretreatment at high temperature allowed removing some precursors of these deactivating compounds, which otherwise were produced during the reaction step (as it happened in the case of AC + HTL-AP). During the storage at low temperature, it has been possible to note the formation of deposit in time (further consideration in paragraph 3.4). As widely pointed out [186], [187], [195], the heat increases the aging process: therefore, the high temperature of APR may favor the polymerization reaction and deposit formation. Indeed, even if the reaction was carried out in the absence of oxygen, it has been highlighted that oxidative coupling phenolic compounds does not require molecular oxygen, being phenol molecules able to react with active sites on the carbon surface itself [196].

Finally, the treatment with activated carbon has been performed also with a sample previously treated with DEE (270 AC + DEE + HTL-AP). In this case, minor differences can be observed in terms of hydrogen productivity compared to the DEE + HTL-AP case; on the other hand, an improvement in terms of selectivity has been reported. Nevertheless, it will be highlighted in the following that the combination of the two steps allowed to improve the stability of the catalyst.

In Figure 56, the adsorption of the actual aqueous phase with activated carbon and Pt/C catalyst is reported. First of all, similar trends can be observed between the two experiments, suggesting that at low temperature the presence of platinum did not strongly affect the adsorption behavior. However, one phenomenon was particularly interesting and refers to the maximum of adsorption reported at 60 minutes for phenol and guaiacol. In the case of the synthetic mixture adsorption indicated in Figure 54, once that the aromatic molecules were adsorbed, there was no change in the product distribution in the liquid phase. The textural analysis of the catalyst reported that the surface area decreased from 831 m^2/g of the fresh catalyst to 583 m^2/g, and it can be ascribed to the adsorption of phenol and guaiacol.

In the case of the actual aqueous phase adsorption, it seemed that after 60 minutes a steady state has not been reached. The study of the dynamic of aromatics adsorption into activated carbon has been majorly explored for a single-component solution. Wang et al. studied the adsorption of a mixture of aromatics into granular activated carbon [197]. It has been highlighted that the solubility and functional groups distribution play a pivotal role in the competitive adsorption capacity. In the current conditions, we suggested that at a first place the aromatic monomers readily interact with the hydrophobic surface of the carbon; however, the oligomers, once overcoming the mass transfer issues (maybe due to their lower diffusion in the aqueous medium) can gradually substitute the monomers being less hydrophilic. The textural analysis of the catalyst reported that the surface area was equal to 285 m^2/g, much less than the synthetic case, despite the lower adsorption of the simple aromatics. Therefore, it is likely that the reduction is due to the high molecular weight compounds.

The slight differences in the adsorption trend between activated carbon and Pt/C may be attributed to the different types of support. In fact, despite the pore volume and average pore size are analogous (0.589 cm^3/g and 6.45 nm for activated carbon and 0.584 cm^3/g and 5.18 nm for Pt/C), the microporosity is different. It is 0.226 cm^3/g for activated carbon and 0.183 cm^3/g for Pt/C (evaluated by t-plot method). Mojoudi et al. reported that phenol adsorption was favored by well-developed porous structure and microporosity [198]. Therefore, the higher value of the latter for activated carbon

may be responsible for the higher adsorption capacity (i.e. corresponding to a lower intensity of the peak in the figure) of phenol.

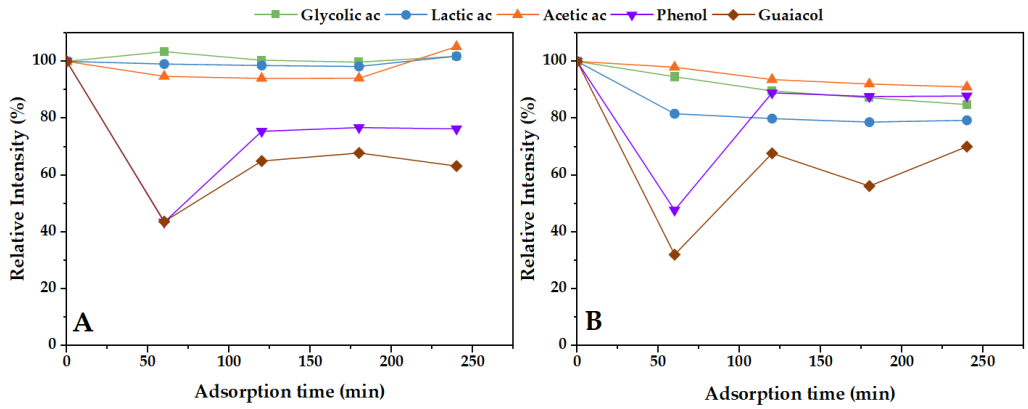


Figure 56. Adsorption of the actual phase with 0.375 g activated carbon (A) and 0.375 g Pt/C catalyst (B). Adsorption conditions: 75 mL solution, room temperature.

The higher affinity of the phenolic oligomers compared to the monomers can also explain some of the peculiar outcomes of the tests reported before. In Figure 57, the chromatograms related to synthetic (A) and actual (B) aqueous phase (HTL-AP) are reported. The feeds are indicated with a black line, the composition obtained after adsorption with the Pt/C catalyst is depicted in red, while the composition after the APR in blue.

Comparing the chromatograms, a) and b), it can clearly be observed that the phenolic compounds were adsorbed in the catalyst (as can be deducted from Figure 56). After the APR, they completely disappeared.

However, making the same comparison for the HTL-AP (Figure 57-B) it is possible to see that catechol, 3-methoxycatechol, phenol, and guaiacol remained entirely in the liquid phase after the adsorption test; however, analogously with the synthetic mixture, they were removed from the liquid phase during the APR. We proposed that in the synthetic mixtures, where no oligomers were present or formed, the monomers could adsorb during the treatment with activated carbon. On the other hand, in the HTL-AP the formation of longer chain molecules, which have a higher affinity with the carbon, prevented the adsorption of the monomers during the first step. Therefore, it was only during the second step (the APR reaction itself) that they were free to adsorb on the catalyst.

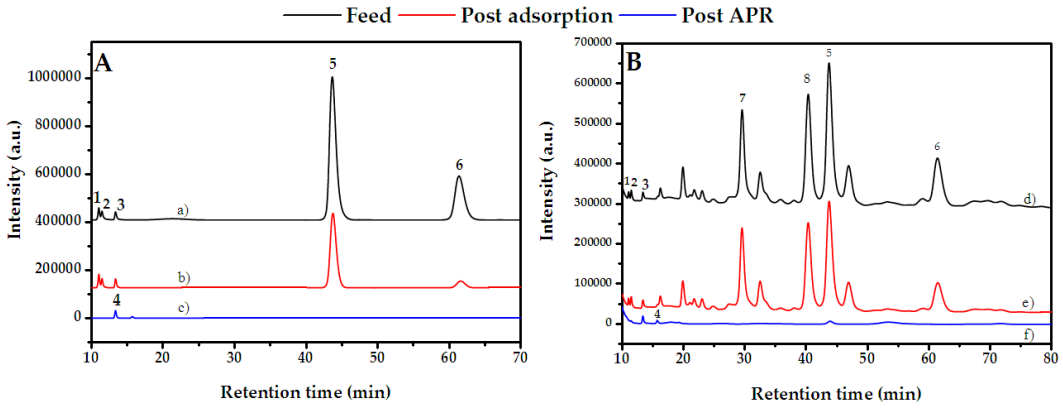


Figure 57. HPLC chromatograms (PDA wavelength: 212 nm) of synthetic (A) and actual (B) mixtures on Pt/C catalyst. 1: glycolic acid, 2: lactic acid, 3: acetic acid, 4: propionic acid, 5: phenol, 6: guaiacol, 7: catechol, 8: 3-methoxycathecol. Adsorption conditions: 75 mL solution, 0.375 g Pt/C catalyst, room temperature, 4 hours. Reaction conditions: 75 mL solution, 0.375 g Pt/C catalyst, 270 °C, 2 hours.

The Pt/C used for the adsorption of the HTL-AP was washed with acetone (50 mL) to get information on the organics present on the surface. 25 mL of the solution were left to evaporate to observe high molecular weight compounds. Indeed, the beaker showed some deposits, that were subjected to ATR analysis (paragraph 3.4). 25 mL of the remaining solution were initially concentrated and then subjected to GC-MS analysis (Figure 58). The spectra revealed the presence of aromatic compounds not identified in the HPLC analysis like 4-ethylguaiacol, 4-propylguaiacol, creosol, and 2,4-di-tert-buthylphenol. These compounds were already present in the initial aqueous phase [199]. This test confirmed that not only small molecules such as guaiacol, phenol, and catechol can be adsorbed on the catalyst surface, but also higher molecular weight compounds can interact with the catalyst as well. Further investigation will be addressed to study deeper the influence of the solvent and time of the washing procedure.

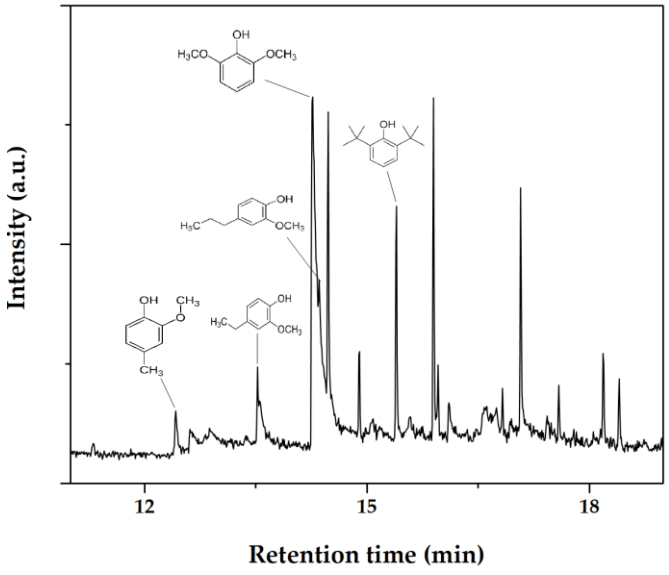
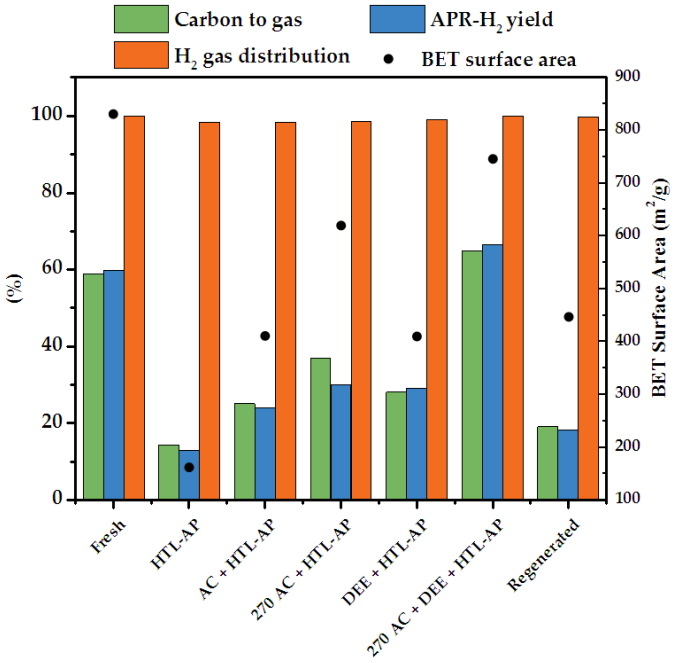


Figure 58. GC-MS analysis of the acetone solution derived from the washing step of the Pt/C catalyst. From left to right: creosol, 4-ethylguaiacol, syringol, 4-propylguaiacol, 2,4-di-tert-buthylphenol.

4.2.3. *Evaluation of catalyst deactivation*

Because of the endogenous nature of the deactivation, it was not possible to evaluate the extent of deactivation conventionally, i.e. re-using the catalyst with a fresh batch of the aqueous phase. Therefore, the APR of a probe molecule (glycolic acid) was used as a reference, whose re-test did not cause appreciable deactivation on the catalyst. The following Figure 59 shows the obtained results comparing catalysts that derive from different tests.



Catalyst	Surface area (m^2/g)	Pore volume (cm^3/g)	Micropore volume (cm^3/g)
Fresh	831	0.604	0.184
HTL-AP	162	0.306	-
Fresh AC	878	0.589	0.226
AC	145	0.342	-
AC + HTL-AP	411	0.506	0.011
270 AC	119	0.317	-
270 AC + HTL-AP	620	0.587	0.074
DEE + HTL-AP	410	0.389	0.024
270 AC + DEE + HTL-AP	746	0.567	0.145
Regenerated	447	0.436	0.068

Figure 59. APR of glycolic acid using second-use Pt/C catalysts and corresponding textural properties. Reaction conditions: 0.375 g Pt/C, 270 °C, 0.9 wt.% C glycolic acid, 2 hours.

In Figure 59, the comparison of the performance after the re-use of the catalyst is reported, together with the information on the surface area. Starting from the reference test (Fresh), which is the APR of glycolic acid using a fresh catalyst, it can be observed that the APR of HTL-AP led to a strong decrease in both the carbon conversion to gas and the hydrogen yield. This result was associated with a steep loss of surface area, moved from 831 to 162 m^2/g. The pretreatment with activated carbon allowed to increase the performance, with the one at higher temperatures confirming the improvement compared to the low-temperature adsorption. As a matter of fact, the surface area of the catalyst after high-temperature adsorption was 620 m^2/g, while it was 411 after room temperature adsorption. Moreover, it is interesting to observe that the surface area of activated carbon after adsorption at room temperature decreased from 878 to 145 m^2/g, further decreasing up to 119 m^2/g at 270 °C. When both the pretreatments have been performed (i.e. use of DEE and AC), the catalyst kept most of its original surface area: this result was reflected on the high performance of APR, similar to the ones obtained with the fresh catalyst.

In the end, it is highlighted here a preliminary attempt on the regeneration of the catalyst. The catalyst after HTL-AP reforming was subjected to a thermal treatment in inert flow (nitrogen) at 410 °C for 2 hours. At the end of this step, it was observed that it partially recovered the surface area (447 m^2/g); however, it was not sufficient to strongly improve the performance compared to the HTL-AP case, with only a slight increase of the carbon conversion and hydrogen yield.

Some of the possible reasons were investigated. One possible explanation was the sintering of the particles due to the high-temperature treatment. In Figure 60, the XRD spectra of the as received (i.e. before its use) and regenerated catalysts are compared. The broad diffraction peak at $2\theta = 20\text{-}30°$ refers to the amorphous carbon structure; the diffraction peaks at $2\theta = 39.6$, 47.4 and 67.1° refer to the face centered cubic structure of platinum. Since the two spectra were analogous, leaching was excluded as main deactivation mode. Moreover, re-oxidation of platinum under the hydrothermal reaction conditions was not found, due to the absence of platinum oxide peaks, while leaching did not occur since ICP-MS did not detect platinum in the HTL-AP and 270 AC + HTL-AP solutions, at the end of the reaction. Finally, it should be considered that, despite the reuse tests have been performed using the same amount of catalyst (0.375 g), it was actually constituted by catalyst plus carbonaceous deposits. In fact, at the end of the reaction with the real aqueous phase, the recovered solid phase weighted more than the original 0.375 g, due to the organics adsorbed on it. Consequently, the effective amount of active sites may vary from one test to the other.

It has been reported that phenolics may adsorb irreversibly into activated carbon so that they cannot actually be removed in water or at high temperatures [200]. Grant et al. reported that the polymerization of phenolics can occur also on the activated carbon support, and that it was favored by higher temperatures [196].

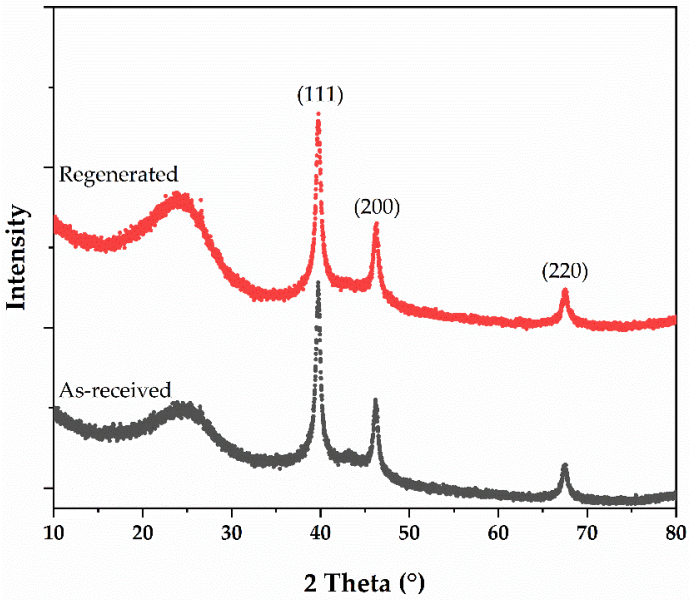


Figure 60. XRD patterns of as-received and regenerated catalyst.

4.2.4. Solid characterization

A filtration step was necessary to eliminate the solid particles from the aqueous phase received by RE-CORD. The use of a simple paper filter was not enough to ensure a clear solution. For this reason, a 0.2 µm PTFE filter was used before the tests. Nevertheless, the mixture was very unstable; indeed, even if filtered and stored in the fridge, new solids were formed.

The solids in the feed presented a dark brown color. They were characterized by attenuated total reflectance (ATR) spectroscopy to evidence its nature through the identification of some key functional groups (Figure 61). The broad peak at 3250 cm^{-1}, corresponding to the O-H stretching, referred to the presence of alcohols, phenols, and carboxylic acids. The band in the range 3000-2840 cm^{-1} can be associated with the presence of alkyl C-H as it represents the C-H stretching vibrations. Please note that the absorption at around 2300 cm^{-1} was referred to a noise due to a not perfect compensation of atmospheric CO_2. The 1200-1000 cm^{-1} band was assigned to the C-O vibrations, therefore it could reveal the presence of acids and phenols. The aromatic skeleton vibration can be identified at 1568 cm^{-1} associated with C=O stretchings and at 1409 cm^{-1} associated with C-H deformations [201]. Finally, the peak at 1315 cm^{-1} can refer to the vibration of siringyl with guaiacyl groups [202]. These peaks evidenced the organic nature of the particles and the presence of phenol-derived groups gradually formed during the low-temperature storage of the solution. This can be an indication that similar phenomena can be accelerated during high-temperature treatment.

The catalyst used for the room-temperature adsorption of the actual aqueous phase was washed with 50 ml of acetone for 10 minutes, as reported in paragraph 3.2. The washing solution was left to evaporate to recover solid species present in the surface. Unfortunately, the amount of recovered deposits was barely enough to perform the analysis, leading to a spectrum with lower peaks intensity.

Despite the explorative nature of this attempt, the characterization showed a different distribution of the functional groups. The bands associated with the aromatic skeleton at 1568 and 1409 cm^{-1} were missing; however, the band of the C-H and C-O stretching vibrations were visible. This result can be due to the fact that the washing step was not able to remove all the species present on the catalyst surface responsible for the observed decrease of surface area during the low-temperature adsorption.

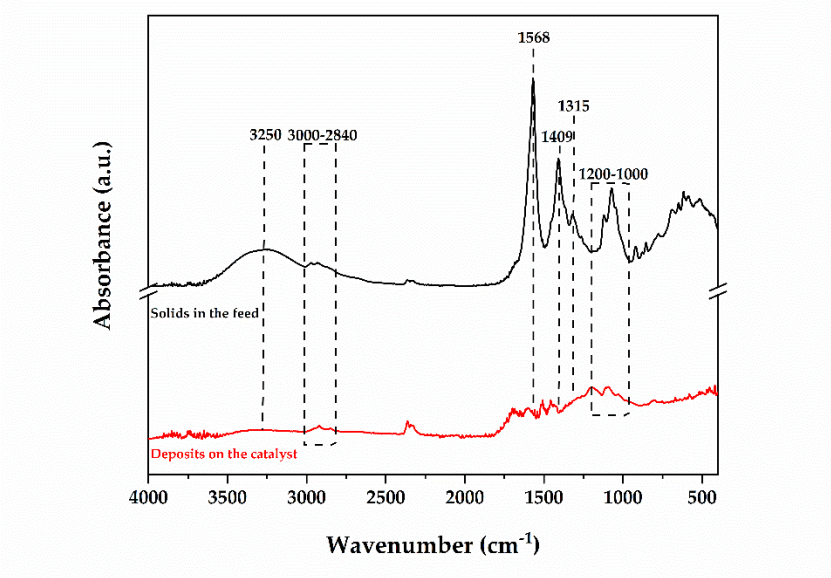


Figure 61. ATR spectra of solid deposits formed during the storage of the aqueous phase.

4.3. Influence of solvent extraction

The results and figure of the paragraph are reported in an accepted paper [203].

As it has been reported in the previous paragraph the phenolic oligomers in the aqueous phase might significantly affect the catalyst performance leading to its deactivation via fouling-like mechanisms. To avoid this inconvenience, one possible route is to carry out a liquid-liquid extraction that selectively removes the aromatics while preserving the content of the other oxygenates prone to produce hydrogen. Diethyl ether has been shown to be an effective solvent for this separation. However, its properties are not fully compatible with its application on a commercial scale plant due to severe issues related with safety, health and environmental criteria [204]. Looking only to the latter, on a scale from 1 (being water) to 10, DEE was ranked 7 as regards to the environmental score due to its low boiling point etc. Butyl acetate is considered a recommended alternative (ranking score 3), being a more environmentally friendly solvent. For this reason, in this paragraph, diethyl ether and butyl acetate were compared as solvents for liquid-liquid extraction of the water fraction collected after the NaOH-assisted hydrothermal liquefaction; moreover, the effect of the S/AP ratio was evaluated. Primarily, the effectiveness of this pretreatment was assessed in terms of selectivity for the extraction. In Figure 62 the extraction of organics acids and aromatics in the case of different solvents and S/AP ratios is reported. Regarding the organic acids, the recovery was defined as the ratio between the sum of glycolic, lactic and acetic acid concentration (the three most present organic acids) in the aqueous phase post-extraction and in the one without extraction (equation 6). The highest

the organic acid recovery, the most effective the treatment: ideally, no organic acids should be removed during this stage.

$$\text{Organic acids recovery (\%)} = 100 \cdot \frac{(\text{glycolic} + \text{lactic} + \text{acetic})_{\text{Treated HTL-AP}}}{(\text{glycolic} + \text{lactic} + \text{acetic})_{\text{Untreated HTL-AP}}} \quad \text{(Eq. 23)}$$

$$\text{Aromatics recovery (\%)} = 100 \cdot \frac{(\text{Aromatics PDA 212 nm Area})_{\text{Treated HTL-AP}}}{(\text{Aromatics PDA 212 nm Area})_{\text{Untreated HTL-AP}}} \quad \text{(Eq. 24)}$$

can be observed that these compounds, thanks to their hydrophilicity, preferentially remained in that phase, and were not removed whatever solvent and S/AP ratios were used. This outcome, which was limited for the sake of clarity to the three most abundant compounds, is reported Figure 62-A, where the HPLC chromatograms are depicted as well. These chromatograms refer to the use of a refractive index detector, which is suitable for organic acids and alcohols detection. This is an important result because the un-selective recovery of the oxygenates would hinder the hydrogen production. In fact, apart from being a cause of deactivation, phenolics were recalcitrant compounds under the reported reaction conditions, therefore their valorization would be difficult [85].

The same evaluation was performed looking at the aromatic fraction of the water-soluble compounds (equation 7). In this case, the chromatograms reported in Figure 62-B are referred to the photo diode array detector, which is more sensitive than the RID to these compounds. Catechol, 3-methoxycatechol, phenol and guaiacol were the most present aromatics and they constituted 50% of the aromatic fraction. Both solvents significantly removed the aromatics. Phenolics showed high affinity with diethyl ether, as reported in [205]. Interestingly, butyl acetate was even more effective, since it allowed a higher recovery at equal S/AP ratio. This is an important element to consider, because it proved that this step can be performed with high selectivity, using a greener solvent. Furthermore, under an industrial point of view, the lower solubility of butyl acetate in water compared to diethyl ether reduces its loss and, consequently, the need for make-up, overall decreasing the operating costs (diethyl ether solubility in water is 69 g/l, while it is only 7 g/l for butyl acetate).

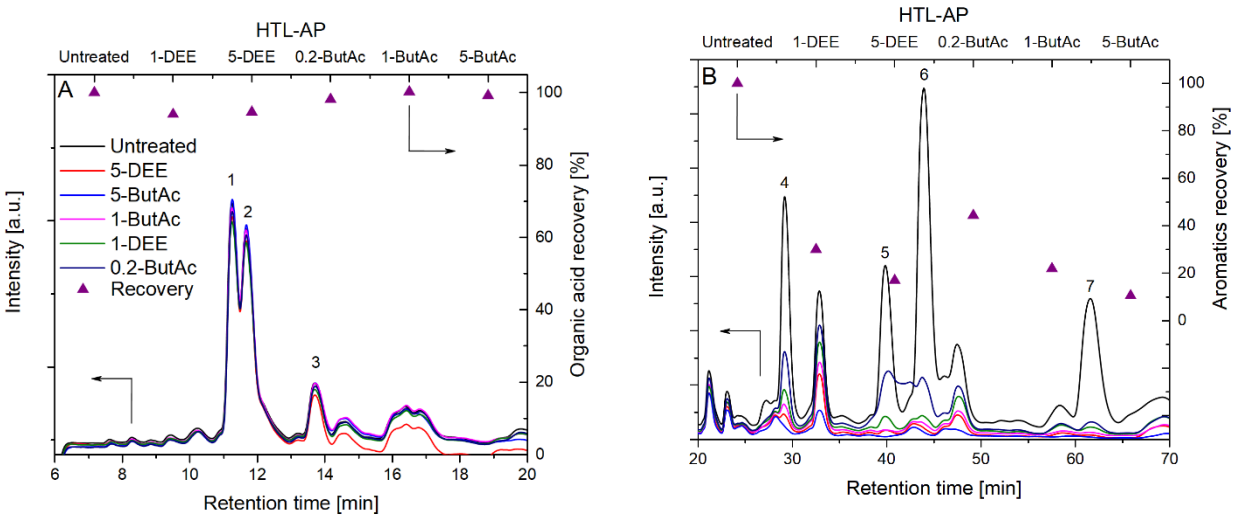


Figure 62. A: Organic acids recovery after liquid-liquid extraction and HPLC-RID chromatograms (1: glycolic acid, 2: lactic acid, 3: acetic acid); B: aromatics recovery after liquid-liquid extraction and HPLC-PDA (212 nm) chromatograms (4: catechol, 5: 3-methoxycatechol, 6: phenol, 7: guaiacol).

The APR results obtained after the liquid-liquid extraction are reported in Figure 63. For comparison, the untreated aqueous phase was added to the graph, showing its lowest gas production for each of the main components. When diethyl ether was used in the pretreatment, an improvement in the hydrogen production was observed both at 1:1 and 5:1 solvent: aqueous phase ratios, with an increase equal to 35% and 48%, respectively. A similar increase rate was observed for methane (40% and 50%), while carbon dioxide production was almost constant. This outcome was likely due to the higher conversion of methanol. In fact, it reacts following the stoichiometry reported in equation 5, so leading to 3 moles of hydrogen per mole of carbon dioxide. Consequently, this may be the reason for the higher H_2/CO_2 ratio. The carbon to gas conversion increased only slightly, being 13.7% at both the S/AP ratios. It should be noted that for the determination of this indicator the carbon content of the solvents was excluded since it was considered as inert.

The same trend was observed when butyl acetate was used as solvent. Again, an increase in the S/AP ratio led to an increase in the hydrogen production and a constant carbon dioxide production; the methane production reported a slight decrease. Comparing the aqueous phases treated with equal amount of solvent, the butyl acetate-treated ones gave better results than the DEE-treated ones, with the 5-ButAc leading to almost double hydrogen production compared to the untreated sample. The carbon to gas showed a greater improvement, reaching up to 19.6% when the highest amount of ButAc was used. It is worth to note that the decrease of phenolic content penalized the occurrence of adsorption, yielding a higher carbon balance closure (85% average).

The reason why butyl acetate led to better performance than diethyl ether is not trivial. The removal of the aromatics, despite significant, does not seem to be the only reason, since the 0.2-ButAc sample had a higher content of these compounds than 1-DEE and 5-DEE, but also higher hydrogen production. It has been reported in literature that the pH can affect the APR performance. However, in this case, the difference cannot be attributed to different pHs, since the two solvents have an almost neutral behavior. Furthermore, blank experiments where only the solvents were subjected to APR, showed a negligible hydrogen production, demonstrating that the solvents did not contribute to the

observed performance. We suggest that the lower solubility of butyl acetate could decrease the onset of competitive adsorption phenomena which, particularly in the liquid phase, can be of great importance [206].

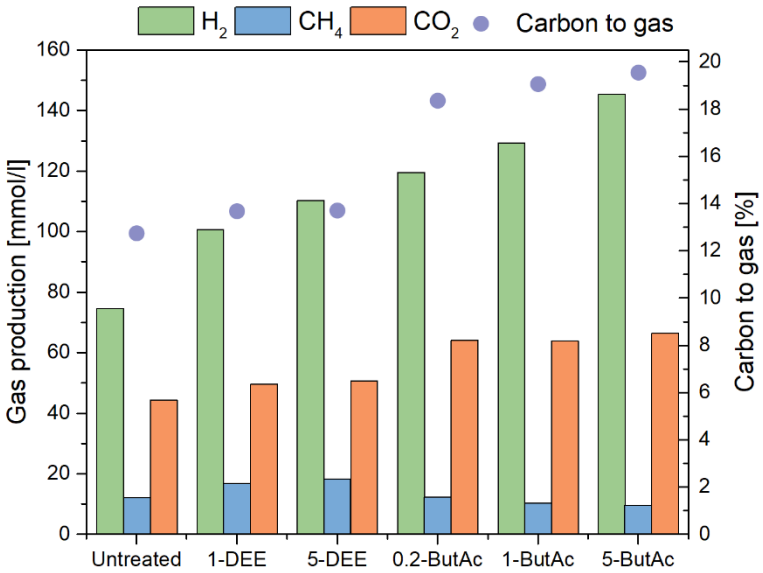


Figure 63. Influence of the nature and amount of the solvent on the APR performance. Reaction conditions: 75 mL aqueous phase, 270 °C, 2 h, 0.375 g 5% Pt/C.

Figure 64 depicts the APR results of the re-use tests, together with the data on the surface area of the spent catalysts. The textural characterization of the catalysts used with treated aqueous phase reported an increase of the surface area compared to the untreated one. However, a clear trend was not observed, since it apparently decreased with the increase of DEE, while increased at higher ButAc/AP ratios. The hydrogen yield and carbon to gas conversion were quite similar for DEE, while they had a slightly increasing trend in the case of butyl acetate. Therefore, despite butyl acetate led to higher hydrogen yield in the reaction stage, it seems that it did not improve the stability of the catalyst to a higher extent than DEE. Further investigations on the influence of the inorganics are ongoing to verify their impact on the catalyst lifetime.

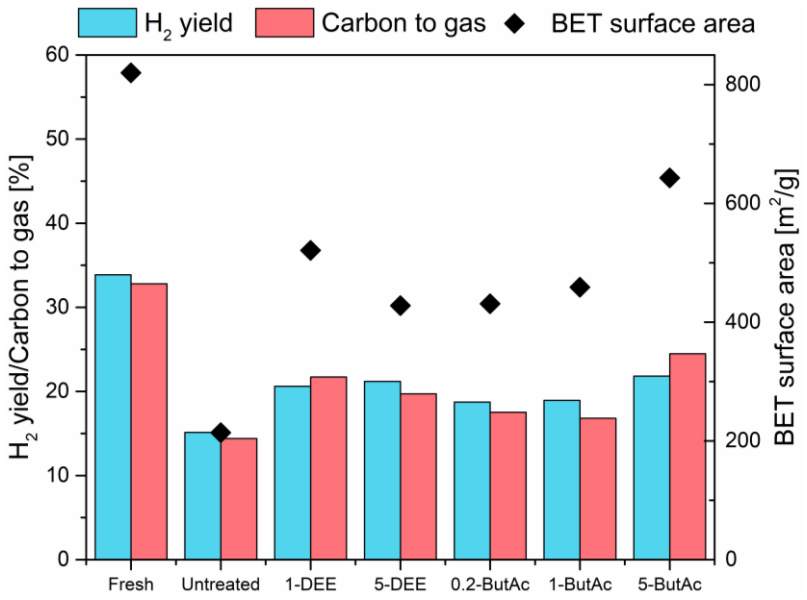


Figure 64. APR of glycolic acid with a spent catalyst. Reaction conditions: 75 mL aqueous phase 2.85 wt.% glycolic acid, 270 °C, 2 h, 0.200 g 5% Pt/C (spent).

Conclusion

The water fraction derived from lignin-rich hydrothermal liquefaction has been valorized through APR for hydrogen production. A screening performed with representative model compounds allowed to identify the molecules prone to reforming, while the study of a synthetic mixture highlighted competitivity issues on the active sites. This outcome is particularly crucial for the valorization of secondary streams as they are complex mixtures constituted by several different classes of compounds. The study of the real water fraction showed a dramatic dependence of the performance on the phenolics content, highlighting the necessity of pretreatment of the water phase to increase the stability of the catalyst. Indeed, the lower was the concentration of phenolics (i.e. phenol, guaiacol, catechol) in the feed, the higher was the hydrogen production. The textural characterization showed that the worsening of the performance may be associated to a decrease of the surface area and pore volume, likely due to the fouling mechanism caused by phenolic oligomers. Tests with synthetic mixtures allowed to exclude that aromatic monomers (phenol and guaiacol) and inorganics (NaCl) may be responsible for the decrease of hydrogen production. Different pretreatments of the aqueous phase were carried out to improve the hydrogen productivity, the carbon conversion to gas and the stability of the catalyst. It was observed that performing the adsorption of the aqueous phase with activated carbon at 270 °C allowed to improve the hydrogen yield, likely because phenolic oligomers, formed at high temperature by condensation reactions, block the active sites of the catalyst. The use of both DEE extraction and activated carbon adsorption increased the stability of the catalyst maintaining the original textural properties. In the last part of the paragraphs a more sustainable alternative to DEE is studied. The ATR spectra of the solids formed during the storage confirmed the presence of organics with peaks referring to aromatic compounds. Although activated carbon is a good support to improve the dispersion of the active metal, alternative supports which may be inert towards high molecular weight molecules adsorption need to be evaluated.

The reasons of catalyst deactivation can be multiple because of the presence of multiple species in the aqueous solution, in this chapter we proved that the presence of aromatics cause the decrease of the surface area and therefore deactivated the catalyst. However due to the complexity of the HTL-AP other causes may be present, which are not detected in batch reactors. Thus, at end of next chapter 5 the presence of sulfate will be investigated in synthetic mixture.

Chapter 5

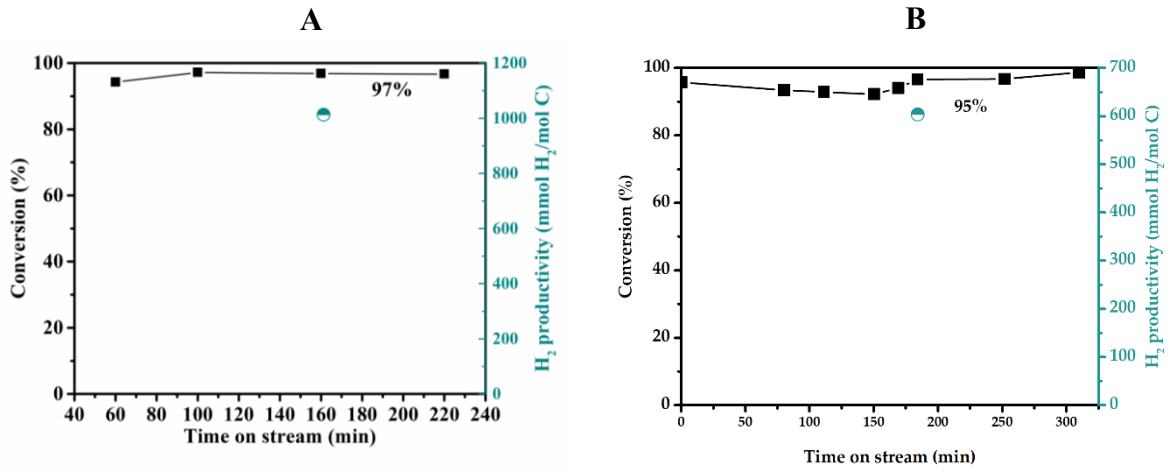
Continuous tests

5.1. Lab scale continuous tests

5.1.1. Model compounds and synthetic mixtures

This chapter describes the tests conducted in the continuous reactor. The reactor is filled with platinum on carbon pellet and the same approach of the batch tests was used. Preliminary tests were conducted with four model compounds representative of the main classes of compounds of HTL: ethanol, glycolic acid, lactic acid and acetic acid. In the following Figure 65 the results of their test are reported. The tests have been conducted for several hours at 270°C and 60 bar to evaluate the stability of the catalyst and to reactivity of the molecules. The reactions had different dilution (glycolic acid was tested at 0.3 wt.% C, ethanol at 1 wt.% C, while acetic and lactic acid at 0.9 wt.%) to be able to compare them with the reference tests in batch reactor.

The compounds followed the activity and selectivity already seen in the batch reactor. The glycolic acid (Figure 65-A) was the most reactive followed by ethanol (Figure 65-B), lactic acid Figure 65-C) and finally, the acetic acid (Figure 65-D). The highest hydrogen productivity was of glycolic acid reached 10000 mmol H_2/molC the lowest is less than 10 mmol H_2/molC of the acetic acid; the compounds with a hydroxyl group confirm their higher reactivity towards APR, while the ones with a carboxylic group led to a higher production of alkanes.



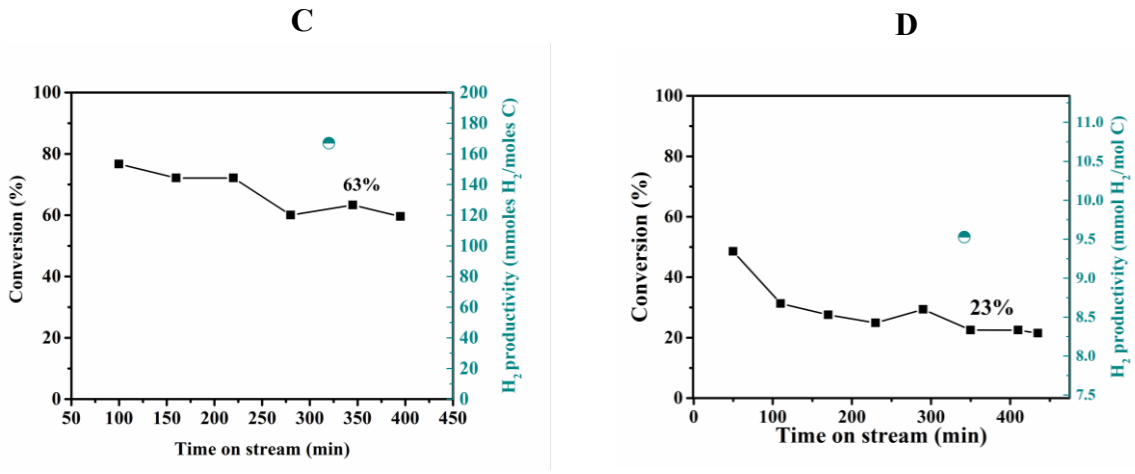


Figure 65. APR of model compounds (A: glycolic acid; B: ethanol; C: lactic acid; D: acetic acid). Reaction conditions: 270 °C, 60 bar, flow 0.6 mL/min, feed concentration 0.3 – 1 wt.% C.

The mixture of the acids was then tested to study the influence of the flow rates between 0.2-0.6 mL/min. The increase of the flow rate affected the conversion of the lactic acid (and glycolic acid) which decreased from 100% (98%) to 55% (89%); generally, the increase of the flow rate decreases the residence time, and this may bring to a decline of the conversion, being the substrate in contact with the catalyst for a shorter period of time. As already observed in previous work [85] the acetic acid conversion dropped when put in mixture, leading to negative conversion due to its lower tendency of the acetic acid to adsorb on the catalyst, together with its production from the glycolic acid hydrogenation (parallel undesired reactions).

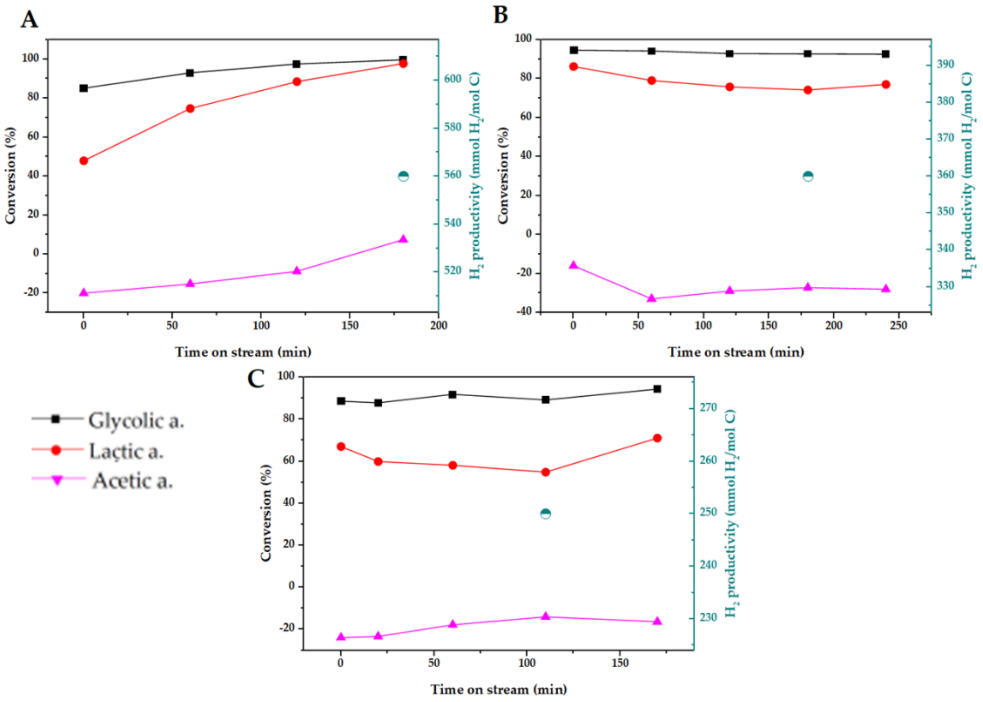


Figure 66. Performance of APR synthetic mixture. 270 °C, 60 bar, A: 0.2 ml/min B: 0.4 ml/min C: 0.6 ml/min

Finally, after the preliminary test to assess how to operate the continuous reactor with simple tests a more representative mixture was prepared based on the characterization of HTL-lignin rich aqueous phase. In the Figure 67 the chromatograms of the aqueous phase (treated HTL-AP) and of the synthetic mixture are reported and compared.

Compound	Wt.%
Glycolic a.	0.16
Lactic a.	0.19
Glycerol	0.05
Acetic a.	0.19
Methanol	0.42

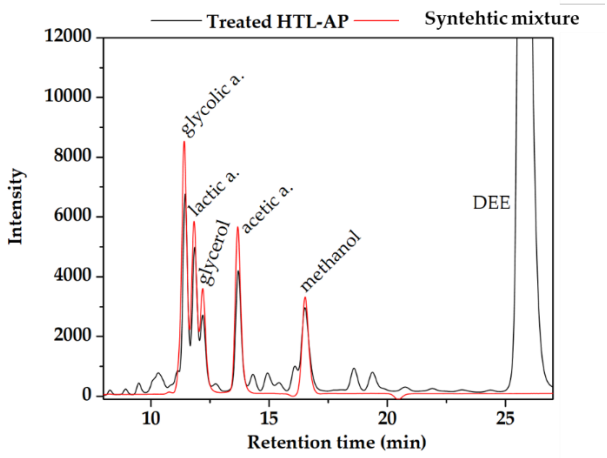


Figure 67: HPLC chromatogram of HTL-AP and synthetic mixture.

The influence of diethyl ether was assessed. Based on the previously reported characterization of the HTL-AP and DEE quantification, a mixture with DEE (1 wt%) was prepared and tested. Comparing Figure 68 shows that the presence of DEE slightly increases the conversion of the compounds but did not change quantitatively the hydrogen productivity; this is coherent with the results obtained in the batch reactor where the DEE did not affect the reaction. In the following tests DEE is not included in the synthetic mixture since its concentration is variable in the HTL-AP.

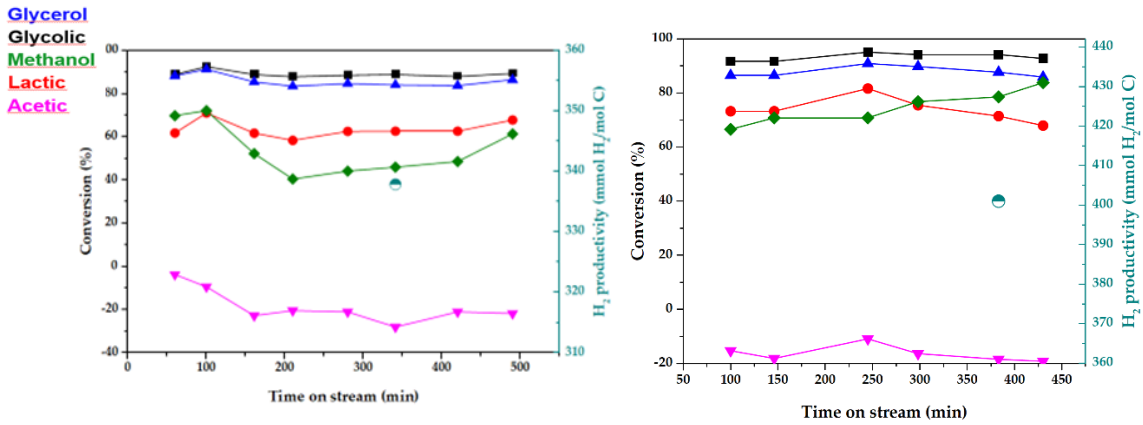


Figure 68. Performance of APR of synthetic mixture 270 °C, 60 bar, 0.8 ml/min without DEE (left) and with DEE (Right)

In Figure 69 gas composition is reported. During the time on stream, the composition of the gas produced is stable with some low variability. The presence of methanol and glycolic acid led to a high selectivity to hydrogen, being the most present compound in the gas phase. The low carbon dioxide concentration compared to conventional APR stoichiometry may be due to the set-up used.

The gas-liquid separation was carried out at 10 °C and high pressure (depending on the reaction temperature). These conditions favored the absorption of carbon dioxide in the water.

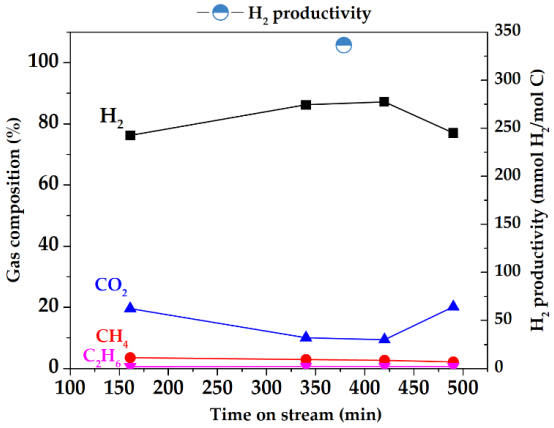


Figure 69. Gas composition of APR of synthetic mixture. 270 °C, 60 bar, 0.8 ml/min.

It is important to highlight that during the synthetic mixture APR the catalyst was stable during the reaction time. The water after the reaction was collected and retested, the results cannot be compared in absolute number as the second test in more diluted conditions. However, it is important to notice the rate of deactivation is close to zero in this case and it is not possible to ascribe the results only to dilution of the water. It is coherent with the test performed in batch and reported before. The textural analysis reported in Table 19 confirmed also that the surface area was higher and close to the fresh catalyst.

The temperature effect (250-260-270°C) on APR performance was analyzed. In the Figure 71 below the conversion of glycolic acid, lactic acid, glycerol and methanol are reported. With the increase of temperature there is for all the molecule an increase of the conversion. This is coherent with the more favourable kinetic of C-C bond breaking, which is a key step in the APR mechanism. At each temperature, the typical conversion ranking was glycolic acid > glycerol > methanol > lactic acid. The acetic acid conversion reported in Figure 70 was negative at each temperature since it was produced along with the reaction by hydrogenation of glycolic acid.

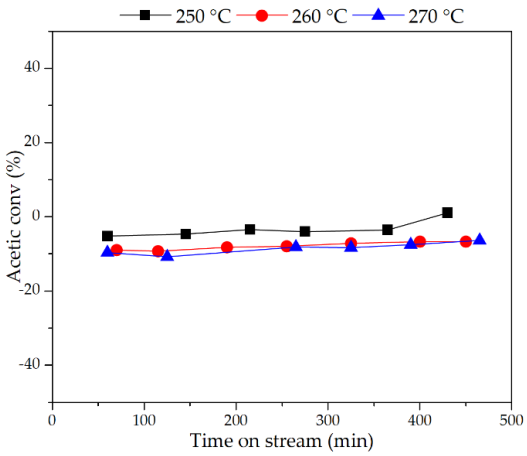


Figure 70: Influence of reaction temperature on acetic acid conversion

Another important compound present in the liquid phase is propionic acid. It is probably obtained via hydrogenation of the hydroxyl group of lactic acid. The selectivity changed drastically with the reaction temperature. It was 65% at 250 °C, while it decreased to 37% at 260 °C and 270 °C. This can be due to the consecutive propionic acid reforming, which gives ethane and carbon dioxide [85].

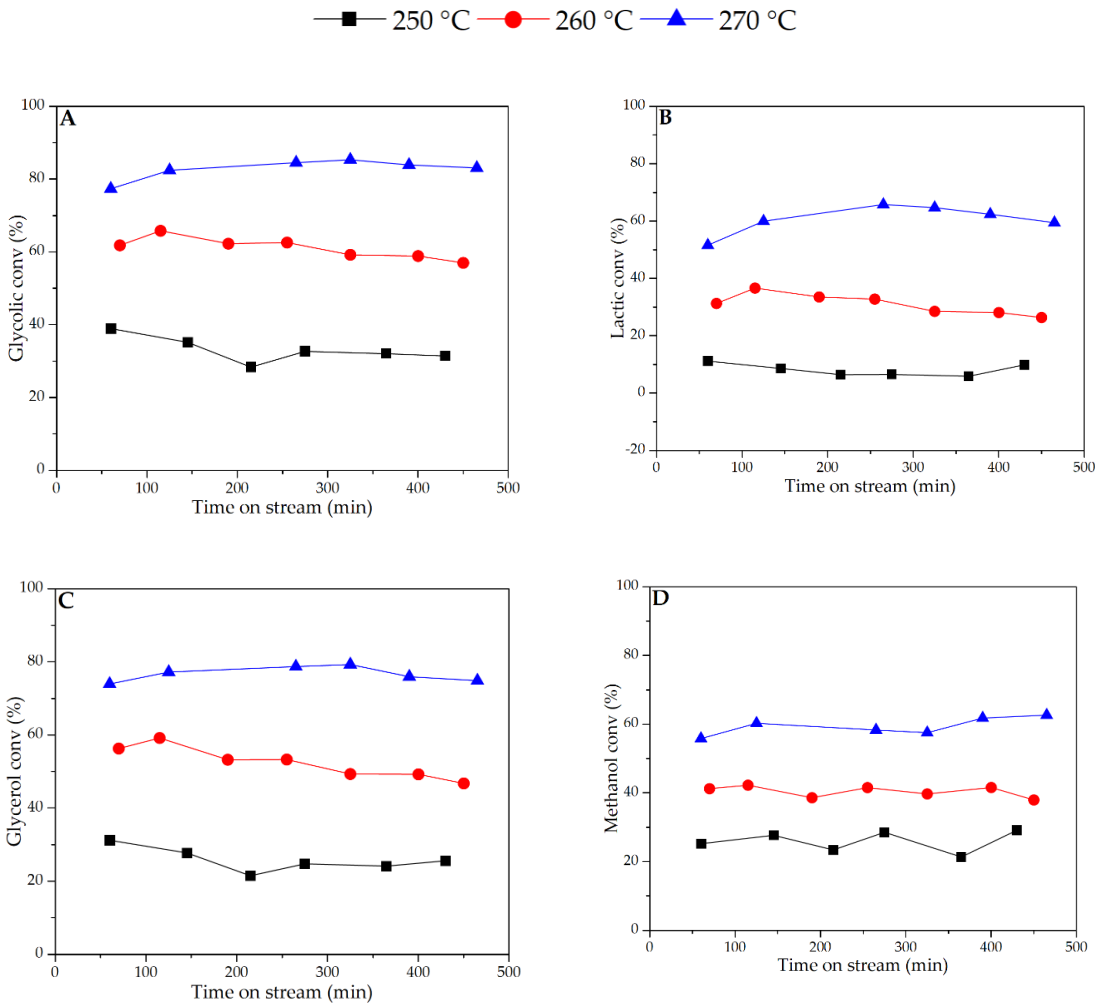


Figure 71. Influence of reaction temperature on substrate conversion. Reaction conditions: 1 g_{feed}/g_{cat} min.

In Table 17 the produced gas is reported for each temperature. Higher temperature led to higher conversion and thus to higher hydrogen production The gas phase composition was similar for each test, indicating that the selectivity for hydrogen production was not strongly affected by the temperature. Globally, the results suggested that working at high temperature is benefic to increase the hydrogen yield, without worsening the selectivity.

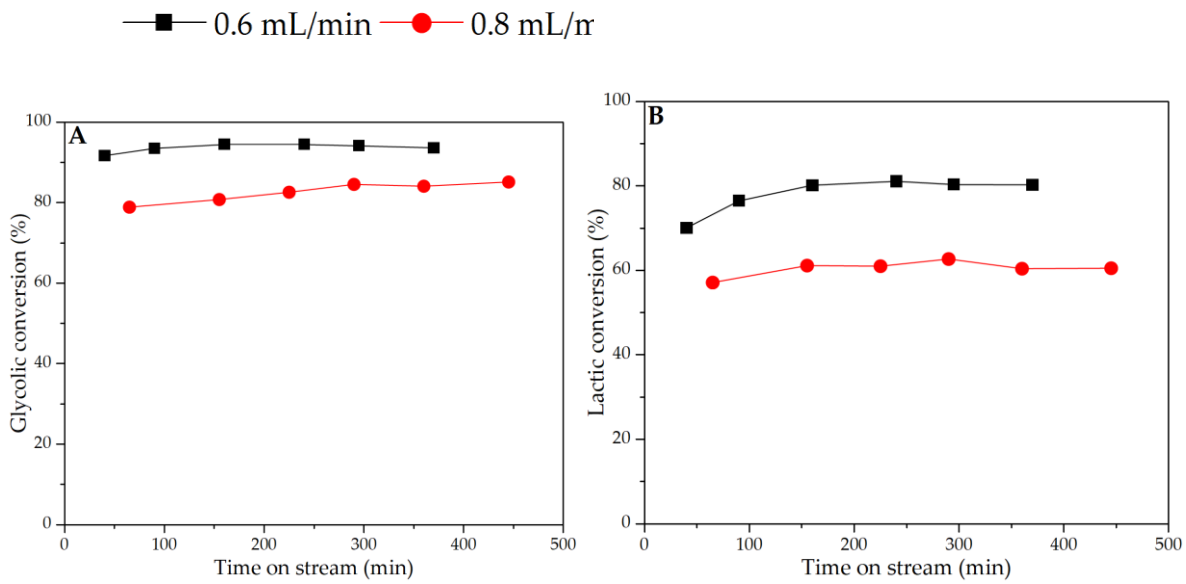
Table 17. Influence of reaction temperature on gas production; average values were reported. Reaction conditions: 1 g_{feed}/g_{cat} min.

Test	H_2 flowrate (mL/min)	H_2 yield (mL H_2/mL AP)	H_2 vol.%	CO_2 vol.%	CH_4 vol.%	C_2H_6 vol.%
250 °C	0.47	0.47	91.5	5.2	2.3	0.2
260 °C	1.62	1.62	87.9	7.7	3.1	0.3
270 °C	3.57	3.57	86.7	9.2	3.0	0.5

5.1.2. Influence of weight-hourly space velocity

The influence of the WHSV was evaluated varying the flowrate (0.6-0.8 mL/min) and maintaining constant the amount of catalyst (1 g). The highest conversion for all the substrates was obtained at highest residence time (lowest flow rate 0.6 mil/min). In Figure 72 these results are reported. Increasing the flowrate the conversion decreased.

Acetic acid conversion remained constant at each WHSV and propionic acid, was obtained with a constant selectivity (approximately 38%) from lactic acid.



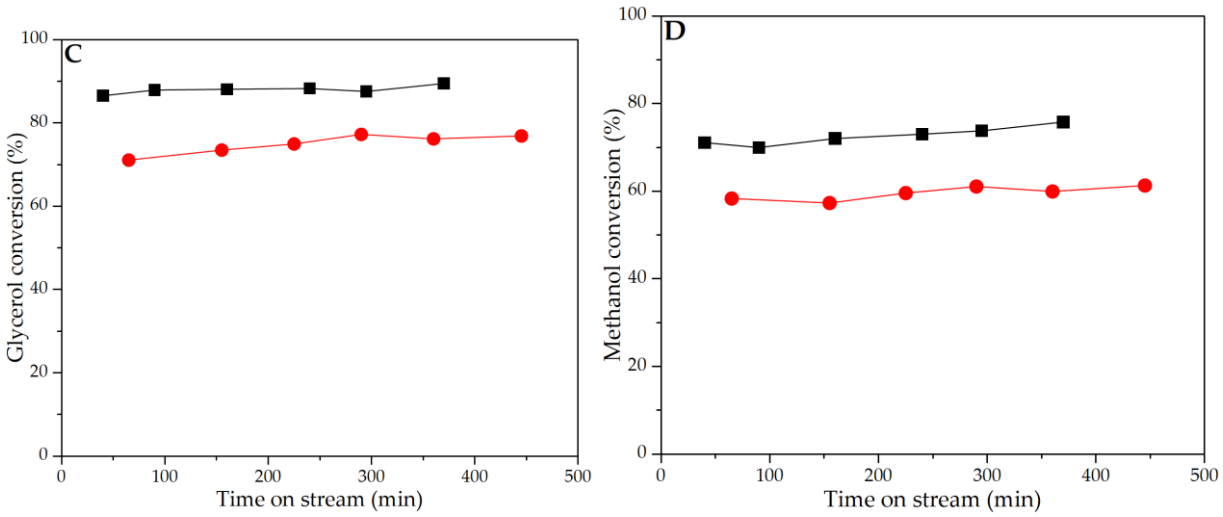


Figure 72. Influence of WHSV on substrate conversion. Reaction conditions: 0.6-0.8 ml/min, 270 °C, 60 bar.

In Table 18 the gas production is reported: the hydrogen flowrate is nearly constant at 3.3 mL/min since it can be seen as the product of the feed flowrate (which increases with the WHSV) and the hydrogen yield (which decreases with the WHSV).

Table 18: gas production. Reaction conditions: 0.6-0.8 ml/min, 270 °C, 60 bar

Test	H_2 flowrate (mL/min)	H_2 yield (mL H_2/mL AP)	H_2 vol.%	CO_2 vol.%	CH_4 vol.%	C_2H_6 vol.%
0.6 g_{feed}/g_{cat} min	3.15	5.26	84.5	11.3	3.1	0.5
0.8 g_{feed}/g_{cat} min	3.24	4.06	87.1	9.5	2.4	0.4

To conclude preliminary tests were conducted with the HTL-AP used in the previous chapter. The water was filtered and send it in the reactor. Looking at the test in the same condition of synthetic mixture is it clear that after 200-250 minutes the catalyst start to deactivate. This is also proven by the textural characterization of the catalyst (Table 19); the surface area is indeed reduced.

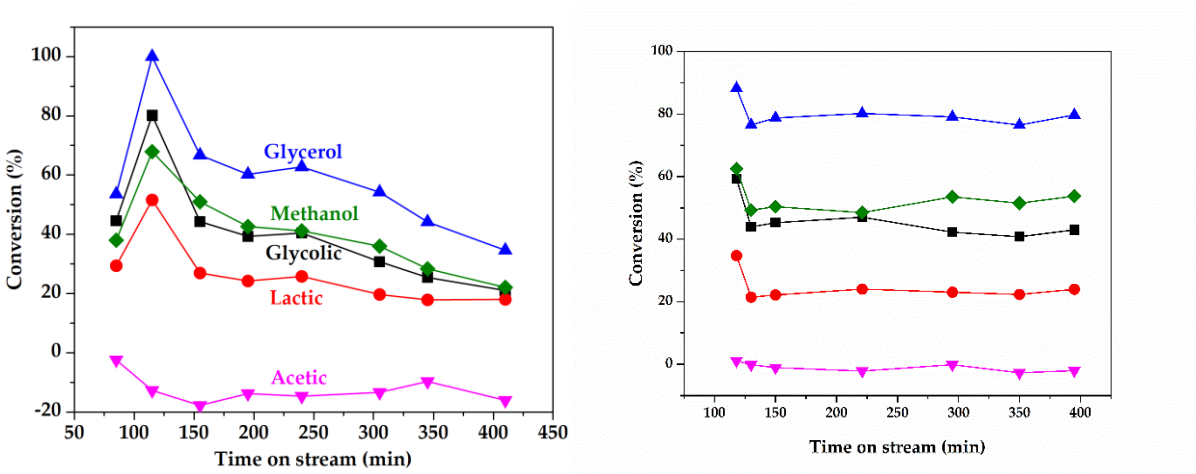


Figure 73. performance of APR of HTL-AP. 270°C, 60 bar, 0.8 ml/min(left); Performance of II use HTL-AP APR. 270°C, 60 bar, 0.8 ml/min (right)

The water after the reaction was collected and retested, the results cannot be compared in absolute number as the second test was in more diluted conditions. However, it is important to notice the rate of deactivation is close to zero in this case and it is not possible to ascribe the results only to the dilution of the water. It is coherent with the test performed in batch and reported before. The textural analysis reported in Table 19 confirmed also that the surface area was higher and close to the fresh catalyst.

Table 19. Surface analysis of fresh and spent Pt/C catalyst.

Sample	Surface area (m2/g)
Pt/C pellet fresh	965
Synthetic mixture	968
HTL-AP	618
HTL-AP II use	857

5.1.3. Influence of sulfate concentration

Continuous reactors allow to deeper study catalyst deactivation compared to batch setup. The study of APR with complex mixture need to consider the presence of inorganics. The HTL-AP derives from the processing of biomass, which normally can contain inorganics. Among the others, sulfur, under the form of sulfate, is commonly present and is particularly dangerous for platinum group metals. Platinum poisoning by sulfur is commonly registered in the oil sector. However, it is not largely reported in aqueous media. In chapter 4 the sulfur was evaluated in batch conditions, however the set-up is not suitable for deep deactivation evaluation. Thus, the sulfur issue was taken in consideration also in continuous mode. The HTL-AP contains 40 ppm of sulfate; in order to understand their effect alone a synthetic mixture was tested with and without sulfate. At 0.6 mL/min,

shifting the feedstock to the one with 40 ppm sulfate, led to a decline in the conversion of each of the molecule along the entire time on stream (Figure 74).

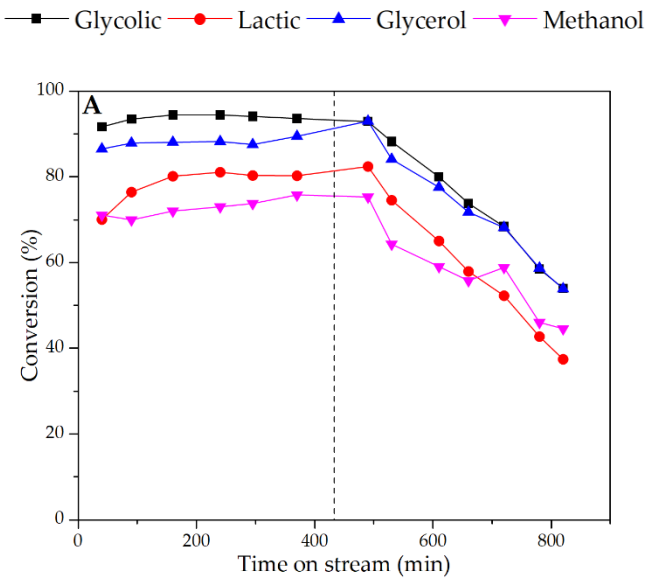


Figure 74. Influence of sulfate 270°C 0.6 mL/min

As already done for aromatics physical or chemical pretreatments should be considered to preserve the catalyst stability (e.g. precipitation of sulfate with addition of salts to the water; adsorption in different media and so on)

Activated carbon and anion exchange resins (Amberlite IRA-) were initially screened to find which adsorbent was able to reach a double scope: maximizing the sulfate adsorption, while minimizing the organic one.

Starting with active carbon in Figure 75: it can be observed that sulfate adsorption increased with the increase of AC amount up to a maximum 60%. However, also the other molecules are unselectively adsorbed. Obviously, this result cannot be accepted since it would drastically reduce the potential of the wastewater for producing hydrogen.

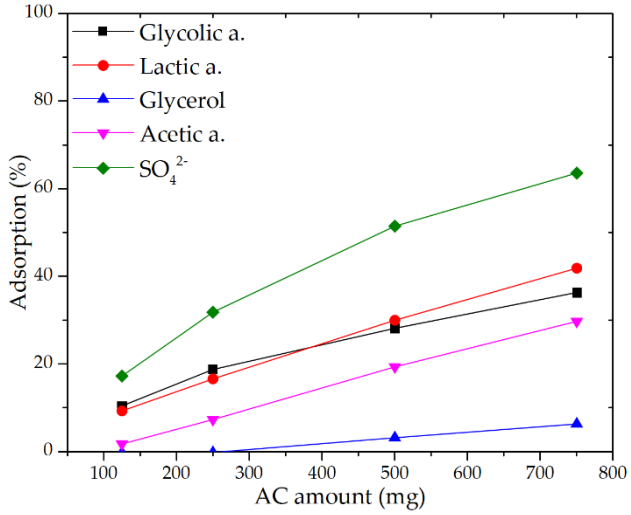


Figure 75: effect of loading in the AC adsorption.

Figure 76 instead shows the results of four types of Amberlite. Each of the anion exchange resins reported very high sulfate adsorption, from 95 to 98%. Moreover, 400, 410 and 900 showed also minor organic uptake which led them to be better compared to active carbon. However, the sulfate adsorption is linked to an exchange mechanism which release a chloride ion, which in turn may be detrimental for platinum. Due to that further attention was given to the study of IRA 67 *free base* which has a different adsorption mechanism. In Figure 76 (right) the representation of mechanism of Amberlite IRA 67 *free base* and IRA 900 is shown. The IRA 900 is an anion exchange resins which release its anion (Cl^-) and adsorb the SO_4^{2-} ; instead, the IRA 67 forms an acid-amine complex for neutralization reaction [207].

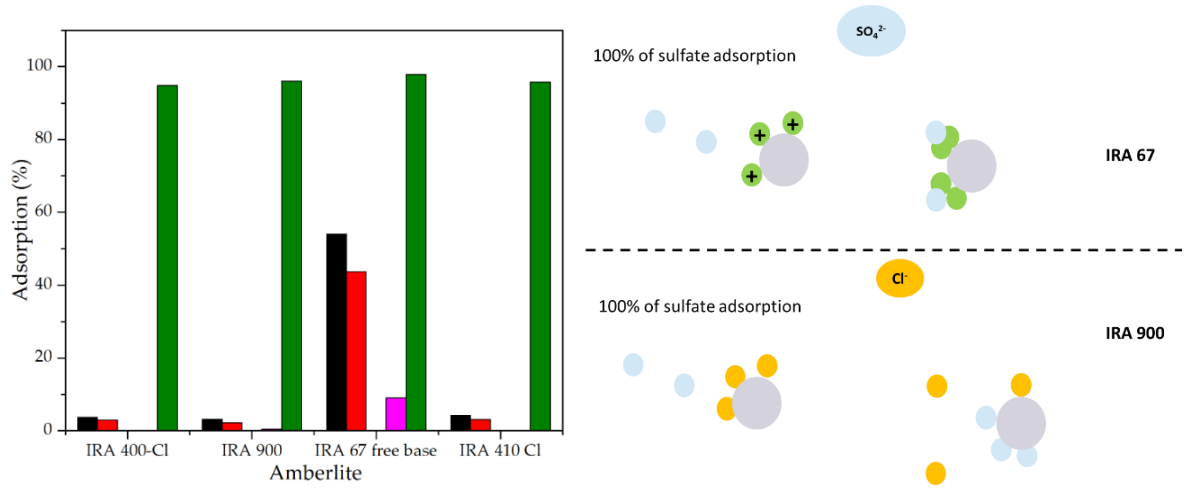


Figure 76: adsorption of four types of Amberlite (left) and mechanism of adsorption (right).

In Figure 77 below the influence of IRA 67 loading is reported. Interestingly, when the amount of Amberlite decreased, linearly decreased only the adsorption of the organic molecules, while sulfate

adsorption remained constant at approximately 95%. This result could be the indication of competitive adsorption between organic and inorganic compounds. Moreover, it allows the use of IRA 67 for an efficient removal of sulfate without compromising the pool of organics able of producing hydrogen. The optimal condition was found at 2mg/ml.

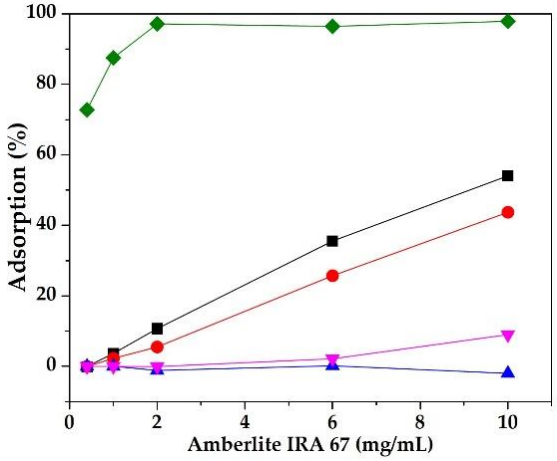


Figure 77: influence of IRA 67 loading

The synthetic mixture with 40 ppm of sulfate was pre-treated with the IRA 900 and IRA 67, the results are reported in the Figure 78 below. The water after IRA 67 treatment recovered the performance of the test without sulfate. Instead, as expected IRA 900 showed catalyst deactivation probably due to the Cl^- in the water.

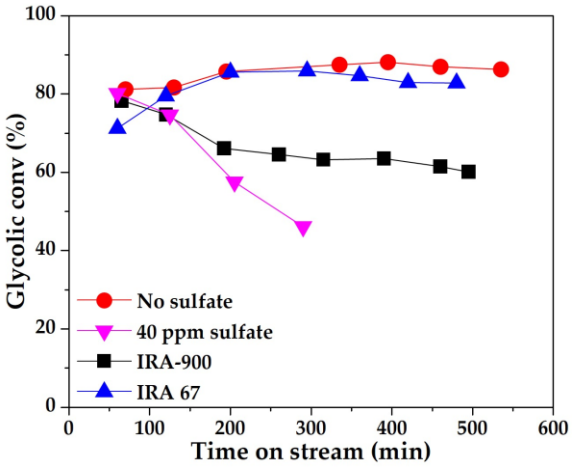


Figure 78: effect of resin pretreatment, 270°C

The real HTL-AP contains both aromatics and sulfate. They have clear effect separately; further investigation should elucidate if one of the mechanisms (fouling and poisoning, respectively) related to their presence, is predominant in order to design the adequate pretreatment and achieve the stability of the catalyst.

5.2. Pilot plant continuous tests

Finally, some tests were conducted in a pilot scale plant to assess the feasibility of the APR reaction at bigger scale. This chapter describes the preliminary results achieved in a pilot-plant scale APR continuous reactor. The reactor was designed based on the continuous results presented before, the plant was constructed and built by BEST (Bioenergy and Sustainable Technologies center) in Wien.

In Figure 79 the picture of the plant is presented. It is constituted by the feeding system which pumps the aqueous phase into the economizer, the final heater and then the reactor. At the outlet, the gas liquid streams are separated. The liquid phase was collected and analyzed at Politecnico di Torino, and the gas phase was constantly analyzed to understand the composition of the produced gas phase.

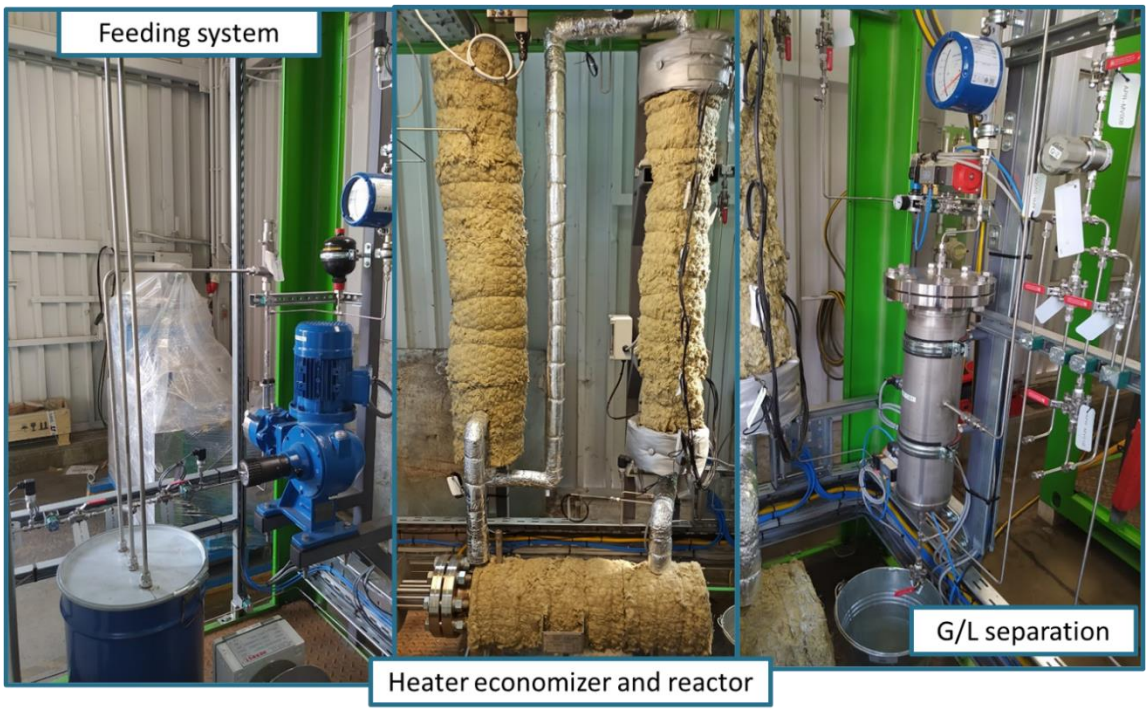


Figure 79: pilot plant pictures, BEST

The reactor is filled with 5% platinum on carbon, in pellet shape. Tests were performed with an aqueous solution constituted by glycolic acid alone to assess the operativity of the plant; afterwards the same synthetic mixture used in the lab scale test presented before was prepared and tested.

Glycolic acid solution at 0.5 weight % was tested at 250 and 265 °C. The first tests were not stable for long time at same temperature and pressure, however looking at average gas flow rate and composition (Table 20) higher temperature led to higher gas production. As expected, the gas

produced by glycolic acid reforming contains mainly hydrogen and carbon dioxide; the only product present in liquid phase was acetic acid (in agreement with the lab scale results)

Table 20: gas production of glycolic acid APR

Temperature °C	**H_2 %**	**CO_2 %**	**CH_4 %**	**Hydrogen flow Nl/h**
250	65.4	34.1	0.5	89
265	64.5	35	0.5	122

Finally, one test with synthetic mixture is shown. In the figure below temperature, pressure, gas flow and the volume percentage of hydrogen in the produced gas are reported. From 150 to 450 minutes the system was stable. The gas flow oscillates due to the opening and closing of the outlet valve.

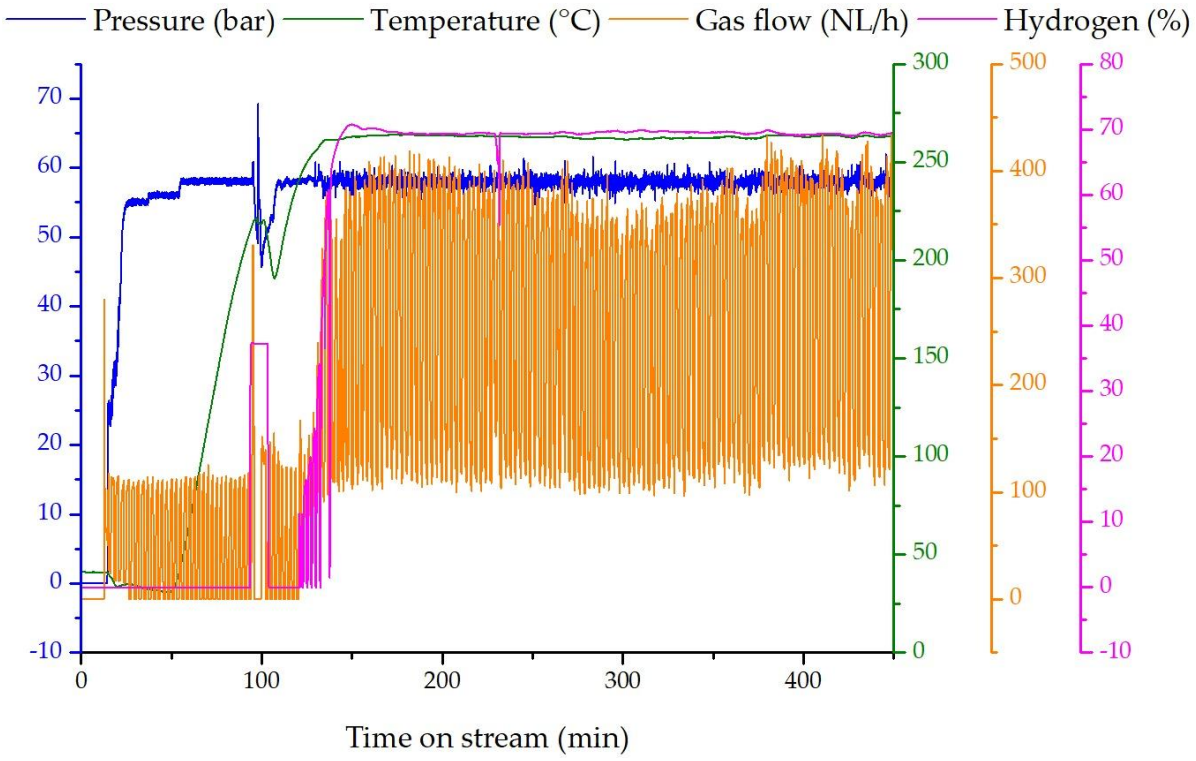


Figure 80: reaction conditions 263°C, 58 bar and 0.56 WHSV

In the Table 21 below is reported the gas composition, which compared to the tests in the lab scale reactor shows higher carbon dioxide due to the separation system at lower pressure. The hydrogen production is 177 Nl/h, the main gas present are hydrogen and carbon dioxide. In Figure 81 the

conversion in liquid phase is reported; glycolic acid and glycerol reached high conversion around 65% lactic acid 45% and methanol 33%.

Table 21: gas composition

Gas	Volume percentage (%)
H_2	70.3
CO_2	26.8
CH_4	2.8

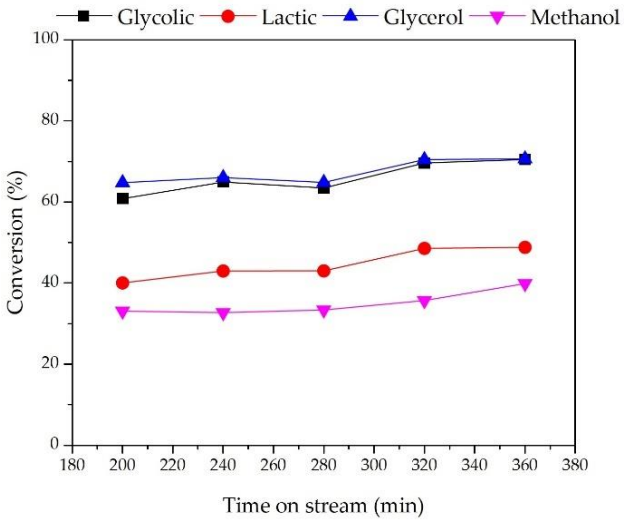


Figure 81: conversion of compounds

These preliminary test on the pilot plant scale showed similarity with the lab scale above presented; the reactivity of the main compounds and their stoichiometry follow what showed in the previous chapter. Future test will be necessary to investigate in the pilot plant also the actual water together with the solution implemented to reduce the catalyst deactivation.

Chapter 6

Techno-economic and life cycle assessment

Coupling HTL with APR can be further exploited using the hydrogen produced by APR for the upgrade of the HTL biocrude. The hydrogenation of the biocrude is a fundamental step due to the presence of heteroatom (O,N,S) in the crude, the hydrogen requirements depends on their concentration and on the reaction condition. Hydrogen in normally produced by steam reforming of natural gas, APR can be a greener options Moreover, the cost of hydrogen can have a strong impact for small-scale production facilities [112]. For example, Zhu et al. reported 0.033 g H_2/g biocrude derived from HTL of woody biomass [25], while 0.041 g H_2/g biocrude were required in the case of algae as starting feedstock [208]. Thus HTL-APR combined plant is a valuable option to improve the carbon efficiency of the hydrothermal liquefaction while producing hydrogen for the upgrade step.

Both technologies are not commercialized yet. HTL of different feedstock (algae, sludge, lignocellulosic biomass) exits in pilot scale ([209]–[211]), while APR for hydrogen production is still at the laboratory scale. In this frame the techno-economic analysis (TEA) and life cycle assessment (LCA) are necessary tool to investigate the feasibility both economically and environmentally of the commercial development. Few TEAs and LCA can be found in literature regarding HTL [25], [212]–[216][217]), fewer TEA work exits about APR, despite its potential application ([112], [123]) and none regarding LCA.

In the previous chapters the APR of lignin rich HTL water was presented. The experimental results from APR and HTL are used to perform the balances and design of the plant. Moreover, a lignocellulosic biomass (corn stover) was chosen as feedstock for HTL.

The chapter present at the beginning the description of the plant and the methodology used for the economic and environmental analysis then the mass and energy balances are presented and finally the design of the main units. The evaluation of TEA and LCA are then reported and compared by the definition of key performance indicators (e.g. minimum selling price, hydrogen cost) and the LCA impact categories.

Results, figures and tables of this chapter are included in two papers under submission.

6.1. Methodology techno-economic assessment

The main processes involved in the plant are the HTL of a wet feedstock and the APR of the aqueous phase produced by the HTL. Two scenarios of HTL-APR coupling with different feedstocks are studied in this work: lignocellulosic biomass (corn stover, CS) and lignin-rich stream (LRS). The scheme is represented in

Figure 82. The battery limit of the plant is from the feedstock pre-treatment to the biofuel production. With the term "biocrude" is hereafter defined the raw oil from HTL, while as "biofuel" is defined the upgraded product.

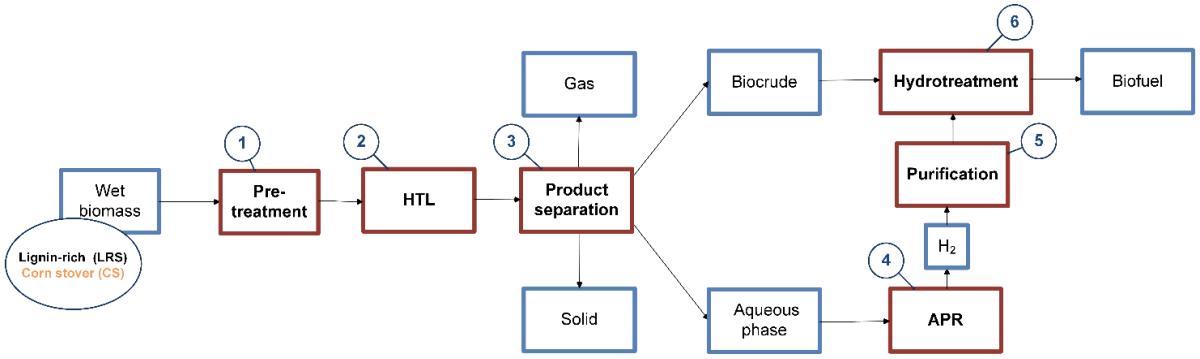


Figure 82: Block flow diagram of the HTL-APR integrated plant. Block numbers are identifiers of plant sections.

The industrial scale for the LRS case is based on the availability of LRS present in an existing bioethanol plant. A 20 MW_{th} of LRS (based on its calorific value) is chosen as the nameplate capacity of the plant, corresponding to 96 kt/y of LRS (70% of humidity) which is coherent with the size of the production of second generation bioethanol plants [218]. The plant was modelled trying to exploit also the solid by-product, i.e. the char.

The same dry feedstock mass rate was considered for the second case (corn stover, CS), with a slight change in the MW_{th} of plant (due to different caloric value of the feedstock). In order to provide a representative scenario of local biomass availability, the corn production in the province of Turin (Italy) was 522 kt in 2019 [219]; since the ratio between corn production and stover is 1:1 [220], 522 kt of corn stover were present in Turin province. Therefore approximately 5% of production was needed to fulfill the plant target capacity, which is a reasonable size that poses no particular problem in terms of biomass collection and transport logistics. The model is developed in a Microsoft Excel© spreadsheet where mass and energy balances were performed based on results from the experimental work and literature. Based on these balances the design details of each equipment are then performed [221], [222]. Equipment of the purification and upgrading section (heat exchangers, trim heater and hydrotreatment reactor) were not designed in detail but their costs were evaluated based on literature correlations. Secondly, the economic evaluation of the process was carried out to compare the two cases and calculate the minimum fuel selling price and the production cost of hydrogen from APR. At the end, a sensitivity analysis was carried out to investigate the effects of some fundamental parameters on the cost of biofuel. Scenarios with different H_2 production (SR plant or alkaline

electrolyzer system) were analyzed, as well as with wider ranges for feedstocks, electricity and natural gas cost and different solid loading.

6.1.1. Process description

The plant is divided in sections and the main units present in each section are reported in Table 22 and highlighted in Figure 82

Table 22: Plant sections and unit operations.

Section number	Section name	Unit operations
1	Biomass pre-treatment	Storage, Mixing, Milling
2	Hydrothermal liquefaction	Heating, HTL reaction, Cooling
3	Product separation	Flash evaporation, Filtration, Centrifugation
4	Aqueous phase reforming	Heating, APR reaction, Flash
5	Purification	Compression, Cooling, PSA
6	Upgrading	Hydrotreatment, H_2 production, Electrolyzer

The first section regards the biomass preparation. In this work, the HTL is fed by a lignin-rich/corn stover stream coming as subproduct of a cellulosic ethanol plant/agricultural residues respectively. Due to the high water-content in the LRS case (70% moisture), the plant should be built next-door to the ethanol one in order to avoid spoiling and dewatering of the LRS matrix. The LRS is therefore temporarily stored, milled, and then mixed with recycled and make-up water. The corn stover is instead harvested three months a year and is stocked to guarantee a continuous flow rate throughout the whole year. After storage for a longer time, which is possible assuming a biological stability guaranteed by the reduced amount of residual moisture (5.4 wt.% [223]), corn stover is milled and mixed with water for slurry formation. The HTL section starts with pressurization of the biomass-water mixture up to 200 bar; afterwards, thanks to economizers and an heater, the temperature reaches the set point of 350 °C. There are four different phases at the outlet of the HTL reactor and the products separation consist in: flash (gas separation), filtration (solid separation) and centrifugation (liquids separation). Among the coproducts, the gas contains mainly CO_2 and is hardly exploitable, the solid is burnt in order to reduce the energy demanded by the process, while the aqueous phase is sent to the APR section.

The APR section involves, similarly to the HTL section, firstly the pressurization of the organic residues laden water (up to 60 bar), followed by heat exchangers to reach 270 °C. Thanks to a platinum-based catalyst, the carbon-laden water fraction is converted into a gas phase rich in hydrogen and the outlet liquid is depressurized at ambient pressure to release all the dissolved gas.

H_2 is the product of interest of the APR, however CO_2 and CH_4 are also present in the gaseous stream. In order to use it for upgrading, a purification step is performed by pressure swing adsorption (PSA) after compression and cooling.

The biocrude cannot be used as drop-in fuel due to the amount of heteroatoms (N, O, S) and a subsequent hydrotreatment step is required. However, hydrotreatment technology is not yet well established for biocrude from HTL; in particular, to the best of our knowledge, no works are known regarding the HTL of LRS. These biocrudes usually contain different concentration of oxygen, nitrogen and sulfur compared to biocrude from lignocellulosic material and therefore further experimental studies on the biocrude are necessary to better understand the process. For this reason, the detailed design of the upgrading section wasn't performed in this work. Based on literature data, correlations were used for fixed costs and operative consumption which included also undesired reaction and the necessary auxiliary unit operations (heating of reactants, cooling and separation of products). Moreover, in the case where the APR is not able to fulfill the hydrogen need of the biocrude upgrading, the production of the missing H_2 quota must be carried out in a small in situ plant, e.g. via an electrolyzer.

6.1.2. Economic assessment

Fixed cost

The economic analysis is performed considering preliminary estimates, with typically ±30% accuracy, in accordance with the Association for the Advancement of Cost Estimating International (AACE International) [224]. The fixed costs of the equipment are calculated based on the module costing technique described in [225]. This approach relates plant costs to the purchased cost of every equipment, taking up what has been done by Guthrie [226]. Compared to it, Turton considers all the improvement occurred in equipment construction between the 30 years gap of the two methods. Moreover, within every equipment type, the Turton method possesses more subgroups within which to choose, leading to a more accurate estimation.

The purchased cost of each piece of equipment (C_P^0) was evaluated through a polynomial equation having as input the capacity or size parameter (A) of the piece of equipment itself (Equation S1.1). This cost is referred to the purchase of base equipment operating at ambient pressure and made of carbon steel. Bare module cost (C_{BM}) considers all the costs (direct and indirect) required for the installations and depends on material (F_M) and pressure factors (F_P) (Equation S1.2-1.3).

$$\log_{10} C_P^0 = K_1 + K_2 \cdot \log_{10}(A) + K_3 \cdot [\log_{10}(A)]^2 \quad \text{(Eq. 23)}$$

$$F_{BM} = B_1 + B_2 \cdot F_P \cdot F_M \quad \text{(Eq. 24)}$$

$$C_{BM} = C_P^0 \cdot F_{BM} \quad \text{(Eq. 25)}$$

Silos and mill weren't described by Turton and the compressor size didn't fit into the useful range. Consequently, these equipment costs were evaluated through Guthrie [226]. Guthrie is based on an exponential law using a base cost (K) multiplied by the characteristic size raised to a size exponent (*n*) (Equation S1.4). Correction factors are a function of material (F_m), pressure (F_p) and design factors (F_d) (Eq. 5). Bare module cost evaluation requires direct field material and labor cost ($F_{M\&L}$) and

indirect cost (F_{IND}), which was assumed to be equal to 1.34 whenever it wasn't reported. Taking into account these contributions, Equation S1.6 was obtained.

$$C_P^0 = K \cdot A^n \quad \text{(Eq. 26)}$$

$$F_c = f(F_m, F_p, F_d) \quad \text{(Eq. 27)}$$

$$C_{BM} = C_P^0 \cdot (F_c + F_{M\&L} \cdot F_{IND} - 1) \quad \text{(Eq. 28)}$$

PSA bare module cost were evaluated with the correlation described by Sladkovskiy et al. (Equation S1.7) [112]. This was based on 85% H_2 recovery; input parameter was the hydrogen production rate (G_{H2}), expressed in kg/h.

$$C_{PSA} = (447846 + 3407 \cdot G_{H2}^{0.8}) \cdot 1.2 \cdot (608/402) \cdot 0.93 / 1.11 \quad \text{(Eq. 29)}$$

Hydrotreatment bare module cost was evaluated through Equation S1.8. The mass rate (kt/y) of biocrude to be hydrotreated was chosen as the size parameter. The coefficients were evaluated through extrapolation of TEA data reported in literature [213], [227].

$$C_{HT} = (357000 \cdot G_{crude}^{0.7727}) \cdot (608/603) \cdot 0.93 / 1.11 \quad \text{(Eq. 30)}$$

Steam reforming (SR) plant bare module costs were evaluated through Equation S1.9. The mass rate (kt/y) of hydrogen produced was chosen as the size parameter. The coefficients were evaluated through extrapolation of TEA data reported in literature [213], [227], [228].

$$C_{H2\ plant} = (4458000 \cdot G_{H2}^{0.70429}) \cdot (608/603) \cdot 0.93 / 1.11 \quad \text{(Eq. 31)}$$

The bare module cost of the alkaline electrolysis system was assumed equal to 800€/kW of installed power [229] and the system efficiency was set to 56% [230].

Total module cost (C_{TM}) also includes contingencies and fees which were assumed equal to 15% and 3% of the bare module cost, respectively (Equation S1.10). Grassroots cost (C_{GR}) takes into account also the auxiliary costs of construction of the new plant and it was calculated as the total module cost plus 50% of the bare module cost of the piece of equipment at base conditions (C_{BM}^0) (Equation S1.11).

$$C_{TM} = C_{BM} \cdot (1 + \text{Contingency\%} + \text{Fee\%}) \quad \text{(Eq. 32)}$$

$$C_{GR} = C_{TM} + 50\% \cdot C_{BM}^0 \quad \text{(Eq. 33)}$$

Operative costs

Operative costs are evaluated based on unit costs shown in Table 23.

Table 23: Data for the operative costs.

	Unit	LRS Case	CS Case	Ref.
Biomass (*db*)	€/t	60	75	[53][54]
Electric power	€/kWh	0.09		[55]
Natural gas	€/Nm^3	0.35		[56]
Cooling power	€/MWh	0.9		[57]
Make up water	€/t	3.5		[58]
Wastewater disposal	€/kg COD	0.064		[59]
APR catalyst	€/kg	45		[25]
HT catalyst	€/kg	28		[60]
SR catalyst	€/t H_2	6.54		[60]
H_2 selling price	€/kg H_2	5		Estimated

Costs for electric power and natural gas are average values present in the EU market in 2019 and feedstocks costs are assumed to be 60 €/t for lignin-rich stream and 75 €/t for corn stover. However, these values could be subjected to strong changes, especially for LRS, due to the fact that its market is not yet consolidated in Europe. Regarding the APR catalyst, Sladkovskiy et al. reported that it is possible to neglect the cost of Pt due to its possible recover at the end of its lifetime [112]; however, compared to that work, the replacement time is cautiously reduced to 1 year. The necessary amount was calculated based on experimental data.
HT catalyst amount was calculated assuming a weight hourly space velocity (WHSV) equal to 0.81, as suggested by PNNL [231], and with a useful life of 2 years. SR catalyst wa based on a 5-years life [231]. The number of operators was calculated based on the Turton method [225], to which other staff members were added (supervisor, logistic, amminstration etc).

Minimum selling price

The objective of the work is to define the minimum selling price (MSP) of the biofuel obtained for the corn stover and LRS case using the “Discounted Cash Flow” (DCF) method. The depreciation and plant life were fixed to 20 years and the main set parameters are reported in Table 24. Maintenance costs take into account both ordinary and extraordinary maintenance due to the long plant life.

Table 24: Economic set parameters.

Startup cost	**5% of fixed cost investment**
Maintenance cost	5% of investment (fixed cost + startup)
Labor cost (average for worker)	56111 €/y
Working Hours	8000 h/y
Depreciation time	20 y
Starting ratio equity/debt ratio	75%/25%
Income tax rate	33%
Internal rate of return (IRR)	0% - 10%

The figures evaluated in the twenty-year projection profile are real values, therefore, maintaining the (real) price fixed for the entire period means that the price itself will have to be subject to (nominal) variations depending on the inflation trend.

As regards the return on invested capital, two hypotheses were considered:

(1) *Contribution of the necessary equity by a public operator, non-profit making, in the pursuit of environmental objectives with generation of positive non-economic externalities.* Considering the cost of capital assumed as debt, it is assumed a return on capital provided as equity equal to zero, with a pure recovery of the invested capital without margins (IRR=0%).

(2) *Contribution of the equity by a private operator, pursuing profit objectives.* In this case the remuneration of the equity invested is set at 10%, considered an adequate rate of return; the Weighted Average Cost of Capital (WACC) of the plan (considered over the entire equity-debt funding structure) is therefore around 8.5%, a prudent rate, taking into account the fact that it is assumed as a real rate (IRR=10%).

Two MSPs values were hence herein evaluated, differentiated by internal rate of return (IRR). The use of an MSP with an IRR=0% (hereafter defined as $MSP^{0\%}$) is justified by the believe that the specificity of the energetic sector and the need for public incentives to the ongoing ecological transition may, legitimately, consider the hypothesis of public intervention in support of the initiative. The public intervention could also be realized by an annual contribution to revenues, or annual capital contribution on the investment, equal to the difference between the price that guarantees remuneration of 10% and 0%. On the other hand, MSP with an IRR=10% (hereafter defined as $MSP^{10\%}$) is usually used as reference parameter to evaluate biofuel profitability [213], [227], [232]–[239]. $MSP^{10\%}$ was hence evaluated to be consistent with literature data and to allow comparison with other TEAs based on technology differences rather than different assumptions about economic management.

Sensitivity analysis

In order to assess the impact of the different cost items on the minimum selling price of the product, a sensitivity analysis was carried out; feedstocks, electricity and natural gas costs were varied over a wider range and the percentage change of the MSP was calculated. The MSP variation was also assessed in case of LRS/CS plants sized to work with a 20% solid loading; fixed and operating costs were evaluated keeping constant the dry biomass flow rate and therefore also the nameplate power capacity of the plant working with 10% solid loading. The carbon distribution and elemental composition of the products, as well as the APR reaction parameters, were maintained equal to those presented below for both LRS and CS case. For the former, this hypothesis is justified by experimental campaigns performed by Re-cord which have shown a substantial non variation in the parameters of HTL and the same composition of organic compounds in the aqueous phase. As regards the corn stover, Zhu et al. [25] performed a techno-economic analysis for an HTL plant using forest residue and corn stover at 15% biomass loading and no additive. Carbon distribution was very similar to those reported below for the 10% biomass loading case: for this reason, we assumed there were no differences in the HTL performances between the 10% and 20% biomass loading cases. In order to take into account the differences in the slurry rheological properties, pumps and heat exchangers for the 20% solid loading case were sized assuming an increase in the slurry viscosity of 10000 fold compared to that of water; this assumption was based on slurry viscosity range from PNNL [240].

As one of the key aspects of this work concerns the production of hydrogen needed for upgrading, the economic impact of replacing the APR section with an alkaline electrolyzer or a SR plant for the production of the hydrogen quota was evaluated. SR is currently the most established way for hydrogen production and is also the cheapest one; however, it is based on fossil sources unlike the green and more expensive electrolysis. Finally, the economic feasibility of a HTL plant without the internal upgrading was assessed in order to better understand how much of the performance of the integrated HTL-APR plant depended on the APR rather than the HTL.

6.2. Methodology life cycle assessment

The environmental analysis of the Heat to fuel plant was carried out using LCA methodology. LCA is standardized by ISO 14040 and ISO 14044, which define the LCA as the compiling and the evaluation of the inputs and the outputs and the potential environmental impacts of a product system during a product life time" [241], [242]. These guidelines have been further detailed by the guidelines of the European Commission: the ILCD (International Reference Life Cycle Data System) Handbook [243], and the PEF (Product Environments Footprint) guidelines [244]. The LCA typically consists of four steps, as reported in Figure 83.

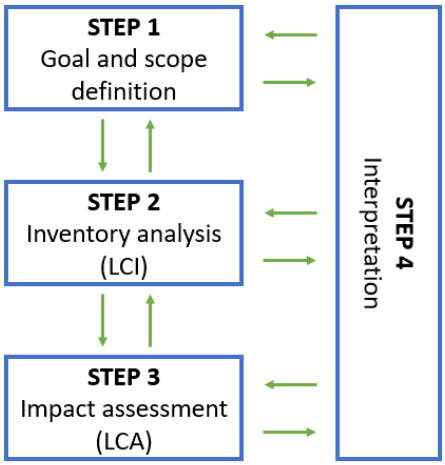


Figure 83: The four steps followed to carry out the life cycle assessment.

1. **Goal and scope definition**: all general decisions are made. The goal must be clearly defined, and it consists of the intended application, the purpose of the work, the intended audience, if it will be used for comparative reason, etc. The scope definition characterizes the product or process system, the defined assumption, as well as the methodology (e.g., function of the product, functional unit, description of the system, system boundaries, allocation procedures, limitation and so on).

2. The **inventory analysis** is constituted by data collection and compilation of the Life Cycle Inventory (LCI). LCI includes data of:

- Resources consumption (raw materials, catalyst, inlet and outlet flows).
- Energy consumption.
- Equipment used.
- Waste treatments.
- Emissions into air, water, soil.

As a result of the LCI phase, input-output flows are converted into a list of elementary flows (flows directly coming from or emitted to the natural environment).

3. **Impact assessment (LCIA)**: the identification and evaluation of the potential environmental impacts from LCI is performed in this phase. Elementary flows are classified and connected to one or more impact categories. The potential impact is quantified according to characterization factors. For the sake of clarity, Figure 84 reports an example showing how emissions to air and water from the LCI are assigned to their categories, together with the adopted "characterization factors", which take into account the severity of each compound and define a common reference (e.g., methane is considered 25 time more "dangerous" than carbon dioxide as greenhouse gas).

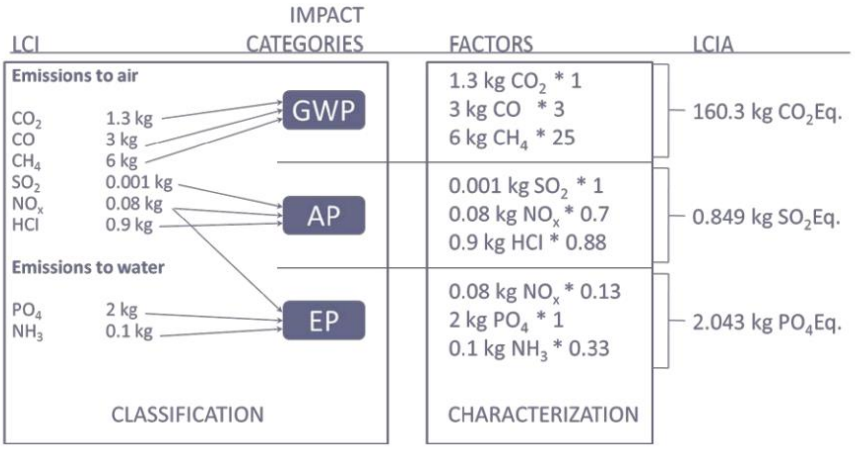


Figure 84: Example of impact categories and factors [245].

4. **Interpretation**: in this transversal phase the consistency among the different steps is checked and the outcomes are evaluated in terms of comparison with other processes, possible improvements to increase the environmental sustainability, etc.

The present LCA was performed with GABI software, using GABI and Ecoinvent database.

6.3.Mass and Energy balances

6.3.1. Mass balance

The nameplate capacity of the plant is fixed equal to 3.6 t/h of dry biomass and the selected solid concentration at the HTL reactor inlet is equal to 10 % for both cases. Due to the difference in LHV values, these plants correspond to an inlet nominal capacity of 20 and 16.5 MW_{th}, respectively.

6.3.2. Hydrothermal liquefaction and separation

HTL experiments were performed in a batch reactor (160 ml Parr) at 350°C for 10 minutes with no additive and 10% of biomass to water ratio. The adopted procedure for biocrude and aqueous phase separation was denoted as Procedure 2 in a work of RE-CORD [246]. Gas composition was not analyzed and the data herein reported are based on literature [25]; for mass balances purpose, methane and ethane are assumed as the only hydrocarbons.

As far as corn stover is concerned, carbon distribution and aqueous composition are calculated as average values of the four experiments conducted by Panisko et al. in a continuous processing bench scale system operating at 350 °C with a solid loading of about 10 wt.% [83], thus being obtained in comparable conditions to the ones of LRS. The elemental compositions of corn stover and its products are assumed from analogous experiments performed by Mathanker et al. [223]: char composition is taken from experiment at 350 °C, while the crude composition is the linear interpolation of

compositions of biocrude obtained at 300 °C and 375 °C. Gas composition is estimated equal to the LRS-derived one (CO_2 88.3 wt.%, H_2 0.9 wt.%, CH_4 1.8 wt.%, C_2H_6 9wt.%). Ash values for biocrude and char for both two cases are evaluated based on mass balances performed with inorganic elements, as explained in the aqueous phase recycling paragraph. In Table 25 the basic compositions and the LHVs of feedstocks, biocrudes and chars are reported.

For both feedstocks, most of the carbon was recovered in the biocrude, respectively 53% for LRS and 49% for CS, and a considerably higher amount of carbon was collected in the AP from CS (38%) compared to LRS (16%). The carbon recovered in gas and solids was respectively 15% and 16% for LRS and 10% and 4% for CS.

The moisture content of the HTL products (Table 25) depends on the designed separation processes: crude oil separation from the aqueous phase leads to a remaining water in the crude of 5 wt.% after centrifugation; char humidity is assumed equal to typical filter press moisture contents; gas is water saturated. Due to the high moisture and CO_2 content, gas has a very low calorific value (LHV= 0.27 MJ/kg) while char is energetically valorized by burning it in a furnace to provide a portion of the heat required by the plant.

Since the results derive from experimental investigations, the uncertainties and measure errors don't allow to fully close the mass balance, although to a little extent. To overcome this issue, the weight percentages of carbon in the AP at APR inlets is derived from the ratio between the carbon flow rate and the total flow rate, being eventually 1.03 and 1.74 wt. C%, for LRS and CS respectively. These values fell within the literature experimental range (0.4-2 wt. C%) [83], [85].

Table 25: Phase compositions and LHV of feedstocks and products.

Stream	**LRS**	**CS**	**Crude LRS**	**Crude CS**	**Char LRS**	**Char CS**
C (wt.% daf)	55.5	43.6	69.3	74.0	77.7	68.2
H (wt.% daf)	6.1	5.8	6.9	8.0	3.2	4.3
O (wt.% daf)	37.4	50	22.8	16.2	19.1	25.4
N (wt.% daf)	1	0.6	1	1.8	n.a.	2.1
Ash (wt.%)	2.6	7.0	0.4	1.0	2.9	34
Moisture (wt.%)	70	5.4	5.0	5.0	32	32
LHV (MJ/kg_{dry})	20.0	16.5*	29.7*	33.2*	25.7*	28.7*

*evaluated with Channiwala and Parikh correlation [247]

6.3.3. Aqueous phase reforming

Experimental APR results from the LRS-derived HTL aqueous phase were taken from chapter 4. In the CS-derived aqueous phase case, APR performances are estimated as linear combination of the

single organic molecules identified in the AP from Panisko et al. [83]; performances of the single molecules and of synthetic mixtures are based on previously performed experimental campaign reported in Chapter 4. In the following Table 26, the APR performances for LRS and CS are reported.

Table 26: APR performances obtained from the HTL-AP valorization of LRS and CS.

APR DATA	LRS	CS
Carbon to Gas (CtoG)	20%	55%
kg H_2/kg C feed	0.037	0.12
Gas composition vol. % (*db*)		
H_2	62%	62%
CO_2	28%	37%
CH_4	9%	1%
C_2H_6	1%	0%
C_3H_8	0%	0%

6.3.4. Aqueous phase recycling

Due to the consistent amount of water required, it is desired to recycle wastewater at the outlet of the APR to dilute inlet feedstocks. This recycling improves the sustainability and cost-effectiveness of the process by reducing the supply of fresh water and the disposal of wastewater. For the LRS case, the effect of the recycling of the aqueous effluent has been tested through preliminary batch experiments.

ICP analysis evaluated the distribution of inorganic compounds between the different HTL phases reported in Table 27. It was assumed that the recirculation doesn't change the inorganic distribution. In the LRS the three main inorganic elements were Na, K and Ca, probably in the form of carbonates. This hypothesis seems to be justified by the fact that if assumed in the form of carbonates, the sum of these ions equals the amount of ash present in the feedstock (measured by combustion at 550 °C). The elemental distribution between biocrude, char and aqueous of Na, K and Ca is used as representative of all inorganic compounds.

Table 27: Main inorganic elements present in LRS and in its HTL products.

Element (ppm)	LRS	Biocrude	Char	AP
Na	6287	293	1270	646
K	3341	266	862	400
Ca	1117	32	3726	68
TOT	10745	590	5858	1114

For the CS case, the main inorganic elements present in the aqueous phase (Na, K) were evaluated from Panisko et al. [83], and their concentration is assumed equal to that one reported minus the contribution of Na coming from Na_2CO_3 used as catalyst. The inorganic distribution to biocrude and char is assumed to be equal to the one of LRS.

In both cases, a large amount of inorganic compounds remain in the aqueous phase; a purge is therefore necessary to avoid their build-up. APR reactions have been tested with water containing up to 3000 ppm of Na and no deactivation was observed. The amount of recycled water is evaluated so as not to exceed this threshold. Purge fractions result equal to 0.29 (LRS) and 0.32 (CS).

Besides inorganic compounds, a build-up of organic is also present, especially acetic acid that it seems in fact not to convert through HTL and APR [85]. Therefore, its presence can be considered as an "inert" carbon. With the previously described purge the amount of inert carbon at APR outlet are 34.8 g C/L (LRS) and 23.3 g C/L (CS).

6.3.5. Purification and upgrading

The pressure swing adsorption (PSA) is necessary to purify the gas stream coming out from the APR reactor and 85% of H_2 recovery is assumed [112]. This stream is used to hydrotreat the biocrude in the upgrading section, while the excess quantity is sold as coproduct.

It was decided to consider only the hydrotreater for the biocrude upgrading [25]. A multiplication factor was derived from literature to estimate the actual amount of hydrogen required from the stoichiometric one to convert all oxygen into water and all nitrogen into NH_3, taking also into account the H_2 consumed by side reactions [215], [231]. As a result, the hydrotreater reactor needs a double amount compared to stoichiometric hydrogen. Therefore, it is necessary to recycle the unreacted hydrogen, which is mixed with alkanes produced during HT. Taking into account 85% of unreacted H2 recovery through PSA [215], the actual H2 make-up is equal to 1.46 times the stoichiometric value. The yield of subproducts is calculated from the carbon distribution of the hydrotreatment (97% biofuel, 1.4% methane, 0.6% ethane, 0.4% propane, 0.1% butane, 0.65% hexane) estimated from [215], [231] and, due to the higher oxygen content contained in biocrudes from LRS and CS compared to the references, the water yield is adapted.

The relative hydrogen consumptions are reported in Table 28, as well as the yields of subproducts from dry biocrude for both cases. Sum of subproducts yields is higher than 100 % due to the reacted hydrogen. Off-gas (LHV=46.6 MJ/kg) is sent to the gas-burning furnace to recover its residual calorific value, while ammonia is assumed to be recovered mostly in the wastewater as reported from literature [227].

Table 28: Hydrotreatment product distribution.

Products	LRS	CS
Biofuel yield	66.9%	72.2%
Water yield	30.5%	24.4%
Gas (C1-C6) yield	6.6%	6.5%
Hydrogen consumption		
H_2 to reactor (kg H_2/kg biocrude)	0.058	0.046
H_2 consumed (kg H_2/kg biocrude)	0.04	0.031
H_2 make-up (kg H_2/kg biocrude)	0.042	0.033

6.3.6. Overall

The main inputs and outputs for a 3.6 t/h plant, for the two different feedstocks, are shown in Table 29 below. In Figure 85 the main mass flow rates inside the plant are reported.

Table 29: Main input and output streams.

	Lignin	***Corn Stover***
Main input (kg/h)		
Feedstock	12 000	3 805
Feedstock (*dry basis*)	3 600	3 600
Water from recycling	23 220	22 489
Make-up water	780	9 706
H_2 required for HT	63	37
Main output (kg/h)		
Wastewater	10 169	11 091
Solid char	619	171
H_2 produced	13	61
H_2 balance	-50	24
Biocrude	1 480	1 105
Biofuel	1047	841

The amount of water required for mixing with LRS and CS was mainly derived from the recycling, promoting the sustainability of the process. The demand for fresh water was limited to 3.3% (LRS) and 30.1% (CS) of the overall water demand.

The char is produced in much greater quantity with LRS and, with a residual humidity of 32 wt.%, this stream was not valued as coproduct but instead is energetically exploited in situ. As regards the production of biocrude, the two cases had a mass yield (dry biocrude/dry feedstock) of 41.1 wt.% (LRS) and 30.7 wt.% (CS); the biofuel yields after upgrading were 29.0% (LRS) and 23.4% (CS). The H2 yield of the HTL-APR integrated plant was lower with LRS (0.039 Nm3/kg dry LRS) than with CS (0.188 Nm3/kg dry CS). The difference was due to the higher organic concentration in the AP for the CS case and to the presence of compounds with high H2 productivity.
In addition, due to the higher oxygen content and mass flow of the biocrude, the H2 required for the upgrading is greater with lignin than with lignocellulosic feedstock. It follows that, while in the lignin case APR is able to provide only 20% of the H2 required for hydrotreatment, for corn stover the HTL-APR coupling is particularly advantageous as it can lead to a surplus of hydrogen (165% of the H2 required) that can be used for other purposes or sold as coproduct.

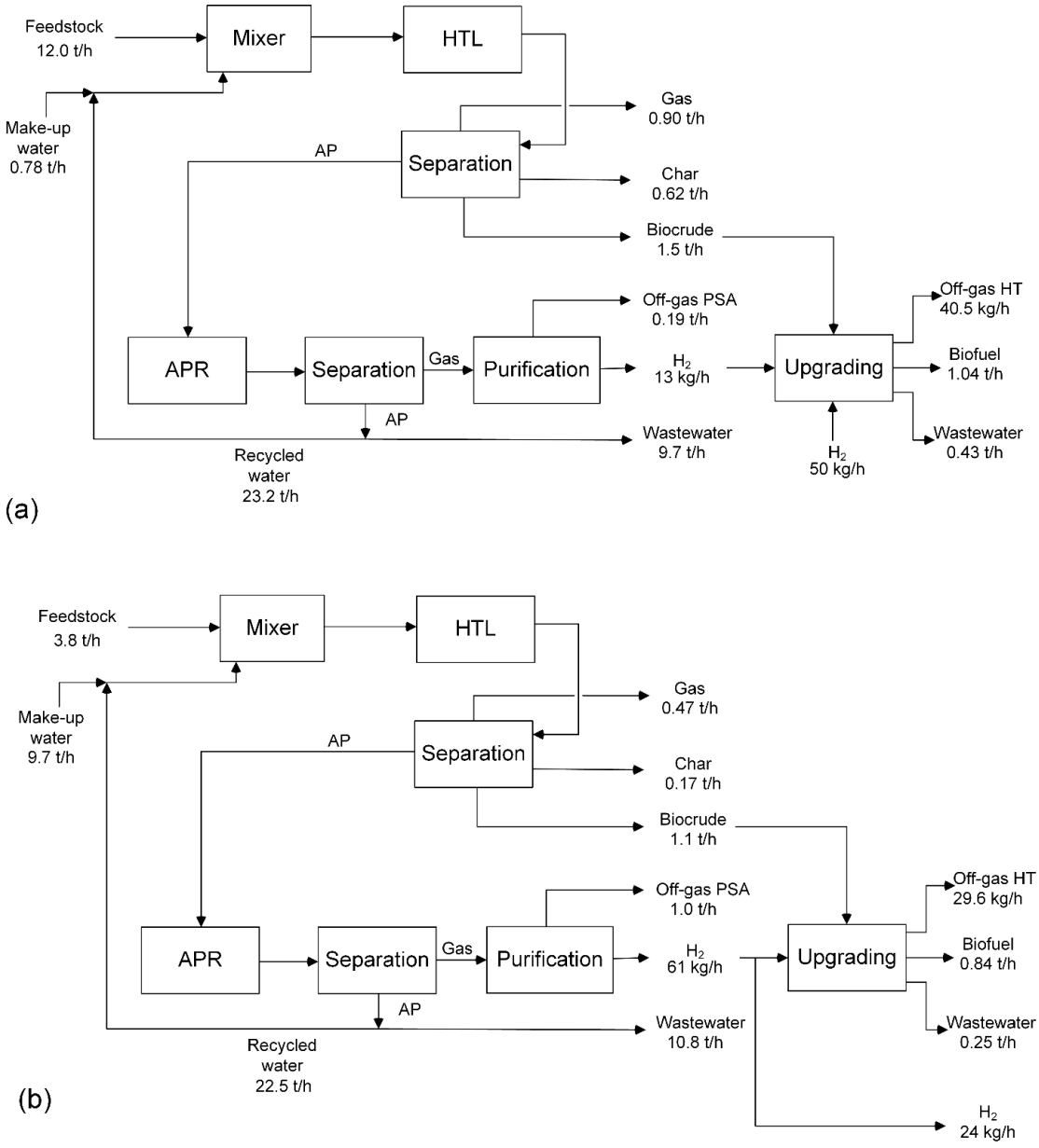
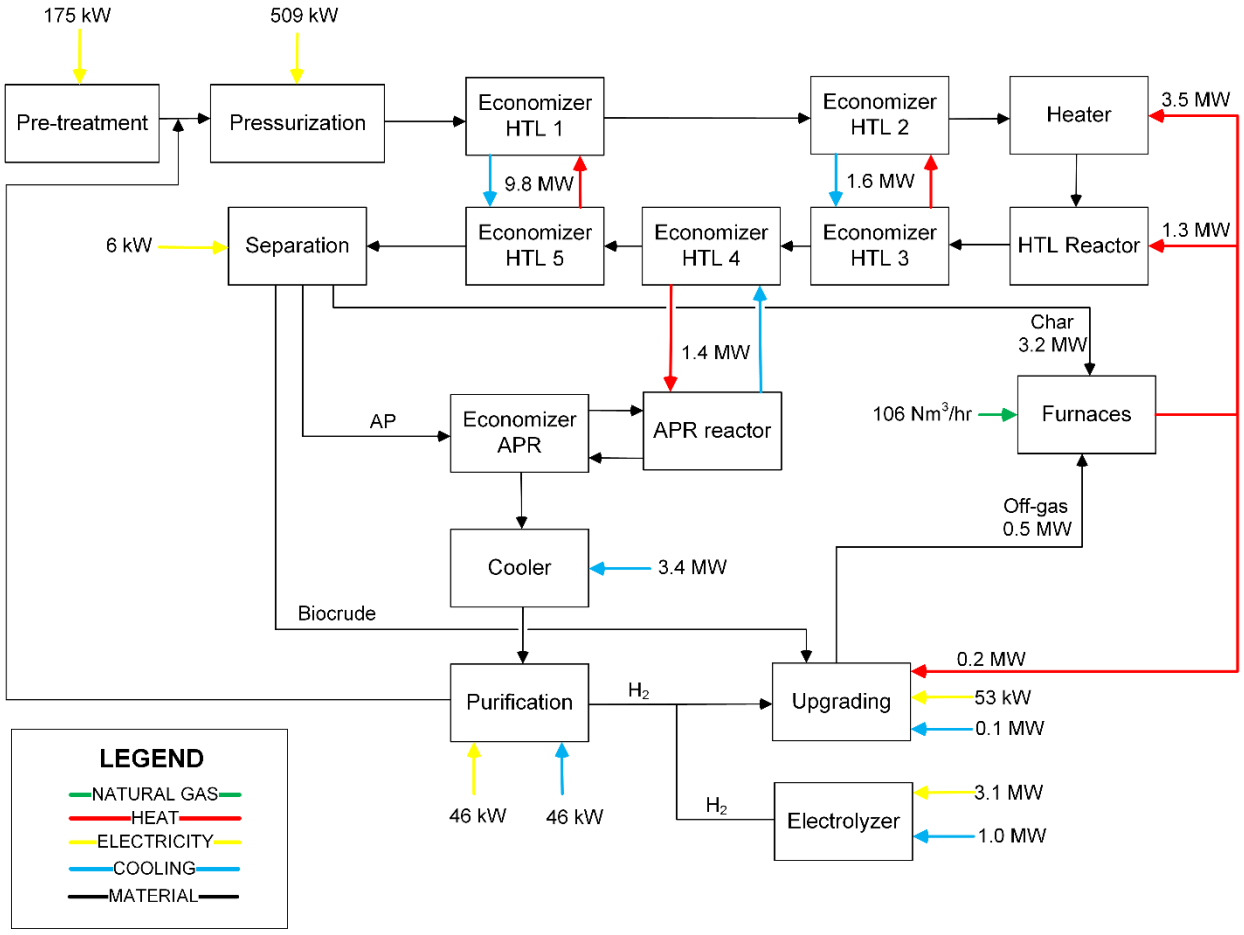


Figure 85: Mass flow for L case (a) and CS (b)

6.3.7. Energy balance

The block diagram in Figure 86 shows the energy streams for the LRS case and CS case. The HTL feed is energy-integrated with the HTL effluent and with the APR reactor by several heat exchangers, 12.8 MW_{th} are hence saved. After the economizers, the remaining heat to be given to the HTL input stream is provided by a final heater and also by the HTL reactor. The HTL effluent preheats the HTL reagent stream by means of two economizers separated by an exchanger able to provide heat to the APR reactor through diathermic oil. 3.2 MW_{th} (LRS) and 0.8 MW_{th} (CS) are recovered after char combustion in a char-burning furnace, assuming a 0.85 combustion efficiency. The heat required for the APR section is completely provided by the APR economizer, able to preheat the feed and to cool down the liquid product, and by the thermal integration with the HTL section. After the APR reaction, further heat must be removed before gas separation and after compression of the product gas for its purification. For the LRS plant, an additional amount of heat from the electrolyzer shall be removed (0.9 MW_{th}). The upgrading section requires 0.2 MW_{th} to heat up the biocrude for hydrotreatment, despite the designed integration of reagents and products. However, the off-gas formed in the upgrading section is sent to the gas-burning furnace, resulting in a 0.5 MW_{th} (LRS) and 0.4 MW_{th} (CS) savings leading to a positive thermal balance of the upgrading section.



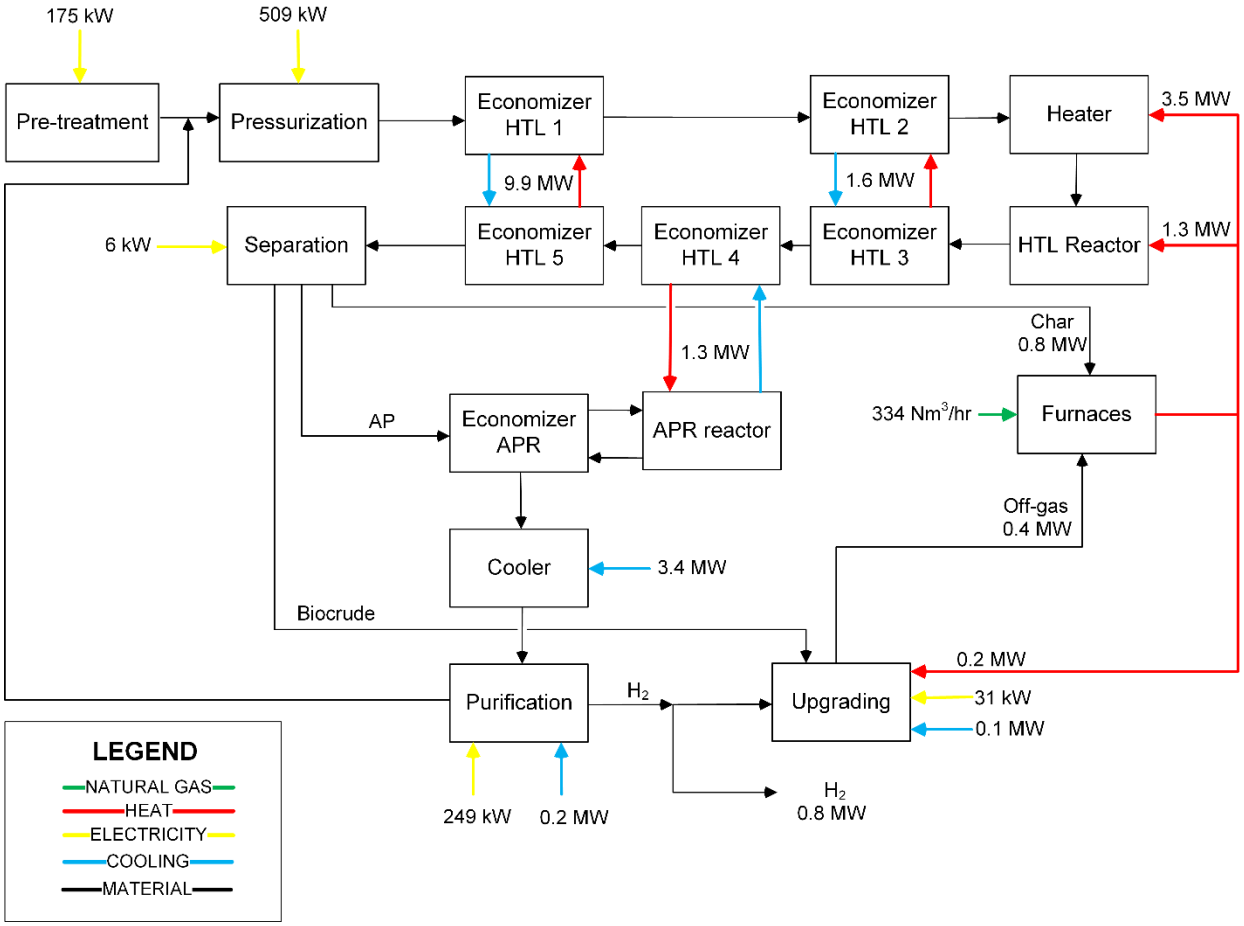


Figure 86: Block diagram and energy stream for LRS and CS

The overall energy consumption is shown in Table 30. The overall required thermal power was similar between the two cases (40 GWh/yr for LRS and 39 GWh/yr for CS), however, due to a lower production of char and off-gas from upgrading, the net thermal demand resulted much higher with CS. Cooling power did not differ strongly between the two cases while the high discrepancy between the electricity consumption was mainly due to the energy cost (24 GWh/yr) of the electrolyzer for the production of the hydrogen quota missing.

Table 30: Electric and thermal yearly inputs of the plant.

	LRS	**CS**
Electric power (GWh)	31.3	7.7
Cooling power (MWh)	7.6	6.1
Natural gas (GWh)	9.5	29.7

6.4. Process and equipment design

The plant layout is reported in Figure 87. In the following paragraphs the main units will be described, together with the performed calculations.

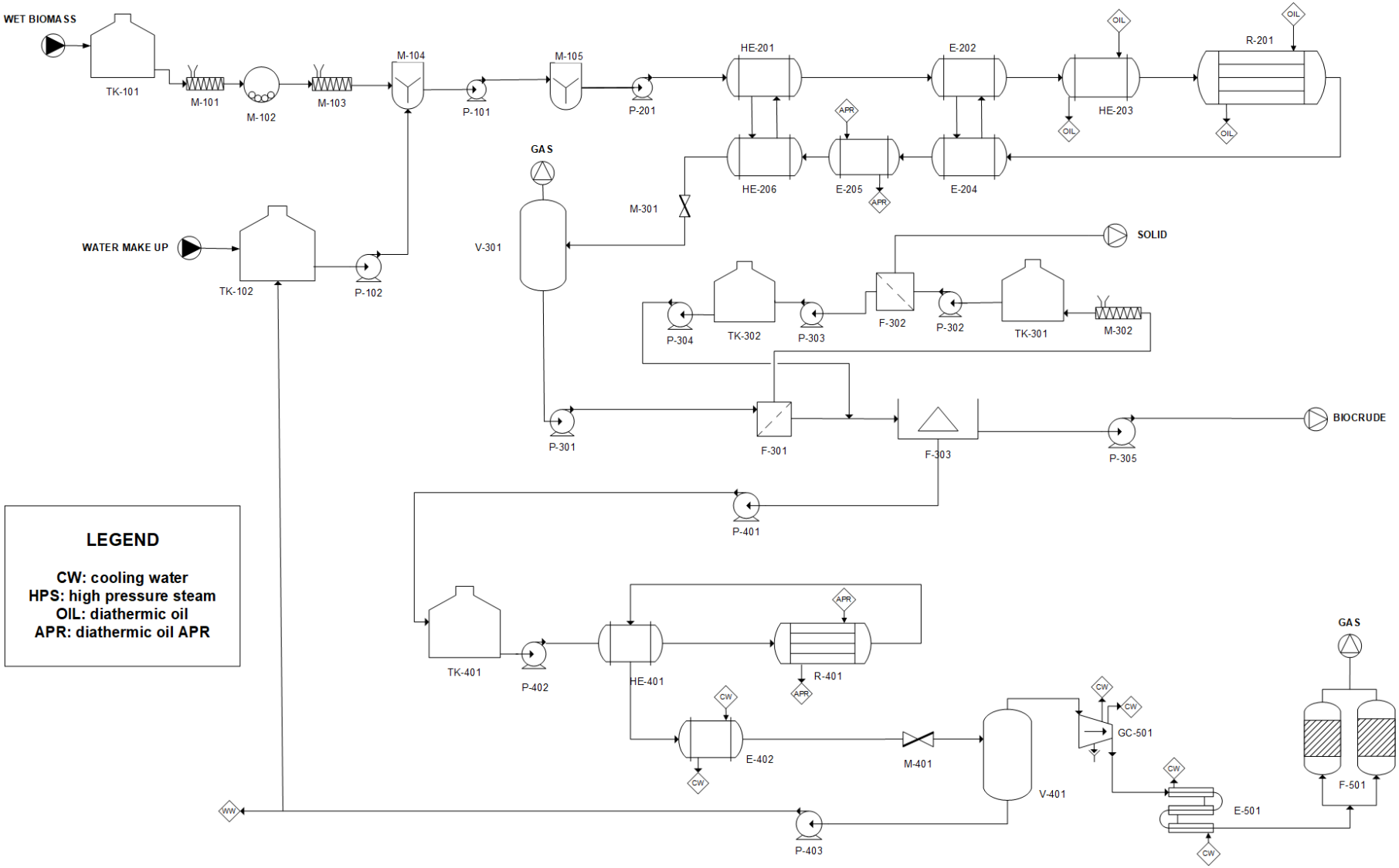


Figure 87: Plant layout.

6.4.1. Pre-treatment

The pre-treatment section is intended to prepare the feedstock to generate a slurry that has an optimal composition for the HTL reaction. The solid phase is transported by means of a screw feeder, while the liquid phase is transported by means of pumps. From the storage, the feedstock is sent to a ball mill where the solid matrix is chipped in order to improve the characteristics of the reagent slurry and avoid problems of sedimentation with particles with larger size. Then the solid is sent to a mixer where is diluted with fresh and warm recirculated water to form the slurry. The mixer is dimensioned assuming a discontinuous operation, in order to maximize the homogeneity of the matrix to be sent to the section of HTL; a high efficiency impeller with three blades (HE-3) was chosen. After mixing, the slurry is pumped in a mixed vessel acting as a buffer tank to ensure continuity of the process. Pumps are sized assuming a slurry viscosity equal to that of water.

6.4.2. HTL reaction

HTL is performed at 350 °C and 200 bar to avoid vaporization of the liquid. The choice of the type of pump suitable for pressurization of the slurry is crucial as currently it represents one of the greatest limits to the development of HTL continuous plants [248]. A commercial diaphragm hose pump is chosen due to the minimal pulsation and possibility to reach the operative pressure in one single stage [249].

A heat exchanger system is design to minimize the thermal expenditure: the reactor outlet preheats the feed up to 300 °C in a double step (couplings HE-201/HE-206 and HE-202/HE-204) and then is brought to the reaction temperature by the final heater. It is important that the heating time from 300 to 350 °C is less than 10% of reaction time due to the reactivity of the feed in this range; this assured that most of the reaction will be performed in the reactor at the desired temperature. The hot outlet stream is thermal integrated to pre-heat the HTL inlet (HE-204 and HE-206) and also to provide the necessary heat to the APR reactor (HE-205).

For all heaters and for the reactor, the shell and tube configuration was preferred. The economizers are thermally connected with a diathermic oil in insulated tubes. This configuration was adopted to avoid high pressure (200 bar) in

both shell (which would lead to high thickness) and tube, as well as to improve the heat exchange (due to high fouling factor of HTL feed and products streams).

Three different type of diathermic oil were used: commercial mineral oil for low temperature heat exchangers, while special synthetic diathermic oil for the high temperature ones (up to 400 °C). The design is performed following the Kern method [222]; fouling factor and necessary data were taken from literature [250]. In order to limit the fixed cost, the choice of custom-made heat exchangers is avoided, preferring the standard commercial dimensions. For this reason, the presence of several reactors in series is set. Economizers are oversized by 20% while the final heater has an over dimension of 100%.

A standard shell & tube configuration is chosen for the HTL reactor; the spatial velocity is set to maintain the residence time of 10 minutes and avoid sedimentation of smaller particles. Having no experimental data, the diathermic fluid flow rate to be sent to the reactor is calculated based on an adiabatic ΔT of 10 °C. As for the exchangers presented above, the tubes must be selected to safely withstand a maximum pressure above the operative one. The selected material is stainless steel 316 with an outer diameter equal to 1.5 in and thickness equal to 0.156 in.

6.4.3. Products separation

The products separation section is a crucial and complex point for the HTL plant. In particular, the critical aspect of this section is represented by the filtration, which results difficult at high temperature, pressure, and solid loading (85 °C, 200 bar, 0.3-1.2 wt.%).

The products were cooled to 85 °C in HE-206, sufficiently above 70 °C to avoid the biocrude to stick in the tube [209]. A suitable pressure letdown system (M-301) shall be chosen to operate with the amount of solid present in the stream; for this reason the choice fall on a system consisting of hydraulic pistons connected to an external oleodynamic circuit able to decrease the pressure up to 3 bar [251]. At this pressure, in flash V-301 incondensable gases (CO_2, CH_4, H_2) are released, avoiding the loss of more volatile organics.

The char, produced during HTL, is separated using a continuous liquid candle filter (F-301). The concentrated slurry coming out of it is then thickened in a filter press (F-302) that works in a discontinuously (4.45 h for cycle). The liquid phases coming from candle filter and filter press are sent to a centrifuge (F-303) to separate the water from the biocrude.

6.4.4. APR reaction

In the APR section, buffer tank TK-401 accumulates the water after the HTL products separation. A surge tank is necessary in case of a problem in one section of the plant since it can avoid stopping all the plant and dampen the fluctuations. A centrifugal pump is used to pressurize aqueous stream to 60 bar.

The economizer HE-401 recovers heat from the APR outlet (115°C after HE-401 for CS, 123 °C for L) and brings the feed up to 240 °C while the final heating is given inside the APR reactor (R-401). HE-401 was designed like the other shell & tube heat exchangers described in the HTL section.

Two shell and tube APR reactors were designed with 99 tubes each (7 cm DI), in which the water stream is fed to the tube side and the diathermic oil in the shell side. The reactor size is chosen based on the same WHSV used in laboratory scale experiments performed on the HTL-AP of LRS. Every reactor has 2 tube passes and the first reactor requires that one third of the first 50 tubes is not filled with catalyst but with inert material that allows the feed to reach the operative temperature. The feed was heated up to 270 °C in the pre-heating section, while reaction section of R-401 must provide the heat necessary to compensate for the endothermicity of the APR. Thanks to thermal integration, this heat is given by the diathermic oil heated up by the hot stream coming out of the HTL reactor.

The APR products were cooled down in the economizer HE-401 and then in HE-402 to 35 °C. The incondensable gas is separated in the flash V-401 operating at 60 °C and 1 bar.

6.4.5. Purification

After separation from the liquid stream, APR is purified through PSA operating at 30 bar. Gas is at first pressurized to the working pressure in a multistage centrifugal compressor with four intercooled stages. Compressed gas comes out at 116 °C and it was cooled to 35 °C before the PSA in a hairpin using tower water as coolant.

6.5. Economic analysis

The overall costs and results are summarized in Table 31 and the details of fixed and material and utilities costs are detailed below.

6.5.1. Fixed costs

Grassroots costs are equal to 24.6 M€ and 22.3 M€, for LRS and CS case, respectively. The distributions of these costs between the sections of the plant are reported in Figure 88; in Figure 89 is presented the distributions of cost between equipment.

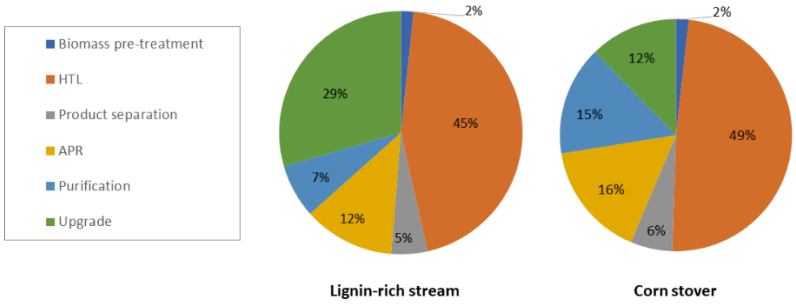


Figure 88: Grassroot costs distribution between sections, with LRS case (left) and CS case (right)

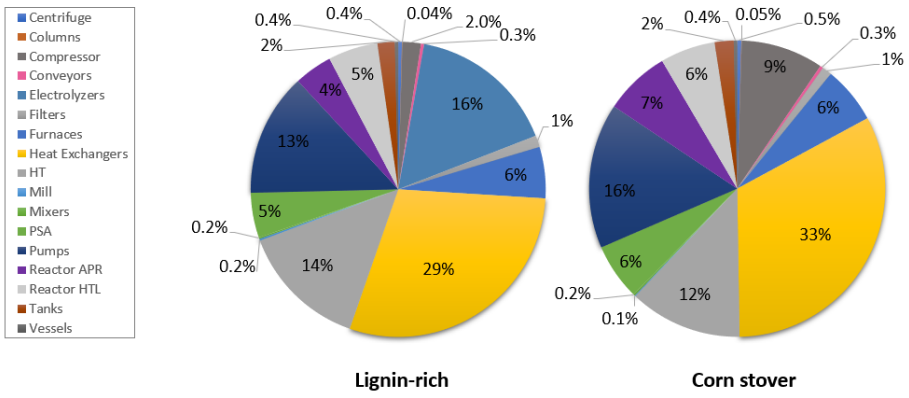


Figure 89: Grassroot costs distribution between equipment, with LRS case (left) and CS case (right).

HTL section is the most expensive of the plant due to the high number of heat exchangers operating at very high pressure (LRS: 25%; CS: 28% of the overall fixed cost), to the hose pump P-201 (LRS: 8.2%; CS: 9.0%) and, secondly to the HTL reactor (LRS: 5.5%; CS: 6.0%). APR is also quite demanding from the economic point of view (LRS: 12%; CS: 16% of the overall cost) and its impact mainly derived from heat exchangers (LRS: 4.3%; CS: 5.0%) and APR reactor (LRS: 4.2%; CS: 7.2%). Biomass pre-treatment has almost no impact on costs, as well as the product separation section.

Cost differences between the LRS and CS case are mainly due to the purification and upgrading sections: 30% of fixed costs for LRS are accounted to the upgrading section because of the electrolyzer (16% of the overall cost), needed to supply the missing amount of hydrogen. On the other hand, in the CS case the purification section cost is twice that of LRS due to the higher amount of hydrogen produced from APR.

6.5.2. Material and utilities costs

Material and utilities costs accounts for 5.4 M€/y and 4.5 M€/y for the LRS and CS case, respectively. As can be seen from Figure 90, one of the two higher cost is related to the purchase of the feedstock. However, the assumption of 60€/t for dry LRS and 75€/t for dry CS may not be economically accurate as a lignin market has not yet been established, as well as for corn stover. For this reason, in the sensitivity analysis the effect of a change in the cost of LRS and corn stover is investigated.

Almost half of the remaining cost is due to electricity in LRS case due to the much higher electric consumption attributable to electrolyzer. In the CS case, natural gas accounts for 20%, due to the increased energy input required, and water make-up accounts for 6%, due to the low feedstock's moisture. Wastewater disposal is relevant in both cases (8%), while catalysts and cooling power costs have low impact.

Within the CS case, the credit deriving from the sale of the produced hydrogen (960 k€/y) is subtracted to the material and utilities costs (4.5 M€/y), resulting in a lower net cost of 3.5 M€/y.

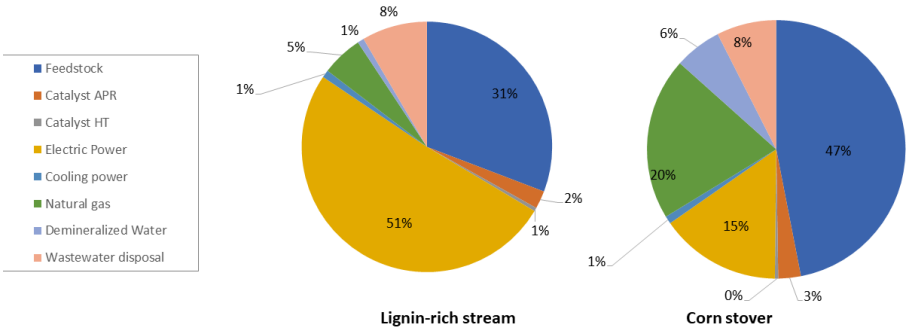


Figure 90: Operative costs, with LRS case (left) and CS case (right)

6.5.3. Minimum selling prices and economic indicators

The resulting $MSPs^{0\%}$ of the biofuels were 1.20 €/kg (LRS) and 1.17 €/kg (CS) and, assuming a distillation cut like diesel (HHV=45 MJ/kg), the gasoline-equivalent prices are equal to 3.39 €/GGE (LRS) and 3.29 €/GGE (CS), which are in the range of the existing biofuel's TEAs. The $MSPs^{10\%}$ were 1.54 €/kg (4.31 €/GGE) and 1.55 €/kg (4.34 €/GGE) for LRS and CS, respectively The $MSP^{10\%}$ of the LRS case is slightly more profitable than CS because, in case of selling price increases, the profitability depends only on the difference in produced quantity of biocrude. In Table 31 the main economic parameters are reported.

Table 31: Economic parameters and main indicators for LRS and CS case

	LRS	**CS**
Total fixed cost (M€)	26.1	24
Start-up cost (5% of fixed cost) (M€)	1.3	1.2
Total investment cost (M€)	27.4	25.2
Maintenance cost (M€/y)	1.4	1.3
Material cost (raw material, catalyst, water) (M€/y)	2.5	3
Utilities cost (M€/y)	3.2	1.6
General cost (M€/y)	0.6	0.6
Labor cost (M€/y)	1	1

Bio-oil production (kt/y)	8.4	6.4
H_2 credit (k€/y)	0	960
$MSP^{0\%}$ (€/kg)	1.20	1.17
$MSP^{10\%}$ (€/kg)	1.54	1.55

The estimated cost of hydrogen production via APR must be evaluated to assess the actual benefit in the HTL-APR coupling. The difference between the sums of fixed, maintenance and operative costs of the integrated HTL-APR plant with a stand-alone HTL plant is normalized compared to the mass of hydrogen produced by the integrated one. H_2 production costs are estimated as 7.6 €/kg (LRS) and 1.7 €/kg (CS). The costs attributable to the APR section are mostly dependent on the amount of aqueous stream to be treated, which is approximately the same for both cases; hence, the higher profitability of the CS case is ascribed to its higher H_2 production rate. APR competitiveness therefore strongly depends on the carbon concentration and H_2 productivity of the organics present in the aqueous phase.

Compared to other TEAs, both these values are lower than hydrogen produced by APR of a sorbitol syrup (11.7 €/kg) [112], which is heavily penalized by the high cost of the feedstock that constitutes up to 91.8 % of the overall costs. In this work, APR is carried out on a waste stream that could not be sold, but rather should be disposed of. In addition to getting rid of the feedstock cost, the HTL-APR coupling also allows the reduction of the COD of HTL water, resulting in lower disposal costs and higher profitability. Also Khodabandehloo et al. assessed economic performance of APR from a sub-product of glycerol stream from biodiesel production [123]. Glycerol was assumed to have a residual value of 45 €/kg, and the resulting H_2 production cost was estimated to be 6.7 €/kg. Although slightly higher than in the LRS case, this value is much higher than in the CS case.

The cost of producing hydrogen from steam reforming (SR) and electrolyzer was also calculated as benchmark. These values were obtained by means of correlations, reported before in the economic evaluation paragraph, with the flow rates required by the two cases. The resulting costs are 2.7-2.9 €/kg for SR and 6.4-6.5 €/kg for the electrolyzer, which fall within the ranges known for these two technologies: 1.3-3.6 €/kg for steam methane reforming [252] and 3-9 €/kg for electrolysis using different electricity sources [253]. The cost of the electrolyzer is proportional to the current to be treated and the cost range is due to the specific electrolysis technology and electricity production cost. For SR there is a scale factor which usually makes

it difficult to produce small hydrogen systems. The required hydrogen flow rates of this work fall within the lower operability limit of the typical SR plant and to make the process more profitable could be favorable the use of a centralized upgrading plant where biocrude from more HTL plants are routed. This does not happen for APR that can therefore be a valid solution for HTL plants within situ upgrading. The comparison with other technologies for hydrogen production will be investigated in detail in the next paragraph.

6.5.4. Sensitivity analysis

Total investment cost and material & utilities cost account in different ways on the minimum selling price: excluding financial items, these account for 13% and 53% with LRS and 14% and 49% with CS. In both cases the material & utilities costs are the most influential on the production cost of the final product. For this reason, the main cost items among the material & utilities, namely feedstock, electricity and natural gas prices, are varied in wider ranges to evaluate how much their variation would affect the economic performances of the plant. The percentage variations on the $MSP^{10\%}$ are reported in Figure 91.

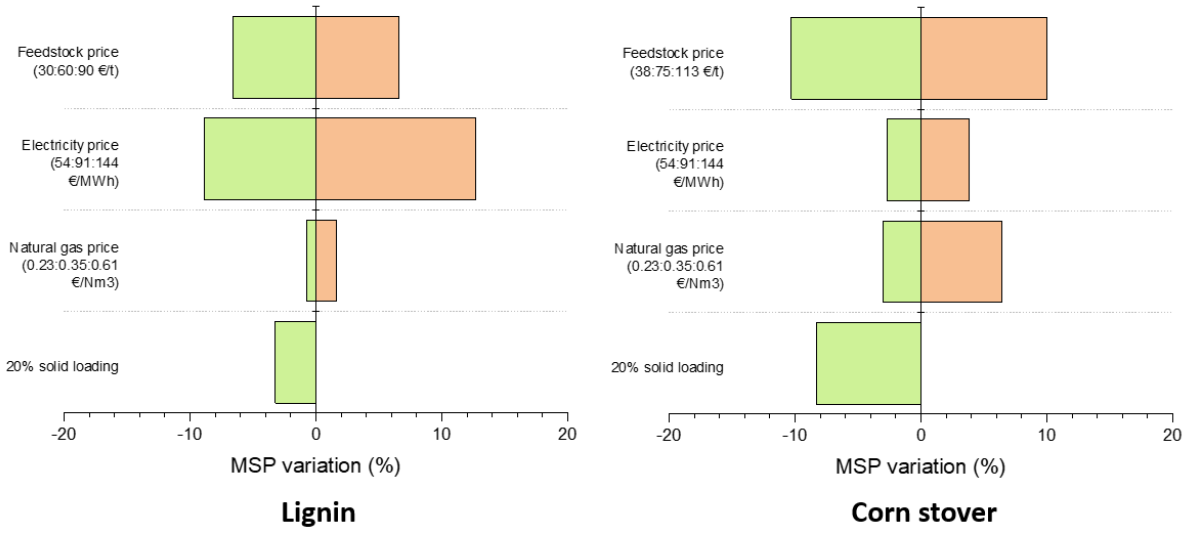


Figure 91: MSP10% variations after feedstock, electricity, natural gas price variation and with an HTL-APR plant operating at 20% solid loading.

The price of feedstocks is subject to strong uncertainties due to the lack of a consolidated market and strong worldwide discrepancies, consequently its value was varied in a big range (± 50%). The LRS $MSP^{10\%}$ varied within ±6.6% while CS $MSP^{10\%}$ varied within ±10%; despite it was important in both cases, the variation was particularly evident for the CS case because of the high share of the feedstock in the material & utility costs of the plant.

As regard electricity and natural gas cost variations, the minimum and maximum costs from EU countries were taken as ranges for the sensitivity. For the LRS case, fluctuations of the electricity price were very important: $MSP^{10\%}$ varies within -8.9% and +13%. This is attributable to the high amount of electricity required by the electrolysis necessary to produce hydrogen that APR is not able to provide. The dependence on electricity is therefore not to be traced directly to the HTL-APR integration, which instead is a green alternative to electricity-demanding electrolysis. As a consequence, an HTL-APR plant capable of being self-sufficient in the production of hydrogen limits the strong influence that electricity has on the selling price of the biofuel. In contrast to electricity, the impact of the cost of natural gas is higher with CS than in the LRS case, because of the almost thermal self-sufficiency of the latter. In this scenario $MSPs^{10\%}$ varied within -0.8%, +1.7% (LRS) and -3.0%, +6.4% (CS). It can be also observed form Figure 91 that the increase of solid loading to 20 wt.% leads to a reduction in fixed and operating costs. This is attributable to the fact that with a double solid loading the biofuel flow rate produced is kept constant while the mass flow to be treated is halved. However, with state-of-the-art technology it is difficult to pump slurry with 20% of solid [26], [238], [254]; this problem is strictly linked to the biomass feature and is currently receiving great attention in order to evaluate, on the different types of substrate, the optimal solution (pre-treatments, basic additives, biocrude recycling). The above-presented result confirms therefore a commendable improvement of the economic performance of a plant operating at a higher solid concentration of solids that will have to be supported by future studies on its technical feasibility.

The different plant configurations for the hydrogen supply are described in Figure 92, as well as the $MSPs^{10\%}$ variations with respect to the base configuration. Table 32 reports the $MSPs^{10\%}$ for every configuration.

Table 32: $MSPs^{10\%}$ for different plant configurations for hydrogen supply.

Upgrade	H_2 production	MSP LRS (€/kg)	MSP CS (€/kg)
Yes	Electrolyzer	1.55	1.78
Yes	SR	1.29	1.61
Yes	APR	-	1.55*
Yes	APR + Electrolyzer	1.54*	-
Yes	APR+SR	1.34	-
No	-	0.65	1.03

*Base case

Looking at the LRS case, an external hydrogen source is always required because APR manages to produce only 20% of the hydrogen needed for the upgrading of biocrude to biofuel. Compared to the production of the remaining 80% via electrolysis (Figure 92 A), the use of SR is economically very advantageous (Figure 92 C) and the $MSP^{10\%}$ is reduced by 13%. The resulting $MSPs^{10\%}$ in configuration E (only electrolyzer) and D (only reforming) turn out to be lower or comparable than with APR. The differences in MSP10% resulting from the removal of the section of APR was -0.8% for electrolyzer compared to the APR+electrolyzer and -3.6% for SR compared to APR+SR.

For the CS case, the integrated HTL-APR plant (Figure 92) was able to produce 165% of the H_2 required by the upgrading section. In this case, the replacement of the APR section with electrolyzer (Figure 92B) or SR (Figure 92 D) led to an increase of $MSP^{10\%}$ (+15% and +3.8%, respectively). These results confirmed the lower H_2 production cost through HTL-APR (2.59 €/kg) compared to the other technologies. The economic performance of the HTL-APR plant was hence further improved by the fact that a surplus of hydrogen can be sold thus increasing the revenue.

Finally, the $MSP^{10\%}$ was evaluated in the case of HTL plant without on-site upgrading and without integration with APR. Without upgrading the final product is no longer a drop-in biofuel but rather a biocrude (Figure 92F) and its $MSPs^{10\%}$ were 0.65 €/kg (LRS) and 1.03 €/kg However, since the product is different, the comparison with the HTL-APR upgraded configuration cannot be done directly because the quality of biocrude is lower than that of a biofuel. This biocrude could be used as a low quality marine fuel for blending [255], due to the high flexibility

of the marine engine regarding fuel [256], could be sent to a centralized upgrading plant [237] or to the upgrading section of existing refineries [257].

$MSP^{10\%}$ for LRS-derived biocrude is much lower than the CS-derived one, as well as for biofuel without APR (Table 32). LRS is thus more economically favorable for biocrude compared to corn stover and this trend is confirmed also for biofuel production without APR (1.53 vs 1.85 €/kg for electrolyzer and 1.26 vs 1.67 €/kg for steam reforming), despite LRS-derived biocrude is more oxygenated and hence requires more upgrading expenses. The difference between $MSP^{10\%}$ of the two cases in their HTL-APR base configurations is instead almost cancelled and it is due to the high H_2 productivity (165% of the hydrogen required) produced through APR of the residual aqueous phase from CS. In conclusion, while HTL plants are more profitable with feedstocks or operating conditions which allows a higher carbon yield towards biocrude, as well as a low content of oxygen and nitrogen in it. Good carbon yield in the aqueous phase and good hydrogen yield (kg H_2/kg C feed) are required to make the HTL-APR integration attractive.

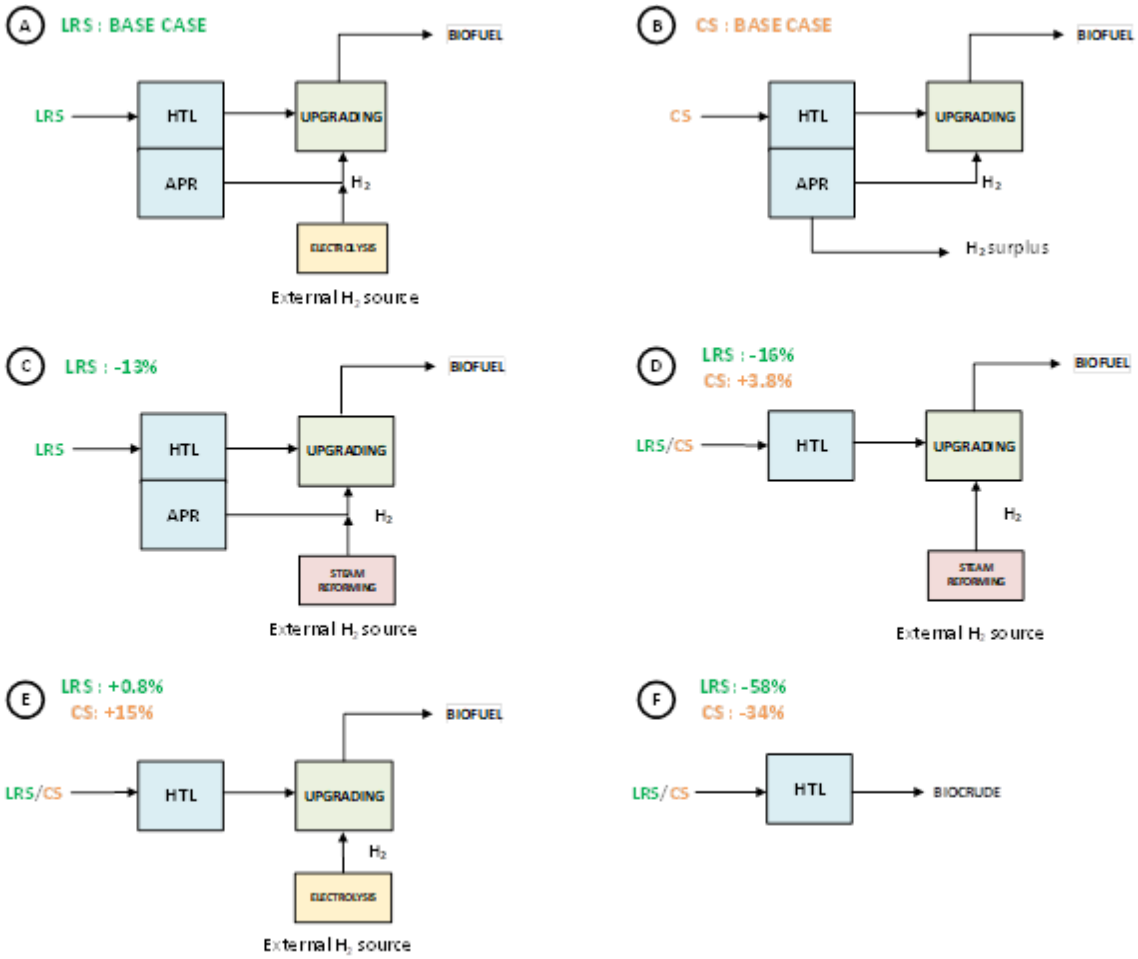


Figure 92: plant configurations for hydrogen supply. A) APR+electrolysis, B) APR alone, C) APR+SR, D) SR alone, E) Electrolysis alone, F) No upgrading. The percentage values refer to the variation of the $MSP^{10\%}$ of the considered configuration compared to the respective base case (A for LRS and B for CS).

6.5.5. Comparison with literature data

In literature there are not many TEAs for HTL of LRS or lignocellulosic material. PNNL studies result in a biofuel's MSP from woody biomass with state-of-the-art technologies of 4.44 $/GGE, which could be further decreased to 2.52 $/GGE through possible future improvements [25]. These mainly included lower operative HTL pressure with equal yields and conversions, better oil-aqueous phase separation and optimization of the upgrading technologies by addition of a hydrocracking section and a single-step hydrotreatment.

Funkenbusch et al. [258] evaluated the production costs for biofuel from Kraft lignin through alkaline HTL with coproduction of benzene, toluene, ethylbenzene, and xylenes (BTEX). The resulting MSPs were 3.52-3.86 $/gallon for the biofuel and 1.65-2 $/L for BTEX. Separation of phenolic compounds via liquid-liquid extraction (LLE) and their hydrotreatment for BTEX production have represented the higher operating and fixed costs of the overall plant and hence currently more technological advancements are required to make BTEX production feasible.

Nie et al. [232] performed a preliminary analysis to evaluate different production systems for HTL biofuel from forest residues, including coupling with anaerobic digestion (AD). MSPs for a plant with a nameplate capacity of 100 million liters per year of biofuel ranged within 3.1-3.4 $/GGE. Despite the higher operating cost, the lower MSP was obtained through a central integrated biorefinery using raw forest residues as feedstock and performing *in situ* upgrading. On the other hand, the other two assessed systems, involving distributed systems with locally produced wood pellet sent to a central biorefinery or smaller HTL plants with a central upgrading plant, resulted in the higher selling prices.

Due to the synergistic effect with wood, also co-liquefaction (co-HTL) with other feedstocks was assessed. Pedersen et al. [259] evaluated the MSP for biofuel from HTL of Aspen wood alone and mixed with glycerol obtained a MSP in the range 3.11-4.31 $/GGE. Blending of wood with microalgae was also evaluated [260] and the MSP was 9.88 $/GGE which results lower than with an algae-only HTL plant, due to the high microalgae production costs.

Another study from PNNL compared biofuel production from forest residue through HTL and fast pyrolysis [215], two of the most promising technologies for biomass processing [261]. The former was more advantageous than the latter: 2 $/GGE against 3.09 $/GGE of MSP. Ramirez et al. [235] compared different technologies for liquid fuel production from sugarcane bagasse, namely gasification coupled with high temperature Fischer-Tropsch (HT FT), HTL and fast pyrolysis. In this case HTL results as the most economically advantageous: MSPs were 7.34 $/gallon (gasification), 3.71 $/gallon (HTL) and 4.50 $/gallon (fast pyrolysis). Brown et al. evaluated MSPs for corn stover-derived biofuel through gasification coupled with HT FT (4.27 $/GGE, [239]) and fast pyrolysis (2.11-2.57 $/GGE without internal H_2 production [233], [234], 3.09 $/GGE with internal H_2 production).

MSP of biofuels from HTL plant fed with other feedstocks have also been evaluated. In particular algae have been used as feedstock due to their high biocrude yield, moisture and growth rate. Gu et al. [213] estimated 7.48 $/GGE and 5.72 $/GGE for single and double stages HTL reactor, respectively. 4.49 $/GGE was evaluated by PNNL [227] through an HTL plant coupled with a catalytic hydrothermal gasification section (CHG) which furnish a portion of the gas to be reformed for biocrude upgrading. In this case, the biggest cost item is the feedstock due to the high cost associated with algae growth. Among other HTL feedstocks, biocrude from food residue (3.48 $/GGE [214]) and wastewater sludge (4.9 $/GGE with HTL+CHG and centralized upgrading plant [237], 3.46 $/GGE with HTL and centralized upgrading plant [231]) were also assessed. In Table 33 below the previously described MSPs are reported.

Table 33: MSPs comparison with literature data

Technology	Feedstock	MSP [$/GGE]	Reference
HTL+APR	LRS	4.48	This work
HTL+APR	Corn stover	4.5	This work
HTL	Wood	4.44	[25]
HTL+LLE	Kraft lignin	3.52-3.86*	[258]
HTL+AD	Forest residue	3.1-3.4	[232]
co-HTL	Wood + glycerol	3.11-4.31	[259]
co-HTL	Wood + microalgae	9.88	[260]
HTL	Forest residue	2	[215]
Fast pyrolysis	Forest residue	3.09	[215]
Gasification+HTFT	Sugarcane bagasse	7.34*	[235]
HTL	Sugarcane bagasse	3.71*	[235]
Fast pyrolysis	Sugarcane bagasse	4.50*	[235]
Gasification+HTFT	Corn stover	4.27	[239]
Fast pyrolysis	Corn stover	2.11-3.09	[231]
Fast pyrolysis	Corn stover	2.57	[232]
HTL	Algae	5.72-7.48	[213]

HTL+CHG	Algae	4.49	[227]
HTL	Food residue	3.48	[214]
HTL+CHG	Sludge	4.9	[237]
HTL	Sludge	3.46	[49]

EUR-USD conversion: 1€=1.11$

*$/gallon

**biocrude

6.6. LCA results

6.6.1. Goal and scope

The goal of this chapter is to assess the environmental impact of the biofuel produced by LRS and CS HTL.

The definition of system boundaries plays a key role in LCA analyses. As showed in Figure 93, there are three common options:

- Cradle-to-grave. The full life cycle of the product is considered: the raw material acquisition, the production, the use and the end-of-life phase (e.g. recycling, disposal)
- Cradle-to-gate. The analysis considers all the processes from the acquisition of raw materials to the production of the product. Use phase and End-of-life phase are excluded.
- Gate-to-gate. The analysis only includes a specific stage of the production. Raw material acquisition, use phase and end-of-life phase are excluded.

The LCA developed here is a cradle-to-gate analysis: it includes the processes from the feedstock acquisition to biofuel production, as showed in Figure 94. The transportation is included only for CS since the LRS plant is built close to the lignin production site.

The functional unit of the study is 1 MJ of HTL biofuel, no allocation is needed, and the plant is located in Europe.

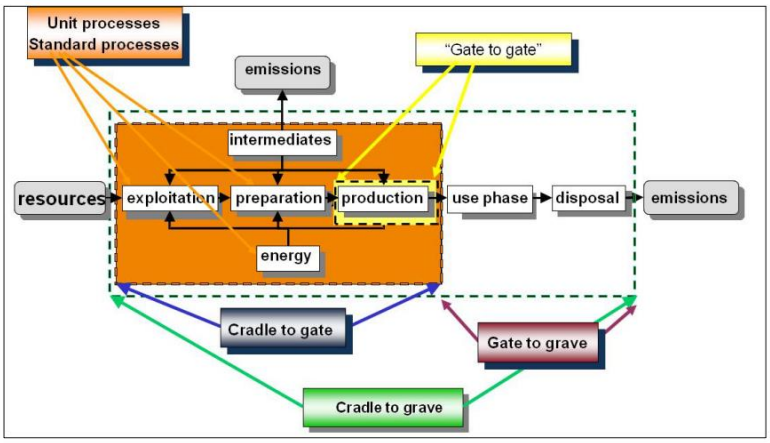


Figure 93: Example of system boundaries in a LCA [245].

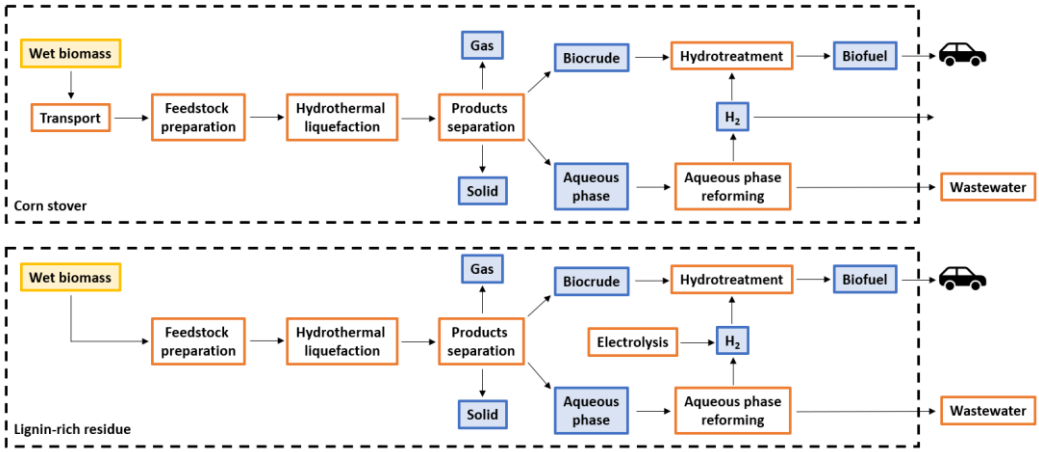


Figure 94: system boundary of studied LCA

In order to perform the LCA some cut-off criteria have to be considered:

1. material and energy of construction of equipment is not considered. Therefore, because of the considerable amount of biofuel that can be produced during the lifespan of the plant (20 years), the impact contribution of equipment would result negligible in the assessment of 1 MJ of biocrude. This is in line with literature and with ILCD Handbook guidelines.

2. Make-up of diathermic oil is not considered for the mass cut-off criteria (<1% of total mass).

Four impact categories were considered for the environmental characterization:

- Global warning potential (GWP). This impact category has been chosen due to the importance of climate change mitigation in the current European and International policies.
- Freshwater Eutrophication Potential (EP). It is due to the discharge of nutrients (e.g., phosphorous and nitrogen) into freshwater bodies, leading to an increasing nutrients uptake of cyanobacteria and algae. This occurrence eventually leads to a potential loss of biodiversity.
- Acidification Potential (AP). It refers to the release into the atmosphere of acid gases (SO2, NOx, N2O) which are the precursors to acid rain.
- Abiotic depletion potential (ADP): it is related to the measure of the use of fossil sources

The method used to evaluate the impact is CML 2015 to facilitate the comparison with previous literature.

When dealing with biomass, an important discussion point is the assessment of biogenic carbon, which is emitted to air as CO_2, CO or CH_4 from the oxidation and/or reduction of biomass. Biogenic carbon could be considered carbon-neutral because carbon emissions derived from the biomass utilization (e.g. through combustion) balance the carbon that has been sequestrated during the growth of the feedstock. However, an overall consensus on the most appropriate way to consider biogenic carbon in LCA, has still not been reached. An issue is the lag time between uptake and release of CO_2, which is particularly severe when dealing with long rotation period biomass. Different approaches can be found in literature:

- "0/0 approach": neither the uptake nor the release of biogenic carbon is considered in the calculation of impacts for the global warming potential
- "–1/+1' approach": the uptake of biogenic CO_2 carbon is considered an environmental credit, while the release is considered an environment burden, with the same impact factor of fossil carbon.
- dynamic approaches based on time-dependent characterization factors [262]–[264]

In this work impact results on climate change are given only as fossil emission, following the "0/0 approach").

Another key point is the definition of the nature of the feedstock (i.e., energy crop, or residue, or waste) and the environmental burden that should be attributed to it. Generally, in LCA waste enters the system free of environmental burdens (and credits). If the feedstock is a by-product (still having economic value), a part of impacts (and eventual credits) of the production should be allocated to it. In the case where energy crops are properly grown for energy production, the feedstock has to be loaded of the total burdens (and eventual credits) of the crop cultivation. In this work the feedstocks are considered as a waste and, consequently, its initial impact is zero. A similar approach was considered by Tews et al. for forest residues [215].

6.6.2. Inventory list

The inventory list presented in literature Table 34 below is described in detailed the previous paragraphs 6.3 mass and energy balances.

In addition, some assumptions have been necessary to fill some inventory gaps. Specifically:

- The cooling power was converted from thermal to electrical energy, as described in literature [250]
- The electrolysis process has been based on literature data [230]
- The data for platinum, are taken from literature.

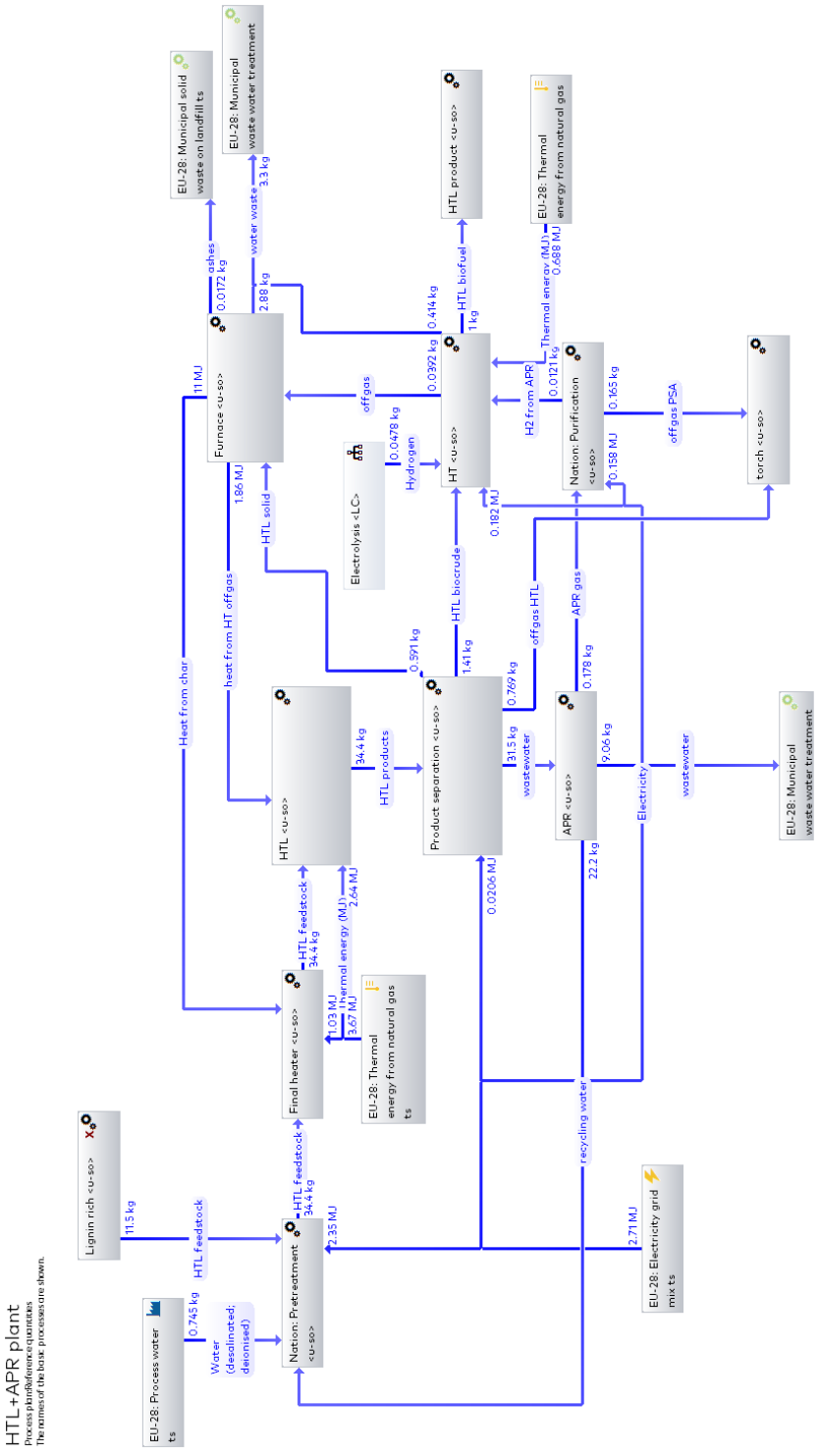
Table 34: Life cycle inventory of 1 kg biofuel for LRS and CS cases.

Process	Stream	Input/Output	Amount LRS case	Amount CS case	Unit
Biomass transport	Biomass transport	Input	-	50	km
Pre-treatment	LRS feedstock	Input	11.5	4.5	kg
	Fresh water	Input	0.74	11.5	kg
	Electricity	Input	0.17	0.21	kWh
Pressurization	Electricity	Input	0.49	0.61	kWh
HTL	External heating	Input	1.1	4.4	kWh
Separation	Cooling	Input	3.2	4.0	kWh
	Electricity	Input	0.006	0.01	kWh
APR	Wastewater	Output	9.3	12.9	kg

Furnaces	Ash	Output	0.02	0.04	kg
	CO2 flue gas	Output	1.2	0.4	kg
Torch	CO2 flue gas	Output	1.1	1.8	kg
Purification	Electricity	Input	0.04	0.30	kWh
	Cooling	Input	0.04	0.24	kWh
HT	External hydrogen	Input (LRS) - Output (CS)	0.05	0.03	kg
	Cooling	Input	0.10	0.12	kWh
	Electricity	Input	0.05	0.04	kWh
	Wastewater	Output	0.83	0.29	kg
	Biofuel	Output	1.0	1.0	kg

6.6.3. Life cycle assessment

The model was built in GABI following the block flow diagram of the TEA. In Figure 95 below the model for lignin case and for corn stover are presented.


HTL+APR plant
Process plant/Reference quantities
The names of the basic processes are shown.
EU-28: Municipal solid waste on landfill ts
EU-28: Municipal waste water treatment
HTL product <u-so>
EU-28: Thermal energy from natural gas
ashes
0.0172 kg
water waste
3.3 kg
2.88 kg
0.414 kg
HTL biofuel
1 kg
Thermal energy (MJ)
0.888 MJ
11 MJ
Furnace <u-so>
offgas
0.0392 kg
H2 from APR
0.0121 kg
Nation: Purification <u-so>
0.165 kg
offgas PSA
torch <u-so>
1.86 MJ
HTL solid
Electrolysis <LC>
0.0478 kg
Hydrogen
HT <u-so>
0.158 MJ
0.182 MJ
Heat from char
heat from HT offgas
0.591 kg
HTL biocrude
1.41 kg
offgas HTL
APR gas
0.178 kg
34.4 kg
HTL products
Product separation <u-so>
0.769 kg
31.5 kg
wastewater
APR <u-so>
9.06 kg
HTL <u-so>
Electricity
wastewater
EU-28: Municipal waste water treatment
HTL feedstock
34.4 kg
Thermal energy (MJ)
2.64 MJ
1.03 MJ
3.67 MJ
Final heater <u-so>
EU-28: Thermal energy from natural gas ts
0.0206 MJ
22.2 kg
Lignin rich <u-so>
11.5 kg
HTL feedstock
34.4 kg
recycling water
2.35 MJ
2.71 MJ
EU-28: Electricity grid mix ts
EU-28: Process water ts
0.745 kg
Water (desalinated; deionised)
Nation: Pretreatment <u-so>

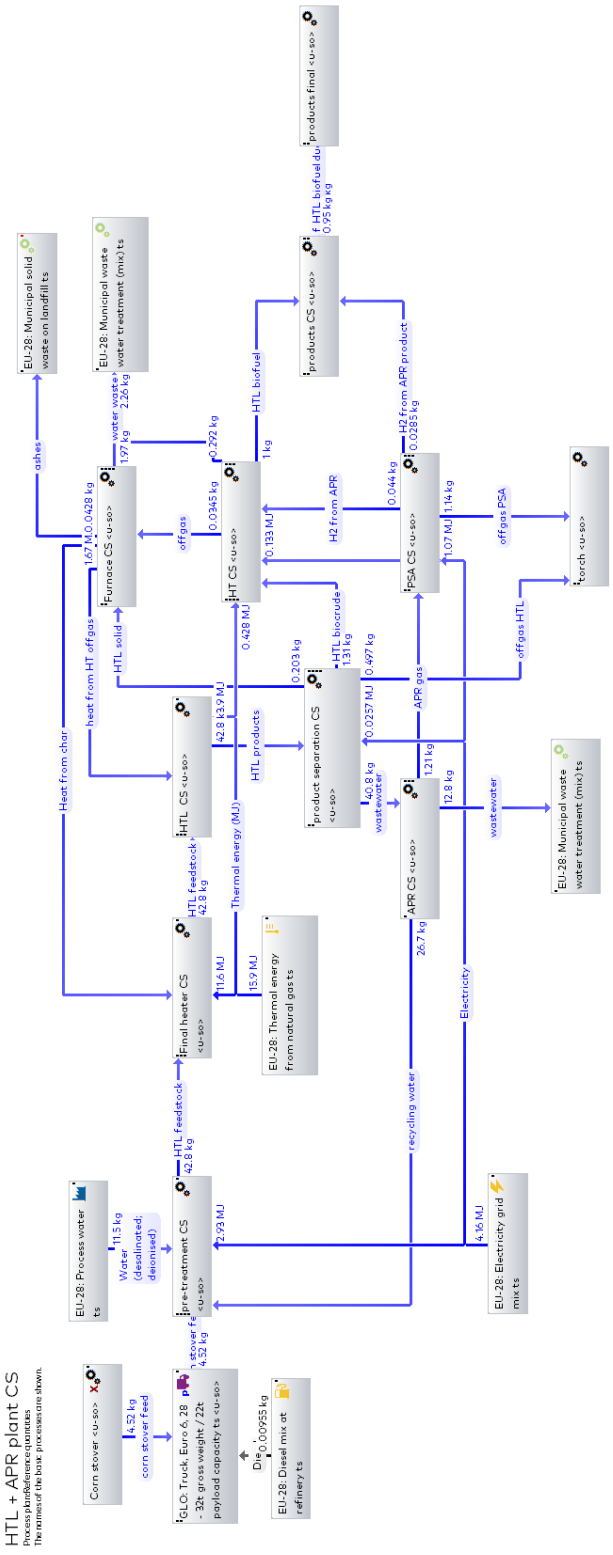


Figure 95: GABI model of HTL+APR plant. LRS above and CS below.

6.6.4. Interpretation step

The interpretation phase includes two steps: first the identification of issues, second the evaluation. This phase is an iterative procedure with the other phases of the LCA. The aim is to draw conclusions, finds limitation and recommendations. The LCA is an intrinsically iterative work. From preliminary results it was clear that some improvements could be achieved by:

1) Burning the off-gas of the hydrotreatment to produce heat and avoiding the release of alkanes (higher GWP extent than CO_2) in the atmosphere.
2) Sending the alkane-containing gas produced by APR and HTL to a torch, reducing its environmental impact (for the same reason cited above).

In Table 35 he chosen impact categories for the entire HTL-APR biorefinery are summarized for the two evaluated scenarios. It can be observed that both reported similar GHG emissions, with the LRS scenario being 31% higher GWP than the CS one. However, this similar cumulative value derives from different reasons. In order to better analyze this outcome, the main contributions are presented in Figure 96. It shows that electrolysis is responsible for 48% of the cumulative LRS-GWP, due to the hydrogen requirement for the biocrude upgrade, while electricity (for mixing, pumping and centrifugation). Thermal energy account for 60% for CS and 11% for LRS case; the higher thermal duty is due to the lower production of char during HTL and alkanes during upgrading. In fact, it was chosen to valorize these by-products by combustion to provide a fraction of the heating energy required by the biorefinery. However, in the CS-plant, this was not sufficient, and the supply of natural gas to compensate this lack of energy caused the discussed difference with respect to the LRS-plant. The second highest impact is due to the catalyst replacement (27% for LRS and 48% for CS) and is due to the platinum of which it is made. Within the CS case, the credit deriving from the surplus of H_2 allows to reduce the environmental burden. The CS-GWP is hence reduced by 29% from the previous value of 58g CO_2/MJ.

Both electrolysis and electricity directly depend on the electricity supply chain; currently The production of electricity is still mainly based on fossil fuels burning. The electric grid mix used in this work is constituted by different sources: fossil fuels is the predominant one (41.5%), followed by nuclear (27.6%), wind (8.0%), hydro (12.8%) and others (e.g., solar, geothermal, etc.). This distribution is similar to the one reported by the European Commission for the 2019 [34]. It derives that the necessity of using electrical energy implies an environmental burden, unless renewable energy sources are strongly deployed. Further evaluations on this topic will be reported in the next paragraph.

Table 35: Environmental impacts of the HTL-APR biorefinery for LRS and CS scenarios (1 MJ biofuel).

	Unit	LRS	CS
Global warming potential (excl. biogenic carbon)	g CO_2 eq.	59.7	40.9
Abiotic resource depletion fossil	MJ	0.68	0.59
Acidification potential	mg SO_2 eq.	22.5	16.9
Freshwater Eutrophication potential	mg PO_4 eq.	474	457

The acidification potential was slightly higher for the LRS-case with respect to the CS-case. Platinum was responsible for most of the AP (77%), followed by electrolysis (17%) this is due to the SO_2 emissions derived from fossil fuel-based thermoelectrical plants [265]. The AP contributions for the CS-biorefinery is almost all derived from platinum replacement.

Finally, LRS-plant showed a higher freshwater eutrophication potential (+24%) than the CS-plant. Electrolysis accounted for 33% of the total eutrophication potential: this is attributed to the nitrogen oxides emissions because of the presence of nitrogen into fossil fuels (i.e., fuel NO_x) and the high temperatures reached during the combustion process (i.e., thermal NO_x). Apart from the influence of electricity, it is noted that the utilization of platinum catalyst contributes as well to the EP (44% and 72% of total contribution in the LR- and CS-case, respectively). This is mainly due to the environmental impact of platinum extraction and purification [266].

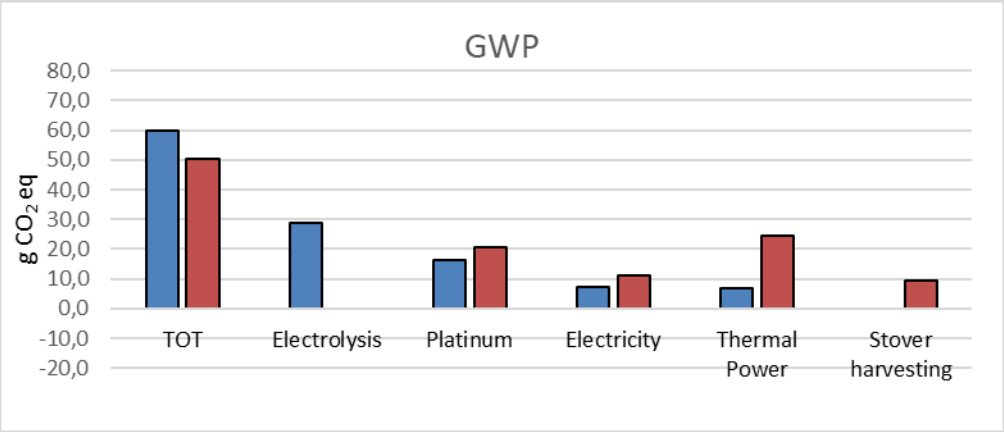
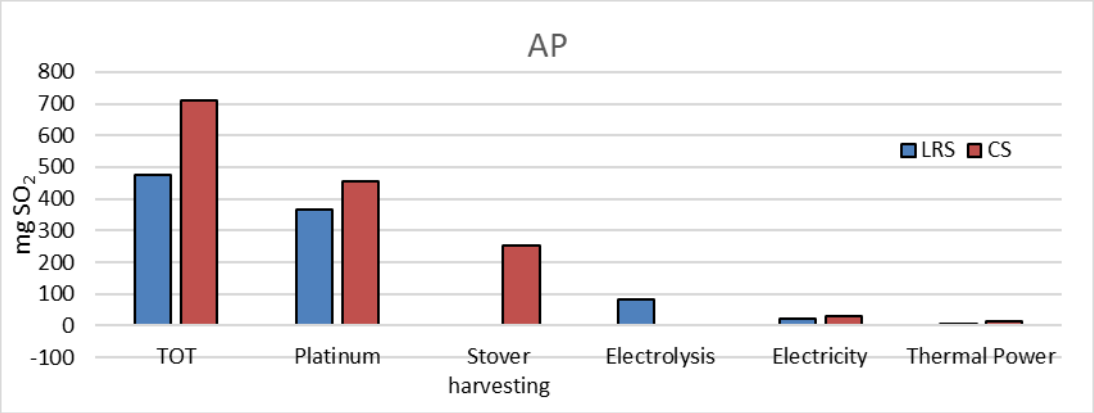
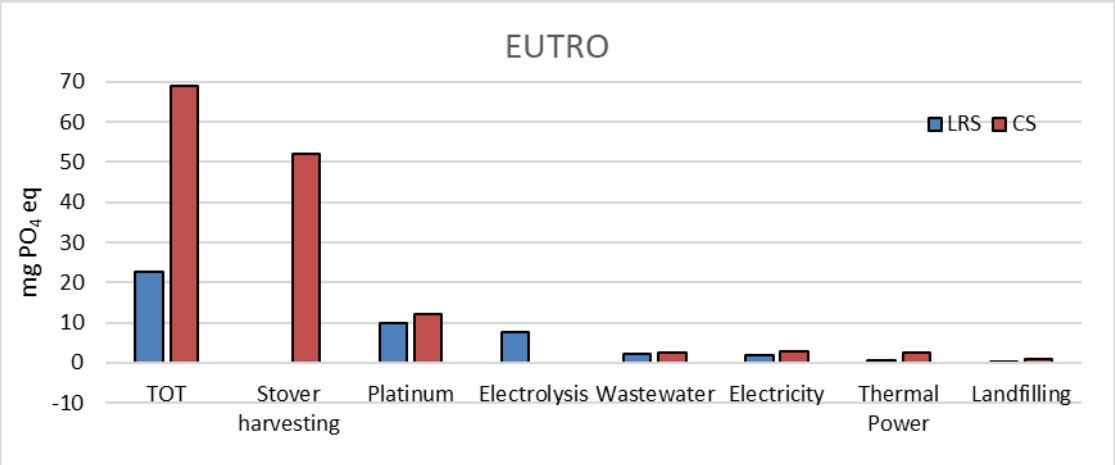


Figure 96: distribution of GWP among the main processes (1 MJ biofuel).





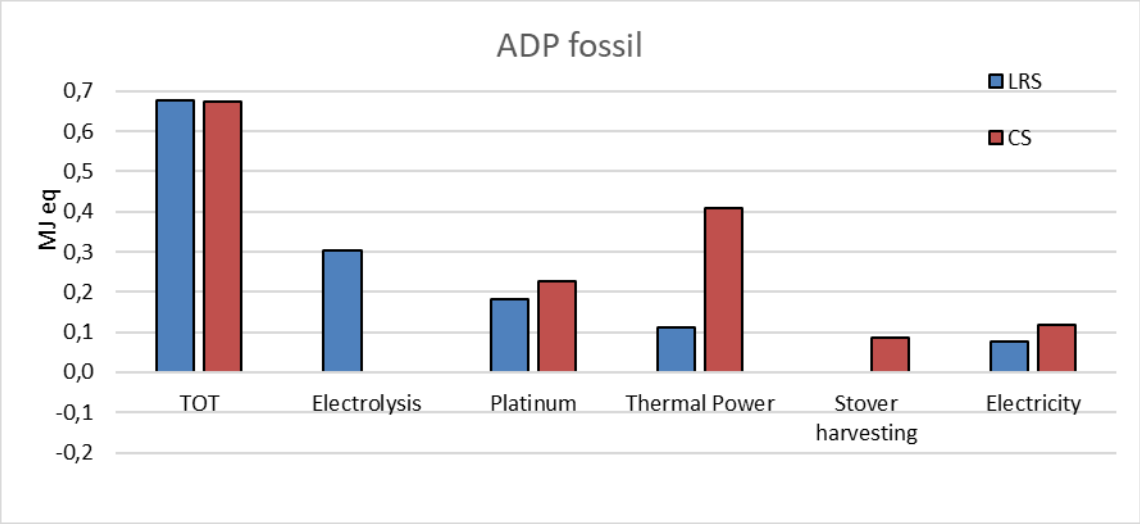


Figure 97:distribution of AP (1) and EP (2) and of abiotic depletion (3) among the main processes (1 MJ biofuel).

6.6.5. Non-biogenic carbon

As reported in the methodology section, the global warming potential of the HTL-APR biorefinery was evaluated following the "0/0 approach", i.e., considering biomass a carbon neutral energy resource. However, an agreement on the way to treat biogenic carbon is still not reached in LCA [267]. This is because the one-time pulse related with the CO_2 emissions from biomass combustion remains in the atmosphere and can therefore influence the delicate greenhouse effect equilibrium. For this reason, in this paragraph the GWP impact including the biogenic carbon is presented as well. In the LR-case, 26.5 g CO_2/MJ biofuel are added due to the torch emissions, and 28.4 g CO_2/MJ biofuel are further attributed to the furnace. The former is attributed to the combustion of the HT gas and the latter is ascribed to the burning of alkanes present in the gas phase derived from HTL and APR. It derived that the global GWP increased from 59.7 to 114.6 g CO2/MJ biofuel (+91%). In the CS-case, the global GWP increased as well, moving from 40.9 to 92.3 g CO2/MJ biofuel (+125%).

6.6.6. Literature comparison

As reported in many LCA works, a fair comparison with other results reported in the scientific literature is not an easy task due to the different choices about the functional unit, impact categories, allocation method and system boundaries, which can have a significant effect on the results. As suggested by Wiloso et al. for bioethanol production, clear and shared guidelines should be created to evaluate the environmental impact of biofuel production thanks to new technologies, and HTL can be an example [26].

Table 36 compares the environmental impact of 1 MJ of biofuel derived from an HTL-APR biorefinery with 1 MJ fuel from alternative biomass-based processes. We took into consideration a fast pyrolysis biofuel [268], bioethanol from fermentation, bio-oil from pyrolysis and jet fuel from gasification of corn stover [269]. When feasible, we derived from the provided data only the impact related to the transport and processing stages (i.e., excluding the use of the fuel), so that these figures could be considered coherent with the ones reported herein.

Table 36: comparison of impacts of different biofuels

	HTL+ APR of lignin	***HTL + APR of cornstover***	***Fast pyrolysis of poplar***	***Pyrolysis***	***Gasification and FT synthesis***	***Fermentation to bioethanol***
GWP 100 year ($g\ CO_2$ eq)	59.7	40.9	90	61	13.2	12.2
EP (mg phosphate eq)	22	17	39	0.15	0.03	0.6
AP (gSO_2 eq)	0.47	0.46	0.20	0.84	0.1	1.1

Finally, the comparison of the GWP with an equivalent fossil fuel can be performed. In this case, it is generally recommended to use a "well-to-wheels" system boundary, so that the growth and utilization stages (i.e. fuel combustion in the engine) are included [268]. Since the biofuels have similar characteristic to fossil ones, the same GHG emission can be applied, however since the origin of the fuel is biomass the GHG emission from the usage stage can be considered as biogenic carbon and thus, as starting point, the impact can be calculated as 0 kg of CO_2 equivalent.

The final GWP values can therefore being evaluated as summation of the biogenic GWP as calculated above in the cradle-to-gate system boundaries and the biogenic GWP related to utilization stage. These values are 40.9 g CO_2/MJ in the corn stover scenario and 59.7 g CO_2/MJ in the lignin-rich stream scenario. If we compare these figures with the ones of a fossil diesel (89.1 g CO_2/MJ) [270], it derives a decrease in the GWP by 54% and 32% for corn stover- and lignin-based HTL-APR biorefineries, respectively. In Figure 98 the comparison of the GWP of this work with fossil fuel and with others biofuel is presented. Moreover, a sensitivity on the electricity and heat sources was performed and the results are shown in figure. Using renewable sources of electricity and or heat can further reduce the GWP impact of the HTL-APR plant.

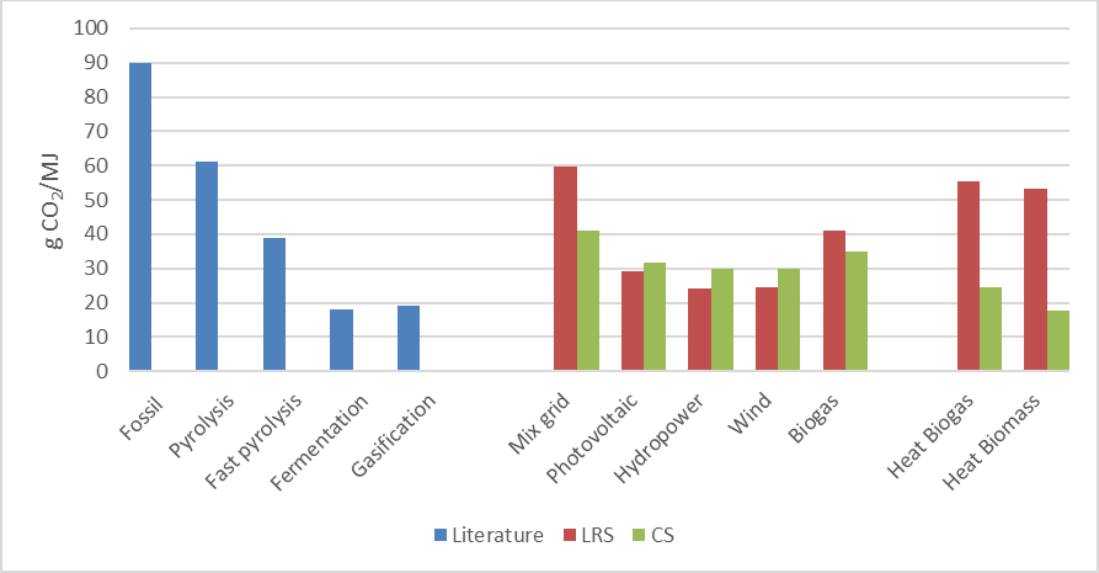


Figure 98: comparison of synfuels and fossil fuels from [268]

For future development deeper study are necessary to enlarge the system boundary and compare with fossil fuel. As reported in many LCA paper, comparison is not easy. Choices about functional units, impact categories, allocation methods and system boundaries can have a great effect on the results. As suggested by Wiloso et al [271] for-bioethanol production, clear and shared guidelines should be created to evaluate biofuel production from new systems. However, in this work the LCI, which is often difficult and lack of information, is consistent and detailed and can be used to improve the detail of the LCA.

6.7.Catalyst deactivation

The assessment carried out so far have not taken into account a possible deactivation of the APR catalyst, which was observed when dealing with real lignin-derived HTL aqueous phases as reported before. The most common impurities are aromatics and corresponding oligomers, which adsorb on activated carbon, blocking the pore and hindering the access to the active sites. This scenario is particularly important when lignin is used as feedstock, being the phenolics concentration in the aqueous phase seven times higher than the lignocellulosic case.

There are different options to tackle it, however none of them is yet costly effective. Different technologies were briefly evaluated herein: liquid-liquid extraction (LLE), adsorption with active carbon, char activation and use of different catalyst

supports. These different solutions will be discussed below, presenting their pros and cons.

6.7.1. Liquid-liquid extraction

The liquid-liquid extraction has been proven to be effective for phenolic compounds removal on a laboratory scale in the previous chapters, however its scale-up to the industrial scale is difficult due to its high operating costs. From experimental campaigns on aqueous phases deriving from HTL of lignin the performances of diethyl ether and butyl acetate were evaluated by the authors (unpublished). Butyl acetate showed better results than diethyl ether and therefore, thanks also to its lower solubility and better environmental compatibility, its use was evaluated for the HTL-APR described above. Besides LLE extraction, a distillation section is necessary to recover the butyl acetate from the oil phase to minimize the amount of fresh solvent to be used. Based on experimental data, extraction and distillation column were sized, using a lower solvent-water ratio compared to laboratory experiments in order to be consistent with industrial applications (0.5 solvent/water). The sums of investment and operative costs for LLE, taking into account also the savings resulting from the reduction of wastewater treatment, are equal to 0.29 (LRS) and 0.39 €/kg biofuel (CS) and are mainly due to the make-up of butyl acetate, which accounts for 76-79% of these costs. Although the distillation column is able to virtually recover all the solvent from the extracted current, most of the losses (99%) are due to the residual solvent in the aqueous current. In fact, despite the low butyl acetate concentration in the raffinate stream (4700 ppm), the overall solvent losses are not acceptable from cost and waste perspective due to the high water flow rate. For this reason, other organic solvents or more efficient technologies for solvent recovery should be sought.

6.7.2. Adsorption with activated carbon

Another option is the use of activated carbon (AC) for the physical adsorption of the aromatics. AC adsorption is the main technique used for the removal of pollutants from water. However, due to the capacity of AC to adsorb only up to 300-400 mg of aromatics (in total) per gram [272], and due to the high quantity of phenolics to be removed, a high amount of carbon is required if the in situ regeneration is not designed. In fact, the AC regeneration is not trivial because of the strong adsorption of the phenolics on them. Experimental studies for phenol desorption showed that at best, only 50% of it can be removed by using an alkali water solution [273]. The cost of commercial AC is higher than 1 €/kg [274].

Assuming an AC cost of 1.5 €/kg and considering the construction of the adsorption columns, the economic impact for phenolic compounds amounts to 0.90 (LRS) and 0.79 €/kg biofuel (CS). For this reason, in literature some works are focusing into finding low cost materials with high adsorbent capacity [272].

6.7.3. Char activation

The char produced inside the plant can be used as internal source of adsorbent for phenols removal. A plant layout of this type could eliminate the demand for expensive external activated carbon allowing, at the same time, the adsorption of phenolic compounds that would be valued at a later time together with the char. Usually, a first activation step, through thermic or chemical treatments, is required to improve physical-chemical properties of the char [275]. The possibility of using a heat treatment at 800 °C for 1 hour has been hereafter taken into consideration. The mass yield for this treatment was assumed equal to 53.8% for lignin and lignocellulosic char [275] and their production cost was taken equal to the production cost of steam activation of sugarcane bagasse to granular AC (2.81 €/kg) from literature [276]. As well as with sugarcane bagasse, a pelletization step is required if granular activated carbon is to be obtained from the pulverized char. The cost of activation is around 0.65 (LRS) and 0.41 €/kg biofuel (CS) to produce 224 kg/h (LRS) and 63 kg/h (CS). With these flow rates, the required capacities of the activated chars are 650 mg/g (LRS) and 403 mg/g (CS) of phenolic compounds; these values are higher than the ones reported by Liu and Zhang [275] towards phenol alone with thermally activated hydrochar (80-40 mg/g). However, Marx et al. [277] have shown that hydrochar has a far higher adsorption capacity towards guaiacol, which represents up to 25 % (LRS) and 10 % (CS) of the identified aromatics, than phenol. Practice et al. [278] also observed a higher adsorption of phenolics in real industrial wastewater than synthetic water composed solely by phenol with hydrochar from HTL of paper sludge. For these reasons, it is possible to infer that, with the presence of different compounds, the total adsorption will be higher than with only phenol.

The cost of removing phenols by activated char is still high. However, it is very likely that the activation cost is overestimated given the greater ease in activating an already carbonized matrix compared to a raw biomass. In addition, Marx et al. [277] studied the possibility of using hydrochar produced by HTL of municipal solid waste without activation treatment, obtaining good adsorption capacity. A deepening on the properties of char produced to the variation of the operating

conditions of HTL could therefore lead to its direct use eliminating the onerous activation costs.

6.7.4. Inert catalyst support

One promising option can be the use a suitable catalytic support, which does not interact with the dissolved compounds. Activated carbon was commonly chosen as a support for APR catalysts since it is known as a stable catalyst for industrial application, especially under hydrothermal conditions. However, as reported before, it has also high affinity with the aromatic compounds. Further research should focus into finding a stable catalyst support, with less surface area and less affinity with the phenols. In this frame, less hydrophobic supports, such as aluminum oxides, could play a role.

6.8.Conclusion

Hydrothermal liquefaction is a very promising technology to produce advanced biofuels, while APR represents a valid technology to exploit the residual organics in the aqueous phase. The APR reaction allows the conversion of these molecules into a gas phase rich in hydrogen, which can be used for in-situ upgrading of the HTL biocrude. A conceptual design of an HTL-APR integrated plant, using a 10 wt.% solid loading in slurry consisting of a LRS (20 MW input) or a lignocellulosic waste (corn stover, 16.5 MW input), has been performed. Firstly, the mass and energy balances were carried out and the main equipment, including the heat exchangers network, was sized. The plant was designed towards energy efficiency, and to valorize the subproducts and to overcome technical issues such as the separation sections.

The economic assessment evaluated the capital and operating costs resulting in a minimum selling price with IRR 0% (IRR 10%) of 1.20 (1.54) €/kg for LRS and 1.17 (1.55) €/kg for CS. A sensitivity analysis has been performed to understand how the main operative cost items affected the $MSP^{10\%}$: for both cases the feedstocks cost variation (±50%) strongly modifies the $MSP^{10\%}$ (±7% for LRS, ±10% for CS). Difference on the electricity price could also lead to significant MSPs variation for the LRS-derived biofuel, mainly due to the high electricity demand for the missing quota of hydrogen, which is produced through electrolysis. For the CS case, natural gas has also a consistent impact.

The APR performances were assessed versus the cost of hydrogen production which is 7.6 €/kg (LRS) and 1.7 €/kg (CS). APR is particularly interesting in combination with CS. The addition of an APR section to the HTL plant fed with

CS allows for a low-price hydrogen, far cheaper than current electrolyzers and steam reformers, which makes HTL-APR coupling very interesting also under the economic point of view. In order to make HTL-APR attractive, good carbon yield for the aqueous phase and good hydrogen yield (kg H_2/kg C feed) should be reached. This in addition to the HTL parameters that still need a specific optimization effort (higher carbon yield and low Oxygen and Nitrogen content).
The preliminary life cycle assessment showed similar value to other biofuels (pyrolysis, biodiesel and so on) deeper study must been done to improve the LCA results.

Chapter 7

Conclusion

The valorization of subproducts is pivotal for the development of biorefineries, since increasing the carbon recovery and reducing the cost of disposal is a key important challenge. In this work the aqueous phase reforming reaction was proposed as solution for the aqueous streams able to convert the organic content in the water into a gas rich in hydrogen.

The thesis focused on the secondary streams of Fischer-Tropsch process and especially of the hydrothermal liquefaction of lignin rich feedstock.

During the FT reaction a water phase, containing small alcohols and carboxylic acids, is produced. the influence of temperature was studied, at higher temperature (270°C) the chemical oxygen demand of the water was reduced up to 90%. The tests on model compound highlighted the difference on the product distribution of primary and secondary alcohols, pointing out the importance of the position of the hydroxyl group on the activation of the molecules.

Then the carbon laden aqueous phase from HTL was subjected to APR to produce hydrogen. Representative model compounds and synthetic mixtures were tested; this allowed the identification of the molecules prone to convert to hydrogen and pointed out competition phenomena in the mixture. The study of the real water fraction showed a dramatic dependence of the performance on the phenolics content, highlighting the necessity of pretreatment of the water phase to increase the stability of the catalyst. The investigation on the actual water fraction showed an important catalyst deactivation which was correlated to the decrease of the surface area. The concentration of aromatics in the water was directly linked to the catalyst stability. Test on single compounds (guaiacol and phenol) excluded their responsibility on the deactivation; thus, the fouling phenomena may be due to the formation of phenolic oligomers. The use of solvent and/ or active carbon to selective remove the aromatics led to an improve in the performance and catalyst

stability. Finally preliminary tests were conducted in continuous mode to deeper study the deactivation, the importance of the sulfate was highlighted, and their impact minimized.

The produced hydrogen can be used to upgrade the oxygenated biocrude, produced by HTL, to biofuel. To understand the feasibility of the HTL and APR combined plant the design, the techno-economic and environmental assessment were performed. Two options were studied: 20 MW lignin rich feedstock to HTL and 16.5 MW corn stover feedstock to HTL. The results regarding the oxygen content of biocrude and the composition of the HTL-AP allowed to understand that the potentiality of the HTL and APR strongly depends on the feedstock. The economic evaluation resulted in a minimum selling price of both fuels comparable with other biofuels presented in literature (1.20 €/kg for lignin and 1.17 €/kg for corn stover). Moreover, regarding the corn stover case, the aqueous phase reforming can produce enough hydrogen at a lower price, compared to the most common electrolyzer and steam reformer, to upgrade the biocrude.

Acknowledgment

The project leading to this research has received funding from the European Union's Horizon 2020 research and innovation program under grant agreement N° 764675.

RE-CORD (Renewable Energy Consortium for Research and Development), BEST (Bioenergy and Sustainable Technologies center) and TU Wien are deeply acknowledged for the supply of the real feedstocks and collaboration.

Bibliography

[1] IEA, "IEA (2021), Key World Energy Statistics 2021," pp. 1–82, 2021, [Online]. Available: https://www.iea.org/reports/key-world-energy-statistics-2021.

[2] P. Singh, S. K. Yadav, and M. Kuddus, *Green nanomaterials for wastewater treatment*, vol. 126. 2020.

[3] "The Sustainable Development Agenda." .

[4] G. S. Simate *et al.*, "The treatment of brewery wastewater for reuse: State of the art," *Desalination*, vol. 273, no. 2–3, pp. 235–247, 2011, doi: 10.1016/j.desal.2011.02.035.

[5] "Kirin Beer University Report. Global Beer Production by Country in 2014. Available at:" .

[6] J. Remón, J. Ruiz, M. Oliva, L. García, and J. Arauzo, "Cheese whey valorisation: Production of valuable gaseous and liquid chemicals from lactose by aqueous phase reforming," *Energy Convers. Manag.*, vol. 124, pp. 453–469, 2016, doi: 10.1016/j.enconman.2016.07.044.

[7] S. Li *et al.*, "Food processing wastewater purification by microalgae cultivation associated with high value-added compounds production — A review," *Chinese J. Chem. Eng.*, vol. 27, no. 12, pp. 2845–2856, 2019, doi: 10.1016/j.cjche.2019.03.028.

[8] L. Leng *et al.*, "Bioenergy recovery from wastewater produced by hydrothermal processing biomass: Progress, challenges, and opportunities," *Sci. Total Environ.*, vol. 748, p. 142383, 2020, doi: 10.1016/j.scitotenv.2020.142383.

[9] L. Leng, J. Li, Z. Wen, and W. Zhou, "Use of microalgae to recycle nutrients in aqueous phase derived from hydrothermal liquefaction process," *Bioresour. Technol.*, vol. 256, no. December 2017, pp. 529–542, 2018, doi: 10.1016/j.biortech.2018.01.121.

[10] R. C. Leitão, A. C. Van Haandel, G. Zeeman, and G. Lettinga, "The effects of operational and environmental variations on anaerobic wastewater treatment systems: A review," *Bioresour. Technol.*, vol. 97, no. 9, pp. 1105–1118, 2006, doi: 10.1016/j.biortech.2004.12.007.

[11] C. Prasse, D. Stalter, U. Schulte-oehlmann, and T. A. Ternes, “Spoilt for choice : A critical review on the chemical and biological assessment of current wastewater treatment technologies,” vol. 87, 2015, doi: 10.1016/j.watres.2015.09.023.

[12] B. A. Black *et al.*, “Aqueous Stream Characterization from Biomass Fast Pyrolysis and Catalytic Fast Pyrolysis,” 2016, doi: 10.1021/acssuschemeng.6b01766.

[13] E. de Jong, H. Langeveld, and R. van Ree, “IEA Bioenergy Task 42 Biorefinery,” *IEA Bioenergy*, p. 28, 2013.

[14] R. Singh, B. B. Krishna, G. Mishra, J. Kumar, and T. Bhaskar, “Strategies for selection of thermo-chemical processes for the valorisation of biomass,” *Renew. Energy*, vol. 98, pp. 226–237, 2016, doi: 10.1016/j.renene.2016.03.023.

[15] H. L. Hwang, S. R. Jadhav, J. R. Silverman, and G. John, “Sweet and Sustainable: Teaching the Biorefinery Concept through Biobased Gelator Synthesis,” *J. Chem. Educ.*, vol. 91, no. 10, pp. 1563–1568, 2014, doi: 10.1021/ed3007764.

[16] J. A. Moulijn, M. Makkee, and A. E. Van Diepen, *Chemical process technology*. 2013.

[17] V. N. Gunaseelan, “Anaerobic digestion of biomass for methane production: A review,” *Biomass and Bioenergy*, vol. 13, no. 1–2, pp. 83–114, 1997, doi: 10.1016/S0961-9534(97)00020-2.

[18] A. Kumar, D. D. Jones, and M. A. Hanna, “Thermochemical biomass gasification: A review of the current status of the technology,” *Energies*, vol. 2, no. 3, pp. 556–581, 2009, doi: 10.3390/en20300556.

[19] T. Kan, V. Strezov, and T. J. Evans, “Lignocellulosic biomass pyrolysis: A review of product properties and effects of pyrolysis parameters,” *Renew. Sustain. Energy Rev.*, vol. 57, pp. 1126–1140, 2016, doi: 10.1016/j.rser.2015.12.185.

[20] A. Kruse, A. Funke, and M. M. Titirici, “Hydrothermal conversion of biomass to fuels and energetic materials,” *Curr. Opin. Chem. Biol.*, vol. 17, no. 3, pp. 515–521, 2013, doi: 10.1016/j.cbpa.2013.05.004.

[21] T. Wang, Y. Zhai, Y. Zhu, C. Li, and G. Zeng, “A review of the hydrothermal carbonization of biomass waste for hydrochar formation: Process conditions, fundamentals, and physicochemical properties,” *Renew. Sustain. Energy*

Rev., vol. 90, no. December 2016, pp. 223–247, 2018, doi: 10.1016/j.rser.2018.03.071.

[22] J. Akhtar and N. A. S. Amin, "A review on process conditions for optimum bio-oil yield in hydrothermal liquefaction of biomass," *Renew. Sustain. Energy Rev.*, vol. 15, no. 3, pp. 1615–1624, 2011, doi: 10.1016/j.rser.2010.11.054.

[23] A. Kruse, "Hydrothermal biomass gasification," *J. Supercrit. Fluids*, vol. 47, no. 3, pp. 391–399, 2009, doi: 10.1016/j.supflu.2008.10.009.

[24] M. Usman *et al.*, "Characterization and utilization of aqueous products from hydrothermal conversion of biomass for bio-oil and hydro-char production: A review," *Green Chem.*, vol. 21, no. 7, pp. 1553–1572, 2019, doi: 10.1039/c8gc03957g.

[25] Y. Zhu, M. J. Biddy, S. B. Jones, D. C. Elliott, and A. J. Schmidt, "Techno-economic analysis of liquid fuel production from woody biomass via hydrothermal liquefaction (HTL) and upgrading," *Appl. Energy*, vol. 129, pp. 384–394, 2014, doi: 10.1016/j.apenergy.2014.03.053.

[26] J. Watson, T. Wang, B. Si, W. T. Chen, A. Aierzhati, and Y. Zhang, "Valorization of hydrothermal liquefaction aqueous phase: pathways towards commercial viability," *Prog. Energy Combust. Sci.*, vol. 77, p. 100819, 2020, doi: 10.1016/j.pecs.2019.100819.

[27] Y. Chen, J. J. Cheng, and K. S. Creamer, "Inhibition of anaerobic digestion process: A review," *Bioresour. Technol.*, vol. 99, no. 10, pp. 4044–4064, 2008, doi: 10.1016/j.biortech.2007.01.057.

[28] O. K. Dalrymple *et al.*, "Wastewater use in algae production for generation of renewable resources: A review and preliminary results," *Aquat. Biosyst.*, vol. 9, no. 1, p. 1, 2013, doi: 10.1186/2046-9063-9-2.

[29] M. H. Waldner and F. Vogel, "Renewable production of methane from woody biomass by catalytic hydrothermal gasification," *Ind. Eng. Chem. Res.*, vol. 44, no. 13, pp. 4543–4551, 2005, doi: 10.1021/ie050161h.

[30] P. N. Kechagiopoulos, S. S. Voutetakis, A. A. Lemonidou, and I. A. Vasalos, "Hydrogen production via steam reforming of the aqueous phase of bio-oil in a fixed bed reactor," *Energy and Fuels*, vol. 20, no. 5, pp. 2155–2163, 2006, doi: 10.1021/ef060083q.

[31] S. P. Zhang, X. J. Li, Q. Y. Li, Q. L. Xu, and Y. J. Yan, "Hydrogen production from the aqueous phase derived from fast pyrolysis of biomass,"

J. Anal. Appl. Pyrolysis, vol. 92, no. 1, pp. 158–163, 2011, doi: 10.1016/j.jaap.2011.05.007.

[32] F. J. G. Ortiz, F. J. Campanario, and P. Ollero, "Supercritical water reforming of model compounds of bio-oil aqueous phase : Acetic acid , acetol , butanol and glucose," vol. 298, pp. 243–258, 2016, doi: 10.1016/j.cej.2016.04.002.

[33] F. J. Campanario and F. J. Gutiérrez Ortiz, "Techno-economic assessment of bio-oil aqueous phase-to-liquids via Fischer-Tropsch synthesis and based on supercritical water reforming," *Energy Convers. Manag.*, vol. 154, no. October, pp. 591–602, 2017, doi: 10.1016/j.enconman.2017.10.096.

[34] K. Chandrasekhar, S. Kumar, B. D. Lee, and S. H. Kim, "Waste based hydrogen production for circular bioeconomy: Current status and future directions," *Bioresour. Technol.*, vol. 302, no. November 2019, p. 122920, 2020, doi: 10.1016/j.biortech.2020.122920.

[35] L. T. Cordova *et al.*, "Valorizing a hydrothermal liquefaction aqueous phase through co-production of chemicals and lipids using the oleaginous yeast Yarrowia lipolytica," *Bioresour. Technol.*, vol. 313, no. June, p. 123639, 2020, doi: 10.1016/j.biortech.2020.123639.

[36] R. D. Cortright, R. R. Davda, and J. A. Dumesic, "Hydrogen from catalytic reforming of biomass-derived hydrocarbons in liquid water.," *Nature*, vol. 418, no. 6901, pp. 964–967, 2002, doi: 10.1038/nature01009.

[37] I. Coronado, M. Stekrova, M. Reinikainen, P. Simell, L. Lefferts, and J. Lehtonen, "A review of catalytic aqueous-phase refCoronado, I., Stekrova, M., Reinikainen, M., Simell, P., Lefferts, L., & Lehtonen, J. (2016). A review of catalytic aqueous-phase reforming of oxygenated hydrocarbons derived from biorefinery water fractions. Interna," *Int. J. Hydrogen Energy*, vol. 41, no. 26, pp. 11003–11032, 2016, doi: 10.1016/j.ijhydene.2016.05.032.

[38] J. J. Baschuk and X. Li, "Carbon monoxide poisoning of proton exchange membrane fuel cells," *Int. J. Energy Res.*, vol. 25, no. 8, pp. 695–713, 2001, doi: 10.1002/er.713.

[39] R. R. Davda, J. W. Shabaker, G. W. Huber, R. D. Cortright, and J. A. Dumesic, "A review of catalytic issues and process conditions for renewable hydrogen and alkanes by aqueous-phase reforming of oxygenated hydrocarbons over supported metal catalysts," *Appl. Catal. B Environ.*, vol. 56, no. 1-2 SPEC. ISS., pp. 171–186, 2005, doi: 10.1016/j.apcatb.2004.04.027.

[40] R. Alcalá, M. Mavrikakis, and J. A. Dumesic, "DFT studies for cleavage of

C-C and C-O bonds in surface species derived from ethanol on Pt(111)," *J. Catal.*, vol. 218, no. 1, pp. 178–190, 2003, doi: 10.1016/S0021-9517(03)00090-3.

[41] I. Coronado, M. Stekrova, M. Reinikainen, P. Simell, L. Lefferts, and J. Lehtonen, "A review of catalytic aqueous-phase reforming of oxygenated hydrocarbons derived from biorefinery water fractions," *Int. J. Hydrogen Energy*, vol. 41, no. 26, pp. 11003–11032, 2016, doi: 10.1016/j.ijhydene.2016.05.032.

[42] J. W. Shabaker, R. R. Davda, G. W. Huber, R. D. Cortright, and J. A. Dumesic, "Aqueous-phase reforming of methanol and ethylene glycol over alumina-supported platinum catalysts," *J. Catal.*, vol. 215, no. 2, pp. 344–352, 2003, doi: 10.1016/S0021-9517(03)00032-0.

[43] B. M. Kabyemela, T. Adschiri, R. M. Malaluan, and K. Arai, "Glucose and fructose decomposition in subcritical and supercritical water: Detailed reaction pathway, mechanisms, and kinetics," *Ind. Eng. Chem. Res.*, vol. 38, pp. 2888–2895, 1999, doi: 10.1021/ie9806390.

[44] G. Pipitone, G. Zoppi, A. Frattini, S. Bocchini, R. Pirone, and S. Bensaid, "Aqueous phase reforming of sugar-based biorefinery streams: from the simplicity of model compounds to the complexity of real feeds," *Catal. Today*, Sep. 2019, doi: 10.1016/j.cattod.2019.09.031.

[45] S. Irmak, M. Kurtuluş, A. Hasanoğlu Hesenov, and O. Erbatur, "Gasification efficiencies of cellulose, hemicellulose and lignin fractions of biomass in aqueous media by using Pt on activated carbon catalyst," *Biomass and Bioenergy*, vol. 49, pp. 102–108, 2013, doi: 10.1016/j.biombioe.2012.12.016.

[46] J. Remón, J. R. Giménez, A. Valiente, L. García, and J. Arauzo, "Production of gaseous and liquid chemicals by aqueous phase reforming of crude glycerol: Influence of operating conditions on the process," *Energy Convers. Manag.*, vol. 110, pp. 90–112, 2016, doi: 10.1016/j.enconman.2015.11.070.

[47] A. Seretis and P. Tsiakaras, "Aqueous phase reforming (APR) of glycerol over platinum supported on Al2O3 catalyst," *Renew. Energy*, vol. 85, pp. 1116–1126, 2016, doi: 10.1016/j.renene.2015.07.068.

[48] B. Roy, H. Sullivan, and C. A. Leclerc, "Effect of variable conditions on steam reforming and aqueous phase reforming of n-butanol over Ni/CeO2 and Ni/Al2O 3 catalysts," *J. Power Sources*, vol. 267, pp. 280–287, 2014, doi: 10.1016/j.jpowsour.2014.05.090.

[49] G. Pipitone, G. Zoppi, R. Pirone, and S. Bensaid, “A critical review on catalyst design for aqueous phase reforming,” *Int. J. Hydrogen Energy*, vol. 47, no. 1, pp. 151–180, 2022, doi: 10.1016/j.ijhydene.2021.09.206.

[50] R. R. Davda, J. W. Shabaker, G. W. Huber, R. D. Cortright, and J. A. Dumesic, “Aqueous-phase reforming of ethylene glycol on silica-supported metal catalysts,” *Appl. Catal. B Environ.*, vol. 43, no. 1, pp. 13–26, 2003, doi: 10.1016/S0926-3373(02)00277-1.

[51] J. W. Shabaker, G. W. Huber, R. R. Davda, R. D. Cortright, and J. A. Dumesic, “Aqueous-phase reforming of ethylene glycol over supported platinum catalysts,” *Catal. Letters*, 2003, doi: 10.1023/A:1023538917186.

[52] G. Wen, Y. Xu, H. Ma, Z. Xu, and Z. Tian, “Production of hydrogen by aqueous-phase reforming of glycerol,” *Int. J. Hydrogen Energy*, vol. 33, no. 22, pp. 6657–6666, 2008, doi: 10.1016/j.ijhydene.2008.07.072.

[53] K. Koichumanova, A. K. K. Vikla, D. J. M. De Vlieger, K. Seshan, B. L. Mojet, and L. Lefferts, “Towards stable catalysts for aqueous phase conversion of ethylene glycol for renewable hydrogen,” *ChemSusChem*, vol. 6, no. 9, pp. 1717–1723, 2013, doi: 10.1002/cssc.201300445.

[54] M. F. Neira D’Angelo, V. Ordomsky, J. Van Der Schaaf, J. C. Schouten, and T. A. Nijhuis, “Aqueous phase reforming in a microchannel reactor: The effect of mass transfer on hydrogen selectivity,” *Catal. Sci. Technol.*, vol. 3, no. 10, pp. 2834–2842, 2013, doi: 10.1039/c3cy00577a.

[55] B. Entezary and M. Kazemeini, “Improved H2 production from the APR of polyols in a microreactor utilizing Pt supported on a CeO2–Al2O3 structured catalyst,” *Int. J. Hydrogen Energy*, pp. 1–14, 2018, doi: 10.1016/j.ijhydene.2018.09.207.

[56] J. W. Shabaker, G. W. Huber, and J. A. Dumesic, “Aqueous-phase reforming of oxygenated hydrocarbons over Sn-modified Ni catalysts,” *J. Catal.*, vol. 222, no. 1, pp. 180–191, 2004, doi: 10.1016/j.jcat.2003.10.022.

[57] T. P. Vispute and G. W. Huber, “Production of hydrogen, alkanes and polyols by aqueous phase processing of wood-derived pyrolysis oils,” *Green Chem.*, vol. 11, no. 9, pp. 1433–1445, 2009, doi: 10.1039/b912522c.

[58] P. D. Vaidya and J. A. Lopez-Sanchez, “Review of Hydrogen Production by Catalytic Aqueous-Phase Reforming,” *ChemistrySelect*, vol. 2, no. 22, pp. 6563–6576, 2017, doi: 10.1002/slct.201700905.

[59] G. Zoppi, G. Pipitone, R. Pirone, and S. Bensaid, “Aqueous phase reforming

process for the valorization of wastewater streams: Application to different industrial scenarios," *Catal. Today*, no. May, 2021, doi: 10.1016/j.cattod.2021.06.002.

[60] Y. Sun and J. Cheng, "Hydrolysis of lignocellulosic materials for ethanol production: A review," *Bioresour. Technol.*, vol. 83, no. 1, pp. 1–11, 2002, doi: 10.1016/S0960-8524(01)00212-7.

[61] K. Sharma, "Carbohydrate-to-hydrogen production technologies: A mini-review," *Renew. Sustain. Energy Rev.*, vol. 105, no. May 2018, pp. 138–143, 2019, doi: 10.1016/j.rser.2019.01.054.

[62] S. Irmak and L. Öztürk, "Hydrogen rich gas production by thermocatalytic decomposition of kenaf biomass," *Int. J. Hydrogen Energy*, vol. 35, no. 11, pp. 5312–5317, 2010, doi: 10.1016/j.ijhydene.2010.03.081.

[63] B. Meryemoglu, S. Irmak, and A. Hasanoglu, "Production of activated carbon materials from kenaf biomass to be used as catalyst support in aqueous-phase reforming process," *Fuel Process. Technol.*, vol. 151, pp. 59–63, 2016, doi: 10.1016/j.fuproc.2016.05.040.

[64] B. Meryemoglu, B. Kaya, S. Irmak, A. Hesenov, and O. Erbatur, "Comparison of batch aqueous-phase reforming of glycerol and lignocellulosic biomass hydrolysate," *Fuel*, vol. 97, pp. 241–244, 2012, doi: 10.1016/j.fuel.2012.02.011.

[65] I. Van Zandvoort *et al.*, "Formation, molecular structure, and morphology of humins in biomass conversion: Influence of feedstock and processing conditions," *ChemSusChem*, vol. 6, no. 9, pp. 1745–1758, 2013, doi: 10.1002/cssc.201300332.

[66] S. Irmak, B. Meryemoglu, A. Hasanoglu, and O. Erbatur, "Does reduced or non-reduced biomass feed produce more gas in aqueous-phase reforming process?," *Fuel*, vol. 139, pp. 160–163, 2015, doi: 10.1016/j.fuel.2014.08.028.

[67] L. I. Godina, H. Heeres, S. Garcia, S. Bennett, S. Poulston, and D. Y. Murzin, "Hydrogen production from sucrose via aqueous-phase reforming," *Int. J. Hydrogen Energy*, vol. 44, no. 29, pp. 14605–14623, 2019, doi: 10.1016/j.ijhydene.2019.04.123.

[68] A. S. Oliveira *et al.*, "Enhanced H2 production in the aqueous-phase reforming of maltose by feedstock pre-hydrogenation," *Appl. Catal. B Environ.*, vol. 281, no. July, p. 119469, 2021, doi: 10.1016/j.apcatb.2020.119469.

[69] M. Alvear, A. Aho, I. L. Simakova, H. Grénman, T. Salmi, and D. Y. Murzin, "Aqueous phase reforming of xylitol and xylose in the presence of formic acid," *Catal. Sci. Technol.*, vol. 10, no. 15, pp. 5245–5255, 2020, doi: 10.1039/d0cy00811g.

[70] B. Kaya, S. Irmak, A. Hasanoglu, and O. Erbatur, "Evaluation of various carbon materials supported Pt catalyts for aqueous-phase reforming of lignocellulosic biomass hydrolysate," *Int. J. Hydrogen Energy*, vol. 39, no. 19, pp. 10135–10140, 2014, doi: 10.1016/j.ijhydene.2014.04.180.

[71] B. Meryemoğlu, A. Hasanoğlu, B. Kaya, S. Irmak, and O. Erbatur, "Hydrogen production from aqueous-phase reforming of sorghum biomass: An application of the response surface methodology," *Renew. Energy*, vol. 62, pp. 535–541, 2014, doi: 10.1016/j.renene.2013.08.018.

[72] S. Irmak, B. Meryemoglu, A. Sandip, J. Subbiah, R. B. Mitchell, and G. Sarath, "Microwave pretreatment effects on switchgrass and miscanthus solubilization in subcritical water and hydrolysate utilization for hydrogen production," *Biomass and Bioenergy*, vol. 108, no. October 2017, pp. 48–54, 2018, doi: 10.1016/j.biombioe.2017.10.039.

[73] S. Irmak and O. Nayman Tiryaki, "Is it economical and beneficial to produce hydrogen from excess corn kernels?," *Fuel*, vol. 272, no. April, p. 117747, 2020, doi: 10.1016/j.fuel.2020.117747.

[74] O. N. Tiryaki, S. Irmak, D. Ramchandran, J. Subbiah, and M. Morton, "Utilization of excess corn kernels for hydrogen gas biofuel production," *Int. J. Hydrogen Energy*, vol. 44, no. 57, pp. 29956–29963, 2019, doi: 10.1016/j.ijhydene.2019.09.212.

[75] O. N. Tiryaki and S. Irmak, "Evaluation of various corn variety kernels for hydrogen gas production by APR," *Biomass and Bioenergy*, vol. 134, no. December 2019, p. 105480, 2020, doi: 10.1016/j.biombioe.2020.105480.

[76] J. Zakzeski and B. M. Weckhuysen, "Lignin solubilization and aqueous phase reforming for the production of aromatic chemicals and hydrogen," *ChemSusChem*, vol. 4, no. 3, pp. 369–378, 2011, doi: 10.1002/cssc.201000299.

[77] G. W. Huber, J. W. Shabaker, and J. A. Dumesic, "Raney Ni-Sn catalyst for H2 production from biomass-derived hydrocarbons," *Science (80-.).*, vol. 300, no. 5628, pp. 2075–2077, 2003, doi: 10.1126/science.1085597.

[78] M. B. Valenzuela, C. W. Jones, and P. K. Agrawal, "Batch aqueous-phase reforming of woody biomass," *Energy and Fuels*, vol. 20, no. 4, pp. 1744–

1752, 2006, doi: 10.1021/ef060113p.

[79] G. Wen, Y. Xu, Z. Xu, and Z. Tian, “Direct conversion of cellulose into hydrogen by aqueous-phase reforming process,” *Catal. Commun.*, vol. 11, no. 6, pp. 522–526, 2010, doi: 10.1016/j.catcom.2009.12.008.

[80] A. Dimitriadis and S. Bezergianni, “Hydrothermal liquefaction of various biomass and waste feedstocks for biocrude production: A state of the art review,” *Renewable and Sustainable Energy Reviews*. 2017, doi: 10.1016/j.rser.2016.09.120.

[81] V. S. Sikarwar, M. Zhao, P. S. Fennell, N. Shah, and E. J. Anthony, “Progress in biofuel production from gasification,” *Prog. Energy Combust. Sci.*, vol. 61, pp. 189–248, 2017, doi: 10.1016/j.pecs.2017.04.001.

[82] S. D. Davidson, J. A. Lopez-Ruiz, Y. Zhu, A. R. Cooper, K. O. Albrecht, and R. A. Dagle, “Strategies to Valorize the Hydrothermal Liquefaction-Derived Aqueous Phase into Fuels and Chemicals,” *ACS Sustain. Chem. Eng.*, vol. 7, no. 24, pp. 19889–19901, 2019, doi: 10.1021/acssuschemeng.9b05308.

[83] E. Panisko, T. Wietsma, T. Lemmon, K. Albrecht, and D. Howe, “Characterization of the aqueous fractions from hydrotreatment and hydrothermal liquefaction of lignocellulosic feedstocks,” *Biomass and Bioenergy*, vol. 74, pp. 162–171, 2015, doi: 10.1016/j.biombioe.2015.01.011.

[84] R. B. R. B. Madsen, P. Biller, M. M. Jensen, J. Becker, B. B. Iversen, and M. Glasius, “Predicting the Chemical Composition of Aqueous Phase from Hydrothermal Liquefaction of Model Compounds and Biomasses,” *Energy and Fuels*, vol. 30, no. 12, pp. 10470–10483, 2016, doi: 10.1021/acs.energyfuels.6b02007.

[85] G. Pipitone *et al.*, “Towards the sustainable hydrogen production by catalytic conversion of C-laden biorefinery aqueous streams,” *Chem. Eng. J.*, vol. 377, Dec. 2019, doi: 10.1016/j.cej.2018.12.137.

[86] L. I. Godina *et al.*, “Aqueous-phase reforming of alcohols with three carbon atoms on carbon-supported Pt,” *Catal. Today*, vol. 301, no. April 2017, pp. 78–89, 2018, doi: 10.1016/j.cattod.2017.03.042.

[87] G. Zoppi *et al.*, “Aqueous phase reforming of pilot-scale Fischer-Tropsch water effluent for sustainable hydrogen production,” *Catal. Today*, Apr. 2020, doi: 10.1016/j.cattod.2020.04.024.

[88] C. Pan, A. Chen, Z. Liu, P. Chen, H. Lou, and X. Zheng, "Aqueous-phase reforming of the low-boiling fraction of rice husk pyrolyzed bio-oil in the presence of platinum catalyst for hydrogen production," *Bioresour. Technol.*, vol. 125, pp. 335–339, 2012, doi: 10.1016/j.biortech.2012.09.014.

[89] L. Chen, Y. Zhu, H. Zheng, C. Zhang, and Y. Li, "Catalytic degradation of aqueous Fischer-Tropsch effluents to fuel gas over oxide-supported Ru catalysts and hydrothermal stability of catalysts," *J. Chem. Technol. Biotechnol.*, vol. 87, no. 8, pp. 1089–1097, 2012, doi: 10.1002/jctb.3719.

[90] I. Coronado, A. Arandia, M. Reinikainen, R. Karinen, R. L. Puurunen, and J. Lehtonen, "Kinetic Modelling of the Aqueous-Phase Reforming of Fischer-Tropsch Water over Ceria-Zirconia Supported Nickel-Copper Catalyst," *Catalysts*, vol. 9, no. 11, p. 936, Nov. 2019, doi: 10.3390/catal9110936.

[91] I. Coronado, M. Pitínová, R. Karinen, M. Reinikainen, R. L. Puurunen, and J. Lehtonen, "Aqueous-phase reforming of Fischer-Tropsch alcohols over nickel-based catalysts to produce hydrogen: Product distribution and reaction pathways," *Appl. Catal. A Gen.*, vol. 567, no. July, pp. 112–121, 2018, doi: 10.1016/j.apcata.2018.09.013.

[92] I. Pavlovič, Ž. Knez, and M. Škerget, "Hydrothermal reactions of agricultural and food processing wastes in sub- and supercritical water: A review of fundamentals, mechanisms, and state of research," *J. Agric. Food Chem.*, vol. 61, no. 34, pp. 8003–8025, 2013, doi: 10.1021/jf401008a.

[93] A. S. Oliveira *et al.*, "Exploration of the treatment of fish-canning industry effluents by aqueous-phase reforming using Pt/C catalysts," *Environ. Sci. Water Res. Technol.*, vol. 4, no. 12, pp. 1979–1987, 2018, doi: 10.1039/c8ew00414e.

[94] M. F. Neira D'Angelo, V. Ordomsky, J. Van Der Schaaf, J. C. Schouten, and T. A. Nijhuis, "Continuous hydrogen stripping during aqueous phase reforming of sorbitol in a washcoated microchannel reactor with a Pt-Ru bimetallic catalyst," *Int. J. Hydrogen Energy*, vol. 39, no. 31, pp. 18069–18076, 2014, doi: 10.1016/j.ijhydene.2014.02.167.

[95] A. S. Oliveira *et al.*, "Production of hydrogen from brewery wastewater by aqueous phase reforming with Pt/C catalysts," *Appl. Catal. B Environ.*, vol. 245, no. October 2018, pp. 367–375, 2019, doi: 10.1016/j.apcatb.2018.12.061.

[96] Y. Guo, M. U. Azmat, X. Liu, Y. Wang, and G. Lu, "Effect of support's basic properties on hydrogen production in aqueous-phase reforming of

glycerol and correlation between WGS and APR," *Appl. Energy*, vol. 92, pp. 218–223, 2012, doi: 10.1016/j.apenergy.2011.10.020.

[97] A. S. Oliveira *et al.*, "Effect of basicity in the aqueous phase reforming of brewery wastewater for H2 production," *Renew. Energy*, vol. 148, pp. 889–896, 2020, doi: 10.1016/j.renene.2019.10.173.

[98] B. Saenz de Miera, A. S. Oliveira, J. A. Baeza, L. Calvo, J. J. Rodriguez, and M. A. Gilarranz, "Treatment and valorisation of fruit juice wastewater by aqueous phase reforming: Effect of pH, organic load and salinity," *J. Clean. Prod.*, vol. 252, p. 119849, 2020, doi: 10.1016/j.jclepro.2019.119849.

[99] Q. Lai, M. D. Skoglund, C. Zhang, A. R. Morris, and J. H. Holles, "Use of Hydrogen Chemisorption and Ethylene Hydrogenation as Predictors for Aqueous Phase Reforming of Lactose over Ni @ Pt and Co @ Pt Bimetallic Overlayer Catalysts," 2016, doi: 10.1021/acs.energyfuels.6b01405.

[100] J. Remón, L. García, and J. Arauzo, "Cheese whey management by catalytic steam reforming and aqueous phase reforming," *Fuel Process. Technol.*, vol. 154, pp. 66–81, 2016, doi: 10.1016/j.fuproc.2016.08.012.

[101] P. F. F. Amaral, T. F. Ferreira, G. C. Fontes, and M. A. Z. Coelho, "Glycerol valorization: New biotechnological routes," *Food Bioprod. Process.*, vol. 87, no. 3, pp. 179–186, 2009, doi: 10.1016/j.fbp.2009.03.008.

[102] G. D. Yadav and P. A. Chandan, "A green process for glycerol valorization to glycerol carbonateover heterogeneous hydrotalcite catalyst," *Catal. Today*, vol. 237, pp. 47–53, 2014, doi: 10.1016/j.cattod.2014.01.043.

[103] N. M. Kosamia, M. Samavi, B. K. Uprety, and S. K. Rakshit, "Valorization of biodiesel byproduct crude glycerol for the production of bioenergy and biochemicals," *Catalysts*, vol. 10, no. 6, pp. 1–20, 2020, doi: 10.3390/catal10060609.

[104] P. M. Walgode, R. P. V. Faria, and A. E. Rodrigues, "A review of aerobic glycerol oxidation processes using heterogeneous catalysts: a sustainable pathway for the production of dihydroxyacetone," *Catal. Rev. - Sci. Eng.*, vol. 00, no. 00, pp. 1–90, 2020, doi: 10.1080/01614940.2020.1747253.

[105] K. Lehnert and P. Claus, "Influence of Pt particle size and support type on the aqueous-phase reforming of glycerol," *Catal. Commun.*, vol. 9, no. 15, pp. 2543–2546, 2008, doi: 10.1016/j.catcom.2008.07.002.

[106] J. Remón, J. Ruiz, M. Oliva, L. García, and J. Arauzo, "Effect of biodiesel-derived impurities (acetic acid, methanol and potassium hydroxide) on the

aqueous phase reforming of glycerol," *Chem. Eng. J.*, vol. 299, pp. 431–448, 2016, doi: 10.1016/j.cej.2016.05.018.

[107] J. Remón, L. García, and J. Arauzo, "Applied Catalysis B : Environmental Effect of acid (CH 3 COOH , H 2 SO 4 and H 3 PO 4) and basic (KOH and NaOH) impurities on glycerol valorisation by aqueous phase reforming," *"Applied Catal. B, Environ.*, vol. 219, pp. 362–371, 2017, doi: 10.1016/j.apcatb.2017.07.068.

[108] A. Seretis and P. Tsiakaras, "Crude bio-glycerol aqueous phase reforming and hydrogenolysis over commercial SiO 2 e Al 2 O 3 nickel catalyst," *Renew. Energy*, vol. 97, pp. 373–379, 2016, doi: 10.1016/j.renene.2016.05.085.

[109] D. A. Boga, F. Liu, P. C. A. Bruijnincx, and B. M. Weckhuysen, "Aqueous-phase reforming of crude glycerol: effect of impurities on hydrogen production," *Catal. Sci. Technol.*, vol. 6, no. 1, pp. 134–143, 2016, doi: 10.1039/c4cy01711k.

[110] "BioForming Technology." .

[111] D. Y. Murzin *et al.*, "Kinetics, Modeling, and Process Design of Hydrogen Production by Aqueous Phase Reforming of Xylitol," *Ind. Eng. Chem. Res.*, vol. 56, no. 45, pp. 13240–13253, 2017, doi: 10.1021/acs.iecr.7b01636.

[112] D. A. Sladkovskiy, L. I. Godina, K. V. Semikin, E. V. Sladkovskaya, D. A. Smirnova, and D. Y. Murzin, "Process design and techno-economical analysis of hydrogen production by aqueous phase reforming of sorbitol," *Chem. Eng. Res. Des.*, vol. 134, pp. 104–116, 2018, doi: 10.1016/j.cherd.2018.03.041.

[113] M. Ouadi, N. Jaeger, C. Greenhalf, J. Santos, R. Conti, and A. Hornung, "Thermo-Catalytic Reforming of municipal solid waste," *Waste Manag.*, vol. 68, no. 2017, pp. 198–206, 2017, doi: 10.1016/j.wasman.2017.06.044.

[114] F. J. Gutiérrez Ortiz, A. Kruse, F. Ramos, and P. Ollero, "Integral energy valorization of municipal solid waste reject fraction to biofuels," *Energy Convers. Manag.*, vol. 180, no. July 2018, pp. 1167–1184, 2019, doi: 10.1016/j.enconman.2018.10.085.

[115] C. Prestigiacomo, V. A. Laudicina, A. Siragusa, O. Scialdone, and A. Galia, "Hydrothermal liquefaction of waste biomass in stirred reactors: One step forward to the integral valorization of municipal sludge," *Energy*, vol. 201, p. 117606, 2020, doi: 10.1016/j.energy.2020.117606.

[116] D. Faria *et al.*, “Sewage treatment using Aqueous Phase Reforming for reuse purpose,” *J. Water Process Eng.*, vol. 37, no. April, p. 101413, 2020, doi: 10.1016/j.jwpe.2020.101413.

[117] M. B. Shemfe, B. Fidalgo, and S. Gu, “Heat integration for bio-oil hydroprocessing coupled with aqueous phase steam reforming,” *Chem. Eng. Res. Des.*, vol. 107, pp. 73–80, 2016, doi: 10.1016/j.cherd.2015.09.004.

[118] T. Yang, L. Shi, R. Li, B. Li, and X. Kai, “Hydrodeoxygenation of crude bio-oil in situ in the bio-oil aqueous phase with addition of zero-valent aluminum,” *Fuel Process. Technol.*, vol. 184, no. July 2018, pp. 65–72, 2019, doi: 10.1016/j.fuproc.2018.10.025.

[119] I. Iliuta, M. C. Iliuta, P. Fongarland, and F. Larachi, “Integrated aqueous-phase glycerol reforming to dimethyl ether synthesis-A novel allothermal dual bed membrane reactor concept,” *Chem. Eng. J.*, vol. 187, pp. 311–327, 2012, doi: 10.1016/j.cej.2012.02.001.

[120] M. F. Neira D’Angelo, V. Ordomsky, J. Van Der Schaaf, J. C. Schouten, and T. A. Nijhuis, “Selective production of methane from aqueous biocarbohydrate streams over a mixture of platinum and ruthenium catalysts,” *ChemSusChem*, vol. 7, no. 2, pp. 627–630, 2014, doi: 10.1002/cssc.201300828.

[121] S. A. W. Hollak, M. A. Ariëns, K. P. De Jong, and D. S. Van Es, “Hydrothermal deoxygenation of triglycerides over Pd/C aided by in situ hydrogen production from glycerol reforming,” *ChemSusChem*, vol. 7, no. 4, pp. 1057–1062, 2014, doi: 10.1002/cssc.201301145.

[122] A. S. Oliveira *et al.*, “Production of hydrogen from brewery wastewater by aqueous phase reforming with Pt/C catalysts,” *Appl. Catal. B Environ.*, vol. 245, pp. 367–375, 2019, doi: 10.1016/j.apcatb.2018.12.061.

[123] M. Khodabandehloo, A. Larimi, and F. Khorasheh, “Comparative process modeling and techno-economic evaluation of renewable hydrogen production by glycerol reforming in aqueous and gaseous phases,” *Energy Convers. Manag.*, vol. 225, no. October, p. 113483, 2020, doi: 10.1016/j.enconman.2020.113483.

[124] M. Kayfeci, A. Kecebaş, and M. Bayat, “Hydrogen production,” in *Solar hydrogen production*, F. Calise, M. D. D’accadia, M. Santarelli, A. Lanzini, and D. Ferrero, Eds. Elsevier Inc., 2019, pp. 45–83.

[125] J. P. Lange, “Catalysis for biorefineries-performance criteria for industrial operation,” *Catal. Sci. Technol.*, vol. 6, no. 13, pp. 4759–4767, 2016, doi:

10.1039/c6cy00431h.

[126] P. B. Weisz and C. D. Prater, “Interpretation of Measurements in Experimental Catalysis,” *Adv. Catal.*, vol. 6, no. C, pp. 143–196, 1954, doi: 10.1016/S0360-0564(08)60390-9.

[127] P. Sabatier and J. B. Senderens, “New synthesis of methane,” *C. R. Hebd. Seances Acad. Sci.*, vol. 134, pp. 514–516, 1902.

[128] F. Fischer and H. Tropsch, “Über die Herstellung von Synthol durch Aufbau aus Kohlenoxyd und Wasserstoff,” *Brennstoff-Chemie*, vol. 5, no. 13, pp. 201–208, 1924.

[129] F. Fischer and H. Tropsch, “Über die Herstellung synthetischer Ölgemische (Synthol) durch Aufbau aus Kohlenoxyd und Wasserstoff,” *Brennstoff-Chemie*, vol. 4, no. 18, pp. 276–285, 1923.

[130] F. Fischer, “Methanol und Synthol aus Kohlenoxyd als Motorbetriebsstoff,” *Brennstoff-Chemie*, vol. 6, no. 15, pp. 234–235, 1925.

[131] F. Fischer and H. Tropsch, “Patent Deutsches Reich - Verfahren zur Gewinnung mehrgliedriger Parffinkohlenwasserstoffe aus Kohlenoxyden und Wasserstoff auf katalytischem Wege,” 1925.

[132] A. de Klerk, “Chapter 4 - Fischer–Tropsch Synthesis,” in *Fischer–Tropsch Refining*, Wiley-VCH Verlag & Co. KGaA, 2011, pp. 73–104.

[133] A. K. Dalai and B. H. Davis, “Fischer – Tropsch synthesis : A review of water effects on the performances of unsupported and supported Co catalysts,” *Appl. Catal. A Gen.*, vol. 348, pp. 1–15, 2008, doi: 10.1016/j.apcata.2008.06.021.

[134] A. J. V Underwood, “Industrial Synthesis of Hydrocarbons from Hydrogen and Carbon Monoxide,” *Ind. Eng. Chem.*, vol. 32, no. 4, pp. 449–454, Apr. 1940, doi: 10.1021/ie50364a002.

[135] M. E. Dry, “Chapter 3 - Chemical concepts used for engineering purposes,” in *Fischer-Tropsch Technology*, A. Steynberg and M. E. Dry, Eds. Elsevier Science & Technology Books, 2004, pp. 196–258.

[136] A. W. Weitkamp and C. G. Frye, “Products of Hydrogenation of Carbon Monoxide - Relation of Product Composition to Reaction Mechanism,” *Ind. Eng. Chem.*, vol. 45, no. 2, pp. 363–367, Feb. 1953, doi: 10.1021/ie50518a035.

[137] V. Subramanian, K. Cheng, and Y. Wang, “Fundamentally Understanding

Fischer–Tropsch Synthesis," in *Encyclopedia of Interfacial Chemistry - Surface Science and Electrochemistry*, K. Wandelt, Ed. Elsevier, 2018, pp. 107–114.

[138] R. B. Anderson, J. F. Schulz, L. J. E. Hofer, and H. H. Storch, "Physical Chemistry of the Fischer-Tropsch Synthesis, report, 1959; Washington D.C," *University of North Texas Libraries, Digital Library, https://digital.library.unt.edu; crediting UNT Libraries Government Documents Department.* .

[139] D. Chakrabarti, V. Prasad, and A. de Klerk, "Chapter 11 - Mechanism of the Fischer-Tropsch Process," in *Fischer-Tropsch Synthesis, Catalysts, and Catalysis: Advances and Applications*, 1st Editio., B. H. Davis and M. L. Occelli, Eds. CRC Press, 2016, pp. 183–222.

[140] A. Lappas and E. Heracleous, "Chapter 18 - Production of biofuels via Fischer-Tropsch synthesis: biomass-to-liquids," in *Handbook of Biofuels Production - Processes and Technologies*, 2nd Editio., R. Luque, C. Lin, K. Wilson, and J. Clark, Eds. Elsevier Ltd, 2016, pp. 549–593.

[141] S. Blakey, L. Rye, and C. W. Wilson, "Aviation gas turbine alternative fuels: A review," *Proc. Combust. Inst.*, vol. 33, no. 2, pp. 2863–2885, 2011, doi: 10.1016/j.proci.2010.09.011.

[142] S. Yang *et al.*, "Linear α-olefin production with Na-promoted Fe–Zn catalysts via Fischer–Tropsch synthesis," *RSC Adv.*, vol. 9, no. 25, pp. 14176–14187, 2019, doi: 10.1039/C9RA02471A.

[143] A. de Klerk and P. M. Maitlis, "Chapter 4 - What Can We Do with Fischer–Tropsch Products?," in *Greener Fischer-Tropsch Processes for Fuels and Feedstocks*, P. M. Maitlis and A. de Klerk, Eds. Wiley-VCH Verlag & Co. KGaA, 2013, pp. 81–106.

[144] R. Miglio, R. Zennaro, and A. de Klerk, "Chapter 15: Environmental Sustainability," in *Greener Fischer-Tropsch Processes for Fuels and Feedstocks*, P. M. Maitlis and A. de Klerk, Eds. Wiley-VCH Verlag & Co. KGaA, 2013, pp. 311–336.

[145] R. J. J. Nel and A. De Klerk, "Fischer-Tropsch aqueous phase refining by catalytic alcohol dehydration," *Ind. Eng. Chem. Res.*, vol. 46, no. 11, pp. 3558–3565, 2007, doi: 10.1021/ie061555r.

[146] M. Majone *et al.*, "High-rate anaerobic treatment of Fischer-Tropsch wastewater in a packed-bed biofilm reactor," *Water Res.*, vol. 44, no. 9, pp. 2745–2752, 2010, doi: 10.1016/j.watres.2010.02.008.

[147] D. Wang, Y. Han, H. Han, K. Li, C. Xu, and H. Zhuang, "New insights into enhanced anaerobic degradation of Fischer-Tropsch wastewater with the assistance of magnetite," *Bioresour. Technol.*, vol. 257, pp. 147–156, Jun. 2018, doi: 10.1016/j.biortech.2018.02.084.

[148] L. Chen, Y. Zhu, H. Zheng, C. Zhang, B. Zhang, and Y. Li, "Catalytic degradation of oxygenates in Fischer-Tropsch aqueous phase effluents to fuel gas via hydrodeoxygenation over Ru/AC catalyst," *J. Chem. Technol. Biotechnol.*, vol. 87, no. 1, pp. 112–122, Jan. 2012, doi: 10.1002/jctb.2690.

[149] B. H. Davis, "Fischer-Tropsch synthesis: current mechanism and futuristic needs," 2001. [Online]. Available: www.elsevier.comrlocaterfuproc.

[150] R. R. Davda *et al.*, "DFT and experimental studies of C-C and C-O bond cleavage in ethanol and ethylene glycol on Pt catalysts," *Stud. Surf. Sci. Catal.*, vol. 145, pp. 79–84, 2003, doi: 10.1016/s0167-2991(03)80168-4.

[151] T. Van Haasterecht, C. C. I. Ludding, K. P. De Jong, and J. H. Bitter, "Stability and activity of carbon nanofiber-supported catalysts in the aqueous phase reforming of ethylene glycol," *J. Energy Chem.*, vol. 22, no. 2, pp. 257–269, 2013, doi: 10.1016/S2095-4956(13)60032-7.

[152] R. Lobo *et al.*, "Understanding the Chemistry of H2 Production for 1-Propanol Reforming: Pathway and Support Modification Effects," *ACS Catal.*, vol. 2, pp. 2316–2326, 2012.

[153] G. Pipitone, D. Tosches, S. Bensaid, A. Galia, and R. Pirone, "Valorization of alginate for the production of hydrogen via catalytic aqueous phase reforming," *Catal. Today*, vol. 304, no. May, pp. 153–164, 2018, doi: 10.1016/j.cattod.2017.09.047.

[154] G. Pipitone *et al.*, "Aqueous phase reforming of the residual waters derived from lignin-rich hydrothermal liquefaction: investigation of representative organic compounds and actual biorefinery streams," *Catal. Today*, vol. 345, pp. 237–250, Sep. 2020, doi: 10.1016/j.cattod.2019.09.040.

[155] G. Zoppi *et al.*, "Aqueous phase reforming of lignin-rich hydrothermal liquefaction by-products: A study on catalyst deactivation," *Catal. Today*, Aug. 2020, doi: 10.1016/j.cattod.2020.08.013.

[156] A. R. K. Gollakota, N. Kishore, and S. Gu, "A review on hydrothermal liquefaction of biomass," *Renew. Sustain. Energy Rev.*, vol. 81, no. August 2016, pp. 1378–1392, 2018, doi: 10.1016/j.rser.2017.05.178.

[157] L. Xu, D. W. F. Wim Brilman, J. A. M. Withag, G. Brem, and S. Kersten,

"Assessment of a dry and a wet route for the production of biofuels from microalgae: Energy balance analysis," *Bioresour. Technol.*, vol. 102, no. 8, pp. 5113–5122, 2011, doi: 10.1016/j.biortech.2011.01.066.

[158] Bioenergy Technology Office, "Multi-Year Program Plan," 2016.

[159] C. U. Jensen, J. K. Rodriguez Guerrero, S. Karatzos, G. Olofsson, and S. B. Iversen, "Fundamentals of Hydrofaction^{TM}: Renewable crude oil from woody biomass," *Biomass Convers. Biorefinery*, vol. 7, no. 4, pp. 495–509, 2017, doi: 10.1007/s13399-017-0248-8.

[160] P. G. Duan *et al.*, "Integration of hydrothermal liquefaction and supercritical water gasification for improvement of energy recovery from algal biomass," *Energy*, vol. 155, pp. 734–745, 2018, doi: 10.1016/j.energy.2018.05.044.

[161] G. Tommaso, W. T. Chen, P. Li, L. Schideman, and Y. Zhang, "Chemical characterization and anaerobic biodegradability of hydrothermal liquefaction aqueous products from mixed-culture wastewater algae," *Bioresour. Technol.*, vol. 178, pp. 139–146, 2015, doi: 10.1016/j.biortech.2014.10.011.

[162] B. Maddi *et al.*, "Quantitative characterization of the aqueous fraction from hydrothermal liquefaction of algae," *Biomass and Bioenergy*, vol. 93, pp. 122–130, 2016, doi: 10.1016/j.biombioe.2016.07.010.

[163] B. Maddi *et al.*, "Quantitative Characterization of Aqueous Byproducts from Hydrothermal Liquefaction of Municipal Wastes, Food Industry Wastes, and Biomass Grown on Waste," *ACS Sustain. Chem. Eng.*, vol. 5, no. 3, pp. 2205–2214, 2017, doi: 10.1021/acssuschemeng.6b02367.

[164] Y. Gu, X. Zhang, B. Deal, L. Han, J. Zheng, and H. Ben, "Advances in energy systems for valorization of aqueous byproducts generated from hydrothermal processing of biomass and systems thinking," *Green Chem.*, vol. 21, no. 10, pp. 2518–2543, 2019, doi: 10.1039/c8gc03611j.

[165] R. M. Ravenelle, J. R. Copeland, A. H. Van Pelt, J. C. Crittenden, and C. Sievers, "Stability of Pt/γ-Al2O3 Catalysts in Model Biomass Solutions," *Top. Catal.*, vol. 55, no. 3–4, pp. 162–174, 2012, doi: 10.1007/s11244-012-9785-3.

[166] T. W. Kim, H. J. Park, Y. C. Yang, S. Y. Jeong, and C. U. Kim, "Hydrogen production via the aqueous phase reforming of polyols over three dimensionally mesoporous carbon supported catalysts," *Int. J. Hydrogen Energy*, vol. 39, no. 22, pp. 11509–11516, 2014, doi: 10.1016/j.ijhydene.2014.05.106.

[167] J. Shabaker and J. Dumesic, “Kinetics of aqueous-phase reforming of oxygenated hydrocarbons: Pt/Al2O3 and Sn-modified Ni catalysts,” *Ind. Eng. Chem.*, pp. 3105–3112, 2004.

[168] Z. Tang, J. Monroe, J. Dong, T. Nenoff, and D. Weinkauf, “Platinum-Loaded NaY Zeolite for Aqueous-Phase Reforming of Methanol and Ethanol to Hydrogen,” vol. 2, no. 3, pp. 2728–2733, 2009.

[169] T. Sakamoto, H. Kikuchi, T. Miyao, A. Yoshida, and S. Naito, “Applied Catalysis A : General Effect of transition metal element addition upon liquid phase reforming of methanol with water over TiO 2 supported Pt catalysts,” vol. 375, pp. 156–162, 2010, doi: 10.1016/j.apcata.2009.12.036.

[170] Y. Liu, Z. Chen, X. Wang, Y. Liang, X. Yang, and Z. Wang, “Highly Selective and Efficient Rearrangement of Biomass-Derived Furfural to Cyclopentanone over Interface-Active Ru/Carbon Nanotubes Catalyst in Water,” *ACS Sustain. Chem. Eng.*, vol. 5, no. 1, pp. 744–751, 2017, doi: 10.1021/acssuschemeng.6b02080.

[171] J. Cueto, L. Faba, E. Díaz, and S. Ordóñez, “Cyclopentanone as an Alternative Linking Reactant for Heterogeneously Catalyzed Furfural Aldol Condensation,” *ChemCatChem*, vol. 9, no. 10, pp. 1765–1770, 2017, doi: 10.1002/cctc.201601655.

[172] R. Ma, K. Cui, L. Yang, X. Ma, and Y. Li, “Selective catalytic conversion of guaiacol to phenols over a molybdenum carbide catalyst,” *Chem. Commun.*, vol. 51, no. 51, pp. 10299–10301, 2015, doi: 10.1039/c5cc01900a.

[173] W. Yang, X. Li, S. Liu, and L. Feng, “Direct hydrothermal liquefaction of undried macroalgae Enteromorpha prolifera using acid catalysts,” *Energy Convers. Manag.*, vol. 87, pp. 938–945, 2014, doi: 10.1016/j.enconman.2014.08.004.

[174] D. Zhou, L. Zhang, S. Zhang, H. Fu, and J. Chen, “Hydrothermal liquefaction of macroalgae enteromorpha prolifera to bio-oil,” *Energy and Fuels*, vol. 24, no. 7, pp. 4054–4061, 2010, doi: 10.1021/ef100151h.

[175] C. Sievers, S. L. Scott, Y. Noda, L. Qi, E. M. Albuquerque, and R. M. Rioux, “Phenomena affecting catalytic reactions at solid−Liquid interfaces,” *ACS Catal.*, vol. 6, no. 12, 2016, doi: 10.1021/acscatal.6b02532.

[176] J. Struijk and Scholten J. J. F, “Selectivity to cyclohexenes in the liquid phase hydrogenation of benzene and toluene over ruthenium catalysts, as influenced by reaction modifiers,” *Appl. Catal.*, vol. 82, no. 2, pp. 277–287, 1992, doi: 10.1016/S0166-9834(00)82297-6.

[177] R. B. Madsen, P. Biller, M. M. Jensen, J. Becker, B. B. Iversen, and M. Glasius, "Predicting the Chemical Composition of Aqueous Phase from Hydrothermal Liquefaction of Model Compounds and Biomasses," *Energy and Fuels*, vol. 30, no. 12, pp. 10470–10483, 2016, doi: 10.1021/acs.energyfuels.6b02007.

[178] X. Bai *et al.*, "Formation of phenolic oligomers during fast pyrolysis of lignin," *Fuel*, vol. 128, pp. 170–179, 2014, doi: 10.1016/j.fuel.2014.03.013.

[179] R. Ni *et al.*, "In-situ glycerol aqueous phase reforming and phenol hydrogenation over," *Chem. Eng. J.*, vol. 350, no. March, pp. 181–191, 2018, doi: 10.1016/j.cej.2018.05.146.

[180] D. Gao, C. Schweitzer, H. T. Hwang, and A. Varma, "Conversion of guaiacol on noble metal catalysts: Reaction performance and deactivation studies," *Ind. Eng. Chem. Res.*, vol. 53, no. 49, pp. 18658–18667, 2014, doi: 10.1021/ie500495z.

[181] D. K. Lee *et al.*, "Deactivation of Pt catalysts during wet oxidation of phenol," *Catal. Today*, vol. 154, no. 3–4, pp. 244–249, 2010, doi: 10.1016/j.cattod.2010.03.052.

[182] P. M. De Souza *et al.*, "Hydrodeoxygenation of Phenol over Pd Catalysts. Effect of Support on Reaction Mechanism and Catalyst Deactivation," *ACS Catal.*, vol. 7, no. 3, pp. 2058–2073, 2017, doi: 10.1021/acscatal.6b02022.

[183] C. Contescu, S. Adhikari, N. Gallego, N. Evans, and B. Biss, "Activated Carbons Derived from High-Temperature Pyrolysis of Lignocellulosic Biomass," *C*, vol. 4, no. 3, p. 51, 2018, doi: 10.3390/c4030051.

[184] W. M. H. S. P. Biloen, J. N. Helle, H. Verbeek, F. M. Dautzenberg, "The Role of Rhenium and Sulfur in Platinum-Based Catalysts," *J. Catal.*, vol. 18, no. 63, pp. 112–118, 1980.

[185] P. Chen, Q. Zhang, R. Shu, Y. Xu, L. Ma, and T. Wang, "Catalytic depolymerization of the hydrolyzed lignin over mesoporous catalysts," *Bioresour. Technol.*, vol. 226, pp. 125–131, 2017, doi: 10.1016/j.biortech.2016.12.030.

[186] H. N. Lyckeskog, C. Mattsson, L. Olausson, S. I. Andersson, L. Vamling, and H. Theliander, "Thermal stability of low and high Mw fractions of bio-oil derived from lignin conversion in subcritical water," *Biomass Convers. Biorefinery*, vol. 7, no. 4, pp. 401–414, 2017, doi: 10.1007/s13399-016-0228-4.

[187] R. N. Hilten and K. C. Das, “Comparison of three accelerated aging procedures to assess bio-oil stability,” *Fuel*, vol. 89, no. 10, pp. 2741–2749, 2010, doi: 10.1016/j.fuel.2010.03.033.

[188] M. Saisu, T. Sato, M. Watanabe, T. Adschiri, and K. Arai, “Conversion of lignin with supercritical water-phenol mixtures,” *Energy and Fuels*, vol. 17, no. 4, pp. 922–928, 2003, doi: 10.1021/ef0202844.

[189] K. Okuda, M. Umetsu, S. Takami, and T. Adschiri, “Disassembly of lignin and chemical recovery - Rapid depolymerization of lignin without char formation in water-phenol mixtures,” *Fuel Process. Technol.*, vol. 85, no. 8–10, pp. 803–813, 2004, doi: 10.1016/j.fuproc.2003.11.027.

[190] B. Zou, Y. juan Xu, J. jun Wu, Y. shan Yu, and G. sheng Xiao, “Phenolic compounds participating in mulberry juice sediment formation during storage,” *J. Zhejiang Univ. Sci. B*, vol. 18, no. 10, pp. 854–866, 2017, doi: 10.1631/jzus.B1600461.

[191] A. G. Gayubo, B. Valle, A. T. Aguayo, M. Olazar, and J. Bilbao, “Pyrolytic lignin removal for the valorization of biomass pyrolysis crude bio-oil by catalytic transformation,” *J. Chem. Technol. Biotechnol.*, vol. 85, no. 1, pp. 132–144, 2010, doi: 10.1002/jctb.2289.

[192] F. Villacañas, M. F. R. Pereira, J. J. M. Órfão, and J. L. Figueiredo, “Adsorption of simple aromatic compounds on activated carbons,” *J. Colloid Interface Sci.*, vol. 293, no. 1, pp. 128–136, 2006, doi: 10.1016/j.jcis.2005.06.032.

[193] C. Moreno-Castilla, “Adsorption of organic molecules from aqueous solutions on carbon materials,” *Carbon N. Y.*, vol. 42, no. 1, pp. 83–94, 2004, doi: 10.1016/j.carbon.2003.09.022.

[194] K. R. Arturi *et al.*, “Hydrothermal liquefaction of lignin in near-critical water in a new batch reactor: Influence of phenol and temperature,” *J. Supercrit. Fluids*, vol. 123, pp. 28–39, 2017, doi: 10.1016/j.supflu.2016.12.015.

[195] X. Hu *et al.*, “Polymerization on heating up of bio-oil: A model compound study,” *AIChE J.*, 2013, doi: 10.1002/aic.13857.

[196] T. M. Grant and C. J. King, “Mechanism of Irreversible Adsorption of Phenolic Compounds by Activated Carbons,” *Ind. Eng. Chem. Res.*, vol. 29, no. 2, pp. 264–271, 1990, doi: 10.1021/ie00098a017.

[197] W. Wang, S. Pan, R. Xu, J. Zhang, S. Wang, and J. Shen, “Competitive adsorption behaviors, characteristics, and dynamics of phenol, cresols, and

dihydric phenols onto granular activated carbon," *Desalin. Water Treat.*, vol. 56, no. 3, pp. 770–778, 2015, doi: 10.1080/19443994.2014.940385.

[198] N. Mojoudi, N. Mirghaffari, M. Soleimani, H. Shariatmadari, C. Belver, and J. Bedia, "Phenol adsorption on high microporous activated carbons prepared from oily sludge: equilibrium, kinetic and thermodynamic studies," *Sci. Rep.*, vol. 9, no. 1, pp. 1–12, 2019, doi: 10.1038/s41598-019-55794-4.

[199] S. Dell'Orco, E. Miliotti, G. Lotti, A. M. Rizzo, L. Rosi, and D. Chiaramonti, "Hydrothermal Depolymerization of Biorefinery Lignin-Rich Streams: Influence of Reaction Conditions and Catalytic Additives on the Organic Monomers Yields in Biocrude and Aqueous Phase," *Energies*, vol. 13, no. 5, p. 1241, 2020, doi: 10.3390/en13051241.

[200] A. Dąbrowski, P. Podkościelny, Z. Hubicki, and M. Barczak, "Adsorption of phenolic compounds by activated carbon - A critical review," *Chemosphere*, vol. 58, no. 8, pp. 1049–1070, 2005, doi: 10.1016/j.chemosphere.2004.09.067.

[201] M. S. Jahan, D. A. N. Chowdhury, M. K. Islam, and S. M. I. Moeiz, "Characterization of lignin isolated from some nonwood available in Bangladesh," *Bioresour. Technol.*, vol. 98, no. 2, pp. 465–469, 2007, doi: 10.1016/j.biortech.2006.01.005.

[202] D. Savy and A. Piccolo, "Physical-chemical characteristics of lignins separated from biomasses for second-generation ethanol," *Biomass and Bioenergy*, vol. 62, no. 0, pp. 58–67, 2014, doi: 10.1016/j.biombioe.2014.01.016.

[203] A. Di Fraia *et al.*, " Coupling Hydrothermal Liquefaction and Aqueous Phase Reforming for integrated production of biocrude and renewable H 2 ," *AIChE J.*, 2022, doi: 10.1002/aic.17652.

[204] D. Prat *et al.*, "CHEM21 selection guide of classical- and less classical-solvents," *Green Chem.*, vol. 18, no. 1, pp. 288–296, 2015, doi: 10.1039/c5gc01008j.

[205] T. Llano *et al.*, "Liquid – Liquid Extraction of Phenolic Compounds from Spent Sulphite Liquor Liquid – Liquid Extraction of Phenolic Compounds from Spent Sulphite Liquor," *Waste and Biomass Valorization*, no. September, 2015, doi: 10.1007/s12649-015-9425-9.

[206] N. S. Gould *et al.*, "Understanding solvent effects on adsorption and protonation in porous catalysts," *Nat. Commun.*, vol. 11, no. 1, pp. 1–13, 2020, doi: 10.1038/s41467-020-14860-6.

[207] Ş. S. Bayazit, I. Inci, and H. Uslu, “Adsorption of lactic acid from model fermentation broth onto activated carbon and amberlite IRA-67,” *J. Chem. Eng. Data*, vol. 56, no. 5, pp. 1751–1754, 2011, doi: 10.1021/je1006345.

[208] D. C. Elliott *et al.*, “Process development for hydrothermal liquefaction of algae feedstocks in a continuous-flow reactor,” *Algal Res.*, vol. 2, no. 4, pp. 445–454, 2013, doi: 10.1016/j.algal.2013.08.005.

[209] A. J. Mørup *et al.*, “Construction and Commissioning of a Continuous Reactor for Hydrothermal Liquefaction,” *Ind. Eng. Chem. Res.*, vol. 54, no. 22, pp. 5935–5947, 2015, doi: 10.1021/acs.iecr.5b00683.

[210] “Steeper Energy.” .

[211] D. Castello, T. H. Pedersen, and L. A. Rosendahl, “Continuous hydrothermal liquefaction of biomass: A critical review,” *Energies*, vol. 11, no. 11, 2018, doi: 10.3390/en11113165.

[212] G. Haarlemmer, M. Briand, A. Roubaud, J. Roussely, and M. Déniel, “Economic evaluation of a hydrothermal liquefaction process,” *Detritus*, vol. 3, no. September, pp. 84–92, 2018, doi: 10.31025/2611-4135/2018.13695.

[213] X. Gu, L. Yu, N. Pang, J. S. Martinez-Fernandez, X. Fu, and S. Chen, “Comparative techno-economic analysis of algal biofuel production via hydrothermal liquefaction: One stage versus two stages,” *Appl. Energy*, vol. 259, no. September 2019, p. 114115, 2020, doi: 10.1016/j.apenergy.2019.114115.

[214] A. Aierzhati, J. Watson, B. Si, M. Stablein, T. Wang, and Y. Zhang, “Development of a mobile, pilot scale hydrothermal liquefaction reactor: Food waste conversion product analysis and techno-economic assessment,” *Energy Convers. Manag. X*, vol. 10, p. 100076, 2021, doi: 10.1016/j.ecmx.2021.100076.

[215] I. Tews *et al.*, “Biomass direct liquefaction options: technoeconomic and life cycle assessment,” *Pacific Northwest Natl. Lab.*, no. July, p. 62, 2014, [Online]. Available: https://www.osti.gov/biblio/1184983.

[216] L. Axelsson, M. Franzén, M. Ostwald, G. Berndes, G. Lakshmi, and N. H. Ravindranath, “Perspective: Jatropha cultivation in southern India: Assessing farmers’ experiences,” *Biofuels, Bioprod. Biorefining*, vol. 6, no. 3, pp. 246–256, 2012, doi: 10.1002/bbb.

[217] M. O. P. Fortier, G. W. Roberts, S. M. Stagg-Williams, and B. S. M. Sturm, “Life cycle assessment of bio-jet fuel from hydrothermal liquefaction of

microalgae," *Appl. Energy*, vol. 122, no. July 2011, pp. 73–82, 2014, doi: 10.1016/j.apenergy.2014.01.077.

[218] D. Chiaramonti, A. Giovannini, S. Pescarolo, and R. Nistri, *2° Generation Bioethanol The world ' s largest demo plant ready to be transferred all over the world - A Handbook - Part II*. 2013.

[219] "Tab. 02.18 Superficie coltivata e produzione di cereali in Piemonte per provincia - Anno 2019." [Online]. Available: https://www.regione.piemonte.it/web/.

[220] S. Menardo, G. Airoldi, V. Cacciatore, and P. Balsari, "Potential biogas and methane yield of maize stover fractions and evaluation of some possible stover harvest chains," *Biosyst. Eng.*, vol. 129, no. 1, pp. 352–359, 2015, doi: 10.1016/j.biosystemseng.2014.11.010.

[221] R. H. Perry and D. W. Green, *Perry's Engineers' Handbook*. 1997.

[222] R. W. Serth and T. Lestina, *Process Heat Transfer*. McGraw-Hill, 2007.

[223] A. Mathanker, D. Pudasainee, A. Kumar, and R. Gupta, "Hydrothermal liquefaction of lignocellulosic biomass feedstock to produce biofuels: Parametric study and products characterization," *Fuel*, vol. 271, no. March, p. 117534, 2020, doi: 10.1016/j.fuel.2020.117534.

[224] G. Towler and R. K. Sinnott, *Chemical Engineering Design - Principles, Practice and Economics of Plant and Process Design (2nd Edition)*. 2013.

[225] R. Turton, R. C. Bailie, W. B. Whiting, J. A. Shaeiwitz, and D. Bhattacharyya, *Analysis, synthesis, and design of chemical processes, 4th edition*. Pearson, 2012.

[226] K. M. Guthrie, "Capital-Cost-Estimating-Guthrie-1969.pdf," *Chem. Eng.*, vol. 76, pp. 114–142, 1969.

[227] S. Jones, Y. Zhu, D. Anderson, R. T. Hallen, and D. C. Elliott, "Process Design and Economics for the Conversion of Algal Biomass to Hydrocarbons : Whole Algae Hydrothermal Liquefaction and Upgrading," *Pnnl*, no. March, pp. 1–69, 2014.

[228] Q. Shi *et al.*, "Clinical and familial characteristics of ten Chinese patients with fatal family insomnia," *Biomed. Environ. Sci.*, vol. 25, no. 4, pp. 471–475, 2012, doi: 10.3967/0895-3988.2012.04.013.

[229] F. Salomone, E. Giglio, D. Ferrero, M. Santarelli, R. Pirone, and S. Bensaid, "Techno-economic modelling of a Power-to-Gas system based on SOEC

electrolysis and CO2 methanation in a RES-based electric grid," *Chem. Eng. J.*, vol. 377, no. October 2018, p. 120233, 2019, doi: 10.1016/j.cej.2018.10.170.

[230] M. Sánchez, E. Amores, D. Abad, L. Rodríguez, and C. Clemente-Jul, "Aspen Plus model of an alkaline electrolysis system for hydrogen production," *Int. J. Hydrogen Energy*, vol. 45, no. 7, pp. 3916–3929, 2020, doi: 10.1016/j.ijhydene.2019.12.027.

[231] L. J. Snowden-Swan *et al.*, "Conceptual Biorefinery Design and Research Targeted for 2022: Hydrothermal Liquefaction Processing of Wet Waste to Fuels," *Pnnl*, vol. 27186, pp. 1–40, 2017.

[232] Y. Nie and X. T. Bi, "Techno-economic assessment of transportation biofuels from hydrothermal liquefaction of forest residues in British Columbia," *Energy*, vol. 153, pp. 464–475, 2018, doi: 10.1016/j.energy.2018.04.057.

[233] M. M. Wright, D. E. Daugaard, J. A. Satrio, and R. C. Brown, "Techno-economic analysis of biomass fast pyrolysis to transportation fuels," *Fuel*, vol. 89, no. SUPPL. 1, pp. S2–S10, 2010, doi: 10.1016/j.fuel.2010.07.029.

[234] T. R. Brown, R. Thilakaratne, R. C. Brown, and G. Hu, "Techno-economic analysis of biomass to transportation fuels and electricity via fast pyrolysis and hydroprocessing," *Fuel*, vol. 106, no. 2013, pp. 463–469, 2013, doi: 10.1016/j.fuel.2012.11.029.

[235] J. A. Ramirez and T. J. Rainey, "Comparative techno-economic analysis of biofuel production through gasi fi cation , thermal liquefaction and pyrolysis of sugarcane bagasse," *J. Clean. Prod.*, vol. 229, pp. 513–527, 2019, doi: 10.1016/j.jclepro.2019.05.017.

[236] Y. Zhu, S. B. Jones, A. J. Schmidt, K. O. Albrecht, S. J. Edmundson, and D. B. Anderson, "Techno-economic analysis of alternative aqueous phase treatment methods for microalgae hydrothermal liquefaction and biocrude upgrading system," *Algal Res.*, vol. 39, no. September 2018, p. 101467, 2019, doi: 10.1016/j.algal.2019.101467.

[237] A. S. LJ Snowden-Swan, RT Hallen, JM Billing, Y Zhu, TR Hart, SB Jones, SP Fox, DC Elliott, GDMaupin, "Hydrothermal Liquefaction and Upgrading of Municipal Wastewater Treatment Plant Sludge: A Preliminary Techno-Economic Analysis, United States Department of Energy, PNNL report," 2016.

[238] S. Li, Y. Jiang, L. J. Snowden-Swan, J. A. Askander, A. J. Schmidt, and J.

M. Billing, “Techno-economic uncertainty analysis of wet waste-to-biocrude via hydrothermal liquefaction,” *Appl. Energy*, vol. 283, no. November 2020, p. 116340, 2021, doi: 10.1016/j.apenergy.2020.116340.

[239] R. M. Swanson, A. Platon, J. A. Satrio, and R. C. Brown, “Techno-economic analysis of biomass-to-liquids production based on gasification,” *Fuel*, vol. 89, no. SUPPL. 1, pp. S11–S19, 2010, doi: 10.1016/j.fuel.2010.07.027.

[240] D. Knorr, J. Lukas, and P. Schoen, “Production of Advanced Biofuels via Liquefaction. Hydrothermal Liquefaction Reactor Design,” *Contract*, vol. 303, no. November, pp. 275–3000, 2013.

[241] The International Standards Organisation, “Environmental management — Life cycle assessment — Principles and framework,” *Iso 14040*, vol. 2006, pp. 1–28, 2006, doi: 10.1136/bmj.332.7550.1107.

[242] The International Standards Organisation, “Environmental management — Life cycle assessment — Requirements and guidelines,” *ISO 14044*, vol. 2006, no. 7, pp. 652–668, 2006, doi: 10.1007/s11367-011-0297-3.

[243] European Commission-Joint Research Center, *ILCD Handbook: General guide for Life Cycle Assessment - Detailed guidance*. 2010.

[244] EC-JRC, “Product Environmental Footprint (PEF) Guide,” *Eropean Commision Jt. Res. Cent.*, p. 154, 2012, [Online]. Available: http://ec.europa.eu/environment/eussd/pdf/footprint/PEF methodology final draft.pdf.

[245] GaBi Hanbook, “GaBi Paper Clip Tutorial,” *Lca*, pp. 1–75, 2012, [Online]. Available: http://www.gabi-software.com/uploads/media/Paper_Clip_Tutorial_Handbook_Part1.pdf.

[246] E. Miliotti, S. Dell’Orco, G. Lotti, A. M. Rizzo, L. Rosi, and D. Chiaramonti, “Lignocellulosic ethanol biorefinery: Valorization of lignin-rich stream through hydrothermal liquefaction,” *Energies*, vol. 12, no. 4, 2019, doi: 10.3390/en12040723.

[247] S. A. Channiwala and P. P. Parikh, “A unified correlation for estimating HHV of solid, liquid and gaseous fuels,” *Fuel*, vol. 81, no. 8, pp. 1051–1063, 2002, doi: 10.1016/S0016-2361(01)00131-4.

[248] D. C. Elliott, P. Biller, A. B. Ross, A. J. Schmidt, and S. B. Jones, “Hydrothermal liquefaction of biomass: Developments from batch to continuous process,” *Bioresour. Technol.*, vol. 178, pp. 147–156, 2015, doi: 10.1016/j.biortech.2014.09.132.

[249] E. Berglin, C. Enderlin, and A. Schmidt, “Review and Assessment of Commercial Vendors / Options for Feeding and Pumping Biomass Slurries for Hydrothermal Liquefaction,” *Pnnl*, vol. 21981, no. November, pp. 1–35, 2012.

[250] R. K. Sinnott, J. M. Coulson, and J. F. Richardson, *Chemical Engineering Volume 6 - Design*. 1983.

[251] A. M. Rizzo, S. Dell’Orco, E. Miliotti, and D. Chiaramonti, “Design, commissioning and start-up of a new hydrothermal liquefaction continuous pilot unit,” *Chem. Eng. Trans.*, vol. 80, no. April, pp. 367–372, 2020, doi: 10.3303/CET2080062.

[252] R. Yukesh Kannah *et al.*, “Techno-economic assessment of various hydrogen production methods – A review,” *Bioresour. Technol.*, vol. 319, no. September 2020, p. 124175, 2021, doi: 10.1016/j.biortech.2020.124175.

[253] “Hydrogen Production Costs 2021,” Aug. 2021.

[254] I. M. Dãrãban, L. A. Rosendahl, T. H. Pedersen, and S. B. Iversen, “Pretreatment methods to obtain pumpable high solid loading wood-water slurries for continuous hydrothermal liquefaction systems,” *Biomass and Bioenergy*, vol. 81, pp. 437–443, 2015, doi: 10.1016/j.biombioe.2015.07.004.

[255] A. M. Rizzo and D. Chiaramonti, “Blending of Hydrothermal Liquefaction Biocrude with Residual Marine Fuel: An Experimental Assessment,” *Energies*, vol. 15, no. 2, p. 450, Jan. 2022, doi: 10.3390/en15020450.

[256] D. M. M. Yacout, M. Tysklind, and V. K. K. Upadhyayula, “Assessment of forest-based biofuels for Arctic marine shipping,” *Resour. Conserv. Recycl.*, vol. 174, no. June, p. 105763, 2021, doi: 10.1016/j.resconrec.2021.105763.

[257] L. Rosendahl, *Direct thermochemical liquefaction for energy applications*. 2017.

[258] L. T. Funkenbusch, M. E. Mullins, L. Vamling, and T. Belkhieri, “Technoeconomic assessment of hydrothermal liquefaction oil from lignin with catalytic upgrading for renewable fuel and chemical production,” no. June 2018, pp. 1–12, 2019, doi: 10.1002/wene.319.

[259] L. A. Pedersen, Thomas Helmer ; Hansen, Nick Høy ; Pérez, Oscar Miralles ; Cabezas, Daniel Esteban Villamar ; Rosendahl, “Renewable hydrocarbon fuels from hydrothermal liquefaction: A techno-economic analysis,” *Biofuels, Bioprod. biorefining*, vol. 12, no. 2, pp. 213–223, 2018, doi:

10.1002/bbb.

[260] Y. Zhu, S. B. Jones, A. J. Schmidt, J. M. Billing, D. M. Santosa, and D. B. Anderson, “Economic impacts of feeding microalgae / wood blends to hydrothermal liquefaction and upgrading systems,” *Algal Res.*, vol. 51, no. August, p. 102053, 2020, doi: 10.1016/j.algal.2020.102053.

[261] M. de Jong, Sierk ; Hoefnagels, Ric ; Faaij, André ; Slade, Raphael ; Mawhood, Rebecca ; Junginger and L. Chichester, UK: John Wiley & Sons, “The feasibility of short-term production strategies for renewable jet fuels – a comprehensive techno-economic comparison,” *Biofuels, Bioprod. Biorefining*, vol. 9, no. 6, pp. 778–800, 2015, doi: 10.1002/bbb.

[262] M. Brandão *et al.*, “Key issues and options in accounting for carbon sequestration and temporary storage in life cycle assessment and carbon footprinting,” *Int. J. Life Cycle Assess.*, vol. 18, no. 1, pp. 230–240, 2013, doi: 10.1007/s11367-012-0451-6.

[263] F. Cherubini, G. P. Peters, T. Berntsen, A. H. Stromann, and E. Hertwich, “CO2 emissions from biomass combustion for bioenergy: atmospheric decay and contribution to global warming,” *GCB Bioenergy*, vol. 3, no. 5, pp. 413–426, 2011, doi: https://doi.org/10.1111/j.1757-1707.2011.01102.x.

[264] A. Levasseur, P. Lesage, M. Margni, and R. Samson, “Biogenic Carbon and Temporary Storage Addressed with Dynamic Life Cycle Assessment,” *J. Ind. Ecol.*, vol. 17, no. 1, pp. 117–128, 2013, doi: https://doi.org/10.1111/j.1530-9290.2012.00503.x.

[265] C. Acar and I. Dincer, *Hydrogen Production*, vol. 3–5. 2018.

[266] L. Duclos, M. Lupsea, G. Mandil, L. Svecova, P. X. Thivel, and V. Laforest, “Environmental assessment of proton exchange membrane fuel cell platinum catalyst recycling,” *J. Clean. Prod.*, vol. 142, pp. 2618–2628, 2017, doi: 10.1016/j.jclepro.2016.10.197.

[267] W. Liu *et al.*, “Analysis of the Global Warming Potential of Biogenic CO2 Emission in Life Cycle Assessments,” *Sci. Rep.*, vol. 7, no. July 2016, pp. 1–8, 2017, doi: 10.1038/srep39857.

[268] J. F. Peters, D. Iribarren, and J. Dufour, “Simulation and life cycle assessment of biofuel production via fast pyrolysis and hydroupgrading,” *Fuel*, vol. 139, pp. 441–456, 2015, doi: 10.1016/j.fuel.2014.09.014.

[269] H. Sun *et al.*, “Comparative life cycle assessment (LCA) of biofuel production via corn stover: fermentation to ethanol, pyrolysis to bio-oil, and

gasification to jet fuel," *Biomass Convers. Biorefinery*, no. 0123456789, 2021, doi: 10.1007/s13399-021-02054-z.

[270] R. Edwards, V. Mahieu, J. C. Griesemann, J. F. Larivé, and D. J. Rickeard, "Well-to-Wheels Analysis of Future Automotive Fuels and Power Trains in the European Context - Report, Version 3c," 2004. doi: 10.4271/2004-01-1924.

[271] E. I. Wiloso, R. Heijungs, and G. R. De Snoo, "LCA of second generation bioethanol: A review and some issues to be resolved for good LCA practice," *Renew. Sustain. Energy Rev.*, vol. 16, no. 7, pp. 5295–5308, 2012, doi: 10.1016/j.rser.2012.04.035.

[272] S. H. Lin and R. S. Juang, "Adsorption of phenol and its derivatives from water using synthetic resins and low-cost natural adsorbents: A review," *J. Environ. Manage.*, vol. 90, no. 3, pp. 1336–1349, 2009, doi: 10.1016/j.jenvman.2008.09.003.

[273] B. Xie, J. Qin, S. Wang, X. Li, H. Sun, and W. Chen, "Adsorption of Phenol on Commercial Activated Carbons: Modelling and Interpretation," *Int. J. Environ. Res. Public Health*, vol. 17, no. 3, 2020, doi: 10.3390/ijerph17030789.

[274] F. Di Natale, A. Erto, A. Lancia, and D. Musmarra, "Experimental and modelling analysis of As(V) ions adsorption on granular activated carbon," *Water Res.*, vol. 42, no. 8–9, pp. 2007–2016, 2008, doi: 10.1016/j.watres.2007.12.008.

[275] Z. Liu and F. Zhang, "Removal of copper (II) and phenol from aqueous solution using porous carbons derived from hydrothermal chars," *DES*, vol. 267, no. 1, pp. 101–106, 2011, doi: 10.1016/j.desal.2010.09.013.

[276] C. Ng, W. Marshall, R. M. Rao, R. R. Bansode, J. N. Losso, and R. J. Portier, "Granular activated carbons from agricultural by-products: process description and estimated cost of production," *Bulletin*, no. 881, pp. 1–32, 2003.

[277] S. Marx, R. J. Venter, A. Louw, and C. T. Dewah, "Upgrading of the aqueous product stream from hydrothermal liquefaction: Simultaneous removal of minerals and phenolic components using waste-derived hydrochar," *Biomass and Bioenergy*, vol. 151, no. July, 2021, doi: 10.1016/j.biombioe.2021.106170.

[278] W. Practice, O. Clean, A. Fuels, and S. Africa, "Utilization of hydrochar derived from waste paper sludge through hydrothermal liquefaction for the

remediation of phenol contaminated industrial wastewater Sanette Marx * and Karina van der Merwe," vol. 16, no. 3, pp. 756–771, 2021, doi: 10.2166/wpt.2021.035.